University of Alberta
Department of Civil & Environmental Engineering

Structural Engineering Report No. 219

SEISMIC EVALUATION OF STEEL BUILDINGS WITH CONCENTRICALLY BRACED FRAMES

by

MANOJ S. MEDHEKAR

and

D.J. LAURIE KENNEDY

October 1997

Recent Structural Engineering Reports

Department of Civil Engineering

University of Alberta

193. *Web Behaviour in Wood Composite Box Beams* by E. Thomas Lewicke, J.J. Roger Cheng and Lars Bach, August 1993.

194. *Experimental Investigation of the Compressive Behavior of Gusset Plate Connections* by Michael C.H. Yam and J.J. Roger Cheng, September 1993.

195. *Some Behavioural Aspects of Composite Trusses* by Berhanu Woldegiorgis and D.J. Laurie Kennedy, January 1994.

196. *Flexural Behavior of High Strength Concrete Columns* by Hisham H.H. Ibrahim and James G. MacGregor, March 1994.

197. *Prediction of Wrinkling Behavior of Girth-Welded Line Pipe* by Luis T. Souza, Alaa E. Elwi, and David W. Murray, April 1994.

198. *Assessment of Concrete Strength in Existing Structures* by F. Michael Bartlett and James G. MacGregor, May 1994.

199. *The Flexural Creep Behavior of OSB Panels Under Various Climatic Conditions* by Naiwen Zhao, J.J. Roger Cheng, and Lars Bach, June 1994.

200. *High Performance Concrete Under High Sustained Compressive Stresses* by Said Iravani and James G. MacGregor, June 1994.

201. *Strength and Installation Characteristics of Tension–Control Bolts* by Scott T. Undershute and Geoffrey L. Kulak, August 1994.

202. *Deformational Behavior of Line Pipe* by Magdi Mohareb, Alaa E. Elwi, Geoffrey L. Kulak and David W. Murray, September 1994.

203. *Behavior of Girth-Welded Line Pipe* by Nader Yoosef-Ghodsi, Geoffrey L. Kulak and David W. Murray, September 1994.

204. *Numerical Investigation of Eccentrically Loaded Tied High Strength Concrete Columns* by Jueren Xie, Alaa E. Elwi, and James G. MacGregor, October 1994.

205. *Shear Strengthening of Concrete Girders Using Carbon Fibre Reinforced Plastic Sheets* by Efrosini H. Drimoussis and J.J. Roger Cheng, October 1994.

206. *Shrinkage and Flexural Tests of a Full-Scale Composite Truss* by Michael B. Maurer and D.J. Laurie Kennedy, December 1994.

207. *Analytical Investigation of the Compressive Behavior and Strength of Steel Gusset Plate Connections* by Michael C.H. Yam and J.J. Roger Cheng, December 1994.

208. *The Effect of Tension Flange Movement on the Strength of Point Loaded I-Beams* by Dean Mullin and J.J. Roger Cheng, January 1995.

209. *Experimental Study of Transversely Loaded Continuous Steel Plates* by Kurt P. Ratzlaff and D.J. Laurie Kennedy, May 1995.

210. *Fatigue Tests of Riveted Bridge Girders* by Daniel Adamson and Geoffrey L. Kulak, July 1995.

211. *Fatigue of Riveted Tension Members* by Jeffery DiBattista and Geoffrey L. Kulak, November 1995.

212. *Behaviour of Masonry Cavity Walls Subjected to Vertical Eccentric Loads* by Ru Wang, Alaa E. Elwi, Michael A. Hatzinikolas and Joseph Warwaruk, February 1996.

213. *Thermal Ice Loads on Structures* by Azita Azarnejad and Terry M. Hrudey, November 1996.

214. *Transmission of High Strength Concrete Column Loads Through Concrete Slabs* by Carlos E. Ospina and Scott D.B. Alexander, January 1997.

215. *Seismic Behaviour of Steel Plate Shear Walls* by Robert G. Driver, Geoffrey L. Kulak, D.J. Laurie Kennedy and Alaa E. Elwi, February 1997.

216. *Extended End Plate Moment Connections under Cyclic Loading* by Bryan T. Adey, Gilbert Y. Grondin and J.J. Roger Cheng, June 1997.

217. *Connection on Infill Panels in Steel Plate Shear Walls* by A. Schumacher, Gilbert Y. Grondin and Geoffrey L. Kulak, August 1997.

218. *Shear Rehabilitation of G-Girder Bridges using CFRP Sheets* by John G.S. Alexander and J.J. Roger Cheng, October 1997.

219. *Seismic Evaluation of Steel Buildings with Concentrically Braced Frames* by Manoj S. Medhekar and D.J. Laurie Kennedy, October 1997.

Seismic Evaluation of Steel Buildings with Concentrically Braced Frames

by

Manoj S. Medhekar

and

D.J. Laurie Kennedy

Structural Engineering Report 219

Department of Civil and Environmental Engineering

The University of Alberta

Edmonton, Alberta, Canada

October, 1997

ABSTRACT

The seismic performance of low-rise steel buildings with concentrically braced frames (CBFs), designed in accordance with the National Building Code of Canada 1995 and CSA Standard S16.1-94, is evaluated. Such buildings possess features such as a flexible roof diaphragm and non-structural partitions. Concerns may arise about limited ductility and brace overstrength. Current seismic design provisions are based on studies on 'tall' buildings and do not address the features of low-rise buildings.

The dynamic behaviour of a single-storey building is investigated with an ambient vibration test. The experimental mode shapes show evidence of roof diaphragm flexibility. Numerical simulations of the dynamic behaviour suggest significant stiffness contributions from the non-structural cladding and built-up roofing.

The seismic evaluation study consists of (i) the design of single-storey and two-storey buildings for five seismic zones in Western Canada, (ii) definition of the intended performance level in the design earthquake, (iii) specification of ground motion consistent with the performance level and the selection of appropriate earthquake accelerograms for dynamic analyses, (iv) development of analytical models accounting for effects such as roof diaphragm flexibility, hysteresis behaviour of steel braces, stiffness and strength contributions from non-structural partitions, (v) use of response spectrum analysis, nonlinear 'pushover' analysis, and nonlinear dynamic time history analyses to estimate the seismic response of the buildings, and (vi) specification of acceptance criteria for the building and its components.

Existing codes provide a reasonable estimate of the maximum drift and brace ductility demand, but do not ensure that yielding is restricted to the braces. In moderate

and high seismic zones, the roof diaphragm response is inelastic and brace connections are overloaded. Recommendations are made to improve the seismic performance of CBFs.

A displacement-based seismic design method, an alternative to the current spectral acceleration-based design method, is used to design CBFs. Design displacement spectra are proposed for five seismic zones in Canada.

A seismic design strategy is proposed as a function of the seismic zone, that considers the importance of the structure, the limit states and governing criteria such as tolerable damage levels, initial and rehabilitation cost implications, and suggests appropriate methods for design and analysis.

ACKNOWLEDGEMENTS

This project was conducted with research funding from the Natural Sciences and Engineering Research Council of Canada. The first author also wishes to acknowledge personal financial support in the form of scholarships from The University of Alberta, The C.W. Carry Chair in Steel Structures, and the Alberta Regional Committee of the Canadian Institute of Steel Construction. Financial support to the first author from both the J.N. Tata Endowment and the R.D. Sethna Scholarship Fund, India, during the early period of graduate study is also gratefully acknowledged.

The authors wish to thank T.E. Little and B.H. Fan of BC Hydro, and D. Weichert of the Pacific Geoscience Centre for their valuable suggestions on selection of earthquake ground motion. Thanks are also extended to Professor C.E. Ventura and the Ambient Vibration Team of The University of British Columbia for conducting the test on the Safeway store, and to C.J. Montgomery of The Cohos Evamy Partners, Edmonton, for providing the necessary drawings and specifications.

The helpful comments of Professors R. Tremblay of École Polytechnique de Montréal, and J.J.R. Cheng, T.M. Hrudey, A.E. Peterson, and A.W. Lipsett of The University of Alberta are also much appreciated.

TABLE OF CONTENTS

LIST OF TABLES

LIST OF FIGURES

LIST OF SYMBOLS

A_f	area of flange member of diaphragm
A_{gn}	area of cross-section of normal brace
A_{go}	area of cross-section of overstrong brace
A_s	shear area
a	zonal acceleration ratio
C	damping, damping matrix
CBF	concentrically braced frame
d	width of diaphragm
D_s	width of CBF in metres
DBF	ductile braced frame
DRS	displacement response spectrum
E	elastic modulus
F	foundation factor
F_Y	static yield strength of steel
G	shear modulus
g	acceleration due to gravity
G′	shear stiffness of diaphragm
h	height of partition
h_n	height of CBF in metres
I	importance factor, moment of inertia
K	lateral stiffness, stiffness matrix, effective length factor
K_{cbf}	lateral stiffness of CBF
K_d	diaphragm stiffness
K_{eff}	effective stiffness
KL/r	effective slenderness ratio of brace or column
L_b	length of brace
LLRS	lateral load resisting system

M	mass, mass matrix, bending moment
M_b	body wave magnitude
M_d	mass of diaphragm
M_f	mass of endframe
M_L	local magnitude
m_{eff}	effective mass
NDBF	nominally ductile braced frame
P	axial load
PGA	peak ground acceleration
PGD	peak ground displacement
PGV	peak ground velocity
PHA	peak horizontal acceleration
PHV	peak horizontal velocity
P_{yn}	compressive capacity of brace, 1st cycle buckling load of brace
P_{ync}	post-buckling capacity of brace
P_{yp}	tensile capacity of brace
R	force modification factor, epicentral distance
r	radius of gyration
S	seismic response factor of the NBCC
S_a	spectral acceleration
SBF	strength braced frame
S_d	spectral displacement
S_v	spectral velocity
T	fundamental period
t	thickness of partition
T_{eff}	effective period
$\ddot{U}_g(t)$	earthquake ground acceleration
V	base shear, shear force

v	zonal velocity ratio
V_e	elastic base shear
W	effective seismic weight
Z_a	acceleration-related seismic zone
Z_v	velocity-related seismic zone
α	mass proportional damping coefficient
β	stiffness proportional damping coefficient
δ	axial displacement of brace
δ_{CBF}	lateral drift of CBF
δ_e	displacement from elastic analysis
δ_{eff}	effective displacement
δ_i	anticipated inelastic displacement in the design earthquake, displacement from nonlinear analysis
δ_{max}	maximum displacement of the structure
δ_{Roof}	lateral drift at mid-span of diaphragm
Δ	lateral displacement of brace, lateral drift of floor
Δ_Y	yield elongation of brace, yield displacement of structure
ϕ	resistance factor
μ	mean
ρ_o	static overstrength ratio
σ	standard deviation
ξ	damping ratio
ξ_{eff}	effective damping ratio
ω	circular frequency

1. INTRODUCTION

1.1 General

The seismic design provisions for buildings as currently reflected in the National Building Code of Canada (ACNBC 1995a) and CSA Standard S16.1-94 (CSA 1994) are undergoing continuous development based on the latest research results. Most analytical studies to date have focused on the seismic design and analysis of tall buildings. Information on the behaviour of low-rise buildings, typically up to four storeys high, is scarce. Such buildings comprise the majority of society's investment in steel structures and provide commercial and industrial space in all seismic zones of Canada. Hence, damage to such structures due to earthquakes poses a significant risk to life and property.

Low-rise buildings may possess one or more of the following features; (a) presence of a flexible roof diaphragm, (b) use of diaphragms as the horizontal lateral load resisting system (LLRS), (c) use of concentrically braced frames (CBFs) as the vertical LLRS for providing lateral stiffness and stability to the structure, [This coupling of a flexible system with a stiff one results in a discontinuity in stiffness and strength], (d) a significant number of non-structural elements such as cladding and partitions, (e) lack of homogeneity in construction due to use of different materials, and (f) irregular building layout.

These features lead to complexities in mathematical modelling and analysis that have limited the development of design recommendations for such buildings. The bases of current seismic design provisions are models that are representative of multi-storey, homogeneous, regular, medium to high-rise buildings with rigid diaphragms. These response models may not be appropriate to determine the earthquake induced force and deformation demands in low-rise buildings, as pointed out by Gupta and Moss (1993).

A large inventory of low-rise buildings exists that were not specifically detailed for ductile response in an earthquake and similar new buildings are also being erected. There is thus a growing concern about the limited strength and ductility of such construction. Analytical studies on the seismic response of such buildings are necessary to arrive at rehabilitation strategies for existing buildings and design recommendations for new construction.

Besides the above concerns, the following issues need to be addressed:

(a) Field measurements of the dynamic behaviour of low-rise buildings are scarce. The empirical expression for determining the fundamental period in the NBCC (ACNBC 1995a) is based on measurements on buildings with rigid diaphragms and may not be representative of such buildings.

(b) Non-structural elements have the potential of contributing significant lateral stiffness and strength to these buildings that is often neglected in design and analysis. The presence of this contribution during severe ground motion and its effect on dynamic response needs to be investigated.

(c) Low-rise buildings may possess a significant oversupply in lateral stiffness and strength with respect to the design requirement due to oversize of the lateral load resisting elements. The effect of this overstrength needs to be assessed.

(d) The NBCC (ACNBC 1995a) specifies three design force levels for CBFs along with the associated detailing requirements given in CSA Standard S16.1-94 (CSA 1994). However, no such provisions exist for design and detailing of diaphragms. The adequacy of the existing requirements and the possible use of a capacity design approach for diaphragms needs to be investigated.

(e) Alternative seismic design methods for such buildings need to be explored.

1.2 Objectives

The objectives of this study are to investigate the dynamic behaviour and seismic performance of low-rise steel buildings designed according to the provisions of the NBCC (ACNBC 1995a) and CSA Standard S16.1-94 (CSA 1994) and thus to make recommendations for:

(a) seismic design including loads in the NBCC,

(b) design of steel members and connections in CSA Standard S16.1,

(c) design of non-structural components, and

(d) further experimental and analytical research.

In addition, an alternative seismic design method based on specifying limiting displacements is reviewed and evaluated by applying it to the design of low-rise and medium-rise buildings.

The buildings in this study have concentrically braced frames (CBFs) as the vertical LLRS as it is the most commonly used system.

1.3 Scope

The work includes:

(a) A review of literature on the seismic behaviour and analytical modelling of low-rise steel buildings and their constituent components such as CBFs, steel deck diaphragms, and non-structural elements.

(b) The development of a methodology for seismic evaluation of such buildings. This involves; (i) design of single-storey and two-storey buildings in various seismic zones of Canada according to the provisions of the NBCC (ACNBC 1995a) and CSA Standard S16.1-94 (CSA 1994), (ii) definition of the performance level intended of these buildings in the design earthquake, (iii) specification of earthquake ground motion consistent with the performance level to be investigated, (iv) selection of appropriate analytical procedures to obtain the earthquake response of such buildings, (v) development of analytical models that simulate the dynamic behaviour of low-rise buildings observed in field measurements on an existing building, (vi) specification of acceptance criteria for the structure and its components, and (vii) formulation of design and detailing recommendations for such buildings based on their seismic performance.

(c) A review of an alternative seismic design philosophy for buildings based on specifying limiting displacements and comparing it qualitatively to the current design philosophy that uses accelerations as the basis.

(d) Application of this alternative seismic design method to both low-rise and medium-rise steel buildings that use CBFs as the LLRS. This constitutes a feasibility study to evaluate the design method, identify potential difficulties in its application, and address issues concerning design office implementation.

1.4 Organization of the thesis

The thesis consists of eleven chapters. Chapter 1 deals with the introduction, objectives, and scope. Chapter 2 reviews some basic concepts of earthquake resistant design of steel structures. Chapter 3 is a literature review on the seismic behaviour and

analytical modelling of CBFs, steel deck diaphragms, and non-structural elements. Chapter 4 describes the methodology adopted for evaluating the seismic performance of low-rise steel buildings designed to the specifications of the NBCC (ACNBC 1995a) and CSA Standard S16.1-94 (CSA 1994). Chapter 5 reports on studies carried out on a single-storey building. Chapter 6 assesses the effect of overstrength in the LLRS of a single-storey building. Chapter 7 reports on studies carried out on a two-storey building. Chapter 8 reviews an alternative displacement-based seismic design method. Chapters 9 and 10 report on the application of this design method to an eight-storey and a two-storey building, respectively. In Chapter 11 the work is summarised and recommendations are made for the design of CBFs. Features of the displacement-based seismic design method are presented and design displacement spectra are proposed. A seismic design strategy is proposed as a function of the seismic zone, that considers the importance of the structure, the limit states and governing criteria such as tolerable damage levels, initial and rehabilitation cost implications, and suggests appropriate methods for design and analysis. Recommendations are made for further experimental and analytical work.

2. EARTHQUAKE-RESISTANT DESIGN

2.1 Introduction

This chapter reviews the basic concepts of earthquake resistant design of steel structures. The characteristics of earthquake ground motion and the concept of an earthquake response spectrum and design spectrum is described. The earthquake-resistant design provisions of the NBCC (ACNBC 1995a) are discussed. The lateral load resisting systems (LLRS) in steel framed structures are described. The design philosophy for concentrically braced frames (CBFs) in the NBCC and CSA Standard S16.1-94 (CSA 1994) is discussed.

2.2 Characteristics of earthquake ground motion

Earthquake ground motion is recorded as a time history of ground acceleration, called accelerograms. Accelerograms are corrected for instrument error and baseline adjustment, and are integrated to give the velocity and displacement time history. The characteristics of ground motion that directly influence structural response are:

(a) the peak ground motion. This refers to the peak ground acceleration, PGA, peak ground velocity, PGV, and peak ground displacement, PGD,

(b) duration of strong motion, and

(c) frequency content.

These characteristics depend on factors such as earthquake magnitude, source mechanism, distance from source to site, geology of the travel path, and soil conditions at the site (Naeim 1989). The peak ground motion influences the amplitude of vibration of the structure. The duration affects the damage to a structure. The frequency content and spectral shapes relate to the period of vibration of the structure. The ground motion is amplified most when the frequency content of the ground motion and the vibration frequencies of the structure are close together.

The PGA, commonly used to indicate severity of ground motions, is not the best measure due to lack of correlation with observed damage in past earthquakes (Campbell 1985). Recent studies suggest that the ratio of PGA to PGV, called a/v ratio, is a good measure of ground motion as it correlates well with magnitude-distance

relationships used in seismology, is indicative of the frequency content and duration of ground motion, and significantly influences the ductility demand of inelastic systems (Zhu *et al.* 1988, Tso *et al.* 1992).

2.3 Earthquake response spectrum

A response spectrum is a plot of the maximum response of a single degree of freedom (SDOF) system with different frequencies and damping ratios to a specific ground motion. It is the most useful tool for the design of earthquake-resistant structures.

The equation of motion of a SDOF system subjected to ground motion is:

$$[2.1] \qquad M\ddot{U} + C\dot{U} + KU = -M\ddot{U}_g(t)$$

where M, C, K, and $\ddot{U}_g(t)$ are the mass, damping, stiffness, and ground acceleration, respectively, and U, $\dot{U}$, and $\ddot{U}$ are the displacement, velocity, and acceleration of the system relative to the ground. The mass is related to the stiffness and damping by

$$[2.2] \qquad K = \omega^2 M$$

$$[2.3] \qquad C = 2\xi\omega M$$

where ω is the circular frequency and ξ is the damping ratio. Using [2.2] and [2.3], [2.1] is written as

$$[2.4] \qquad \ddot{U} + 2\xi\omega\dot{U} + \omega^2 U = -\ddot{U}_g(t)$$

Equation [2.4] may be solved numerically to obtain the maximum relative displacement of the system during the ground motion, S_d, which is also called the spectral displacement. A plot of S_d versus the fundamental period, T (equal to $2\pi/\omega$), is called the displacement response spectrum (DRS). The maximum force in the system is equal to $K S_d$. Equating this to an equivalent static force $M S_a$, where S_a is the spectral acceleration or pseudo-acceleration, gives

$$[2.5] \qquad S_a = \omega^2 S_d$$

The plot of S_a versus T for a given damping ratio is called a pseudo-acceleration response spectrum and is related to the maximum base shear in the system. Let S_v be a pseudo-velocity or spectral velocity such that the kinetic energy associated with it

$(1/2\ M\ S_v^2)$ is equal to the maximum strain energy stored in the system $(1/2\ K\ S_d^2)$. Equating the two energy terms gives

[2.6] $$S_v = \omega\ S_d$$

The plot of S_v versus T for a given damping ratio is called a pseudo-velocity response spectrum. It is related to the maximum strain energy stored in the system during the ground motion. The relations between the spectral quantities may be summarised as

[2.7] $$S_a = \omega\ S_v = \omega^2\ S_d$$

With this relationship, all three spectra can be plotted on a tripartite logarithmic plot. Figure 2.1 shows such a plot for the N04W component of the Western Washington earthquake of April 1949 recorded at the Olympia Highway Laboratory. At zero period, the spectral acceleration is equal to the PGA. At very long periods, the spectral displacement is equal to the PGD. Chopra (1995) states that a response spectrum may be considered to consist of three regions; an acceleration sensitive region typically from 0 s to 0.5 s, a velocity sensitive region from 0.5 s to 3.0 s, and a displacement sensitive region thereafter.

2.4 Design spectrum

A response spectrum is unique to a given accelerogram and is therefore influenced by all the factors that affect ground motion. For design purposes, the effect of several earthquake events of various magnitudes, occurring at different distances from the site may have to be considered. Hence, the response spectra from a number of accelerograms are often averaged and smoothed to obtain a design spectrum that specifies the relative strength of structures of different periods. Figure 2.1 shows the design spectrum specified in Appendix J of NBCC (ACNBC 1995b) for the three cases that arise depending on the relative value of the acceleration-related seismic zone, Z_a, to the velocity-related seismic zone, Z_v.

Inelastic design spectra are obtained by reducing elastic design spectra to account for inelastic behaviour (Newmark and Hall 1982) and are specified in building codes when inelastic response is permitted in the design earthquake.

2.5 NBCC provisions for seismic design

The NBCC (ACNBC 1995a) uses the spectral acceleration-based approach to specify the minimum lateral seismic force (base shear) for buildings as

[2.8] $$V = \left(\frac{V_e}{R}\right)U$$

where R is a force modification factor, U is a calibration factor (equal to 0.6), and V_e is the elastic base shear given by

[2.9] $$V_e = (v\,S\,I\,F)\,W$$

W is the dead load plus 25% of the design snow load for most buildings. The factors v, S, I, and F are defined as follows:

(a) v is the zonal velocity ratio that varies from 0 for the least seismic zone to 0.4 for the highest seismic zone and corresponds to a PGV with a probability of exceedance of 10% in 50 years,

(b) S is the seismic response factor that varies with the period of vibration as shown in Fig. 2.2. For periods less than 0.5 s, S depends on both Z_a and Z_v, where Z_a is the acceleration-related seismic zone and Z_v is the velocity-related seismic zone. The S factor curve is an elastic design spectrum obtained by averaging several 5% damped acceleration response spectra of accelerograms scaled to a PGV of 1 m/s (Tso *et al.* 1992),

(c) I is the importance factor and is specified as 1.5 for post-disaster buildings, 1.3 for schools, and 1.0 for all other buildings, and

(d) F is the foundation factor that depends on the soil category at the site. It varies from 1.0 for rock to 2.0 for deep deposits of soft soil.

The force modification factor, R, depends on the type of LLRS used and varies from 1.0 for systems with limited ductility to 4.0 for ductile systems. The elastic design spectrum at any location is given by the product, v S. This spectrum is reduced by the force modification factor, R, to give the inelastic design spectrum. The period of vibration, T, has to be specified to obtain the S factor from Fig. 2.2. As the period is not known a-priori, the period for CBFs is specified in the NBCC as:

[2.10] $$T = \frac{0.09\, h_n}{\sqrt{D_s}}$$

where h_n is the height and D_s is the width of the CBF in metres. Alternatively, Rayleigh's method or any other analytical method may be used to estimate the period. The base shear specified by [2.8] may be reduced up to 20% if the analytically computed period is greater than that by [2.10]. The lateral seismic force is distributed over the building height as lateral forces, F_x, that act at each level, of magnitude

[2.11] $$F_x = (V - F_t)\, \frac{W_x\, h_x}{\sum_{i=1}^{n} W_i\, h_i}$$

where W_x is the weight at level 'x', h_x is the height to level 'x', and F_t is a force applied at the roof level that is taken as zero for period, T, less than 0.7 s and as 0.07 T V for T greater than 0.7 s, subject to a maximum of 0.25 V. This force increment at the roof level is introduced to account for the effect of higher modes of vibration.

For floors and roofs acting as diaphragms, the lateral force for design is

[2.12] $$V_p = v\, I\, S_p\, W_p$$

where v and I are as defined before, S_p is 0.7, and W_p is the tributary weight of the diaphragm. However, the force F_x from [2.11] is used if it is greater than V_p.

A minimum design torsional moment, T_x, about the vertical axis of the building, given by

[2.13] $$T_x = F_x\, (1.5\, e_x \pm 0.1\, D_{nx}),\ \text{and}$$

[2.14] $$T_x = F_x\, (0.5\, e_x \pm 0.1\, D_{nx})$$

is considered, where e_x is the structural eccentricity and D_{nx} is the dimension of the building perpendicular to the direction of seismic load. The product $0.1\, F_x\, D_{nx}$ is the minimum accidental torsion that must be considered even when the structural eccentricity is zero.

The anticipated deflection, δ_i, of the structure in an earthquake is assumed equal to the product of the deflection, δ_e, obtained from a linear elastic analysis under the forces, F_x (from 2.11), and the force modification factor, R. Thus,

[2.15] $\delta_i = R\,\delta_e$

The allowable interstorey drift is specified as 1% of the storey height for post-disaster buildings and 2% for all other buildings.

2.6 Lateral load resisting systems in steel framed structures

All buildings must have a structural system to resist lateral loads due to earthquakes. Concentrically braced frames (CBFs), moment resisting frames (MRFs), and eccentrically braced frames (EBFs) are the common vertical LLRS in steel framed buildings. Alternatively, steel plate shear walls, base isolation techniques, and energy absorbing elements in braced frames are also used.

CBFs are used extensively in low-rise buildings. They are appropriate in situations with low to moderate ductility demand. CBFs have simple beam to column connections. Lateral stiffness and strength are provided by diagonal braces that are attached concentrically to the beam to column connection by means of gusset plates. Energy dissipation is provided by the ability of the braces to yield in tension. The braces may also be designed to buckle inelastically in compression. CBFs are economical due to the relative ease in design, detailing, and construction, and are efficient because the members are primarily subjected to axial loads. CBFs are stiff systems and provide good control of lateral drift and thus damage to non-structural components is minimised. Damaged brace members can also be replaced with relative ease. This system is not preferred in high seismic zones due to its low redundancy. The absence of alternative load paths may lead to severe consequences should components fail. The compressive resistance of diagonal braces tends to degrade under cyclic loading and thus the frame may deteriorate substantially in strength and stiffness. Frames that rely only on the tension diagonal to resist lateral force may have components subject to impact loads due to slackness that can develop in the diagonals.

MRFs have beam to column connections that are capable of transferring moment. They are more ductile than CBFs. Energy dissipation takes place by flexural yielding in plastic hinges that are formed at the ends of the members. This system causes no obstruction between the columns and thereby gives maximum freedom in interior planning and fenestration. It is also highly redundant. Hence, it is preferred in high

seismic zones. It is a rather flexible system and may not provide adequate drift control. Consequently, non-structural components may be damaged in moderate events. Furthermore, the frame design is often governed by stiffness considerations rather than by the strength of the individual members. This has lead to the evolution of dual systems comprising both CBFs and MRFs. The former provides drift control in moderate but frequent events and the latter provides the ductility required to survive an extreme event.

EBFs combine the advantages of CBFs and MRFs. They have beam to column connections that are capable of moment transfer. In addition, braces are provided that have at least one eccentric connection. The force in the brace is transferred through a 'link' element to the beam to column connection. EBFs are detailed to dissipate energy by shear yielding or flexural yielding in the link elements only. The braces are designed to remain elastic (and not to buckle).

The earthquake force on roof and floor diaphragms is an in-plane horizontal load that is resisted by diaphragm action wherein the diaphragm web (roof or floor deck) resists the shear force while the flange members (diaphragm chords) resist the bending moment. Horizontal bracing may also be provided in the plane of the diaphragm to increase its shear capacity.

Of the three vertical LLRS described above, this study deals with CBFs only as it is the most common system used in low-rise steel buildings.

2.7 Design philosophy for CBFs

CBFs are vertical cantilever trusses. Some common configurations are shown in Fig. 2.3. Earthquake excitation results in lateral inertia forces at each floor level. The resulting storey shear is resisted by the diagonal bracing. The overturning moment is resisted by tensile and compressive axial forces in the columns of the braced bay. The diagonal bracing may be designed as tension members only or as tension-compression members. The former relies on the tension diagonal only to resist the storey shear while the latter relies on both.

The NBCC classifies CBFs into the three categories of: ductile braced frame (DBF), nominally ductile braced frame (NDBF), and ordinary (strength) braced frame (SBF) having force modification factors, R, of 3.0, 2.0, and 1.5, respectively. CSA

Standard S16.1-94 (CSA 1994) specifies detailing that endeavours to provide ductility that is consistent with the R factor assumed in design. Each category has to meet the strength requirement of the Standard, i.e., each must resist the lateral load specified by the NBCC. In addition, DBFs and NDBFs have to satisfy special detailing provisions outlined in clause 27 of the Standard that is often referred to as the 'ductility design' process (Redwood and Channagiri 1991).

The diagonal bracing in a DBF is detailed to absorb significant energy by yielding in tension and inelastic buckling in compression. Brace configurations such as chevron (V-bracing) and K-bracing are not permitted in view of the problems anticipated in their response (Redwood and Jain 1992). A tension-only bracing system is also not permitted due to its limited energy absorbing capacity and lack of redundancy. Severe limits are imposed on the slenderness ratio of the braces and the width-thickness ratio of the brace cross-section to ensure good ductility. The brace connections, beams, and columns are designed for loads induced by yielding of the braces.

A NDBF is detailed to absorb a limited amount of energy. Some restrictions are imposed on the selection of diagonal braces. A tension-only bracing system may be adopted provided that the beams, columns, and brace connections are designed for the possible overload due to impact.

SBFs are anticipated to respond elastically in an earthquake and no provisions are outlined to ensure ductile behaviour. They are assigned an R factor of 1.5 in view of the inherent ductility of structural steel. Often, they are designed so that the lateral load is resisted entirely by braces in tension. Such CBFs are also referred to as tension-only concentrically braced frames. The brace diagonals are slender and buckle elastically under low compressive load. The NBCC does not permit the use of such frames in buildings more than three storeys high in acceleration or velocity related seismic zones of 2 and higher.

Low-rise buildings use SBFs extensively. The only limitation placed on the braces is that their effective slenderness ratio should not exceed 300 for use as tension members, and should not exceed 200 if they are to resist significant compressive loads.

2.8 Some concerns in design practice

Some questions that arise in applying the NBCC 1995 provisions to the seismic design of steel buildings with CBFs are:

(a) Do current design procedures result in CBFs that are of consistent performance in all seismic zones, or are more stringent design requirements needed in the higher zones ?

(b) Is the empirical expression for estimating the period of braced frames valid for CBFs with and without flexible diaphragms ? Should the design period be a function of the seismic zone ?

(c) Are current procedures adequate for the design of metal diaphragms and their connections ?

(d) Is the consideration of non-structural components with respect to their contributions to stiffness and strength, and their susceptibility to damage, adequate ?

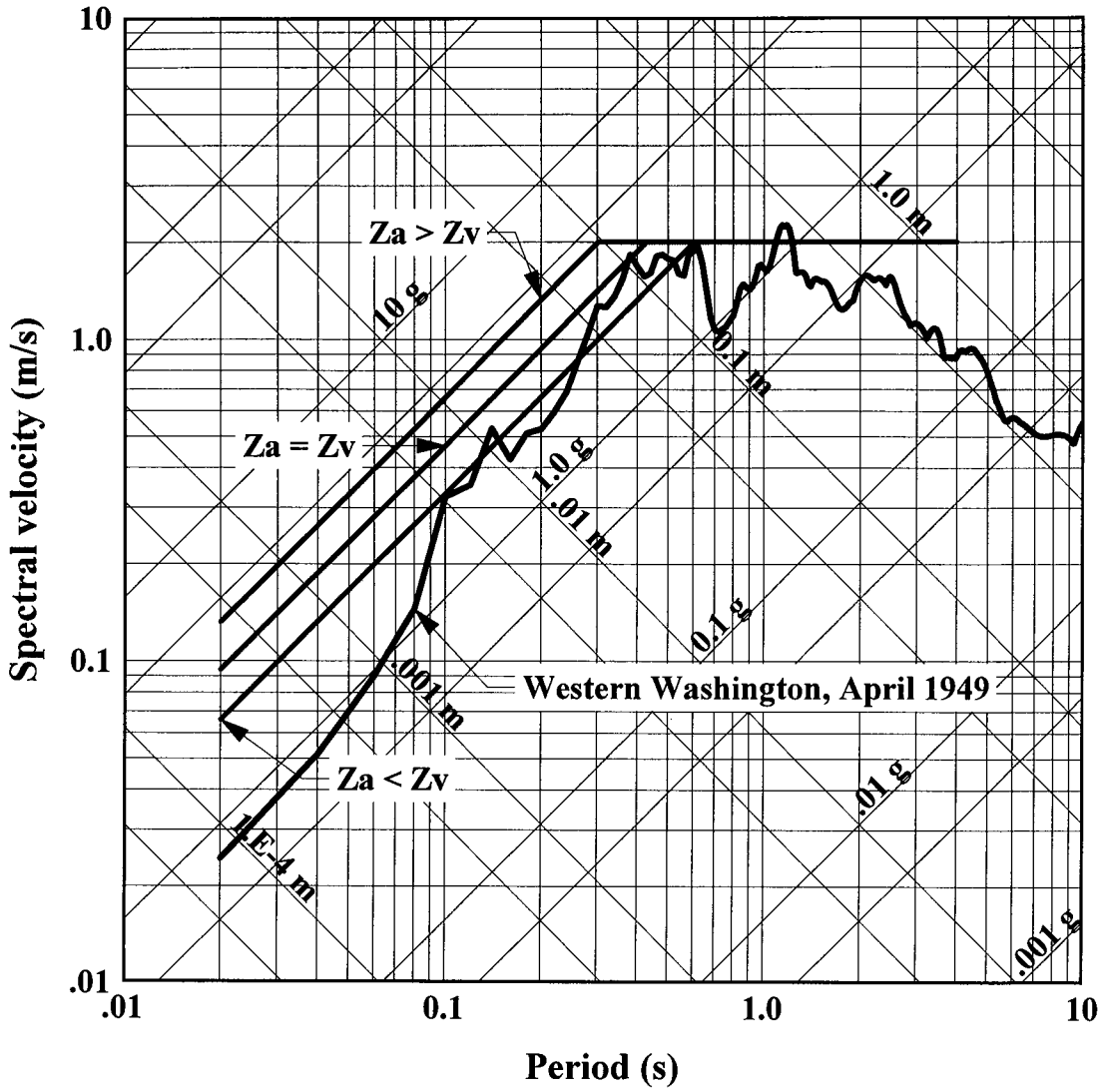

Figure 2.1 Earthquake response spectrum and the NBCC design spectrum

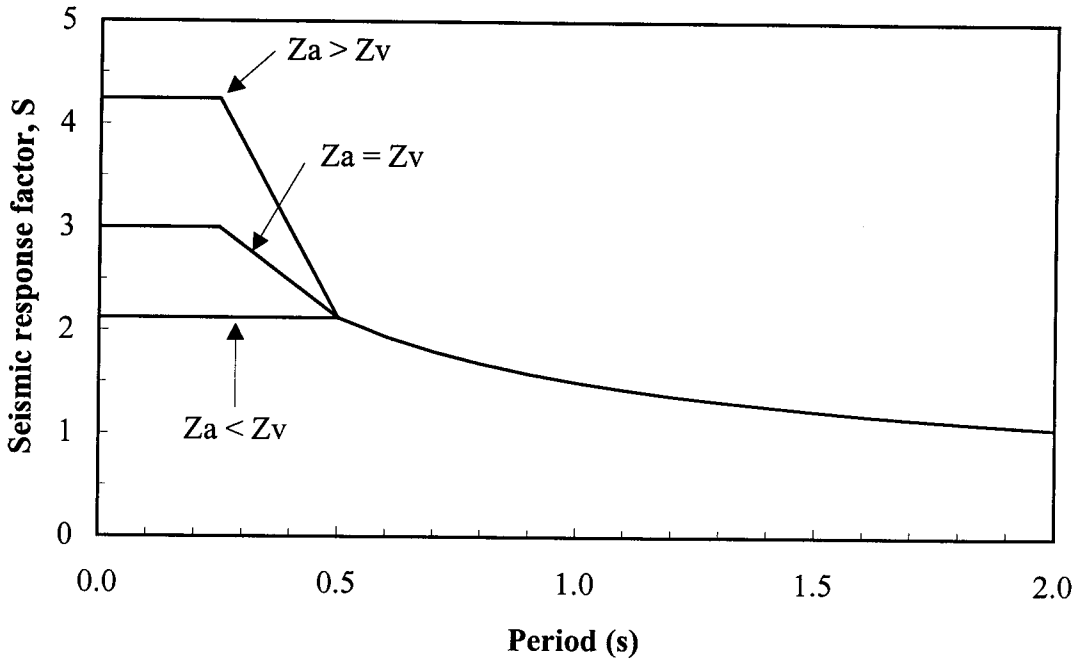

Figure 2.2 Seismic response factor S for NBCC (1995)

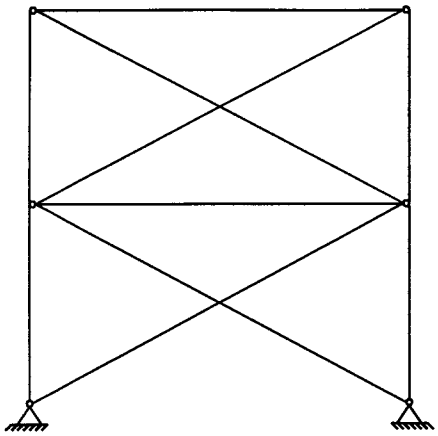

X-bracing

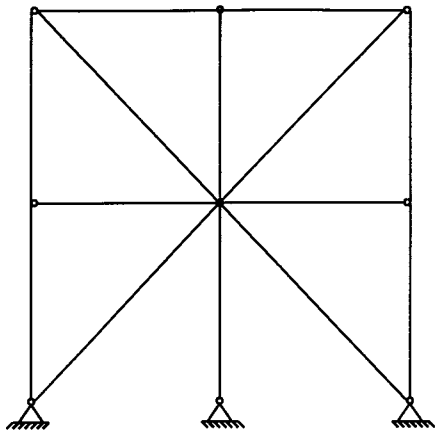

Split-X bracing

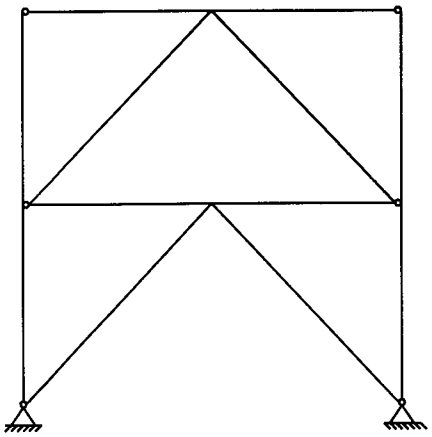

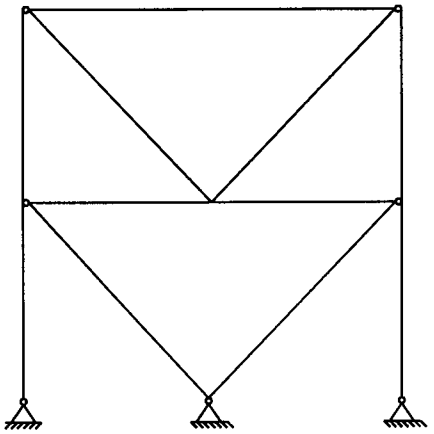

Chevron bracing

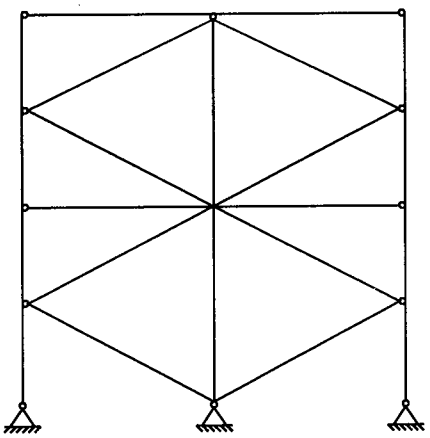

K-bracing

Figure 2.3 Typical CBF configurations

3. LITERATURE REVIEW

3.1 Introduction

Analytical modelling of buildings for earthquake response analysis requires definition of the cyclic force-deformation behaviour of the structural and non-structural elements in the lateral load path. Previous studies on the experimental behaviour and analytical modelling of concentrically braced frames (CBFs), steel shear diaphragms, non-structural components, and low-rise steel buildings are reviewed.

3.2 Concentrically braced frames

In the following, the performance of CBFs in past earthquakes, experiments on brace members and connections, and analytical modelling of the cyclic behaviour of braces are reviewed. The factors affecting the inelastic seismic response of CBFs are identified.

3.2.1 Performance in past earthquakes

The American Iron and Steel Institute (AISI 1991) has documented the performance of engineered steel buildings in 11 major earthquakes that have occurred over the past three decades. The seismic performance of CBFs has been variable. Most of the damaged frames were in minor structures that had rod or angle braces as the tension bracing. Typical damage patterns observed were buckling of braces, fracture of brace members at welded splices, fracture at the net section in bolted connections, and fracture in gusset plates. In most of the buildings investigated, the gravity load carrying system was relatively undamaged. Consequently, collapse of an entire building due to failure in the CBF was rare. The damage to CBFs is considered to be largely a result of poor detailing, inadequate design of connections, and a rather low lateral design force for the frame (Walpole 1985).

Tremblay *et al.* (1995) investigated the damage to steel buildings with CBFs in the Northridge earthquake of 1994. Although no collapse of steel buildings occurred, there were numerous occurrences of in-plane and out-of-plane brace overall buckling, tension yielding and fracture of braces, buckling and bending in gusset plates, uplifting of

columns of the CBF, and significant damage to non-structural elements. Several large braces composed of hollow structural sections developed brittle cracks due to excessive strains because of local buckling.

Tremblay *et al.* (1996) carried out similar investigations in the Hyogo-ken Nanbu (Kobe) earthquake of 1995. Most buildings surveyed had tension-only X-bracing or chevron bracing with rods, angles, flat bars, round tubes, wide flange sections, square tubes, and channels used as braces. Damage in the smaller braces consisting of rods, angles, and flat bars was more severe than in the larger braces. Brittle fracture at bolt holes and welded connections was typical. The slender tension-only bracing experienced inelastic stretching and developed significant slackness. However, some tension-only CBFs with well-designed brace connections performed well. The slender braces buckled almost elastically and were less susceptible to low cycle fatigue. In addition, the gussets were subjected to lower loads due to the limited compressive capacity of the slender bracing. Tension-compression braces showed signs of low-cycle fatigue fracture at plastic hinge locations, fracture of bolted brace to gusset connections, and failure of the welded connections between the gusset and the frame. The out-of-plane buckling of the braces also caused failure in adjacent wall partitions. Local buckling and brittle fracture in the columns of the CBF were also observed. Several severely damaged buildings survived collapse due to redundancy in the lateral load resisting system (LLRS). This investigation reiterated the need for well designed connections in CBFs and redundancy in the LLRS.

3.2.2 Tests on brace members and connections

In the following, results of cyclic tests on brace members typically used in CBFs are reviewed. These tests serve a two fold purpose: they help in formulating provisions for detailing of brace members and connections; they also provide experimental data that is useful for the mathematical modelling of brace behaviour under cyclic loading.

3.2.2.1 Kahn and Hanson (1976)

In one of the earliest experimental investigation on the hysteresis behaviour of steel members, Kahn and Hanson (1976) tested 16 small hot-rolled steel bars with a

rectangular cross section of 25.4 x 12.7 mm. The bars were welded to steel plates at either end. The effective slenderness ratio, KL/r, ranged from 85 to 210. All bars were preloaded to yield in tension and then subjected to cyclic axial load. Each cycle consisted of loading to a prescribed displacement into the post-buckling region followed by tension loading to the elastic limit and then return to zero load.

The first cycle buckling load was found to be somewhat less than that predicted by the Column Research Council formula (Johnson 1966). The maximum compressive load reduced progressively with increasing number of cycles. The greatest reduction was observed between the first and the second cycles. With increasing number of cycles, the maximum compressive load became almost constant for a given KL/r ratio. All specimens exhibited a net elongation after a complete cycle of deformation. Short columns were found to dissipate greater energy for the same relative deformation than long columns. The dynamic hysteresis behaviour was almost the same as the static hysteresis behaviour for all KL/r ratios. A similar observation had been made by Hanson (1966) in tests on steel structures.

3.2.2.2 Jain *et al.* (1978)

Jain *et al.* (1978, 1980) investigated the hysteresis behaviour of small tube and angle specimens. They tested 17 cold-rolled steel tube specimens with a nominal cross section of 25 x 25 mm and a wall thickness of 2.67 mm. Hot rolled gusset plates of various sizes were welded to the members to form the end connections. The gussets had greater axial strength than the tubes. The flexural strength of the gussets was varied so that some had less flexural strength than the tube (weak gussets) while others had greater flexural strength (strong gussets). The KL/r ratio of the tubes ranged from 30 to 140. The specimens were annealed before testing. The angle sections were hot-rolled single angles of size ranging from 25 x 25 x 6 mm to 40 x 40 x 3 mm. These specimens were welded to steel end plates. The KL/r ratio of the angles ranged from 85 to 120. All tube and angle specimens were pretensioned to yield and then subjected to cyclic axial load.

The KL/r ratio was found to be the single most important parameter that influenced the hysteresis behaviour. The flexural stiffness of the connection affected the effective length factor, K. Hence, its effect was similar to that of a change in the KL/r

ratio. For a given KL/r ratio, the connection flexural strength (i.e., presence of a weak or a strong gusset) did not have any significant effect on the hysteresis loops. It influenced the mode of buckling and failure of the tube specimens only. Tube specimens with weak gussets buckled in a plane perpendicular to the gusset and did not develop any cracks at the welds. Those with strong gussets buckled in a bi-axial mode and developed cracks only if the KL/r ratio was less than 80. All angle specimens buckled about the minor principal axis and no cracks were observed. This lead the investigators to conclude that weak gussets should be used to avoid bi-axial buckling. Local buckling did not influence the hysteresis behaviour of the tube specimens; some effect was noticed in the angle specimens. A comparison of the hysteresis loops of tube, angle, and bar specimens indicated that the hysteresis behaviour was influenced by the shape of the cross section. Reasons cited for the difference were heat treatment, strain hardening, residual stresses, the Bauschinger effect, and local buckling.

The first cycle buckling load for tube specimens was slightly greater than that predicted by the AISI Specifications. For angle specimens, the load predicted was in good agreement with measured capacity. Residual elongation or 'growth' of the member was found to be directly proportional to the maximum displacement in compression and inversely proportional to the KL/r ratio. The reduced compressive capacity due to cyclic buckling ranged between 0.3 to 0.6 times the compressive resistance of the original column and was expressed as an empirical function of the KL/r ratio, as shown in Fig. 3.1.

3.2.2.3 Popov and Black (1981)

Popov and Black (1981) carried out cyclic tests on 24 struts of rolled steel shapes. These included wide flange, structural T, thick and thin walled circular pipe and tube sections, and built-up double angle and double channel sections. The struts had either a pinned-pinned or a pinned-fixed end condition and a KL/r ratio of 40, 80, or 120.

The KL/r ratio was found to control the hysteresis behaviour. Members with a KL/r ratio of 80 and 120 exhibited pinched hysteresis loops. The end condition of the specimen had a minor effect on the hysteresis loop for the same KL/r ratio. The cross sectional shape had little influence on the hysteresis behaviour. The shapes were ranked

in order of decreasing performance as follows; tube, wide flange, structural T, double channels, and finally double angles. The difference in performance was attributed to the susceptibility of the members towards lateral-torsional buckling, local buckling, and in the built-up members, web buckling between stitch fasteners. The pattern of loading was found to influence the first cycle buckling load of the member. Those members that were initially loaded to yield in tension could only attain a compressive capacity which was 0.75 times that of the original specimen. The reduced compressive resistance in subsequent cycles of loading could be predicted approximately by applying load reduction factors to the compressive resistance of the original specimen. These reduction factors accounted for the Bauschinger effect and for the residual curvature developed in the plastic hinges.

3.2.2.4 Astaneh-Asl *et al.* (1985)

Astaneh-Asl *et al.* (1985a, 1985b, 1986) carried out cyclic tests on 17 full size, double angle specimens. The angles were stitched together and were connected to end gusset plates with bolts or fillet welds. Some specimens were designed to buckle in-plane and others out-of-plane. The direction of buckling had a significant influence on the cyclic behaviour and the failure mode. The in-plane buckling specimens behaved as fixed-ended columns. One plastic hinge formed at mid-span while the other two formed within the member at the connection to the gusset. The out-of-plane buckling specimens behaved as pin-ended columns. One plastic hinge formed at mid-span while the other two formed within the gusset plate. The provisions for stitch fasteners in accordance with the AISC Specification (1978) were found to be inadequate for double angles. The investigators recommended; (a) an adequate free length of gusset plate be provided to allow for the formation of the plastic hinge and to improve the ductility of the gusset, (b) connections be designed for the yield strength of the brace members, and (c) stitch welds be designed for an eccentric force equal to half the yield capacity of a single angle.

3.2.2.5 El-Tayem and Goel (1986)

El-Tayem and Goel (1986) conducted cyclic tests on five full-scale single angle and one double angle X-braced specimens. The members had end gusset plates and fillet

welds were used for all connections. At small deformation levels, the complete compression diagonal showed symmetrical lateral deformation in the out-of-plane direction. At large deformation levels, only one half of the compression diagonal buckled about the weak axis where the tension diagonal provided some restraint to the compression diagonal. The investigators concluded that the design of X-braced systems should be based on consideration of the effective length of one half the diagonal only. An effective length of 0.85 times the half diagonal length was suggested for X-braced systems made from single equal leg angles.

3.2.2.6 Walpole (1995)

Walpole (1995) carried out cyclic tests on three cold-formed 150 x 100 x 6 mm hollow sections with a specified yield stress of 350 MPa. The overall slenderness ratios were 40, 60, and 80 with a fixed-fixed end condition for the first and pinned-pinned end condition for the other two.

Local buckling occurred relatively quickly. The magnitude of the local buckles increased under cyclic loading and eventually lead to fracture. The specimen with slenderness ratio of 80 formed a local buckle in the plastic hinge at mid-span when it was compressed to four times the yield elongation. The member was then stretched to 5 times the yield elongation, that is, a ductility ratio of 5. After a cycle at a ductility ratio of 10, cracks occurred in the corners of the section and fracture followed. The specimen with slenderness ratio of 60 formed a local buckle that grew in size with number of cycles. Fracture occurred in the member after a cycle at a ductility ratio of 10. The specimen with slenderness ratio of 40 formed a local buckle at a ductility ratio of 3. After a cycle at a ductility ratio of 5, a major crack formed under tensile loading. Local buckling was more significant with the less slender specimen. Walpole recommended more stringent width-thickness ratio for cold-formed sections in high seismic zones.

3.2.2.7 Rabinovitch and Cheng (1993)

Rabinovitch and Cheng (1993) investigated the cyclic behaviour of steel gusset plates. A 'strong brace-weak gusset' design was employed wherein the gusset was designed to dissipate energy by buckling in compression and yielding in tension and the

brace was designed to remain elastic. The cyclic loading did not affect the tensile capacity of the gusset but caused a reduction in its compressive resistance. The provision of extra length for the free formation of a plastic hinge in the gusset, as recommended by Astaneh-Asl *et al.* (1986), was found to be questionable as it resulted in reduced stiffness and compressive resistance of the gusset. Gusset plates with stiffeners were found to exhibit a more stable post buckling behaviour than unstiffened ones.

3.2.3 Analytical modelling of brace behaviour

The behaviour of braces under cyclic loading has been modelled in several ways. Some of the early models shown schematically in Fig. 3.2 include (a) elastic behaviour only, (b) tension-yield and compression-buckling, and (c) tension-yield and compression-yield. The elastic model is appropriate in situations where no yielding in tension and buckling or yielding in compression is anticipated. The tension-yield and compression-buckling model is appropriate for slender braces with low compressive resistance. The tension-yield and compression-yield model is appropriate for short braces that do not buckle in compression. None of these models is considered appropriate for braces of intermediate length (that are most prevalent) that buckle inelastically in compression. These models either under-estimate or over-estimate the energy dissipated in the compression region of the hysteresis loop. Hence, significant research has been directed towards analytical modelling of intermediate length braces (Nakashima and Wakabayashi 1992).

The complexity of modelling the axial hysteresis behaviour of intermediate length braces is best described with an idealized hysteresis loop for a pin-ended member as shown in Fig. 3.3. A typical hysteresis loop is composed of several characteristic zones. Zone OA represents the elastic compression of a virgin column up to its critical buckling load at point A. Zone AB is characterised by a constant axial load accompanied by column shortening due to lateral displacement, Δ. The P-Δ moment results in a plastic hinge at mid-span and a mechanism is formed. Zone BC describes the compression induced plastic rotation of this mechanism. Zones CD and DE represent elastic unloading and tension reloading of the brace, respectively. The stiffness in these zones is significantly less than that in zone OA due to residual curvature of the brace. With an

increase in axial load along path EF, the strut elongates and gradually straightens. This is accompanied by an increase in stiffness. The P-Δ moment now causes the plastic hinge to rotate in the opposite sense until all plastic rotation is recovered. The brace becomes straight at point F. Zone FG represents uniaxial yielding of the member. This zone may have some stiffness due to strain hardening.

Ikeda and Mahin (1986) have reviewed brace models and classified them into three general categories; finite element, physical theory, and phenomenological models.

In finite element models, the brace is discretised into a number of elements with elastic or elastic-plastic constitutive laws. These models can provide realistic representation of brace behaviour. However, they are computationally expensive for practical analyses of large structures. Their use has therefore been restricted to analysis of individual brace members and end connections.

Physical theory brace models are formulated with simplified theoretical assumptions that are based on physical considerations. The input parameters for these models are based on material, geometric, and engineering properties of the brace (e.g., the cross sectional area, moment of inertia, effective length, and plastic section modulus). The geometric representation of a brace is considerably simpler than that in a finite element model. The brace member is typically modelled with two elastic beam segments connected to a plastic hinge at mid-span. Analytical expressions for the axial force versus axial deformation behaviour of the brace are derived on the basis of the classical beam-column equation and a plastic flow rule for the plastic hinge. This approach has been used by Higginbotham and Hanson (1976), Nonaka (1977), Prathuangsit *et al.* (1978), Ikeda and Mahin (1986), and a few others. However, these models were also considered unsuitable for dynamic analysis due to the highly nonlinear analytical solutions that require iterative solution schemes. Furthermore, they cannot account for a reduction in compressive resistance due to cyclic buckling and the residual elongation that is observed in experiments. These factors can only be accounted for by introducing some empiricism into the models.

Phenomenological models (Jain *et al.* 1980, Maison and Popov 1980, Andreaus and Gaudenzi 1989) mimic the observed hysteresis loops of a brace with piecewise linear approximations. This is the most common approach adopted for dynamic structural

analysis. These models are based on linearization of the physical theory models to avoid an iterative solution and give the most realistic result when calibrated against experiment. They account for effects such as the reduction in compressive resistance and residual elongation by using empirical equations that are derived from regression analyses of experimental data.

3.2.4 Factors affecting the inelastic seismic response of CBFs

The inelastic seismic response of a CBF depends on the following factors:

(a) Behaviour of the braces in compression. Most braces are of intermediate length and buckle inelastically. The maximum compressive load occurs only briefly, and within a narrow range of compressive strains. The compressive load capacity reduces significantly as the brace buckles and affects the behaviour of the CBF. Brace buckling is accompanied by a redistribution of forces from the compression braces to the tension braces which affects the distribution of forces in all elements of the braced bay. The effective slenderness ratio of the brace, KL/r, is the single most important parameter that influences its compressive behaviour and the shape of the hysteresis loop. Braces with a KL/r ratio exceeding 80 have pinched hysteresis loops. A greater KL/r ratio also results in a lower compressive resistance that makes the hysteresis loop more asymmetric. The post-buckling capacity of a brace diminishes with repeated cycles of loading. This reduction due to cyclic buckling depends on: (i) KL/r ratio of the brace, (ii) residual curvature from buckling in previous cycles, (iii) extent of tensile yielding, and (iv) number of alternating tension-compression cycles,

(b) Configuration of the bracing. Chevron (V-bracing) and K-bracing have an inherent disadvantage over X-bracing due to the brace configuration. The compression and tension brace have unequal capacities so that once the compression brace buckles, there is an unbalanced load that has to be resisted by beams in the V-bracing or columns in the K-bracing,

(c) The number of storeys in the CBF. Once the braces in a particular storey yield, there is a tendency to form a 'soft storey' sway mechanism where yielding is localized in that storey only,

(d) Design and detailing of connections between the braces and the surrounding beams and columns of the braced bay. The connections should have adequate strength and toughness so as not to fail under loads induced by brace yielding or buckling, and

(e) Characteristics of the earthquake ground motion.

3.3 Steel shear diaphragms

Light gage steel shear diaphragms are used extensively as roof and floor diaphragms in steel buildings. They transfer dead and live load to the gravity load resisting system and provide lateral stability to the structure by transferring in-plane lateral loads to the vertical LLRS.

The basic unit of a diaphragm is an individual panel. Each panel is composed of a number of elements, namely, the corrugated steel sheeting, primary supporting members (rafters), secondary supporting members (purlins), shear connectors, sheet to purlin fasteners, and seam fasteners, as illustrated in Fig. 3.4. For design purpose, the diaphragm is considered analogous to a deep plate girder that is supported by the vertical LLRS. The panels make up the web and carry the shear force and the flange members (also called diaphragm chords) resist the bending moment. Roof diaphragms are flexible as compared to concrete topped floor diaphragms that are relatively rigid.

3.3.1 Assessment of stiffness and strength

The stiffness and strength of a diaphragm must be assessed for its design. The stiffness of a diaphragm is affected by profile distortion of the corrugated sheeting, shear deformation of individual panels, stiffness of the various fasteners, and axial stiffness of the flange members. The shear strength is a function of the seam strength, the strength of the shear connectors, the strength of the sheet to purlin connection, and the shear buckling strength of individual panels.

Davies (1976, 1977) suggests three approaches to estimate the stiffness and strength of a diaphragm: (a) experimental tests, (b) approximate methods, and (c) finite element analysis. Of the three, the approximate methods such as the Tri-Service method (NAVFAC 1982, CSSBI 1991), the SDI method (Luttrell 1981), and the European method (Davies and Bryan 1982) are widely used.

The Tri-Service method is based on test data from welded diaphragms. The stiffness and strength of a deck are tabulated as a function of its span, profile depth, sheet thickness, and the weld layout. The CSSBI manual (1991) adapts the Tri-Service method for limit states design in Canada. This method is applicable to welded decks only. It cannot account for non-standard weld patterns. Further, failure modes cannot be explicitly identified.

The European method (Davies and Bryan 1982) is the most comprehensive diaphragm design method developed to date. Detailed expressions to estimate the diaphragm stiffness and strength are given. These are based on an assumed internal force distribution within the panel. Extensive tests and finite element analyses of cantilever diaphragm panels have been made to justify them. It is applicable to welded or mechanically fastened decks and can account for non-standard fastener layout. It is ideal for seismic design of diaphragms as one can explicitly identify failure modes and ensure a ductile failure.

3.3.2 Behaviour under cyclic loading

Tests on diaphragm panels typically employ a monotonic loading. Information on their hysteresis behaviour is scarce. Most failure modes of a diaphragm will involve shear failure of the fasteners. Experiments on fasteners indicate that they have adequate fatigue life (Davies and Bryan 1982). Mazzolani (1994) has reported cyclic tests of various fasteners used in diaphragm design. Spot welds were found to have the best hysteresis behaviour followed by screws and finally rivets.

Strnad and Pirner (1978) carried out dynamic shear tests on full scale sheeting panels with loading that simulated the gust effect of wind. The hysteresis loops observed were repeatable and became pinched with increasing level of deformation. The dynamic loading did not affect the strength or the fatigue life of the panels.

3.4 Non-structural elements

A building has many non-structural elements such as the exterior cladding and interior partitions. The exterior cladding is typically made up of glass, metal, masonry, and precast concrete. Interior partitions typically consist of metal or wood stud frames

with gypsum wallboard or plywood facing. Traditionally, the stiffness and strength contributions of these elements are ignored in seismic design. They are assumed to be either isolated from the structural frame so that no interaction occurs, or brittle enough to fail at low drift during an earthquake.

There is evidence of the interaction between structural frame and non-structural elements. Palsson *et al.* (1984) performed vibration tests and analytical studies on a 25 storey steel building with precast concrete cladding panels. The cladding was found to contribute significant lateral stiffness that affected the dynamic response of the building. The difference between the measured and computed deflection in clad steel frames suggests that the cladding contributes to the stiffness (Strnad and Pirner 1978, Sockalingam *et al.* 1994). Several low-rise steel building systems used in Britain, as cited by Davies and Bryan (1982), rely substantially on structural cladding for lateral stiffness and stability. Steel cladding has also been used to reduce drift due to wind in high-rise buildings (Tomasetti *et al.* 1984). Cohen and Powell (1993) have suggested the use of steel cladding panels with energy-dissipating connections for seismic design.

3.4.1 Tests on non-structural partitions

Experimental data on the stiffness and strength characteristics, and the damage threshold of common non-structural partitions is rather scarce. Previous experimental work is reviewed below.

3.4.1.1 Freeman (1977)

Freeman (1977) reports on racking tests carried out on 54 wall panels that were 8 feet high by 8 feet long of gypsum wallboard, plaster, plywood, and combinations of plywood and gypsum wallboard. The frames were of wood or metal stud construction. On cyclic loading, the first signs of distress were observed at a drift ratio of 0.0025. The ultimate load capacity was attained at a drift ratio of 0.008. Gypsum wallboard panels of 1 inch equivalent thickness had a tangent modulus of rigidity, G, varying from 40 MPa to 120 MPa, and a secant modulus of 30 MPa at a drift ratio of 0.003.

3.4.1.2 Rihal (1986)

Rihal (1986) performed cyclic racking tests to study the earthquake resistance and damage threshold of 10 feet high by 8 feet long wood-stud framed partitions with 1/2 inch gypsum panels on either side. Partitions that were well anchored to the floor by means of holdowns were capable of resisting cyclic load. Damage to the partitions initiated by crumbling of gypsum board around nail-heads at a drift ratio of 0.002. Severe damage to the partitions occurred at drift ratios from 0.007 to 0.010 and comprised failure of taped joints in the gypsum board and a further increase in crumbling of gypsum board around nail-heads.

3.4.1.3 Adham *et al.* (1990)

Adham *et al.* (1990) conducted racking tests on 6 gypsum wallboard panels that were 8 feet high by 8 feet long and were supported on a lightgage steel framing system with diagonal straps. The wallboards developed local cracks at corners at a drift ratio of 0.005. An increase in the area of diagonal straps increased the overall load carrying capacity of the panel at intermediate and high drift ratios. Under cyclic loading, the panel stiffness and strength degraded by 15% and 40%, respectively. The average value of equivalent viscous damping was about 12%.

3.4.1.4 Mazzolani *et al.* (1996)

Mazzolani *et al.* (1996) performed monotonic and cyclic tests on steel cladding panel assemblies. In the monotonic tests, the maximum load was attained at a drift ratio of about 0.016. In cyclic tests of panel assemblies that were fastened with bolts to the external frame and with self-tapping screws as seam fasteners, slip-type hysteresis loops were obtained with low energy dissipation. The fastener holes ovalized and consequently force transfer occurred only when the fasteners came into bearing against the sheet at the end of the holes.

3.5 Analytical studies on low-rise steel buildings with CBFs

Only a few analytical studies on low-rise steel buildings are reported in literature. However, recent earthquakes such as the Loma Prieta earthquake of 1989, the Northridge

earthquake of 1994, and the Kobe earthquake of 1995 have caused researchers to focus attention on such buildings.

Montgomery and Hall (1979) investigated the inelastic seismic response of a three-storey steel building with tension-only bracing. Maximum inelastic response from time history analyses was observed in the first storey. Once yielding occurred in this storey, the upper storeys remained largely elastic. The P-Δ effect was found to increase the inelastic drift of the CBF by only 1.03 times.

Dumanoglu and Severn (1985) investigated the dynamic behaviour and seismic response of Clasp-type buildings (that use minimal diagonal bracing and rely on the cladding for stability). Experiments on a full-scale three-storey building and studies with analytical models were both performed. Damping of about 8% to 13% was estimated from vibration tests on the structure. The stiffness contribution from the cladding influenced the frequencies of the building significantly. The dynamic response of calibrated computer models of the building to recorded ground motion indicated no sign of distress in both the diagonal bracing and the cladding.

Naman and Goodno (1986) performed a detailed seismic evaluation of an existing two-storey office building that was designed for gravity and wind loads only. The effect of roof diaphragm flexibility was investigated with a three-dimensional computer model of the building and was found to affect the lateral load distribution to the frames significantly. The earthquake load was found to be the governing lateral load case for design.

Léger and Romano (1992) investigated the response of a two-storey building with tension-only X-braced CBFs to the Saguenay earthquake of 1988. The ductility demand on the braces was found to depend on the real strength of the LLRS (as against the code specified design base shear). They suggested that this overstrength should be explicitly considered in design.

Tremblay and Stiemer (1996) investigated the nonlinear seismic response of 36 rectangular single-storey steel buildings designed to the prevailing Canadian practice. The analytical models accounted for flexible diaphragm behaviour and nonlinear behaviour of the CBF. The analytically computed fundamental period of the buildings was found to be significantly greater than the empirical estimate in the NBCC

(ACNBC 1990). The lateral force on the roof diaphragm was also found to exceed the design force recommended in the NBCC and an amplification factor of 2.3 was proposed on the design bending moment. The maximum lateral drift of the buildings was reported to be within the NBCC limit of 0.02 times the building height. The ductility demand on the CBF was rather high with values up to 80 reported.

3.6 Summary

The experimental work on brace members and their connections, steel shear diaphragms, and non-structural elements under cyclic loading is relatively limited.

Further cyclic tests on full-size brace members of different shapes and their connections to investigate the effect of the slenderness ratio on the hysteresis behaviour, the propensity towards development of cracks as a function of the width-thickness ratio, and the connection behaviour itself would be invaluable.

There is a lack of experimental data on the cyclic behaviour of steel deck diaphragm assemblies, the means used to fasten the deck sheets together and to fasten the diaphragm to the collector elements. Both welded and mechanically fastened connections need to be examined.

Non-structural elements for which experimental data on stiffness, strength, and damage threshold should be established include masonry, exterior insulation and finish systems, glazing, and roofing. Even the information on gypsum partitions is limited.

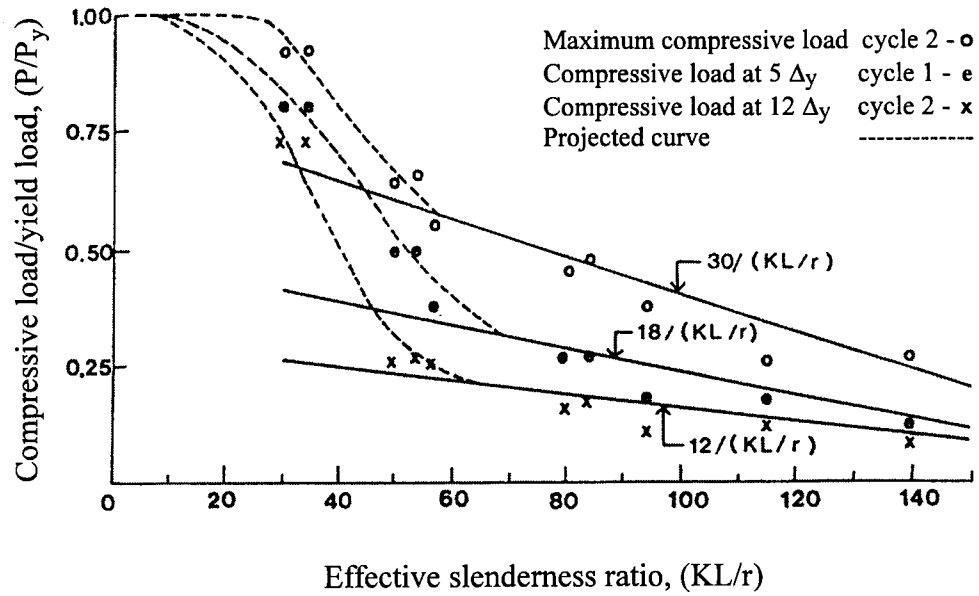

Figure 3.1 Compressive load vs. KL/r ratio for tube specimens (Jain *et al.* 1980)

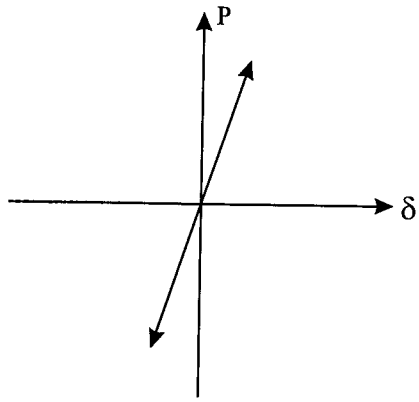

(a) Elastic

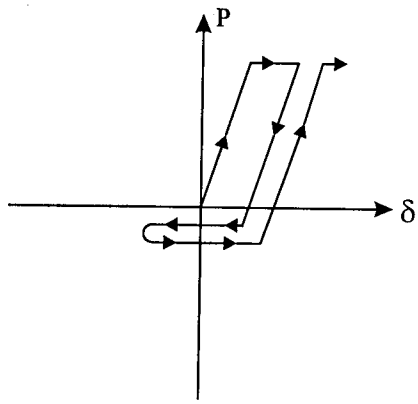

(b) Tension-yield and compression-buckling

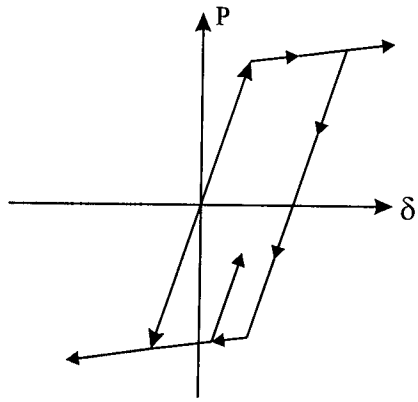

(c) Tension-yield and compression-yield

Figure 3.2 Various brace models

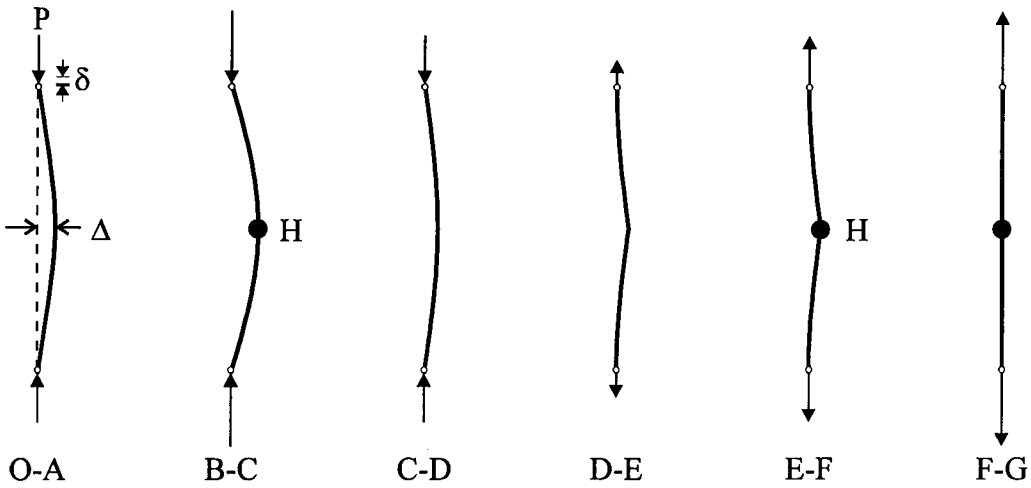

(a) Deformed state of brace

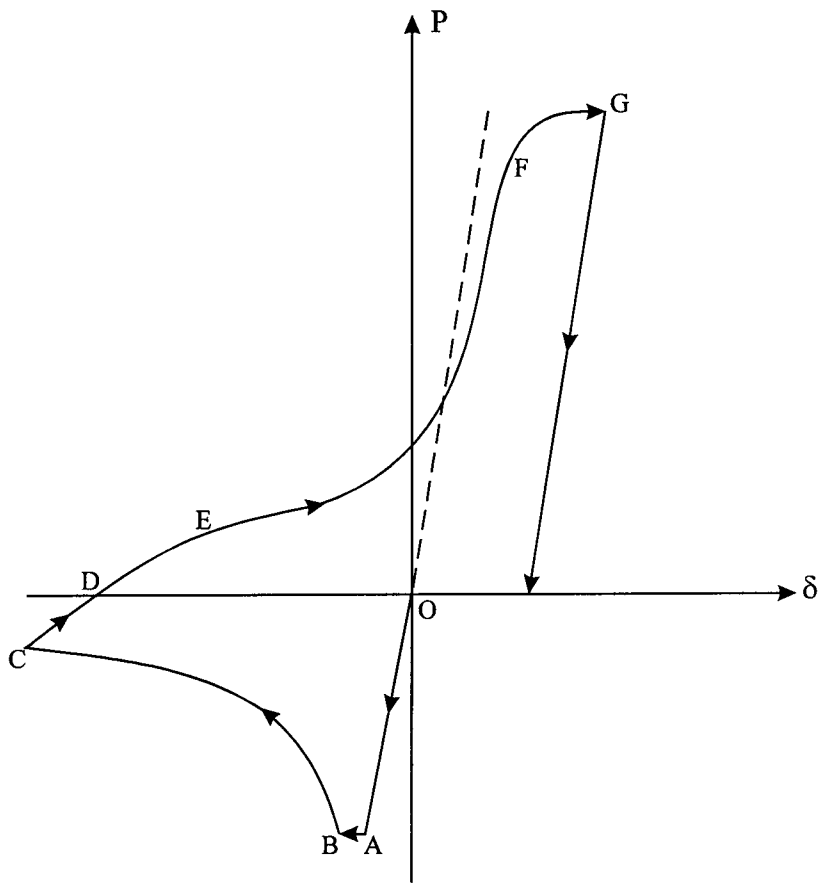

(b) Idealized hysteresis Loop

Figure 3.3 Axial-hysteresis behaviour of brace

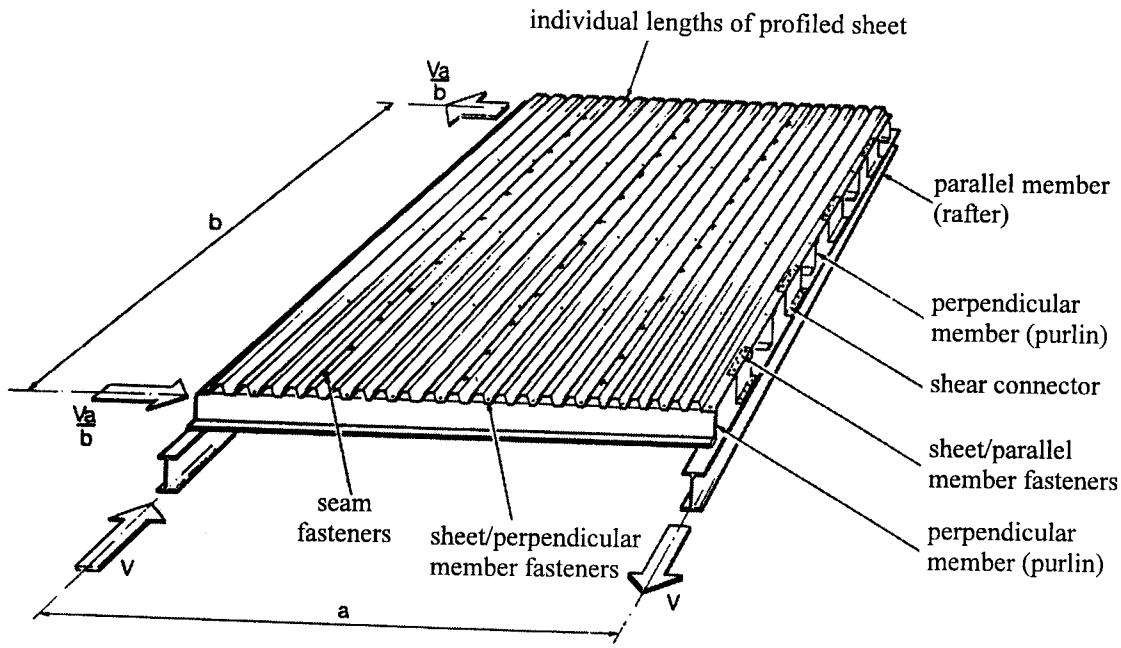

Figure 3.4 Basic shear panel

4. METHODOLOGY

4.1 Introduction

The methodology adopted for seismic evaluation of low-rise steel buildings is presented. It is based on the systematic procedure for seismic rehabilitation of buildings recommended by the Applied Technology Council (ATC 1995) with several additions specific to this work. The intended performance level of buildings designed according to the earthquake-resistant design provisions of the NBCC (ACNBC 1995a) is defined. The criteria for selection of design ground motion for use in seismic analysis are then described. Response spectra of the selected accelerograms are developed and compared with the NBCC design spectrum. The use of various analytical procedures for earthquake response analysis of buildings is discussed. Some aspects of structural modelling relevant to dynamic analysis of low-rise buildings are discussed. The parameters used for quantifying the seismic response are identified. Finally, acceptance criteria for evaluating the structural response are defined.

4.2 Performance levels

A performance level is the intended post-earthquake condition of the building and indicates how much earthquake damage is sustained. Typically four performance levels are specified by seismic design codes in order of decreasing damage: the collapse prevention level, life safety level, immediate occupancy level, and the operational level.

The collapse prevention level is that state in which the building is on the verge of experiencing a partial or total collapse. There is substantial damage to the structure, significant degradation in the stiffness and strength of the lateral load resisting system (LLRS), possible permanent lateral drift, some degradation in vertical load carrying capacity, and extensive damage to non-structural components.

The life safety level is that state in which significant damage has occurred, but some margin against either partial or total structural collapse remains.

The immediate occupancy level is that state in which only limited structural and non-structural damage has occurred. The vertical and lateral load resisting systems retain nearly all of their pre-earthquake characteristics and capacities.

The operational level is that state in which the building is available for normal occupancy and use and most utility systems are functional.

The earthquake-resistant design provisions of the NBCC (ACNBC 1995a) endeavour to provide an acceptable level of public safety by designing to prevent major failure and loss of life. Thus, the intended performance level for most buildings is the life safety level. The immediate occupancy level and the operational level are specified for post-disaster buildings such as schools, hospitals, and fire stations.

4.3 Specification of design ground motion

The design ground motion selected should correspond to the performance level to be investigated. It may be specified as response spectra, simplified force coefficients representative of such spectra, or as ensembles of earthquake time histories. The choice depends on the method of analysis selected. There are two procedures for selecting ground motion; (a) the general procedure involving use of probabilistic ground motion maps specified in the NBCC, and (b) site-specific procedures wherein detailed studies are carried out for a given site. In this work, the first of these is adopted to select earthquake time histories for five seismic zones in Canada. These time histories are then used to develop response spectra for comparison with the NBCC design spectrum in each of the five zones.

4.3.1 Earthquake accelerogram selection criteria

The seismic hazard at typical sites is influenced by earthquakes of various magnitudes that occur nearby and by earthquakes of large magnitude that are distant. The former contribute significantly to the peak horizontal acceleration, PHA, at the site while the latter contribute to the peak horizontal velocity, PHV. Both parameters are specified in the NBCC (ACNBC 1995a) for each seismic zone for the 1 in 475 year design earthquake. Hence in this work, two sets of historical earthquake accelerograms are selected for each seismic zone. The first set, comprising accelerograms that have peak ground accelerations, PGA, that are scaled to match the zonal PHA, is referred to as the 'acceleration set.' The second set, comprising accelerograms that have peak ground velocities, PGV, that are scaled to match the zonal PHV, is referred to as the 'velocity

set.' The criteria for selecting accelerograms for each set evolved from discussions with BC Hydro[1] and with Weichert[2]. The recommendations of BC Hydro for selection of accelerograms are given in Appendix A. The accelerogram selection criteria used in this work are as follows:

(a) only earthquake events with local magnitude, M_L, or body wave magnitude, M_b, exceeding 5 are considered as these have historically caused structural damage,

(b) only horizontal accelerograms obtained from the free field and from building basements at sites on bedrock or stiff soils are considered,

(c) only one accelerogram is selected per event to avoid bias towards any particular event,

(d) the accelerograms are selected to keep the scaling required to match the zonal PHA or PHV to a factor in the range 0.5 to 2.0, and

(e) the accelerograms selected in either the acceleration set or the velocity set are unique, i.e., they are not repeated in the other set.

When using this procedure, the ratio of PGA to PGV (a/v ratio) is not considered and thus may be greater than, less than, or equal to 1.0. The periods of the buildings may also lie in the range where the NBCC 1995 considers the a/v ratio not to be a factor.

When dynamic time history analysis is used to assess the structural response, FEMA (1994) recommends that at least 4 spectrum compatible time histories should be used while the ATC (1995), BC Hydro[1], and the ICBO (1997) recommend the use of at least 3 time histories. Spectrum compatibility is considered a desirable characteristic when only a few accelerograms are used in analysis; their response spectrum must match the design spectrum over most of the period range of interest. However, when a significantly greater number of accelerograms are used, some relaxation of this condition is justifiable because the design spectrum itself is a smoothed average of a number of response spectra from events that have different characteristics. For example, a nearby earthquake may have frequency content predominantly in the high frequency range. A more distant earthquake may have frequency content in the intermediate and low

---

[1] Little, T.E., and Fan, B.H. 1995. Personal communication.

[2] Weichert, D. 1995. Personal communication.

frequency range. A greater number of time histories are recommended for use in nonlinear dynamic analysis (than for linear dynamic analysis) due to the greater sensitivity of nonlinear structural response to characteristics of the ground motion such as duration, phase, and the sequence of pulses.

4.3.2 Application of the earthquake accelerogram selection criteria

The criteria mentioned above are applied to select accelerograms from the 'STRONGMO' earthquake database at Lamont-Doherty Geological Observatory of Columbia University (Friberg and Susch 1990) and from the California Strong Motion Instrumentation Program server on the internet (CSMIP). Accelerograms are selected for the acceleration set and the velocity set for five seismic zones in Canada with the acceleration-related seismic zone, Z_a, assumed equal to the velocity-related seismic zone, Z_v. The acceleration set has zonal acceleration ratios, a, of 0.05, 0.10, 0.15, 0.20, and 0.30 in zones 1 to 5, respectively. Similarly, the velocity set has zonal velocity ratios, v, of 0.05, 0.10, 0.15, 0.20, and 0.30 in zones 1 to 5, respectively. A total of 100 accelerograms are selected, of which 90 are from the 'STRONGMO' database that has over 1900 horizontal accelerograms, and the remaining from the CSMIP. The selected accelerograms represent 36 earthquake events that occurred in the Americas from 1933 up to 1994. A regional break up of events is as follows; Alaska (5), California (22), Eastern Canada (1), Western Canada (1), Chile (2), Mexico (1), Montana (1), Nicaragua (1), and Washington (2). The accelerograms selected for the acceleration and the velocity sets for each of the five seismic zones are listed in Tables 4.1 through 4.10. In the tables, the epicentral distance is denoted by R, the local magnitude is denoted by M_L, and the body wave magnitude, M_b, is indicated by an asterisk. The duration of the accelerogram used in the analyses is taken from initiation until the last pulse that exceeds 0.02 g, except that for some accelerograms of long duration, this limit is set at 0.05 g.

4.3.3 Response spectra of selected accelerograms

Response spectra of the accelerograms are developed by integrating numerically the response of a 5% damped elastic oscillator by the constant-average acceleration method, as explained in Appendix B. Figures 4.1 to 4.10 present the 5% damped elastic

acceleration response spectra for three levels of response: the mean, mean plus one standard deviation (mean + 1 sigma), and the maximum, together with the elastic response spectrum given in the NBCC. Note that the vertical scales in these figures change by a factor of 4 from Fig. 4.1 to Fig. 4.10. The accelerograms of the 'acceleration set' have their PGA scaled to equal the zonal PHA. Hence, all the spectra converge to the zonal PHA at zero period on the spectrum. As these accelerograms have been scaled to a common PHA, the scatter tends to be less in the acceleration sensitive region of the spectrum, that is, for periods less than 0.5 s, as established by Nau and Hall (1984). Similarly, the accelerograms of the 'velocity set' have their PGV scaled to equal the zonal PHV. As these accelerograms have been scaled to a common PHV, the scatter is less in the velocity sensitive region of the spectrum, that is, for periods greater than 0.5 s. The average effect of the ensemble of accelerograms selected for each zone is a smoothed response spectrum that represents the effect of different seismic events of different magnitudes and source-to-site distances. The NBCC elastic design spectrum is the product of the zonal velocity ratio, v, and the S factor for seismic zones with Z_a equal to Z_v. For a given period, a comparison of spectral ordinates of the NBCC curve with the smoothed response spectra for each zone, indicates if the structure is subjected to an earthquake force greater or smaller than the NBCC lateral force requirement. The response level for evaluating the results of dynamic analysis against the acceptance criteria, may be chosen to be compatible with the NBCC design spectrum in the period range of interest.

4.4 Response analysis procedures

The analysis procedures available for determining the earthquake response of a building range from simple to rather sophisticated. Depending on the material behaviour assumed, they may be classified into two general categories of linear analysis procedures and nonlinear analysis procedures. Each may be further classified into a dynamic or a static analysis procedure depending on whether inertial effects are considered or not. Linear static and linear dynamic procedures are widely used in seismic design. Nonlinear procedures are typically used for detailed evaluation studies.

4.4.1 Linear static analysis

This is the analysis that is intended to be used with the NBCC equivalent lateral force procedure for seismic design. The NBCC specifies the magnitude and distribution of the equivalent lateral forces that the building should resist. These static lateral forces are applied on an appropriate structural model and are used for design and analysis of the building.

4.4.2 Linear dynamic analysis

A linear dynamic analysis may be further classified into a response spectrum analysis or a time history analysis. The former is recommended by the NBCC to determine the distribution of lateral forces in buildings that have irregularity in the distribution of mass or stiffness, for example, buildings with vertical or horizontal setbacks. Its intent is to determine the maximum structural response directly from an earthquake response (or design) spectrum. This procedure is considered to be sufficiently accurate for building design (Gupta 1990, FEMA 1994). A linear dynamic time history analysis is more involved. The response of each mode to a specific ground acceleration is computed by numerical integration and the resulting modal responses are superposed by suitable modal combination rules. Details of both methods are given by Chopra (1995).

4.4.3 Nonlinear static analysis

This is also referred to as a static "pushover analysis" (Lawson *et al.* 1994, ATC 1995). It is an incremental nonlinear analysis wherein the structure is loaded with a lateral force profile that is considered to represent, at least approximately, the relative inertia forces that are generated at locations of substantial mass. The structure is pushed laterally by the forces of this load pattern until the level of deformation expected in the design earthquake is attained. The following information may be obtained from such an analysis; (a) estimates of the strength and deformation demands on the structural elements, (b) effect of deterioration of individual components on the behaviour of the structure, (c) overload of brittle elements, and (d) identification of possible weak links in the lateral load path. Test data may also be used directly in this procedure by specifying appropriate force-deformation relations for the structural elements.

A nonlinear static analysis is not a dynamic procedure and hence cannot predict ductility demand on the structural elements; nor can it account for the effect of higher modes and changes in dynamic response and inertial load distributions that occur as the structure degrades in stiffness. Nevertheless, it is superior to linear analysis methods as it considers the actual strength of the structural elements. Several yield situations may be studied by varying the lateral force profile on the structure and increasing the forces proportionately until significant yielding occurs. In this work, the program DRAIN-2DX (Prakash *et al.* 1993) is used to perform this analysis.

4.4.4 Nonlinear dynamic time history analysis

This is considered to be the most sophisticated earthquake response analysis in that it employs numerical integration in the time domain and explicitly accounts for nonlinear stiffness and strength characteristics of the structural elements. It also accounts for the effect of higher modes and shifts in inertial load patterns as structural softening takes place. The strength and deformation demands are computed explicitly for each component of the structure. Use of this method for assessing the building response is necessary because the structure may exhibit a nonlinear response in the design earthquakes. However, it is sensitive to the characteristics of ground motion and therefore an adequate number of appropriately selected accelerograms should be used to obtain meaningful results.

4.4.4.1 Selection of a computer program

A number of commercial programs are available that can perform a nonlinear dynamic time history analysis of reasonably symmetric structures. Among them are DRAIN-2D (Kannan and Powell 1973), ANSR-1 (Mondkar and Powell 1975), and DRAIN-2DX (Prakash *et al.* 1993). The program DRAIN-2D was selected for this study as it has been used widely in the past. This choice is also governed by the fact that it has the EL9 buckling element (Jain and Goel 1978) that represents, at least approximately, the hysteresis behaviour of steel braces.

4.4.4.2 Description of computer program DRAIN-2D

DRAIN-2D is a general purpose computer program for the dynamic response analysis of inelastic plane structures. The structure to be analysed is idealized as a planar assemblage of discrete elements. Analysis is by the direct stiffness method with the nodal displacements as the unknowns. Each node may possess up to 3 degrees of freedom with the provision of constraining any degree of freedom as desired. The structural mass is assumed to be lumped at the nodes so that the mass matrix is diagonal. Earthquake excitation is defined by time history of ground acceleration with all support points assumed to move in phase. Separate time histories may be specified in the vertical and horizontal directions. Static loads may be applied to the structure prior to dynamic loading. However, yielding of the elements is not permitted under static loads. The dynamic response is determined by step-by-step integration of the equations of motion by the constant-average acceleration method.

A number of structural elements are available for idealizing the structure. These include; (a) an inelastic truss element capable of yielding in tension and buckling in compression, (b) a beam-column element capable of flexural yielding by the formation of plastic hinges at its ends, (c) a semi-rigid connection element with a bilinear moment-rotation relationship, (d) an inelastic shear panel element capable of failing in a ductile or a brittle mode, and (e) the EL9 buckling element capable of representing the hysteresis behaviour of steel braces.

4.5 Structural modelling

The use of a two-dimensional structural model of the building is adequate if torsion is absent or is accounted for separately. The stiffness, strength, and post-yield behaviour of all elements in the lateral load path should be considered explicitly in the analysis. Masses should be distributed appropriately to model all important dynamic effects. Some aspects of structural modelling relevant to dynamic analysis of low-rise buildings are discussed in the following.

4.5.1 Braces

Because the nonlinear behaviour of a concentrically braced frame (CBF) occurs due to yielding or buckling of the braces, these elements deserve particular attention. In this study, the EL9 buckling element of DRAIN-2D is used to model the braces. Appendix C describes the hysteresis behaviour of this element. The model considers the tensile and compressive resistance of the brace and accounts for the reduction in compressive resistance due to cyclic buckling. The ATC (1995) recommends a post-buckling strength of 33% of the compressive capacity for cold formed brace sections and 25% for all other sections excluding circular tubes. Experimental data on the reduction in brace compressive resistance by Jain *et al.* (1980) is reviewed in section 3.2.2.2.

4.5.2 Flexible diaphragms

The ATC (1995) recommends that the effect of diaphragm flexibility should be considered if its inclusion in the model changes the force or deformation demands by more than 20%. Diaphragm flexibility results in; (a) an increase in the period of the fundamental mode, (b) vibration modes of the diaphragm and the CBF that can be considered independently, and (c) a redistribution of lateral load applied to the diaphragm itself. The assumption of a rigid diaphragm instead of a flexible one is conservative insofar as the design forces are concerned because the shorter fundamental period of the former is generally associated with a greater design base shear. The stiffness and strength estimates given in diaphragm design manuals may be used in analysis.

4.5.3 Non-structural elements

Non-structural elements that dynamically interact with the structure and add significant mass and stiffness should be modelled explicitly. The brittle failure mode of such elements should also be modelled appropriately. Interior partitions have to be framed directly into the structural roof or floor at the top and bottom to have any effect on the dynamic response. They may be isolated from the structural framing by provision of appropriate connections.

4.5.4 Geometric nonlinearity (P-Δ effect)

The P-Δ effect refers to the movement of gravity loads through the lateral displacement of a structure that generate second-order forces in the structure. Its effect is significant when the building response is severely inelastic, i.e., large Δ (Montgomery 1981), or when the vertical forces are large. It may also be important in low-rise buildings with flexible diaphragms (Tremblay 1993). This is typically the case when the LLRS has to stabilize a substantial gravity load, i.e., large P, on the remainder of the structure that has gravity load (leaner) columns only. The P-Δ effect results in increased lateral drift of the frame. A suitable method to account for it in dynamic analysis involves reducing the lateral stiffness of the structure by a geometric stiffness (Wilson and Habibullah 1987). The latter is based on the axial force due to the static gravity load in the columns. This method is available as an option in DRAIN-2D with the reduced lateral stiffness used as the initial tangent stiffness for dynamic analysis. The P-Δ effect may also be modelled by using dummy leaner columns with the appropriate gravity load on them.

4.5.5 Damping

A dynamic analysis with any numerical integration scheme requires that the damping matrix be defined explicitly. In DRAIN-2D, Rayleigh damping which is proportional to mass and stiffness may be specified such that

[4.1] $$C_T = \alpha M + \beta K_T$$

where α and β are constants to be specified by the program user and C_T, M, and K_T are the tangent damping matrix, the mass matrix, and the tangent stiffness matrix, respectively. One method of selecting the constants α and β is based on the estimated modal damping ratios for the structure that may be obtained from forced vibration tests on similar structures or from the recorded motion of structures in past earthquakes.

Let λ_i and λ_j be the modal damping ratios for the i th and j th mode with corresponding periods T_i and T_j. The constants α and β are given by

[4.2] $$\alpha = \frac{4\pi (T_j \lambda_j - T_i \lambda_i)}{T_j^2 - T_i^2}$$

[4.3] $$\beta = \frac{T_i T_j (T_j \lambda_i - T_i \lambda_j)}{\pi (T_j^2 - T_i^2)}$$

Table 4.11 gives damping values for clad and unclad steel structures based on recommendations of the New Zealand National Society for Earthquake Engineering (Patton 1985). Table 4.12 gives damping values obtained from vibration tests on light gage metal buildings (Sockalingam 1988, Sockalingam *et al.* 1994). Newmark and Hall (1982) recommend a damping ratio between 5% and 7% for steel structures with welded connections and between 10% and 15% for steel structures with bolted connections.

4.5.6 Observations from an ambient vibration test of a single-storey steel building

Appendix D describes the dynamic behaviour of a single-storey steel building with a flexible roof diaphragm and with CBFs as the LLRS. The first three periods and corresponding mode shapes of this building were obtained from an ambient vibration test (Ventura 1995). Analytical studies were performed to investigate suitable computer models for dynamic analysis. Based on the experiment and the analytical work, the following suggestions were made: (a) diaphragm flexibility should be considered in analytical models of such buildings, (b) non-structural cladding and partitions should be considered as they may contribute significant stiffness and strength, and (c) for buildings that are fairly regular in plan, a two-dimensional model may be used instead of a three-dimensional one.

4.6 Parameters for quantifying the seismic response

Inherent in the concept of performance levels is the assumption that this performance can be measured using appropriate parameters. The fundamental period and the distribution of lateral forces on the building, obtained from a response spectrum analysis, may be compared with the NBCC recommendations. The force and deformation demands on the structural elements obtained from a nonlinear static analysis or a nonlinear dynamic analysis may be compared to their strength and deformation capacity. Nonlinear dynamic time history analysis typically gives time histories of element forces and deformations. Information on the global drift, interstorey drift,

strength and ductility demand on the structural elements, number of yield occurrences, cumulative ductility demand (damage), maximum base shear developed in the building, and the state of the non-structural elements after the earthquake, are common parameters that are used to quantify the seismic response.

4.7 Acceptance criteria

Acceptance criteria relate to permissible earthquake induced forces and deformations for various structural elements of the building and correspond to the intended performance level. Table 4.13 from the ATC (1995) gives the levels of structural and non-structural damage that may be used to quantify the performance of the structure. The performance levels of "immediate occupancy" and "operational level" are grouped together because the distinction between them is in the functionality of the utilities after the earthquake. Additional data on other materials such as concrete, masonry, wood, and precast concrete are given by the ATC (1995).

The drift limits for CBFs given in Table 4.13 may not be appropriate because the yield deformation of the CBF is a function of its geometry and material property only. The ductility demand on the braces is a better indicator of the severity of response. The maximum ductility attained in the earthquake may be compared with test results (which are scant) to qualify the response. A rule of thumb used in this work is that the ductility demand in the CBF should not exceed the R factor used in design. The number of yield events that occurs in the braces is a function of the duration of ground shaking and the characteristics of the ground motion. As information on the duration dependent damage to structural elements is scarce, these duration dependent parameters are difficult to interpret.

Lack of full-scale cyclic tests on diaphragm assemblies makes the interpretation of the roof diaphragm response rather judgemental. In general, inelastic action in the roof diaphragm is to be avoided. Forces in excess of the diaphragm strength may cause a brittle failure in the welded connections, or failure in the mechanical connections, or may even cause buckling of the deck panels.

For non-structural partitions, the interstorey drift ratio may be used to assess the likely damage. Based on the literature reviewed (Freeman 1977, Rihal 1986), an

interstorey drift ratio of 0.0025 is considered the threshold to initiate damage in non-structural partitions and 0.0050 is the lower bound of significant damage. An interstorey drift ratio of 0.0075 may be considered as failure of the partitions requiring their complete replacement.

Table 4.1 Acceleration set of earthquake records for analysis in zone 1

Event	*Date*	*Site*	M_L M_b*	*R*	*PGA*	*PGV*	*a/v*	*Duration*
				km	*g*	*m/s*		*s*
Morgan Hill, California	4/24/84	1028, Hollister City Hall Basement, 1°	6.2	58	0.07	0.07	0.97	29
Humboldt County, California	6/7/75	1278, Shelter Cove 2, 70°	5.2	62	0.06	0.02	2.95	4
Loma Prieta, California	10/18/89	58133, Stockton Basement, SFO, 0°	7.0	100	0.05	0.07	0.80	4
Saguenay, Quebec	11/25/88	GSC site 9, St. Pascal P.O., 0°	6.0*	129	0.05	0.03	1.79	19
Michoacan, Mexico City	9/19/85	Teacalco, 0°	6.8*	329	0.05	0.07	0.71	18
Alaskan Subduction Zone	10/9/85	BKJ 2773, Big Koniuji, 345°	-	48	0.05	0.02	2.89	14
Valparaiso, Chile	3/3/85	Chilean Institute, 2 story bldg., 350°	6.7*	319	0.05	0.09	0.62	41
Northridge, California	1/17/94	Mojave, Oak Creek Canyon, 0°	6.6	94	0.05	0.03	1.59	16

Table 4.2 Velocity set of earthquake records for analysis in zone 1

Event	*Date*	*Site*	M_L M_b*	*R*	*PGA*	*PGV*	*a/v*	*Duration*
				km	*g*	*m/s*		*s*
Imperial Valley, California	10/15/79	5056, El Centro Array # 1, 140°	6.6	37	0.06	0.05	1.24	5
Northern California	9/22/52	1023 FER, Ferndale City Hall, 134°	5.2	43	0.08	0.05	1.59	16
Morgan Hill, California	4/24/84	47380, Gilroy Array # 2, 0°	6.2	39	0.16	0.05	3.14	22
Humboldt Bay, California	2/7/37	1023 FER, Ferndale City Hall, 315°	5.8	75	0.04	0.04	0.97	9
Mount Diablo	1/27/80	1226, Livermore VA Hospital, 38°	5.8	13	0.06	0.04	1.41	7
Michoacan, Mexico City	9/19/85	Teacalco, 90°	6.8*	329	0.03	0.05	0.53	17
Alaskan Subduction Zone	7/30/72	2714 SMO, Sitka Observatory, 90°	7.6*	48	0.10	0.06	1.51	31
Valparaiso, Chile	4/9/85	Llolleo Basement, 1 story bldg., 100°	6.3*	166	0.17	0.06	2.79	30
Northridge, California	1/17/94	Rancho Palos Verdes, 0°	6.6	53	0.07	0.05	1.45	17

Table 4.3 Acceleration set of earthquake records for analysis in zone 2

Event	*Date*	*Site*	M_L M_b*	*R* *km*	*PGA* *g*	*PGV* *m/s*	*a/v*	*Duration* *s*
Coyote Lake, California	8/6/79	1408 G01, Gavilan College, 320°	5.7	16	0.11	0.10	1.10	9
San Francisco, California	3/22/57	1080 STA, State Bldg., SFO, 171°	5.3	20	0.09	0.05	1.69	29
Whittier, California	10/1/87	141 GPK, Griffith Park Obs., 360°	6.1	21	0.12	0.13	0.94	10
Humboldt County, California	6/7/75	1249, Cape Mendocino, 30°	5.2	33	0.11	0.03	3.18	9
Oroville, California	8/1/75	1051, Oroville Seismic Station, 307°	5.7	13	0.08	0.04	1.89	3
Loma Prieta, California	10/18/89	58222, 145 - SFO Presidio, 0°	7.0	102	0.10	0.13	0.75	22
Imperial Valley, California	10/15/79	931, El Centro Array # 12, 230°	7.0	30	0.12	0.19	0.60	31
Saguenay, Quebec	11/25/88	GSC site 8, La Malbaie P.O., 63°	6.0*	93	0.12	0.05	2.67	25
Nahanni, N.W.T.	12/23/85	Nahanni site 1, Iverson, 280°	5.4*	11	0.09	0.03	2.80	7
Michoacan, Mexico City	9/19/85	Zihuatanejo Aeropuerto, 180°	6.8*	131	0.10	0.16	0.65	34
Alaskan Subduction Zone	4/6/74	2744 SAN, Sand Point School, 120°	-	51	0.10	0.07	1.45	10
Northridge, California	1/17/94	Featherly Park, Maint. Bldg., 90°	6.6	86	0.10	0.06	1.74	21

Table 4.4 Velocity set of earthquake records for analysis in zone 2

Event	*Date*	*Site*	M_L M_b*	*R* *km*	*PGA* *g*	*PGV* *m/s*	*a/v*	*Duration* *s*
Dutch Harbour, Alaska	2/27/87	2743 DUT, Dutch Harbor, Alaska, 17°	6.2*	65	0.06	0.10	0.63	20
Morgan Hill, California	4/24/84	47381, Gilroy Array # 3, 0°	6.2	39	0.18	0.11	1.64	25
Whittier, California	10/1/87	4407 Jasper Street, Los Angeles, 40°	6.1	10	0.22	0.11	1.95	15
Humboldt County, California	6/7/75	1023 FER, Ferndale City Hall, 224°	5.2	11	0.18	0.11	1.59	14
Hollister, California	11/28/74	1028, Hollister City Hall, 271°	5.2	11	0.17	0.11	1.44	13
Loma Prieta, California	10/18/89	58133, Stockton Basement, SFO, 90°	7.0	100	0.09	0.10	0.96	7
Imperial Valley, California	10/15/79	117, El Centro Array # 9, 90°	6.6	27	0.20	0.10	1.94	11
Northern California	3/9/49	1028, Hollister City Hall, 271°	5.2	19	0.20	0.11	1.75	10
Valparaiso, Chile	3/3/85	Santa Maria University, 160°	6.7*	26	0.17	0.09	1.92	65
Michoacan, Mexico City	9/19/85	CUIP, UNAM, 0°	6.8*	373	0.03	0.10	0.32	27
Alaskan Subduction Zone	7/30/72	2714 SMO, Sitka Observatory, 180°	7.6*	35	0.07	0.11	0.66	29
Northridge, California	1/17/94	Leona Valley #6, 360°	6.6	52	0.13	0.10	1.31	21

Table 4.5 Acceleration set of earthquake records for analysis in zone 3

Event	*Date*	*Site*	M_L M_b*	*R* *km*	*PGA* *g*	*PGV* *m/s*	*a/v*	*Duration* *s*
Coyote Lake, California	8/6/79	1445 CYC, Coyote Creek, 160°	5.7	5	0.14	0.11	1.22	15
Whittier, California	10/1/87	24157, Baldwin Hills, Los Angeles, 0°	6.1	27	0.14	0.08	1.84	11
Loma Prieta, California	10/18/89	1413 G06, Gilroy Array # 6, 90°	7.0	28	0.17	0.14	1.22	24
Western Washington	4/13/49	2101, Olympia Highway Lab., 356°	7.1	30	0.16	0.21	0.77	48
Kern County, California	7/21/52	1095 TAF, Lincoln School, 21°	7.5*	50	0.16	0.16	0.99	44
Helena, Montana	10/31/35	323, Carroll College, 270°	6.0	10	0.15	0.13	1.09	5
San Fernando, California	2/9/71	Hollywood Storage P.E. Lot, 180°	6.6	36	0.17	0.17	1.03	32
Michoacan, Mexico City	9/19/85	La Union, 90°	6.8*	80	0.15	0.12	1.28	53
Puget Sound, Washington	4/29/65	2101, Olympia Highway Lab., 176°	6.3*	63	0.14	0.08	1.72	35
Valparaiso, Chile	3/3/85	Talca, 1 storey bldg., 280°	6.7*	228	0.17	0.12	1.41	25
Northridge, California	1/17/94	San Marino, Southwestern Acad., 360°	6.6	39	0.15	0.06	2.35	28

Table 4.6 Velocity set of earthquake records for analysis in zone 3

Event	*Date*	*Site*	M_L M_b*	*R* *km*	*PGA* *g*	*PGV* *m/s*	*a/v*	*Duration* *s*
Borrego Mountain	4/9/68	117, El Centro Array # 9, 270°	6.0*	76	0.06	0.15	0.39	43
Whittier, California	10/1/87	4407 Jasper Street, Los Angeles, 130°	6.1	10	0.33	0.15	2.23	20
Loma Prieta, California	10/18/89	USCG Bldg., Yerba Buena Island, 90°	7.0	99	0.07	0.15	0.46	15
Santa Barbara, California	8/13/78	Santa Barbara Court House, 220°	5.1	8	0.20	0.15	1.34	11
Imperial Valley, California	10/15/79	5055, Holtville Post Office, 315°	6.6	21	0.25	0.16	1.55	12
Morgan Hill, California	4/24/84	57382, Gilroy Array # 4, 360°	6.2	37	0.33	0.17	2.00	22
Michoacan, Mexico City	9/19/85	Tacubaya, 180°	6.8*	376	0.04	0.14	0.25	47
Long Beach, California	3/11/33	136 SUB, Subway Terminal, 39°	6.3	55	0.06	0.17	0.37	26
Northridge, California	1/17/94	Leona Valley #5, Ritter Ranch, 0°	6.6	51	0.15	0.15	0.98	24

Table 4.7 Acceleration set of earthquake records for analysis in zone 4

Event	*Date*	*Site*	M_L M_b*	*R* *km*	*PGA* *g*	*PGV* *m/s*	*a/v*	*Duration* *s*
Coyote Lake, California	8/6/79	1445 CYC, Coyote Creek, 250°	5.7	5	0.25	0.20	1.22	13
Morgan Hill, California	4/24/84	57383, Gilroy Array # 6, 0°	6.2	37	0.22	0.11	1.95	12
Humboldt County, California	6/7/75	1249, Cape Mendocino, 120°	5.2	33	0.20	0.06	3.43	9
Loma Prieta, California	10/18/89	58222, 145 - SFO Presidio, 90°	7.0	102	0.20	0.34	0.59	23
Imperial Valley, California	10/15/79	5055, Holtville P.O., 315°	7.0	20	0.22	0.48	0.45	29
Imperial Valley, California	5/19/40	117, El Centro Array # 9, 270°	6.6	5	0.21	0.36	0.59	51
San Fernando, California	2/9/71	Hollywood Storage P.E. Lot, 90°	6.6	36	0.21	0.21	1.00	32
Parkfield, California	6/28/66	1097 TM2, Temblor Array # 2, 295°	5.6	20	0.27	0.15	1.86	11
Michoacan, Mexico City	9/19/85	Papanoa, 270°	6.8*	83	0.23	0.07	3.25	31
Puget Sound, Washington	4/29/65	2101, Olympia Highway Lab., 266°	6.3*	63	0.20	0.12	1.60	30
Valparaiso, Chile	4/9/85	Llolleo Basement, 1 story bldg., 10°	6.3*	166	0.20	0.14	1.46	27
Northridge, California	1/17/94	Los Angeles, 116th St. School, 90°	6.6	41	0.20	0.16	1.26	35

Table 4.8 Velocity set of earthquake records for analysis in zone 4

Event	*Date*	*Site*	M_L M_b*	*R* *km*	*PGA* *g*	*PGV* *m/s*	*a/v*	*Duration* *s*
Morgan Hill, California	4/24/84	57382, Gilroy Array # 4, 270°	6.2	37	0.22	0.19	1.15	21
Loma Prieta, California	10/18/89	58132, 138 - 1090 Pt. Lobos, 90°	7.0	104	0.11	0.21	0.51	16
Imperial Valley, California	10/15/79	5053, Calexico Fire Station, 225°	7.0	15	0.27	0.19	1.41	33
Kern County, California	7/21/52	Santa Barbara Court House, 132°	7.5*	105	0.13	0.19	0.68	43
Managua, Nicaragua	12/23/72	3501, ESSO Refinery, Managua, 180°	5.2*	20	0.33	0.21	1.55	15
Whittier, California	10/1/87	709 GVR, Garvey Reservoir, 330°	6.1	3	0.48	0.20	2.41	17
Michoacan, Mexico City	9/19/85	Zihuatenejo Aeropuerto, 270°	6.8*	131	0.16	0.18	0.90	34
Northridge, California	1/17/94	Los Angeles, Temple & Hope, 180°	6.6	32	0.18	0.20	0.92	32

Table 4.9 Acceleration set of earthquake records for analysis in zone 5

Event	*Date*	*Site*	M_L M_b*	*R* *km*	*PGA* *g*	*PGV* *m/s*	*a/v*	*Duration* *s*
Coyote Lake, California	8/6/79	1413 G06, Gilroy Array # 6, 320°	5.7	9	0.32	0.25	1.28	10
Whittier, California	10/1/87	709 GVR, Garvey Reservoir, 60°	6.1	3	0.37	0.15	2.43	17
Morgan Hill, California	4/24/84	57383, Gilroy Array # 6, 90°	6.2	37	0.29	0.37	0.78	14
Loma Prieta, California	10/18/89	58135, 138 - UCSC / Lick Lab., 90°	7.0	23	0.41	0.21	1.93	26
Imperial Valley, California	5/19/40	117, El Centro Array # 9, 180°	6.6	5	0.35	0.32	1.08	51
Nahanni, N.W.T.	12/23/85	Nahanni site 2, Slide Mountain, 330°	5.4*	4	0.39	0.33	1.20	19
Western Washington	4/13/49	2101, Olympia Highway Lab., 86°	7.1	30	0.28	0.17	1.65	50
Parkfield, California	6/28/66	1097 TM2, Temblor Array # 2, 205°	5.6	20	0.35	0.23	1.54	12
Michoacan, Mexico City	9/19/85	Papanoa, 180°	6.8*	83	0.26	0.08	3.37	32
Alaskan Subduction Zone	7/12/83	VHS 2748, Valdez High School, 180°	-	52	0.32	0.19	1.74	14
Valparaiso, Chile	3/3/85	Valparaiso El Almendral, 50°	6.7*	26	0.30	0.29	1.04	64
Northridge, California	1/17/94	Pacoima, Kagel Canyon, 90°	6.6	18	0.30	0.31	0.97	34

Table 4.10 Velocity set of earthquake records for analysis in zone 5

Event	*Date*	*Site*	M_L M_b*	*R* *km*	*PGA* *g*	*PGV* *m/s*	*a/v*	*Duration* *s*
Coyote Lake, California	8/6/79	1410 G03, Gilroy Array # 3, 140°	5.7	13	0.25	0.29	0.85	19
Managua, Nicaragua	12/23/72	3501, ESSO Refinery, Managua, 180°	5.2*	37	0.32	0.30	1.07	31
Loma Prieta, California	10/18/89	47125, 137 - Capitola Fire Stn., 90°	7.0	15	0.40	0.31	1.30	36
Imperial Valley, California	10/15/79	5115, El Centro Array # 2, 140°	7.0	32	0.32	0.31	1.01	33
Nahanni, N.W.T.	12/23/85	Nahanni site 2, Slide Mountain, 240°	5.4*	4	0.54	0.30	1.80	18
Long Beach, California	3/11/33	131, Public Utilities Bldg., 180°	6.3	26	0.20	0.29	0.67	14
Northridge, California	1/17/94	Pacoima Dam, downstream, 265°	6.6	19	0.43	0.31	1.42	16

Table 4.11 Recommended viscous damping for steel structures (Patton 1985)

Type of structure	Behaviour	Welded connections	Bolted connections
Clad	Elastic	2.5	5.0
Clad	Ductile	5.0	10.0
Unclad	Elastic	2.0	5.0
Unclad	Ductile	5.0	7.5

Note: A clad structure has concrete or composite steel flooring and may be open or fully enclosed around its perimeter. An unclad structure is one with an open floor system and no exterior covering.

Table 4.12 Viscous damping for steel buildings with light gage roofing and cladding from vibration tests (Sockalingam 1988, Sockalingam *et al.* 1994)

Type of structure	Period (s)	Damping (%)
80' x 60' enclosed metal building with moment resisting frames and 26 gage sheeting.	1st mode - 0.220 2nd mode - 0.098	3.00 5.08
Open ended aircraft hanger with moment resisting frames and 26 gage sheeting.	1st mode - 0.895 2nd mode - 0.375 3rd mode - 0.272	2.84 not measured 9.13
125' x 60' x 20' metal building with moment resisting frames and 26 gage sheeting.	1st mode - 0.247 2nd mode - 0.090	4.20 6.50

Table 4.13 Performance levels and anticipated damage (ATC 1995)

Type	Collapse prevention level	Life safety level	Immediate occupancy and Operational level
Braced steel frames	Transient drift about 1.5%. Extensive yielding and buckling of braces. Many braces and their connections may fail.	Transient drift about 1%. Many braces yield or buckle but do not totally fail. Many connections may fail.	Essentially linear response. Minor yielding or buckling of braces.
Metal deck diaphragms	Large distortion with buckling of some units and tearing of many welds and seam attachments.	Some localised failure of welded connections of deck to framing and between panels. Minor local buckling of deck.	Connections between deck units and deck units and framing intact. Minor distortions.
Cladding	Severe damage to connections and cladding. Some panels fall off.	Severe distortion in connections. Distributed bending, crushing, and spalling of cladding elements. Some fracturing of cladding but panels do not fall off.	Connections yield. Minor cracks (< 1/16" width) or bending in cladding.
Partitions	Severe racking and damage in many cases.	Distributed damage. Severe cracking, crushing, and racking in some areas.	Cracking to about 1/16" width at openings. Minor crushing and cracking at corners.

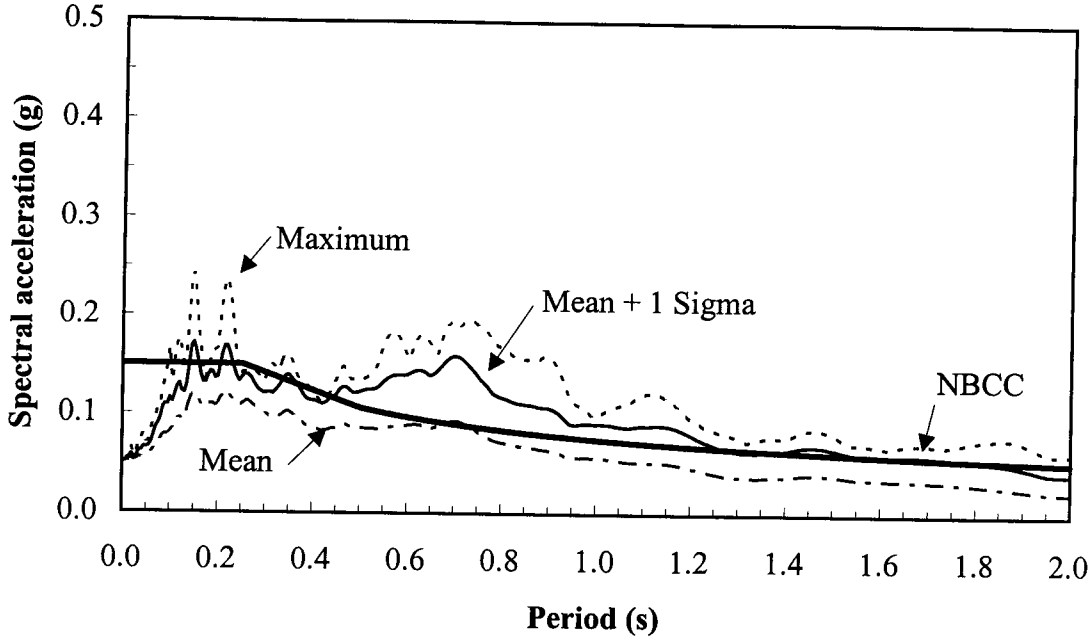

Figure 4.1 Response spectra for acceleration set of records for zone 1

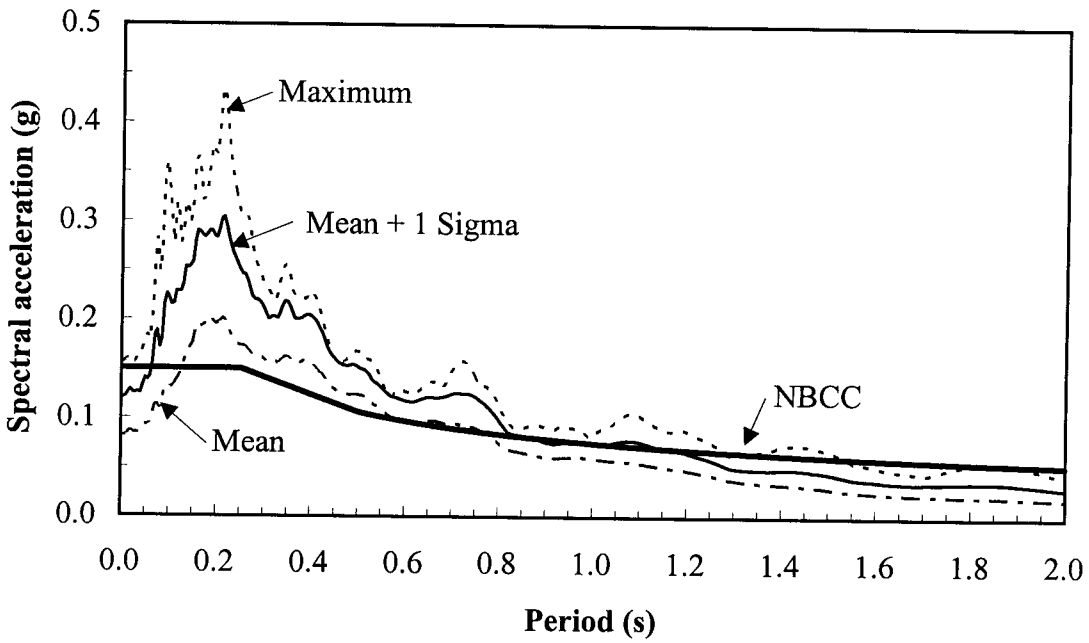

Figure 4.2 Response spectra for velocity set of records for zone 1

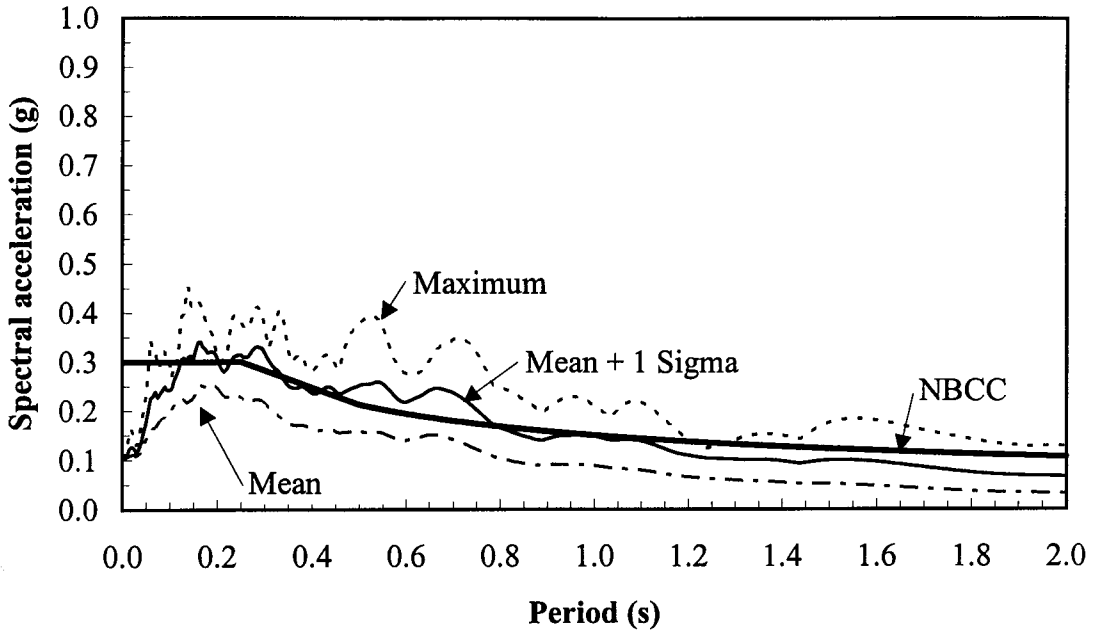

Figure 4.3 Response spectra for acceleration set of records for zone 2

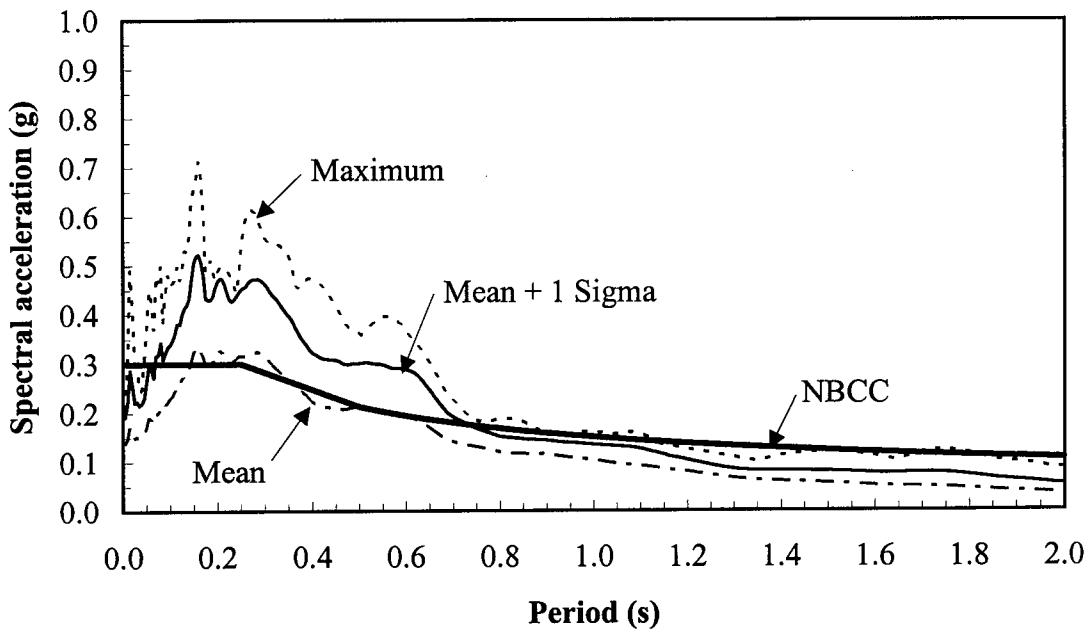

Figure 4.4 Response spectra for velocity set of records for zone 2

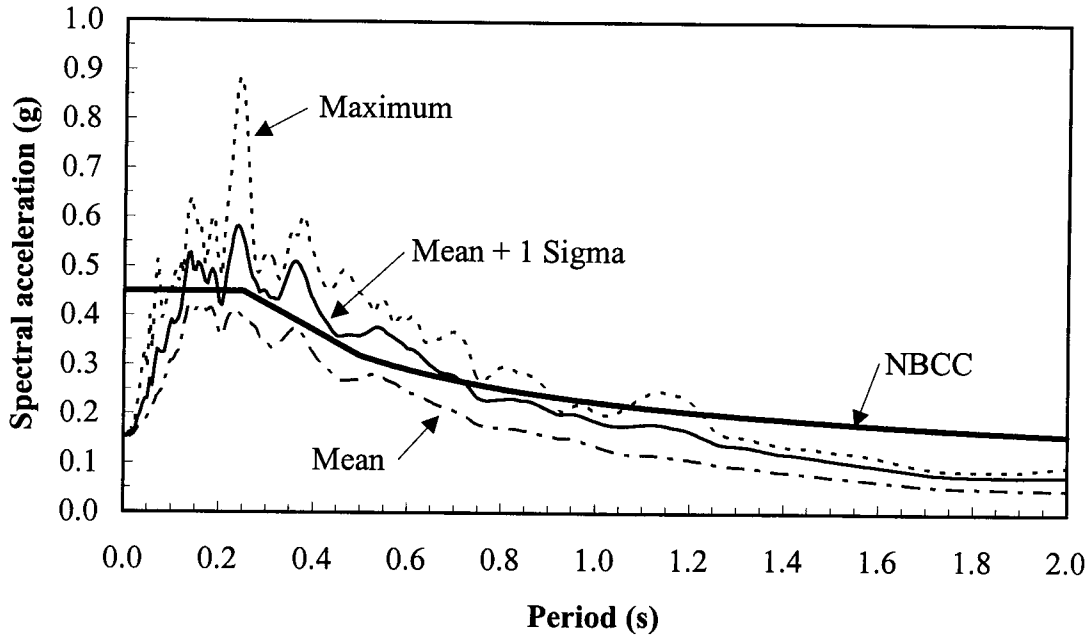

Figure 4.5 Response spectra for acceleration set of records for zone 3

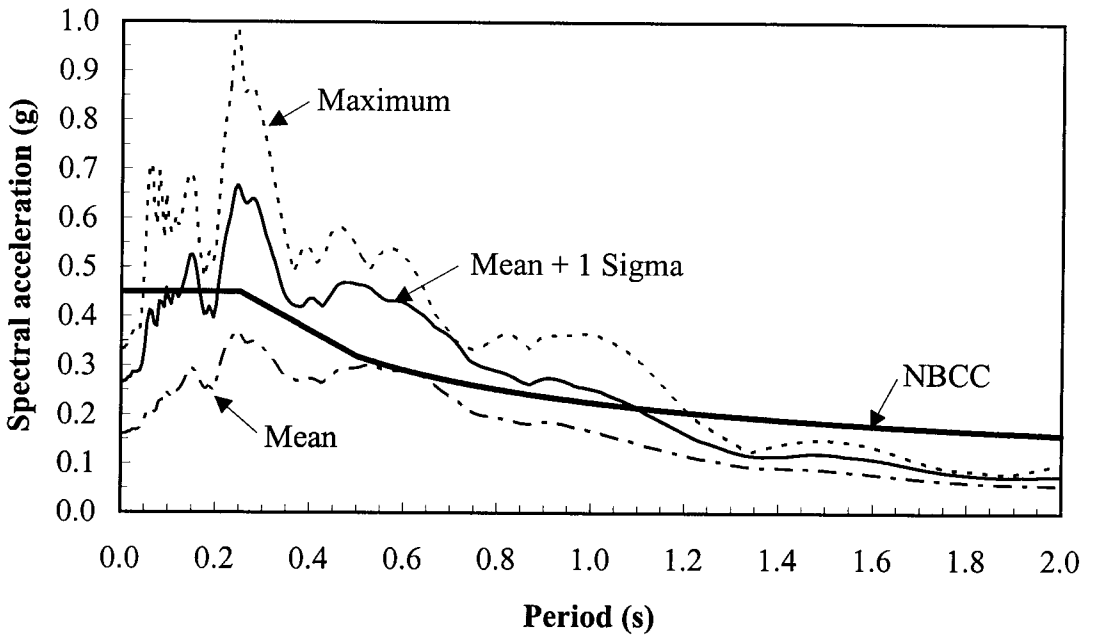

Figure 4.6 Response spectra for velocity set of records for zone 3

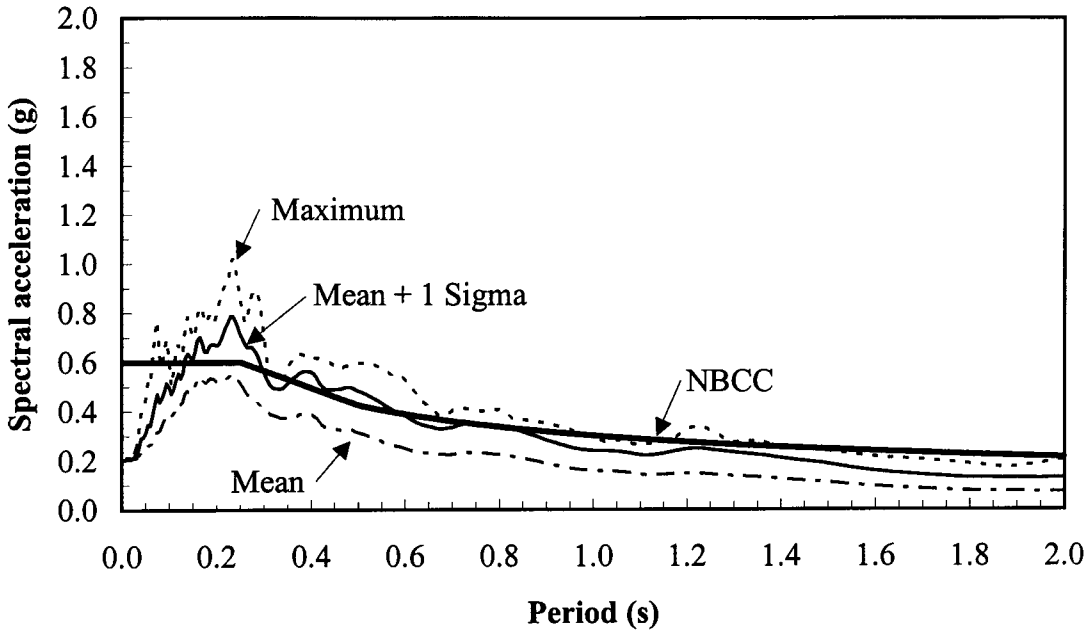

Figure 4.7 Response spectra for acceleration set of records for zone 4

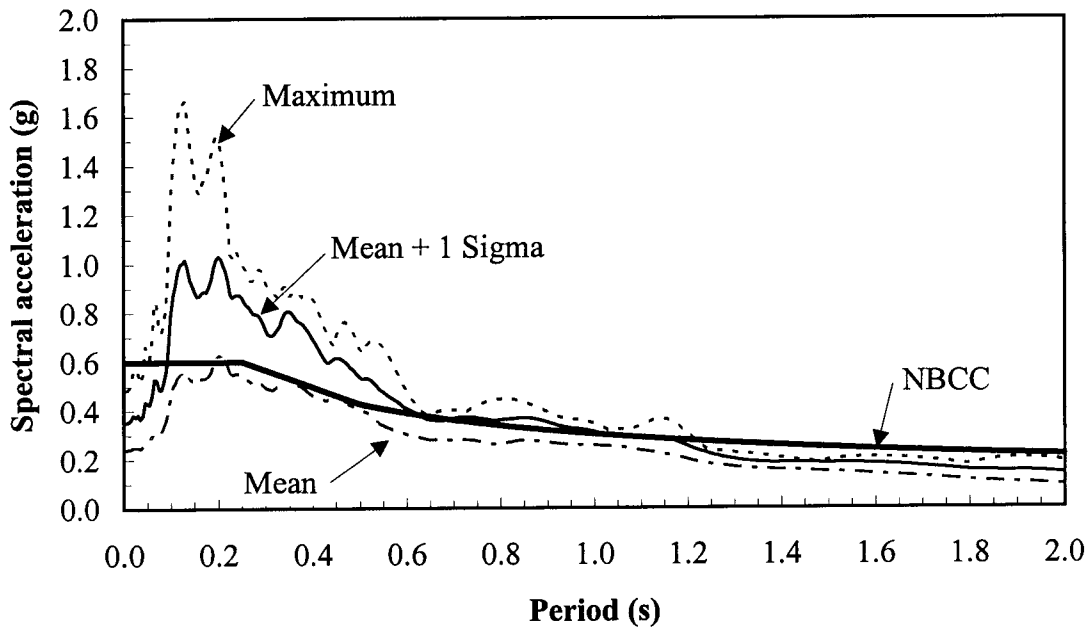

Figure 4.8 Response spectra for velocity set of records for zone 4

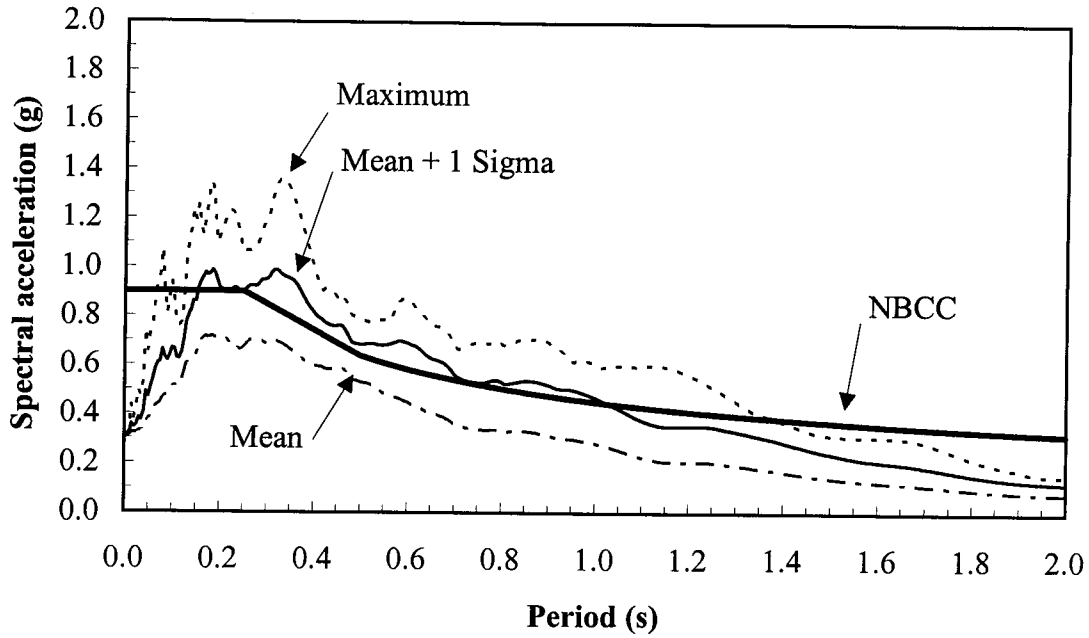

Figure 4.9 Response spectra for acceleration set of records for zone 5

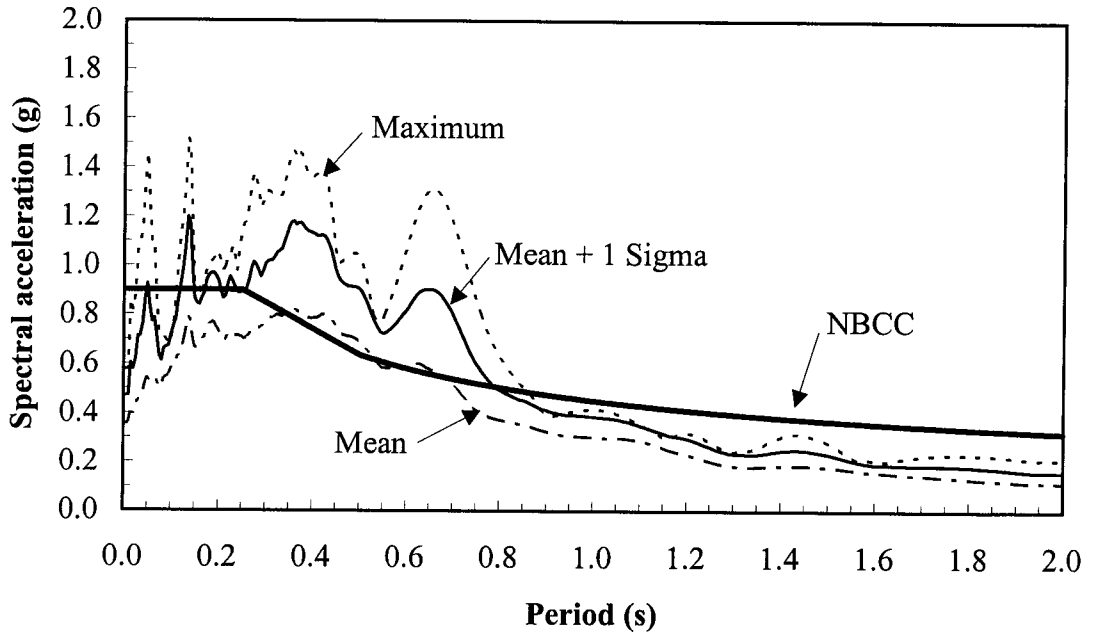

Figure 4.10 Response spectra for velocity set of records for zone 5

5. CASE STUDY I: SINGLE-STOREY BUILDING

5.1 Introduction

Analytical studies are performed with a single-storey steel building that is designed in accordance with the provisions of the NBCC (ACNBC 1995a) and CSA Standard S16.1-94 (CSA 1994) for five seismic zones of Canada that have seismicities ranging from low to high. A two-dimensional structural model is developed that considers the nonlinear seismic behaviour of the concentrically braced frame (CBF), the strength and stiffness contribution of the cladding, and the flexibility, strength, and distributed mass of the roof diaphragm. The dynamic behaviour of the building is investigated with a number of models. The excess supply of strength to the building is identified. The analytical procedures described in Chapter 4, namely, linear static analysis, response spectrum analysis, nonlinear static analysis, and nonlinear dynamic time history analysis, are used to estimate the seismic response of the building and assess its conformance with the acceptance criteria. Recommendations are made for the seismic design and analysis of such buildings.

5.2 Description of the building

The building considered in this study is adapted from the "Single storey building design aid" published by the Canadian Institute of Steel Construction (Chien 1985). This standard document is used widely by the steel construction industry. The building is rectangular in plan as shown in Fig. 5.1. It has a metal roof deck and relies on the diaphragm action of the deck to transfer lateral loads to the CBFs. The deck is supported by open web steel joists, supported in turn by girders that constitute a cantilever-suspended-span system that is continuous over the interior columns. The latter are typically 178 x 178 x 8 hollow structural sections of grade 350W steel. The vertical lateral load resisting system (LLRS) consists of four CBFs that are present along the exterior walls. They are typically two bays wide and comprise a split-X bracing system. The exterior cladding is composed of an insulated sheet steel wall that is supported by side girts and the exterior columns. Interior partitions are neglected for simplicity.

5.3 Design of the building

The building is designed for 5 locations in Western Canada that have the acceleration-related seismic zone, Z_a, equal to the velocity-related seismic zone, Z_v, as given in Table 5.1. The snow load at these locations is different in the 1995 edition of the NBCC (ACNBC 1995a) that was only available after this study had progressed considerably. A constant intensity of ground snow load, S_s, and rain snow load, S_r, is assumed for all zones so that its contribution to the effective seismic weight in each zone is the same. The base shear prescribed by the NBCC in each seismic zone is directly proportional to the product of the zonal velocity ratio, v, given in Table 5.1, and the seismic response factor, S, assuming that all other factors are invariant.

The roof dead load is taken as 0.95 kPa inclusive of structural steel. The gravity load resisting system given by Chien (1985) is found to be adequate. The seismic design assumes a strength braced frame (SBF) with tension-only bracing. Hence, a force modification factor, R, of 1.5 is used. This represents an ordinary steel frame where the detailing provisions in clause 27 of CSA Standard S16.1-94 (CSA 1994) need not be adopted. A large number of existing buildings fit into this category. A SBF may also qualify as a nominally ductile braced frame (NDBF) if the connections are detailed to resist the impact load from slender braces. Most CBFs are designed and detailed as NDBFs as the prescribed base shear is lower than that of SBFs and the ductility provisions of CSA Standard S16.1 (1989, 1994) can be satisfied relatively easily as compared to the more stringent requirements for ductile braced frames (DBFs).

The base shear specified by the NBCC is given by [2.8]. The importance factor, I, and the foundation factor, F, are both assumed equal to 1.0. The effective seismic weight, W, is estimated as 6710 kN, as given in Table 5.2, and is assumed to be the same in all 5 seismic zones. In the East-West (E-W) direction, about 82% of this weight is attributed to the roof diaphragm and the remainder to the CBFs and the cladding. An estimate of the fundamental period, T, is required to define the seismic response factor, S. The NBCC estimate of the fundamental period of a braced frame is given by [2.10]. For this CBF, h_n is 9 m, slightly less than the overall height, and D_s is 12 m in the E-W direction and 10.5 m in the North-South (N-S) direction. Thus, the period is 0.23 s in the E-W

direction and 0.25 s in the N-S direction. This places the building in the short period range ($T \leq 0.25$ s) and the S factor, shown in Fig. 2.2, is equal to 3.0 for both directions. Hence, the base shear from [2.8] is also the same in both directions. The analytically computed period of the building, verified by subsequent analyses, is significantly greater than 0.25 s in all the zones. In such an event, the NBCC allows a seismic base shear that is 0.80 times that obtained from [2.8] to be used. This base shear is reported in line 1 of Table 5.3 which gives the summary of building design in the E-W direction in each zone. The factored wind load on line 2, based on the 1 in 30 hourly wind pressure, is less than the base shear in all the zones.

The seismic load prescribed for design of the roof diaphragm is an in-plane uniformly distributed lateral load equal to the base shear. Using the plate girder analogy for the roof diaphragm design (CSSBI 1991, Davies and Bryan 1982), it is assumed that the diaphragm panels resist the shear force while the flange members resist the bending moment. The design involves selection of a metal deck profile of adequate thickness to resist gravity loads and lateral loads, provision of appropriate fasteners to transfer the lateral load, and design of the flange members. Details of the deck diaphragm and estimates of its shear stiffness and strength are given in lines 3 to 9 of Table 5.3. Both the CSSBI method (CSSBI 1991) and the European method (Davies and Bryan 1982) are used to assess the stiffness and strength of the diaphragm. The latter is a more rational method for seismic design of diaphragms as it accounts explicitly for the various failure modes and enables a designer to detail the diaphragm to fail in a ductile mode. The following hierarchy is assumed when greater shear capacity in the diaphragm is to be provided; (a) decrease seam fastener spacing, (b) provide sheet to purlin fasteners in every corrugation (7 per sheet width) instead of every other corrugation (4 per sheet width), and (c) increase the profile (sheet) thickness. The profile depth is assumed equal to 38 mm (1.5 inches) in all zones as is usual for roof decks that are not topped with concrete.

The shear force at the edge of the diaphragm is 'collected' by the collector element (a beam) and transferred to the braced bay. The collector element may also function as the flange member of the diaphragm for earthquake load acting in the N-S direction (Chien 1985). It may also support the entire weight of the exterior cladding [if

the latter is tied back to it by means of sag rods.] Hence, it is designed to resist these actions and those due to the tributary gravity loads acting on it. A W310x31 section is adequate in zones 1 to 4 and a W310x39 in zone 5.

For design of each CBF, one half the base shear is applied as a concentrated load at the top of the CBF and then the torsion provisions of the NBCC are applied. Although the building plan is symmetric, the centre of mass is positioned a distance equal to the 'accidental eccentricity' from the centre of stiffness. This accidental eccentricity is specified as 0.1 times the dimension of the building perpendicular to the direction of seismic load. The base shear is applied at this location and the equilibrating forces are found in the CBFs assuming the four of them to have equal lateral stiffness and assuming a rigid roof diaphragm. The base shear for the CBFs is increased by 12% and 8% in the E-W and N-S direction respectively, due to this accidental eccentricity. [Logically, the analyses should also account for accidental torsion as could be accomplished by scaling the earthquake records by the torsion increment. This was not done because (a) the torsion increment is based on a rigid roof diaphragm that does not reflect the true behaviour, and (b) when inelastic action occurs, the effect of a slightly larger earthquake would be essentially limited to increasing the ductility demand.] This amplified base shear is then applied at the top of each CBF and an approximate P-Δ analysis is carried out with the elastic drift amplified by the force modification factor, R (ACNBC 1995a). The factored base shear for each CBF, including increments for torsion and the P-Δ effect, is given in line 11 of Table 5.3, and is used for the design of the CBF and the collector element.

The computer program SODA (Acronym Software 1994) is used for structural design of the CBF. It produces a least weight design that satisfies the strength requirements of CSA (1989) and any additional user specified nodal displacement constraints. For structural design, a two-dimensional model of the CBF is used as shown in Fig. 5.2. Only the tension diagonal is physically modelled as it is assumed to resist the entire lateral load due to wind or earthquake. This is consistent with the detailing assumed for the R factor of 1.5 that is characterised by the absence of an adequate constraint on the effective slenderness ratio that would give the brace any significant compressive capacity. The braces are constrained to be hollow structural sections (HSS)

and their effective slenderness ratio, KL/r, is limited to 300, as is required for tension members by CSA Standard S16.1-94 (CSA 1994). The load combinations considered in design are as follows;

(a) 1.25 D + 1.5 L,

(b) 1.25 D + 1.5 W,

(c) 1.25 D + 0.7 (1.5 L + 1.5 W), and

(d) 1.0 D + 0.5 L + 1.0 E

where D, L, W, and E are the specified dead load, live load (including snow), wind load, and earthquake load, respectively. Load combination (d) governs the design of the braces and columns of the CBF in all the zones. The slenderness constraint is found to affect the brace selection in zone 1 only, resulting in a 14% excess in brace cross-sectional area provided over that required. In the other zones, the brace cross-sectional area provided is within 5% of that required. The KL/r ratio of the braces reduces with increasing base shear. This implies an increased compressive capacity of the brace. The estimate of CBF strength in line 12 of Table 5.3 assumes a resistance factor, ϕ, of 1.0 to obtain the most likely strength of the member. In addition, the compressive capacity of the brace is taken as only 25% of that found from CSA Standard S16.1-94 (CSA 1994), to account for the reduction in compressive resistance due to cyclic buckling, as discussed in section 3.2.2.

5.4 Stiffness and strength contribution of the cladding

The building is enclosed on all sides by an insulated sheet steel wall that is fixed to the exterior girts and columns. Lateral pressure due to wind is the governing load for these elements. The 1 in 30 hourly wind pressure is used for strength design and the 1 in 10 hourly wind pressure for the serviceability check on deflections. The influence of cladding is usually neglected in seismic analysis and design because such cladding is either too weak to resist any significant lateral load or is structurally isolated from the LLRS. However, it does contribute some stiffness and strength to the structure. This contribution may be particularly important in low-rise steel buildings (Sockalingam 1988). Hence, two bounding cases are considered in this work. The first assumes that the cladding is 'absent' and does not provide any stiffness and strength. The second assumes that it is 'present' and is effective. In both cases, the entire weight of the

cladding contributes to the effective seismic weight as it is suspended from the collector element.

A commercially available profile (Indal Metals 636M) is assumed for the sheet steel cladding. A typical cladding panel along the E-W exterior wall is shown in Fig. 5.3. The strength and stiffness of such a panel are estimated by the European method (Davies and Bryan 1982). The individual sheets are assumed to be attached to the girts (purlins) and not to the columns (rafters). The girts are assumed to be spaced equally along the panel height. The sheet to purlin fasteners are assumed to be self-tapping screws of 6.3 mm diameter and the seam fasteners are assumed to be self-tapping screws of 4.8 mm diameter. Davies and Bryan (1982) give the strength and stiffness characteristics of common connections in light gage metal structures. The lateral stiffness of each panel, as shown in Fig. 5.3, is estimated as 0.46 kN/mm and its shear strength is estimated as 19 kN. For the case with cladding present, these stiffness and strength contributions are added to those of the CBF to get the total value for the end wall in the E-W direction. As the same cladding system is assumed to be present in the building in all the 5 zones, its contribution of stiffness and strength is the same in all zones and decreases proportionately as those of the CBFs increase.

5.5 Estimate of static overstrength

The LLRS of the buildings designed by the above procedure have excess strength with respect to the prescribed base shear. This is typical for most buildings and is referred to as 'static overstrength' in this work. The static overstrength ratio, denoted by ρ_o, is defined as the ratio of the strength provided by the LLRS to that prescribed by the NBCC in [2.8].

Static overstrength of the diaphragm is largely due to the discrete spacing of seam fasteners, discrete number of sheet to purlin fasteners, and the sheet thickness itself. For the CBF, it is a product of several factors: (a) torsion increment due to the consideration of accidental torsion in design and not in analysis. One possible way to account for this would be to increase the earthquake records by this amount, (b) the overstrength due to use of resistance factor, ϕ (< 1.0), in the calculation of member resistance in design, (c) a discretisation factor due to the availability of sections in discrete sizes only that is itself

affected by considerations such as the allowable KL/r ratio and the P-Δ effect, (d) the small contribution of the compression diagonal in a tension-only CBF, and (e) the possible contribution of non-structural components.

Table 5.4 gives a summary of the strength provided and ρ_0 for the roof diaphragm and the CBF. The factored shear force for the diaphragm and the factored base shear for the CBF are one-half the base shear for the building given in line 1 of Table 5.3. The value of ρ_0 for the diaphragm reduces with an increase in seismic zone, as shown in Fig. 5.4. For the CBF, ρ_0 is calculated assuming the two cases of cladding absent and cladding present, to study the significance of the cladding contribution. The value of ρ_0 for the CBF with cladding absent is almost constant in all zones except zone 1 where the constraint on the KL/r ratio affects the brace design. The value of ρ_0 for the CBF with cladding present reduces with an increase in seismic zone. The difference between the curves for cladding absent and cladding present gives the contribution to the strength of the end wall by the cladding. The ratio of static overstrength of the diaphragm to the CBF is also given in Table 5.4 and shown in Fig. 5.5, and is of importance when studying the performance of a strong diaphragm-weak frame (SD-WF) design and its reverse. The diaphragm is stronger than the CBF (cladding absent case) in zones 1 and 2 only.

The capacity design approach has been recommended for design of roof and floor diaphragms by Tremblay and Stiemer (1996). In this approach, elements of the primary LLRS are chosen and suitably designed and detailed for energy dissipation in a severe earthquake. All other structural elements in the load path are then provided with adequate strength so that the chosen means of energy dissipation can be maintained. Use of this approach would require that the diaphragm be stronger than the CBF in all the zones. For the present designs, the diaphragms are weaker than the CBFs in zones 3, 4, and 5. Hence in a severe earthquake, the diaphragm would be expected to yield prior to the CBF in these zones.

Table 5.5 gives factors contributing to the static overstrength in the CBFs. The quantities designated "ratio a" and "ratio b" are obtained by taking the product of the contributing factors and are equal to ρ_o, without and with cladding for the CBF in Table 5.4. For example, for zone 1 the torsion increment is 1.12 for the E-W direction

while the overstrength due to the resistance factor, ϕ (= 0.9), is the inverse of it, $1/\phi$, and gives a more likely strength of the member. A brace cross-sectional area of 715 mm^2 is required to resist a base shear of 180 kN (1.12 x 161 kN). The discretisation factor of 1.26 is the ratio of the brace cross-sectional area provided to that required (903/715). The limit of 300 on the KL/r ratio and the increment due to the P-Δ effect influence the brace selection. The assumed post-buckling capacity of the compression brace (equal to 5 kN) increases the strength of the CBF by 2% (from 253 kN to 257 kN). The product of these factors is 1.60. On considering the cladding contribution, ρ_o increases to 2.78.

5.6 Structural models and assumptions

The static and dynamic analyses of the building are performed for earthquake ground motion in the E-W direction only. Three different structural idealizations are used to model the building. These idealizations differ in how the distributed mass and flexibility of the roof diaphragm are modelled. The models include; (a) a single degree of freedom elastic model (SDOFE), (b) a two-dimensional, multi-degree of freedom nonlinear model (MDOFN), and (c) a three-dimensional model (3-D).

The SDOFE model is the simplest idealization of the building and is used for free vibration analysis only. The roof diaphragm is assumed to be rigid and is represented by a single mass as shown in Fig. 5.6. Lateral stiffness is provided by the tension diagonal of the CBFs only. This linear model and does not account for the strength of the LLRS.

The two-dimensional model used for structural design with SODA is enhanced to obtain the MDOFN model, shown in Fig. 5.7. This model accounts for the nonlinear seismic behaviour of the CBF, the strength and stiffness contribution of the cladding, and the flexibility, strength, and distributed mass of the roof diaphragm. The CBF is modelled as a pin-connected truss. The lateral displacement of the nodes at the top of the CBF is constrained to be equal so that there is only one lateral degree of freedom. The cladding panels are modelled with panel or shell elements that have a calibrated thickness to give the required shear stiffness. They are attached in parallel to the CBF at the roof level. The diaphragm is modelled by an equivalent Timoshenko beam that is simply supported between the two end walls along the E-W direction (Tremblay and

Stiemer 1996). The flexural rigidity, EI, is based on the collector element that functions as the diaphragm flange member. The moment of inertia, I, is defined as

[5.1] $$I = 2 A_f (d/2)^2$$

where A_f is the cross-sectional area of the flange member and d is the width of the diaphragm (equal to 60 000 mm in the E-W direction). The shear rigidity of the beam, GA_s, is taken equal to that of the diaphragm. The shear area, A_s, is defined as

[5.2] $$A_s = G' d / G$$

where G′ is the shear stiffness of the diaphragm and G is the shear modulus. The flexural strength of the diaphragm is the product of the maximum axial capacity of the flange member and the diaphragm width, d. The former is obtained from a beam-column interaction equation as one of the flange members is subjected to axial compression due to the earthquake lateral load and bending due to tributary gravity loads acting on it. The flexural strength of the diaphragm is considered by specifying elastic-plastic rotational springs at the two ends of the beam elements. The translational mass of the diaphragm is lumped at nodes along the equivalent beam. Rotational inertia is neglected. The P-Δ effect is modelled with dummy columns that carry appropriate gravity load and are attached to the diaphragm and the CBF with rigid links. As this symmetric building is assumed to be subjected to in phase earthquake excitation at all support points, anti-symmetric modes of vibration of the roof diaphragm are not excited. Hence, only one half of the building is modelled as shown. The node at mid-span of the diaphragm is free to translate in the horizontal direction but is constrained against rotation because a zero slope is required at mid-span in all the symmetric modes. A total of 7 beam elements are used to model the half-span of the diaphragm. The adequacy of this idealization is discussed in the section on free vibration analysis.

A rigid-plastic link transfers the shear force from the diaphragm edge to the CBF. As a series connection is implied, the maximum force in this link will depend on the strength of the CBF and the diaphragm. The behaviour of the connections between the roof diaphragm and the CBF and those within the CBF itself are not modelled explicitly. The maximum force developed in the diaphragm and the braces will suggest the strength required of these connections. The idealized rigid-plastic link that connects the

diaphragm to the CBF does not represent the actual behaviour of such connections. Mazzolani *et al.* (1996) have shown that a typical diaphragm panel assembly, fastened with bolts to the external frame and with self drilling screws as seam fasteners, displays a slip type hysteresis loop. This occurs due to ovalization of the fastener holes and consequently force transfer occurs only when the fasteners bear against the sheet at the end of the holes. Welded connections, however, may demonstrate brittle behaviour under cyclic loading. The tension and compression yield level of the rigid-plastic link are set equal to the strength of the diaphragm. The maximum force that can be transferred from the diaphragm to the CBF is limited by the capacity of this link. This idealization permits an investigation of the effect of different strength levels of the diaphragm relative to the CBF.

The 3-D model is used for free vibration analysis only. The CBF is modelled with truss elements. The remaining framework is modelled with beam-column elements that have pinned ends. The roof diaphragm and the cladding panels are modelled with plane stress elements with an effective thickness equal to the ratio of the shear stiffness, G′, to the shear modulus, G. Translational masses are distributed in the plane of the roof diaphragm in both horizontal directions.

Table 5.6 summarises the modelling details used in each zone. The reduction factor for the CBF applies to the compressive resistance of the brace and is used to define its post-buckling capacity, P_{ync}. The reduction factors given in CSA Standard S16.1-94 (CSA 1994) were not used because they apply only to stockier braces.

5.7 Free vibration analysis

Table 5.7 summarises the fundamental period obtained from a free vibration analysis in the E-W direction. The design period specified by the NBCC is also given for comparison. All the models assume that only the tension diagonal contributes to the stiffness of the LLRS. For a given design, the SDOFE model that assumes a rigid roof diaphragm has a significantly lower period than that of the MDOFN and the 3-D models because of consideration of the distributed mass and flexibility of the diaphragm in the latter. There is a significant difference between the calculated fundamental period and the NBCC estimate. One might expect the SDOFE model that neglects diaphragm

flexibility to give a period close to that determined from the NBCC, but this is not the case. The ratio of the period by the SDOFE model (cladding present) to the NBCC estimate ranges from 4.56 in zone 1 to 2.43 in zone 5. Because the SDOFE model is the stiffest among the three considered, the period estimates from the other models will give higher ratios when compared with the NBCC estimate.

The stiffness contribution of the cladding may be evaluated by taking the ratio of the period of the cladding absent case to that of the cladding present case. For the SDOFE model, this results in a difference in period ranging from 26% in zone 1 to 7% in zone 5. A similar comparison for the MDOFN model gives a range from 15% in zone 1 to 3% in zone 5. This range is lower than that for the SDOFE model due to diaphragm flexibility. The cladding stiffens the end walls where the CBFs are present and does not stiffen the diaphragm. The diaphragm may be stiffened by interior partitions that are attached to it and are anchored to the floor below, but the contribution of such partitions is neglected in this work.

Because the MDOFN model is used extensively for nonlinear static and dynamic analyses, it is important to verify the adequacy of the model in representing the dynamic behaviour of the structure. The results of free vibration analysis are compared with those obtained from the more appropriate 3-D model of the building. Comparison is also made with a classical solution for a simple boundary condition.

Figure 5.8 illustrates the first, second, and third mode shapes obtained with the MDOFN model. Note that these are the first, third, and fifth mode shapes of the complete building. Figure 5.9 compares the period of the first three modes obtained with the MDOFN model (cladding present case) with those of the 3-D model that have corresponding mode shapes. The periods are in good agreement with a maximum difference of 5% for the first mode. This suggests that the two-dimensional MDOFN idealization is adequate for dynamic analysis of this symmetric building.

The frequency of the n th mode of vibration, ω_n, of a simply supported diaphragm is derived in Appendix E and is given by [E.19]. The results from [E.19] are compared with those obtained from a numerical beam model of the simply supported diaphragm that uses similar modelling techniques as the MDOFN model. The roof diaphragm of the building in zone 1 is considered as an example. The entire diaphragm is modelled with

14 beam elements with flexural and shear rigidity obtained from the parameters listed in Table 5.6. Table 5.8 compares the first five periods of the numerical beam model of the diaphragm with those obtained from [E.19]. The fundamental period is seen to be within 0.2% of the classical estimate and suggests that 7 beam elements are adequate to model a half-span of the diaphragm.

5.8 Analytical estimate of the building period

The NBCC estimate of the building period is empirical and does not account for diaphragm flexibility, stiffness of the CBFs, cladding, and interior partitions. Hence, a classical estimate of the period for such a building is derived from fundamental principles in Appendix E. The relevant equations are [E.19] and [E.21] to [E.26]. The classical estimate of the fundamental period is reported in line 7 of Table 5.7. The results are in good agreement with those from the MDOFN and the 3-D models.

5.9 Dynamic strength-to-demand ratio

When nonlinear dynamic time history analysis is used, a difference in strength demand may arise due to; (a) the difference between the code prescribed design period and the fundamental period of the analytical model used in analysis, and (b) the difference between the inelastic design spectrum and the average elastic response spectrum of the accelerograms used in analysis. The dynamic strength-to-demand ratio is defined as the ratio of the spectral ordinate obtained from the inelastic design spectrum at the prescribed design period to the spectral ordinate obtained from the average elastic response spectrum of the accelerograms at the analytical estimate of the fundamental period. The strength supplied is in accordance with the base shear per unit weight prescribed by the NBCC, given by

$$\frac{V}{W} = \left(\frac{v\,S\,I\,F\,U}{R} \right) \qquad [5.3]$$

The base shear per unit weight demand of the earthquake is

$$\frac{V}{W} = \left(\frac{S_a}{g} \right) \qquad [5.4]$$

where S_a is the spectral acceleration and g is the acceleration due to gravity. The dynamic strength-to-demand ratio is the ratio of [5.3] to [5.4]. Note that [5.3] is evaluated at the prescribed period and [5.4] at the analytical estimate of the fundamental period.

Consider the building in zone 1. Figure 5.10 shows the inelastic design spectrum defined by [5.3] and the mean + 1 sigma elastic response spectrum of the velocity set of accelerograms used for analysis in zone 1. The design period by the NBCC, from [2.10], is 0.23 s in the E-W direction. The S factor specified at this period is 3.0, but is reduced by a maximum of 20% because the analytical period (equal to 1.42 s from the MDOFN model in line 5 of Table 5.7) is greater than the design period. The base shear per unit weight from [5.3] is 0.048, and is marked as 'prescribed strength' in Fig. 5.10. The spectral ordinate of the elastic response spectrum at the analytical period of 1.42 s is 0.049. Thus, the dynamic strength-to-demand ratio is equal to 0.98.

5.10 Effective overstrength

The effective overstrength is a measure of the excess capacity provided to the LLRS with respect to the demand from the earthquakes used in the analysis. The latter is obtained from the average elastic response spectrum of an appropriate set of accelerograms selected for seismic analysis at a given location. The effective overstrength ratio is the product of the static overstrength ratio, ρ_o, and the dynamic strength-to-demand ratio, and is shown in Fig. 5.10.

Consider the building in zone 1. The value of ρ_o for the CBF with cladding present is 2.78, as given in Table 5.4. The dynamic strength-to-demand ratio is 0.98, as discussed in section 5.9. Hence, the effective overstrength ratio is 2.72. A value exceeding 1.0 suggests that the CBF is likely to have an elastic response in the earthquakes while a value less than 1.0 is indicative of inelastic response.

Figures 5.11 and 5.12 give the effective overstrength ratio for the diaphragm and the CBF in the 5 zones considered. As the dynamic strength-to-demand ratio depends on the response spectra of the accelerograms used, the results are presented separately for the acceleration and the velocity set in each zone. The mean + 1 sigma response spectrum of

the set of accelerograms is used to obtain the dynamic strength-to-demand ratio. The figures indicate that there is significant overstrength in seismic zones 1 and 2 and the response is likely to be elastic. The overstrength reduces with increase in seismic zone and is the least in zone 5. Yielding may occur in zones 3, 4, and 5 as the effective overstrength ratio is less than 1.0.

5.11 Response spectrum analysis

The NBCC recommends the use of a response spectrum analysis to determine the distribution of lateral forces in buildings that have irregularities in the distribution of mass or stiffness. In the single-storey building, there is a discontinuity in stiffness because the end wall containing the CBF and the cladding has significantly greater lateral stiffness than the roof diaphragm. Moreover, the flexibility of the diaphragm also affects the distribution of lateral forces. Hence, a response spectrum analysis is carried out with the MDOFN model. The NBCC design spectrum for locations with Z_a equal to Z_v is used, as shown in Fig. 2.1.

Figures 5.13 and 5.14 show the distribution of shear force along the half-span of the diaphragm for the MDOFN model with cladding absent and present, respectively. The co-ordinates along the half-span correspond to the 7 beam elements used to model it, with the CBF and the cladding located at the origin. The shear force is normalised with respect to the base shear developed. The flexibility of the roof diaphragm results in a nonlinear distribution of shear force with greater ordinates as compared to the linear distribution assumed in design. Diaphragms in zones 1 and 2 show greater deviation from the assumed linear distribution.

The nonlinear variation of shear force along the diaphragm has implications on the provision of shear strength. Diaphragms of small to moderate sizes are usually provided with the same details along the entire span, resulting in a uniform distribution of stiffness and strength. Large diaphragms may have a nonuniform distribution of strength. Figures 5.13 and 5.14 suggest that some caution needs to be exercised in reducing the shear strength along the diaphragm. The static overstrength of the diaphragm, as discussed in section 5.5, provides extra capacity and hence tends to mitigate this potential problem.

The ATC (1995) recommends that the total lateral load on the diaphragm, V, be distributed in a parabolic manner with an ordinate of 1.5 V/L at mid-span, where L is the span of the diaphragm. The resulting variation in shear force is cubic and is also plotted in Figs. 5.13 and 5.14. The distribution from response spectrum analysis is seen, for the first quarter-span of the diaphragm, to lie between that recommended by the ATC (1995) and the linear distribution assumed in design. The parabolic and linear distributions may therefore be considered as bounding cases for distribution of shear force in the quarter-span of the diaphragm near the supports.

5.12 Nonlinear static analysis

A nonlinear static analysis (NSA) of the building is performed to assess the behaviour under the prescribed lateral force and under displacements that might occur in the design earthquake. The MDOFN model described in section 5.6 is used. A bilinear elasto-plastic model is assumed for the braces with the buckling load equal to the post-buckling capacity, P_{ync}, given in Table 5.6. The cladding panels are modelled with an equivalent truss element because the program DRAIN-2DX (Powell 1993) does not have an inelastic panel element. Two lateral force profiles are used in analysis under the prescribed base shear given in Table 5.3. The first assumes a uniform distribution of base shear along the span of the diaphragm, as assumed in its design. The second corresponds to the average of the normalised shear force distribution obtained from response spectrum analysis, as shown in Figs. 5.13 and 5.14. The two lateral force profiles result in nodal displacements that differ by a maximum of 5%. The profile from response spectrum analysis results in greater displacements and is used for further study.

Figure 5.15 shows the drift under the prescribed lateral force for the case with cladding absent. The CBF and the cladding are located at co-ordinate zero on the graph. The compression diagonal buckles in all zones due to its low resistance. The drift in zone 2 is greater than that in the other zones because the diaphragm is marginally stiffer than that in zone 1 while the lateral force is twice as large.

The drift at mid-span of the diaphragm is next amplified by an arbitrary factor of 2.0 to force inelastic action in the building. This amplified drift is used as a target displacement for static 'pushover analysis', as discussed in section 4.4.3. Figure 5.16

shows the displaced shape of the diaphragm at this target displacement. In zones 1, 2, and 3, the braces of the CBF yield in tension at a base shear of 239 kN, 422 kN, and 650 kN, respectively, while the roof diaphragm remains elastic. In zones 4 and 5, the diaphragm yields in flexure at mid-span at a base shear of 769 kN and 1110 kN, respectively, while the CBF remains elastic. A comparison of shear strength of the diaphragm to the CBF, as shown in Fig. 5.5, suggests that this should be the case.

Figures 5.17 and 5.18 show results for the case with cladding present. The drift in Fig. 5.17 is less than that in Fig. 5.15 due to the stiffening of the end wall by the cladding. The compression diagonal buckles in all zones.

The target displacement for static 'pushover analysis' is assumed as 3 times the drift at mid-span. Figure 5.18 shows the displaced shape of the diaphragm at this target displacement. In zones 1 and 2, the CBF in the end wall containing the CBF and the cladding, yields at a base shear of 421 kN and 605 kN, respectively, while the diaphragm remains elastic. In zones 3, 4, and 5, the diaphragm yields in flexure at mid-span at a base shear of 768 kN, 771 kN, and 1110 kN, respectively.

The NSA suggests that in a severe earthquake, the diaphragm may yield prior to the end wall in zones 3, 4, and 5. An appropriate measure may be to strengthen the diaphragm so that the end wall yields first, resulting in a strong diaphragm-weak frame (SD-WF) design. Such a measure is not adopted herein as it is not mandatory in the current design philosophy for such buildings.

5.13 Nonlinear dynamic time history analyses

The MDOFN model of the building is used for nonlinear dynamic time history analysis with the program DRAIN-2D. The braces of the CBF are modelled with the EL9 buckling element described in Appendix C, with the parameters given in Table 5.6. The reduction factor applied to the compressive resistance of the brace to define its post-buckling strength, is assumed as 0.25 because the KL/r ratio exceeds 125 in all the zones. Experimental data by Jain *et al.* (1980) shown in Fig. 3.1 suggests that this value is appropriate. CSA Standard S16.1-94 (CSA 1994) recommends a larger reduction factor as given in Table 5.6. The cladding panels are modelled with the inelastic panel element of DRAIN-2D. This element has shear stiffness only and may be specified to fail

in a brittle manner. A bilinear hysteresis behaviour is assumed with the failure deformation equal to twice the yield deformation. The latter is about 42 mm and is greater than that required to yield the braces in the CBF. Hence, brace yielding will always precede yielding of the cladding panels. All analyses are carried out with an integration time step of 0.001 s. Rayleigh damping is used with the constants chosen to obtain 3% and 5% damping in the first and second mode, respectively. The P-Δ effect is considered in all analyses.

Earthquake accelerograms for analysis in each seismic zone are listed in Tables 4.1 to 4.10. The accelerograms of the 'acceleration set' have their PGA scaled to match the zonal PHA, while the accelerograms of the 'velocity set' have their PGV scaled to match the zonal PHV. The structure is analysed with each accelerogram and the peak value of the response parameters of interest is recorded. The mean value, μ, mean + 1 sigma value, $\mu + 1\ \sigma$, and the maximum value of the peak responses for each set of accelerograms is calculated.

A response level has to be selected for evaluating the dynamic response of the structure with the acceptance criteria for the life safety level given in Table 4.13. The elastic design spectrum for the 1 in 475 year design earthquake is defined by the product v S, where v is the zonal velocity ratio and S is the seismic response factor. The response level may be selected such that the response spectrum of the accelerograms used in analysis is compatible with the elastic design spectrum, in the period range of interest.

Consider the building in zone 1. The fundamental period from the MDOFN model in Table 5.7 is 1.42 s with the cladding present, and 1.63 s with the cladding absent. In the period range from 1.4 s to 1.6 s in Fig. 4.1, the $\mu + 1\ \sigma$ response spectrum of the acceleration set of records is closest to the NBCC design spectrum. Similarly, in Fig. 4.2, the maximum response spectrum of the velocity set of records is closest to the NBCC design spectrum. Hence, these response levels are selected to evaluate the dynamic response of the building. Similar comparisons are carried out for each set of accelerograms in all 5 zones and the appropriate response levels are given in Table 5.9.

The dynamic response of the building in zones 1 to 5 is reported in Tables 5.10 to 5.14, respectively. Results for the two cases of cladding absent and cladding present are

reported in each table. The 'A-set' and 'V-set' refer to the acceleration set and velocity set of accelerograms, respectively, that are used for analysis in each zone. The 'number of records' gives the total number of accelerograms used in each set. The 'CBF drift' refers to the lateral drift at the top of the CBF that is expressed as a percentage of the height, h_n. Similarly, the 'Roof drift' refers to the lateral drift at the mid-span of the diaphragm that is expressed as a percentage of the height, h_n. The column and brace response ratios are the ratio of the maximum axial force in these elements to their nominal capacity. The ductility demand in the brace is its maximum extension in tension divided by its yield elongation. The 'number of records with yielding (or buckling)' gives the number of accelerograms within the set in which yielding (or buckling) of the braces occurs. The cladding response ratio is the ratio of the shear force developed in the cladding panel to its shear capacity. The bending response ratio is the ratio of the bending moment developed in the diaphragm to its yield moment given in Table 5.6. The shear force response ratio is the ratio of the shear force developed in the diaphragm to its shear strength given in Table 5.4. The base shear response ratio is the ratio of the base shear developed to the strength provided by the CBF given in Table 5.4. The dynamic response in each zone is discussed briefly in the following sections.

5.13.1 Response in zone 1 (Kamloops)

Table 5.10 presents the summary of dynamic response in zone 1. The $\mu + 1\,\sigma$ response level is used to evaluate the response of the acceleration set, as given in Table 5.9. For the acceleration set with cladding absent, the $\mu + 1\,\sigma$ drift of the CBF is 0.28% while that of the roof is 0.51%, and is considerably less than the 1% limit in Table 4.13. The column response ratio is 0.49. The braces do not yield in tension as indicated both by brace response ratios and ductility demands less than 1.0. They do however buckle in compression in almost all records due to their low compressive resistance. The maximum brace response ratio and maximum ductility demand, even though the braces are responding elastically in tension, are different because of the nonlinear behaviour of the Jain and Goel hysteresis model. The bending and shear force response ratios of the diaphragm indicate elastic response. The $\mu + 1\,\sigma$ base shear

response ratio is 0.77. With the cladding present, the $\mu + 1\ \sigma$ drift of the CBF reduces from 0.28% to 0.22% while that of the roof from 0.51% to 0.50%. The response ratio for the columns, braces, and the base shear reduces while the bending and shear force response ratios of the diaphragm increase. The cladding panels remain elastic.

The response of the velocity set is evaluated at the maximum level and is qualitatively similar to that of the acceleration set. In summary, the response in zone 1 is elastic. The slender braces buckle in compression but do not yield in tension with a maximum ductility demand of 0.9 in the acceleration set with cladding absent. The response of the roof diaphragm and the cladding is also elastic. Damage may initiate in the non-structural interior partitions that are not isolated from the roof diaphragm as the drift exceeds 0.25%.

5.13.2 Response in zone 2 (Princeton)

Table 5.11 presents the summary of dynamic response in zone 2. The maximum response level is used to evaluate the dynamic response of both the acceleration set and the velocity set. For the acceleration set with cladding absent, the maximum drift of the roof is 0.88% and is less than the 1% limit. The column response ratio has a maximum value of 0.93. The braces yield in tension in only one record with a maximum ductility demand of 1.2, and buckle in compression extensively. The bending and shear force response ratios of the diaphragm indicate elastic response. The maximum base shear response ratio of 1.0 is developed in the same record that causes yielding of the brace. With the cladding present, the response ratios of the CBF reduce while those of the diaphragm increase. The cladding panels remain elastic.

The response of the velocity set is similar qualitatively with the exception that the braces do not yield in tension. In summary, the response in zone 2 is largely elastic. The braces yield in just one record with a maximum ductility demand of 1.2. Non-structural interior partitions that are not isolated from the roof diaphragm may suffer some damage.

5.13.3 Response in zone 3 (Hope)

Table 5.12 presents the summary of dynamic response in zone 3. The maximum response level is used to evaluate the dynamic response of the acceleration set. For the

acceleration set with cladding absent, the maximum drift of the roof is less than the 1% limit. The column response ratio has a maximum value of 0.74. The braces do not yield in tension but buckle in compression extensively. The bending and shear force response ratios of the diaphragm indicate elastic response. The base shear response ratio has a maximum value of 0.93. With the cladding present, the drift of the CBF reduces while that of the roof increases. The column and brace response ratios reduce marginally. The cladding panels remain elastic. The bending and shear capacity of the diaphragm are attained in one record with a maximum slip of 2 mm in the rigid-plastic link element between the diaphragm and the CBF.

The response of the velocity set is evaluated at the $\mu + 1\ \sigma$ level. The $\mu + 1\ \sigma$ drifts are greater than the maximum drifts of the acceleration set. The $\mu + 1\ \sigma$ response ratios for the CBF are almost the same as the maximum response ratios of the acceleration set. However, the braces do yield in 2 records with a maximum ductility demand of 1.8. The shear force response ratio also attains a value of 1.0 is one record. With the cladding present, the response of the CBF reduces while that of the diaphragm increases. The shear capacity of the diaphragm is attained in 2 records with a maximum slip of about 16 mm in the link. The cladding panels remain elastic.

In summary, the response in zone 3 shows limited inelastic action in the CBF and the roof diaphragm. The ratio of diaphragm to CBF strength, as shown in Fig. 5.5, is less than 1.0 for both cases of cladding absent and present. Hence, the diaphragm is expected to yield during severe ground motion. Non-structural interior partitions not isolated from the roof diaphragm may suffer significant damage.

5.13.4 Response in zone 4 (Vancouver)

Table 5.13 presents the summary of dynamic response in zone 4. The $\mu + 1\ \sigma$ response level is used to evaluate the response of both the acceleration set and the velocity set. For the acceleration set with cladding absent, the $\mu + 1\ \sigma$ drift of the CBF is 0.38% while that of the roof is 0.74%. The $\mu + 1\ \sigma$ response ratio for the column and the braces is 0.86 and 0.96, respectively. The braces yield in 3 records with a maximum ductility demand of 1.3, and buckle in compression extensively. The $\mu + 1\ \sigma$ response ratio for bending and shear in the diaphragm is 0.97 and 1.0, respectively, with the

bending capacity attained in 3 records and the shear capacity in 4 records. The maximum slip in the link is 25 mm. The base shear capacity is attained in the same 3 records that cause brace yielding. With the cladding present, the drift of the CBF reduces while that of the roof increases. The response ratio of the column, brace, and base shear reduces while those of the diaphragm increase. The braces do not yield and the cladding panels remain elastic. The maximum slip in the rigid-plastic link element increases from 25 mm to 35 mm.

The response of the velocity set is similar qualitatively. The braces yield in 3 records only when the cladding is considered absent, with a maximum ductility demand of 1.3. In summary, the response in zone 4 shows inelastic action in the CBF and the roof diaphragm. The maximum brace ductility demand of 1.3 may have been greater if the roof diaphragm response were elastic. The maximum slip of 35 mm in the link between the diaphragm and the CBF suggests severe deformation along the edge of the diaphragm. The ratio of diaphragm to CBF strength, as shown in Fig. 5.5, suggests that the diaphragm is expected to yield in severe ground motion as observed in this zone. Non-structural interior partitions not isolated from the roof diaphragm may be damaged beyond repair as the drift ratio exceeds 0.75%.

5.13.5 Response in zone 5 (Victoria)

Table 5.14 presents the summary of dynamic response in zone 5. The $\mu + 1\,\sigma$ response level is used to evaluate the response of the acceleration set. For the acceleration set with cladding absent, the $\mu + 1\,\sigma$ drift of the CBF is 0.39% while that of the roof is 1%. The $\mu + 1\,\sigma$ response ratio for the column and the brace is 0.68 and 0.87, respectively. The braces yield in 2 records with a maximum ductility demand of 1.4, and buckle in compression extensively. The response ratios of the roof diaphragm suggest significant inelastic action in about half the records. The base shear capacity is attained in the same records that cause brace yielding. With the cladding present, the drift of the CBF reduces while that of the roof increases. The response ratio for the column, brace, and base shear reduces marginally while those of the diaphragm increase. The maximum brace ductility demand reduces from 1.4 to 1.0. The cladding panels remain elastic.

The response of the velocity set is evaluated at the μ level and is similar qualitatively to that of the acceleration set. The braces yield in 2 records with a maximum ductility demand of 1.7 when the cladding is absent. The bending capacity of the roof diaphragm is attained in 6 of the 7 records. This results in large maximum drifts for the roof that exceed the 1% limit in Table 4.13 and marginally exceed the 2% drift limit in the NBCC.

In summary, the response in zone 5 shows some inelastic action in the CBF and extensive inelastic action in the roof diaphragm. The deformation of the diaphragm suggests severe damage to it. Non-structural interior partitions not isolated from the roof diaphragm may be damaged beyond repair because of excessive drift.

5.14 Estimate of lateral drift

Figure 5.19 shows the $\mu + 1\,\sigma$ drift of the CBF and the mid-span of the roof diaphragm, and the maximum drift of the roof diaphragm obtained from time history dynamic analyses for the case with cladding absent. Two interpretations of the NBCC estimate of the total inelastic drift given by [2.15] are also shown. The $\mu + 1\,\sigma$ drift shown is the greater of that obtained from the acceleration set and the velocity set in each zone. Because the lateral stiffness of the CBF is considerably greater than that of the diaphragm, the two variations of [2.15] investigated are

[5.5] $$\delta_i = R\,\delta_{CBF} + (\delta_{Roof} - \delta_{CBF})$$

[5.6] $$\delta_i = R\,\delta_{Roof}$$

where δ_{CBF} and δ_{Roof} are the lateral drift of the CBF and the mid-span of the roof diaphragm, respectively. In [5.5], the R factor is applied to the drift of the CBF only, while in [5.6] it is applied to the total drift. The elastic drifts intended for use in [2.15] are obtained from nonlinear static analysis (NSA) of the building under the prescribed lateral force. Referring to Table 5.9, the maximum response level is selected to evaluate the response in zones 1, 2, and 3, and the $\mu + 1\,\sigma$ response level in zones 4 and 5. In zones 1 and 2, the drift from [5.5] and [5.6] bound the maximum drift of the roof, while in zone 3, the maximum drift of the roof is marginally greater. In zone 4, the drift from [5.5] and [5.6] bounds the $\mu + 1\,\sigma$ drift of the roof, while in zone 5 the $\mu + 1\,\sigma$ drift of the

roof is greater because of inelastic action in the diaphragm. The maximum drift of the roof is less than the 1% limit of the ATC (1995) in zones 1 to 4, and is less than the 2% limit of the NBCC in all the zones. The $\mu + 1\ \sigma$ drift of the CBF is less than 0.5% in all the zones.

Figure 5.20 presents data for the case with cladding present that shows a similar trend. Nonlinear response of the roof diaphragm in zones 3, 4, and 5 results in the maximum roof drift being greater than the estimate from [5.6]. The maximum drift of the roof is less than the 1% limit of the ATC (1995) in zones 1 to 4, and is marginally greater than the 2% limit of the NBCC in zone 5 only.

Thus, [5.5] and [5.6] provide a reasonable estimate of the maximum drift when the diaphragm response is elastic. Although the maximum drift exceeds these estimates when the diaphragm response is inelastic, it is still within the 2% limit.

5.15 Brace ductility demand in tension

Figure 5.21 shows the brace ductility demand in tension at the maximum and the $\mu + 1\ \sigma$ response levels. The maximum response level is used to evaluate the response in zones 1, 2, and 3. With the cladding absent, the maximum ductility demand exceeds the 'rule of thumb' limit of 1.5 (the R factor for a SBF) in zone 3 only. In zones 4 and 5, the $\mu + 1\ \sigma$ ductility demand is also less than 1.5. With the cladding present, the ductility demand is reduced significantly in all zones with no value exceeding 1.5. Although the presence of the cladding results in additional stiffness to the end wall, it does provide some strength to the end wall and shares the lateral load with the CBF. Consequently, the ductility demand on the braces is reduced. Examination of the time history output of the braces that yield in tension reveals that the maximum number of times a particular brace yields in a given earthquake record is limited to 3. The maximum strain rate in the brace just prior to tension yield is 25×10^{-3}/s. Filiatrault and Tremblay (1996) have reported strain rate demand on slender braces between 10×10^{-3}/s to 40×10^{-3}/s from shake table tests on tension-only CBFs.

5.16 Design of CBF connections

It is implicitly assumed in dynamic analyses that the connections of the CBF are strong enough to transfer whatever force is developed. In practice, a designer has the following options; (a) design the connection for the factored load prescribed by the NBCC, and (b) design the connection so that it can develop the tensile strength of the brace member. Option (b) is recommended in high seismic zones and in the capacity design approach (Feeney and Clifton 1995). The adequacy of both these options is discussed with respect to the results obtained from dynamic analyses.

Consider the design of the CBF connections for the building in zone 1. Line 11 of Table 5.3 gives a factored base shear of 195 kN for design of each CBF, resulting in a factored load of 244 kN (equal to 195/cos θ) for connection design. Assuming a resistance factor of 1.0 to obtain the most likely strength of the member, the tensile capacity of the brace is 316 kN. Hence, the factored load for design of the connection by option (a), normalised with respect to the tensile capacity of the brace, is 0.77 (equal to 244/316). For the acceleration set with cladding absent, the maximum and $\mu + 1\ \sigma$ brace response ratio in tension is 0.90 and 0.77, respectively, as given in Table 5.10. These values are divided by the connection design force by option (a) and are shown in Fig. 5.22 by curves labelled 'maximum' and 'mean + 1 sigma,' respectively. Also shown in the figure is the weld overstrength ratio that is simply the inverse of the weld resistance factor of 0.67 used by CSA Standard S16.1-94 (CSA 1994). The latter is intended to ensure failure in the member and not in the weld. It is evident from Fig. 5.22 that the maximum and the $\mu + 1\ \sigma$ brace force developed are greater than the factored load from option (a) in almost all zones. This reduces the margin of safety for the weld that is implicit in the resistance factor used for its design. A similar figure could be drawn comparing the brace response force to the net section resistance of a bolted connection.

Filiatrault and Tremblay (1996) report that an increase in brace yield force in tension-only CBFs occurs because of an increase in yield strength of steel under high strain rates. This has the potential of reducing further the margin of safety provided to the connection. The increase in yield strength of steel with strain rate may be estimated by the following expression (Wakabayashi *et al.* 1984):

[5.7] $$\frac{F_{Yd}}{F_{Ys}} = 1 + 0.0473 \log_{10}\left(\frac{\dot{\varepsilon}}{\dot{\varepsilon}_o}\right)$$

where F_{Yd} is the dynamic yield strength for a strain rate $\dot{\varepsilon}$ and F_{Ys} is the quasi-static yield strength at a strain rate $\dot{\varepsilon}_o$ of 50×10^{-6}/s. Using [5.7] with the maximum strain rate of 25×10^{-3}/s obtained from dynamic analyses, gives an increase in the yield strength of about 13%. Thus, the brace yield force is expected to increase by this amount. The same increase may not apply to the connection if its failure mode is brittle or is based on the tensile strength of steel that does not increase as much with strain rate as the yield strength does.

Consider the building in zone 5 where some instances of brace yielding occur. The ratio of the maximum brace response force to the connection design force is 1.13, as shown in Fig. 5.22. Multiplying this factor by 1.13 to account for the increase in yield strength of steel for a strain rate demand of 25×10^{-3}/s, results in a factor of 1.28. This reduces the margin of safety provided to the connection. Further, a comparison of brace cross-sectional area required (line 13 in Table 5.3) with that provided (line 15) indicates that braces in zones 2 to 5 have little overstrength with respect to the design requirement. Hence, it appears rational to design the connections to develop the tensile strength of the brace member. For braces that have significant overstrength with respect to the design requirement, special studies may be carried out to arrive at an appropriate design force for the connections.

5.17 Capacity design approach for roof diaphragm

The seismic performance of the building in zones 3, 4, and 5 may be improved by implementing the capacity design approach. This will require a strong diaphragm-weak frame (SD-WF) design where the diaphragm has greater shear capacity than the strength of the CBF. A designer may use a force modification factor, R, of 1.5, 2, or 3 for design of the CBF when a SBF, NDBF, and DBF, are used respectively. While the design base shear reduces with a greater R factor, the ductility provisions of Clause 27 of CSA Standard S16.1-94 (CSA 1994) place restrictions on the brace cross section selected for use. This affects the lateral load design significantly.

Consider the design of the building in Victoria (zone 5). The capacity design force for the roof diaphragm for each of the three categories of CBFs is given in Table 5.15. The lateral load capacity of the pair of CBFs is seen to be greater than the base shear for the building and the lateral force for design of the diaphragm, V_p. To implement the SD-WF approach for the SBF designed with a R factor of 1.5 will require the ratio of diaphragm strength to the prescribed shear (equal to 966 kN) of 1.4. For a NDBF, this ratio reduces to 1.3 because of the greater R factor and detailing requirements that are easy to satisfy. However, for a DBF which is supposed to be the superior CBF in terms of energy dissipation capability, this ratio is equal to 4.7 and is rather high due to severe restrictions on the brace member by CSA Standard S16.1-94 (CSA 1994). This will require the use of either a thicker deck diaphragm or horizontal bracing in the plane of the diaphragm to increase its shear resistance. In either case, the cost of the diaphragm is significantly increased and may render its use uneconomical as a lateral load transfer mechanism. An additional difficulty may arise due to the presence of non-structural elements in the plane of the vertical bracing. These elements have the potential of decreasing significantly the difference in strength between the diaphragm and the vertical bracing provided by the designer. This could transform a SD-WF design into the reverse if adequate reserve capacity is not provided. Hence, the SD-WF approach seems feasible (economically viable) for NDBFs and possibly SBFs but does not seem to be a viable alternative for DBFs.

An alternate approach for CBFs is to provide a ductile shear link between the roof diaphragm and the frame. This link is designed to have a yield capacity less than the shear strength of the diaphragm and the CBF. It will, in theory, isolate the roof diaphragm from the effects of severe ground motion and also limit the loads in the CBF.

The capacity design approach is illustrated with the SBF in zone 5 (Victoria). This requires a reversal in the design sequence to that previously adopted. The CBF is designed and detailed first. The roof diaphragm is then provided with adequate capacity in flexure and shear to ensure that in a severe event the CBF will yield prior to the roof diaphragm. The CBF is the same as used for zone 5 in Table 5.3. The base shear capacity of the CBF is 1340 kN. The diaphragm details are revised to provide it with a shear capacity greater than 1340 kN. The seam fastener spacing of 600 mm is reduced to

150 mm to result in a shear capacity of 1470 kN and a shear stiffness, G', of 19.5 kN/mm. The diaphragm is then provided with adequate capacity in flexure so that the shear strength is developed prior to its flexural strength. The capacity design force, V_c, of 2940 kN (2 times 1470 kN) is distributed over the span of the diaphragm. A parabolic distribution of load intensity is assumed with an ordinate of $1.5\ V_c/L$ at mid-span (ATC 1995), where L is the span of the diaphragm. This gives a bending moment of 34×10^6 kN mm at mid-span that is resisted by the flange member. The eave beams in the N-S direction function as the flange members of the diaphragm for earthquake loads acting in the E-W direction. They also act as the collector element for earthquake loads in the N-S direction. Hence, they are designed for the appropriate loads and a W250x58 section is selected instead of the W310x39 given in Table 5.3. The revised properties of the diaphragm are; shear stiffness, G', of 19.5 kN/mm (giving an equivalent shear area, A_s, of 15000 mm^2), moment of inertia, I, of 13.36×10^{12} mm^4, yield moment of 53.7×10^6 kN mm, and shear strength of 1470 kN. These properties are used for modelling the diaphragm. The strength and stiffness of the diaphragm are not varied along the span. Free vibration analysis with the MDOFN model gives a fundamental period of 0.72 s.

Table 5.16 presents the summary of the dynamic response obtained in zone 5 for the cladding absent case with the capacity design. In the following discussion, the results for the cladding absent case in Table 5.14 are compared with those in Table 5.16 to indicate the change in response. The maximum drift of the CBF increases from 0.62% in Table 5.14 to 0.73% in Table 5.16. The maximum drift of the roof reduces from 1.51% to 1.03%. While the maximum column response ratio is the same, the other response levels indicate an increase in response. The brace response increases with yielding in a greater number of records and the maximum ductility demand is about 2.0. The bending response is significantly different with totally elastic response for the capacity design as expected. The shear force response indicates almost elastic response for the capacity design with only one instance of yield. The base shear response is seen to increase indicating more severe response in the CBF.

Thus, the capacity design approach *does* protect the diaphragm from inelastic action that is now concentrated in the CBF. The maximum ductility demand of 2.0 is considered reasonable for the brace member. The connections of the CBF should develop the brace capacity in tension and compression. The increased cost of the capacity design arises from the close spacing of seam fasteners required to increase the shear strength of the diaphragm.

5.18 Conclusions and recommendations

Based on the analytical studies performed with the single-storey building in 5 seismic zones, conclusions and recommendations for seismic design of such buildings are developed as follows:

5.18.1 Estimate of period

The empirical estimate of the fundamental period of braced frames in the NBCC is unrealistic for buildings with flexible diaphragms and does not reflect the dynamic behaviour of the structure appropriately. The closed form analytical expression developed in this work accounts for all significant characteristics of such buildings and gives excellent results when compared with more elaborate numerical methods.

The consequence of adopting a significantly lower design period given by the NBCC estimate, as against a longer period from analytical models, is that the structure is provided with a greater base shear capacity. Although this gives greater safety to the structure, the use of expressions that do not reflect the dynamic characteristics of such buildings is considered inappropriate. Were the rational expressions developed here to be used, the base shear would be reduced. As for any structure, the ductility demands should be assessed.

5.18.2 Design of diaphragms

5.18.2.1 Distribution of lateral force

Figure 5.23 shows the envelope of maximum shear force and bending moment developed along one half-span of the diaphragm from time history dynamic analysis in zone 4 normalized to a maximum ordinate of 1.0. The variation of maximum shear force

along the span of the diaphragm is nonlinear as against the linear distribution usually assumed in design. The ATC (1995) recommends a parabolic distribution of distributed lateral force on the span with an ordinate of 1.5 V/L at mid-span, where V is the lateral force and L is the span. The resulting shear force distribution is shown in Fig. 5.23. The response envelope, in this case, suggests that even the ATC (1995) force distribution is unconservative.

5.18.2.2 Use of the capacity design approach

The inelastic response of the roof diaphragm obtained in zones 3, 4, and 5, may be considered unsatisfactory. Full scale experiments on typical diaphragm assemblies are needed to provide information on the allowable damage and possible remedial measures. The alternatives for improving the seismic performance are the capacity design approach or the use of ductile shear links to connect the diaphragm to the CBF. The former is a viable alternative for SBFs and NDBFs.

5.18.2.3 Lateral stiffness

Other things being equal, it is recommended that where a choice exists, a stiffer rather than more flexible diaphragm be used to control deformations.

5.18.3 Use of various analytical procedures in seismic design

A linear elastic static analysis of the structure is adequate for the equivalent lateral force procedure of the NBCC. The designer should identify the lateral load path clearly and provide the required strength to various elements along it. As the relative strength of elements in the load path is of utmost importance, a hierarchy in the provision of strength should be adopted so that the weakest component selected has a ductile failure mode.

A nonlinear static analysis (NSA) is a useful analytical technique when used in conjunction with a response spectrum analysis. The latter suggests the distribution of the lateral force (considering the dynamic characteristics of the structure) that may be used in a NSA to study the behaviour of the structure under amplified drifts and provide adequate strength to the components. In this study, the NSA suggested that the diaphragm would yield in a severe earthquake in seismic zones 3, 4, and 5. This is deduced from statics as

well because the load path is statically determinate. A NSA will be particularly useful for provision of strength and stiffness in buildings with redundancy in the load path.

5.18.4 Anticipated deformations of the structure

The NBCC amplifies the elastic deformations of the structure by the force modification factor, R, to give the anticipated deformations in the design earthquake. The two variations of this approach, given by [5.5] and [5.6], bound the maximum drift when the diaphragm response is elastic. Although the maximum drift exceeds these estimates when the diaphragm response is inelastic, it is still within the 2% limit of the NBCC. Hence, these expressions may be used to estimate the maximum deformation of the building.

5.18.5 Design of brace members

Dynamic analyses with the capacity design in zone 5 gives the maximum brace ductility demand in tension of 2.0, and a maximum number of 3 yield excursions. The response of the traditional design has lower demand on the CBF. The braces selected in all zones are class 1 HSS and should be capable of meeting this demand.

5.18.6 Design of connections

Connections of CBFs in all zones should be designed to develop the strength of the member in tension and compression. This study shows that it is possible to select braces that have a capacity within 5% of the design requirement. Dynamic response in all zones suggests that such braces may yield. Special studies are recommended to assess measures for braces that are several times stronger than the requirement.

5.18.7 Design of non-structural components

The exterior cladding makes a significant contribution to the lateral strength and stiffness relative to the CBF, and is particularly so in zones 1 and 2. The placement of non-structural elements in parallel (same vertical plane) with the CBF is worthwhile. The CBF has a high in-plane stiffness that limits its deformation and thus offers protection to non-structural elements from excessive drift. Non-structural partitions that do not lie in the same vertical plane as the CBF should be isolated from the roof diaphragm by

provision of appropriate connections. The drifts obtained exceed the damage threshold of 0.25% and in many instances exceed the failure limit of 0.75%. Hence, isolation appears to be a rational alternative. In the capacity design approach, the strength contribution of the non-structural components should be explicitly considered to ensure a strong diaphragm-weak frame design.

Table 5.1 Locations selected for study and environmental loads (NBCC 1990)

Location	Snow load (kPa) Actual*		Assumed*		Wind load (kPa)		Seismic zone		
	S_s	S_r	S_s	S_r	$q_{1/10}$	$q_{1/30}$	Z_a	Z_v	v
Kamloops	1.3	0.2	1.6	0.3	0.30	0.37	1	1	0.05
Princeton	1.8	0.5	1.6	0.3	0.24	0.32	2	2	0.10
Hope	2.5	0.3	1.6	0.3	0.41	0.55	3	3	0.15
Vancouver	1.6	0.2	1.6	0.3	0.45	0.55	4	4	0.20
Victoria	1.0	0.2	1.6	0.3	0.48	0.58	5	5	0.30

* The snow load at these locations is different in the NBCC 1995

Table 5.2 Estimate of effective seismic weight

Item	Load (kN)
Roof dead load (@ 0.95 kPa)	4190
25% roof snow load (@ 0.40 kPa)	1742
100% cladding weight (@ 0.25 kPa)	617
50% column weight	161
Total	**6710**

Table 5.3 Building design parameters in the East-West direction

Line	Parameter	Zone 1	Zone 2	Zone 3	Zone 4	Zone 5
1	base shear for building (kN)	322	644	966	1288	1932
2	factored wind load (kN)	280	242	417	417	439
	Roof diaphragm					
3	factored shear force (kN)	161	322	483	644	966
4	shear strength (kN)	377	582	630	681	1152
5	shear stiffness, G′ (kN/mm)	2.92	3.31	10.00	10.80	17.37
6	profile depth (mm)	38	38	38	38	38
7	profile thickness (mm)	0.76	0.76	0.76	0.91	1.22
8	number of sheet/purlin fasteners per sheet	4	4	7	7	7
9	seam fastener spacing (mm)	600	300	300	450	600
10	collector element	W310x31	W310x31	W310x31	W310x31	W310x39
	CBF					
11	factored base shear (kN)	195	377	558	739	1100
12	strength provided (kN)	257	444	666	864	1343
13	brace cross-section required (mm^2)	789	1502	2217	2932	4363
14	HSS brace used (class 1)	89x64x3	102x76x5	152x102x5	152x102x6	152x152x8
15	brace cross-section provided (mm^2)	903	1550	2280	2960	4430
16	effective slenderness ratio (KL/r)	294	250	181	185	128
17	column section used	W310x52	W310x52	W310x60	W310x67	W310x79

Table 5.4 Static overstrength ratio for roof diaphragm and CBF

Parameter	Zone 1	Zone 2	Zone 3	Zone 4	Zone 5
Roof diaphragm					
factored shear force (kN)	161	322	483	644	966
shear strength provided (kN)	377	582	630	681	1152
static overstrength ratio	2.34	1.81	1.30	1.06	1.19
CBF					
factored base shear (kN)	161	322	483	644	966
strength provided					
(a) cladding absent (kN)	257	444	666	864	1343
static overstrength ratio	1.60	1.38	1.38	1.34	1.39
(b) cladding present (kN)	447	634	856	1054	1533
static overstrength ratio	2.78	1.97	1.77	1.64	1.59
ratio of diaphragm/CBF strength					
(a) cladding absent	1.47	1.31	0.95	0.79	0.86
(b) cladding present	0.84	0.92	0.74	0.65	0.75

Table 5.5 Contributions to static overstrength in the CBF

Contributing factors	Zone 1	Zone 2	Zone 3	Zone 4	Zone 5
Torsion	1.12	1.12	1.12	1.12	1.12
Material resistance factor	1.11	1.11	1.11	1.11	1.11
Discrete size of brace member	1.26	1.08	1.06	1.04	1.03
Contribution of compression brace	1.02	1.02	1.04	1.04	1.08
ratio a, without cladding	1.60	1.38	1.38	1.34	1.39
Contribution from cladding	1.74	1.43	1.29	1.22	1.14
ratio b, with cladding	2.78	1.97	1.77	1.64	1.59

Table 5.6 Modelling details for buildings

Parameter	Zone 1	Zone 2	Zone 3	Zone 4	Zone 5
Roof diaphragm					
moment of inertia, I (mm^4 x 10^{12})	7.24	7.24	7.24	7.24	8.89
shear area, A_s (mm^2)	2246	2542	7682	8302	13352
equivalent thickness, t (mm)	0.037	0.042	0.128	0.138	0.222
yield moment (kN mm x 10^6)	15.67	15.67	15.67	15.67	22.32
CBF					
brace cross-sectional area (mm^2)	903	1550	2280	2960	4430
tension yield force, P_{yp} (kN)	316	543	798	1036	1551
compressive capacity, P_{yn} (kN)	21	49	135	170	504
reduction factor for P_{ync} (CSA 1994)	0.42	0.46	0.54	0.54	0.63
reduction factor used for P_{ync}	0.25	0.25	0.25	0.25	0.25
post-buckling capacity, P_{ync} (kN)	5	12	34	42	126
capacity of CBF (kN)	257	444	666	864	1343
Cladding (for 10 panels)					
stiffness contribution (kN/mm)	4.55	4.55	4.55	4.55	4.55
equivalent thickness, t (mm)	0.087	0.087	0.087	0.087	0.087
yield force (kN)	190	190	190	190	190

Table 5.7 Fundamental period from free vibration analysis in the E-W direction

Line	Model description	Zone 1	Zone 2	Zone 3	Zone 4	Zone 5
				Period (s)		
1	NBCC empirical estimate	0.23	0.23	0.23	0.23	0.23
2	SDOFE model rigid diaphragm cladding absent	1.32	1.01	0.83	0.73	0.60
3	SDOFE model rigid diaphragm cladding present	1.05	0.87	0.75	0.67	0.56
4	MDOFN model flexible diaphragm cladding absent	1.63	1.36	1.00	0.91	0.74
5	MDOFN model flexible diaphragm cladding present	1.42	1.27	0.93	0.86	0.72
6	Three dimensional model flexible diaphragm cladding present	1.49	1.33	0.97	0.90	0.75
7	Classical model flexible diaphragm cladding present	1.42	1.26	0.93	0.86	0.71

Note: All models assume a tension-only bracing system.

Table 5.8 Period of vibration of simply supported diaphragm

Mode number	1	2	3	4	5
Model			Period (s)		
(a) Classical model - [E.19]	1.11	0.54	0.36	0.27	0.21
(b) Numerical beam model	1.11	0.54	0.37	0.28	0.23
ratio b/a	1.00	1.01	1.02	1.03	1.05

Table 5.9 Response level for evaluating the time history dynamic response

Accelerogram set	Zone 1	Zone 2	Zone 3	Zone 4	Zone 5
Acceleration set	$\mu + 1\,\sigma$	max.	max.	$\mu + 1\,\sigma$	$\mu + 1\,\sigma$
Velocity set	max.	max.	$\mu + 1\,\sigma$	$\mu + 1\,\sigma$	μ

Table 5.10 Summary of dynamic response in zone 1 (Kamloops)

Response parameter	Response level	Cladding			
		Absent		Present	
		A-set	V-set	A-set	V-set
Number of records		8	9	8	9
CBF drift (%)	maximum	0.33	0.24	0.28	0.24
	$\mu+1\sigma$	0.28	0.17	0.22	0.15
	μ	0.16	0.11	0.12	0.10
Roof drift (%)	maximum	0.62	0.45	0.62	0.54
	$\mu+1\sigma$	0.51	0.32	0.50	0.36
	μ	0.30	0.22	0.28	0.24
Column response ratio	maximum	0.56	0.45	0.50	0.41
	$\mu+1\sigma$	0.49	0.36	0.42	0.31
	μ	0.35	0.29	0.30	0.25
Brace response ratio	maximum	0.90	0.66	0.77	0.69
	$\mu+1\sigma$	0.77	0.48	0.61	0.43
	μ	0.45	0.32	0.34	0.28
Ductility demand	maximum	0.88	0.62	0.73	0.64
No. of records with yielding		0	0	0	0
No. of records with buckling		7	9	7	9
Cladding response ratio	maximum	-	-	0.60	0.52
Roof diaphragm					
Bending response ratio	maximum	0.23	0.21	0.29	0.23
	$\mu+1\sigma$	0.20	0.15	0.25	0.16
	μ	0.13	0.11	0.15	0.12
No. of records with yielding		0	0	0	0
Shear force response ratio	maximum	0.55	0.40	0.70	0.62
	$\mu+1\sigma$	0.46	0.30	0.56	0.41
	μ	0.28	0.22	0.32	0.28
No. of records with yielding		0	0	0	0
Base shear response ratio	maximum	0.90	0.67	0.70	0.62
	$\mu+1\sigma$	0.77	0.49	0.56	0.39
	μ	0.46	0.33	0.32	0.26
No. of records with yielding		0	0	0	0

Table 5.11 Summary of dynamic response in zone 2 (Princeton)

Response parameter	Response level	Cladding			
		Absent		Present	
		A-set	V-set	A-set	V-set
Number of records		12	12	12	12
CBF drift (%)	maximum	0.44	0.28	0.28	0.23
	$\mu+1\sigma$	0.28	0.22	0.21	0.18
	μ	0.15	0.16	0.12	0.14
Roof drift (%)	maximum	0.88	0.62	0.68	0.65
	$\mu+1\sigma$	0.60	0.51	0.58	0.53
	μ	0.35	0.40	0.35	0.42
Column response ratio	maximum	0.93	0.74	0.75	0.65
	$\mu+1\sigma$	0.70	0.62	0.60	0.54
	μ	0.45	0.50	0.40	0.46
Brace response ratio	maximum	1.00	0.76	0.77	0.65
	$\mu+1\sigma$	0.70	0.60	0.57	0.50
	μ	0.39	0.45	0.33	0.40
Ductility demand	maximum	1.20	0.71	0.72	0.59
No. of records with yielding		1	0	0	0
No. of records with buckling		11	12	11	12
Cladding response ratio	maximum	-	-	0.60	0.49
Roof diaphragm					
Bending response ratio	maximum	0.55	0.41	0.52	0.48
	$\mu+1\sigma$	0.41	0.36	0.44	0.41
	μ	0.25	0.29	0.27	0.33
No. of records with yielding		0	0	0	0
Shear force response ratio	maximum	0.69	0.49	0.65	0.59
	$\mu+1\sigma$	0.48	0.42	0.52	0.48
	μ	0.29	0.33	0.32	0.38
No. of records with yielding		0	0	0	0
Base shear response ratio	maximum	1.00	0.76	0.72	0.61
	$\mu+1\sigma$	0.71	0.61	0.55	0.48
	μ	0.42	0.46	0.33	0.38
No. of records with yielding		1	0	0	0

Table 5.12 Summary of dynamic response in zone 3 (Hope)

Response parameter	Response level	Cladding			
		Absent		Present	
		A-set	V-set	A-set	V-set
Number of records		11	9	11	9
CBF drift (%)	maximum	0.35	0.65	0.34	0.40
	$\mu+1\sigma$	0.30	0.45	0.29	0.34
	μ	0.23	0.29	0.21	0.24
Roof drift (%)	maximum	0.53	0.95	0.65	0.80
	$\mu+1\sigma$	0.50	0.71	0.54	0.67
	μ	0.38	0.48	0.40	0.46
Column response ratio	maximum	0.74	0.80	0.73	0.80
	$\mu+1\sigma$	0.68	0.74	0.66	0.72
	μ	0.53	0.56	0.50	0.53
Brace response ratio	maximum	0.92	1.00	0.91	1.00
	$\mu+1\sigma$	0.83	0.91	0.81	0.89
	μ	0.62	0.66	0.58	0.63
Ductility demand	maximum	0.89	1.79	0.86	1.09
No. of records with yielding		0	2	0	2
No. of records with buckling		10	9	10	9
Cladding response ratio	maximum	-	-	0.73	0.87
Roof diaphragm					
Bending response ratio	maximum	0.84	0.90	1.00	0.97
	$\mu+1\sigma$	0.72	0.84	0.84	0.91
	μ	0.57	0.62	0.65	0.67
No. of records with yielding		0	0	1	0
Shear force response ratio	maximum	0.78	1.00	1.00	1.00
	$\mu+1\sigma$	0.74	0.92	0.88	0.98
	μ	0.59	0.68	0.67	0.72
No. of records with yielding		0	1	1	2
Slip in link (mm)	maximum	-	0	2	16
Base shear response ratio	maximum	0.93	1.00	0.87	0.97
	$\mu+1\sigma$	0.83	0.92	0.77	0.86
	μ	0.64	0.69	0.57	0.62
No. of records with yielding		0	2	0	0

Table 5.13 Summary of dynamic response in zone 4 (Vancouver)

Response parameter	Response level	Cladding			
		Absent		Present	
		A-set	V-set	A-set	V-set
Number of records		12	8	12	8
CBF drift (%)	maximum	0.43	0.47	0.36	0.36
	$\mu+1\sigma$	0.38	0.43	0.34	0.34
	μ	0.25	0.33	0.22	0.27
Roof drift (%)	maximum	0.93	0.97	0.96	0.85
	$\mu+1\sigma$	0.74	0.78	0.77	0.75
	μ	0.49	0.59	0.51	0.57
Column response ratio	maximum	0.90	0.90	0.85	0.85
	$\mu+1\sigma$	0.86	0.90	0.81	0.81
	μ	0.59	0.75	0.56	0.67
Brace response ratio	maximum	1.00	1.00	0.95	0.95
	$\mu+1\sigma$	0.96	1.01	0.89	0.90
	μ	0.63	0.82	0.59	0.73
Ductility demand	maximum	1.17	1.28	0.91	0.92
No. of records with yielding		3	3	0	0
No. of records with buckling		10	8	10	8
Cladding response ratio	maximum	-	-	0.78	0.78
Roof diaphragm					
Bending response ratio	maximum	1.00	1.00	1.00	1.00
	$\mu+1\sigma$	0.97	1.03	1.04	1.01
	μ	0.72	0.86	0.77	0.87
No. of records with yielding		3	3	3	3
Shear force response ratio	maximum	1.00	1.00	1.00	1.00
	$\mu+1\sigma$	1.00	1.02	1.05	1.04
	μ	0.73	0.86	0.78	0.88
No. of records with yielding		4	3	4	3
Slip in link (mm)	maximum	25	18	35	21
Base shear response ratio	maximum	1.00	1.00	0.92	0.92
	$\mu+1\sigma$	0.95	1.01	0.86	0.87
	μ	0.66	0.83	0.60	0.71
No. of records with yielding		3	3	0	0

Table 5.14 Summary of dynamic response in zone 5 (Victoria)

Response parameter	Response level	Cladding			
		Absent		Present	
		A-set	V-set	A-set	V-set
Number of records		12	7	12	7
CBF drift (%)	maximum	0.53	0.62	0.40	0.44
	$\mu+1\sigma$	0.39	0.48	0.33	0.39
	μ	0.24	0.35	0.21	0.30
Roof drift (%)	maximum	1.48	1.51	2.01	2.03
	$\mu+1\sigma$	1.00	1.12	1.19	1.37
	μ	0.60	0.78	0.67	0.86
Column response ratio	maximum	0.78	0.78	0.77	0.78
	$\mu+1\sigma$	0.68	0.78	0.66	0.74
	μ	0.45	0.64	0.44	0.60
Brace response ratio	maximum	1.00	1.00	1.00	1.00
	$\mu+1\sigma$	0.87	1.01	0.84	0.96
	μ	0.56	0.81	0.54	0.76
Ductility demand	maximum	1.43	1.70	1.00	1.21
No. of records with yielding		2	2	2	1
No. of records with buckling		7	7	7	7
Cladding response ratio	maximum	-	-	0.85	0.95
Roof diaphragm					
Bending response ratio	maximum	1.00	1.00	1.00	1.00
	$\mu+1\sigma$	1.01	1.03	1.02	1.01
	μ	0.82	0.98	0.84	0.99
No. of records with yielding		5	6	5	6
Shear force response ratio	maximum	1.00	1.00	1.00	1.00
	$\mu+1\sigma$	0.96	1.01	0.98	1.01
	μ	0.73	0.90	0.75	0.92
No. of records with yielding		3	2	3	3
Slip in link (mm)	maximum	5	1	6	17
Base shear response ratio	maximum	1.00	1.00	0.98	0.99
	$\mu+1\sigma$	0.90	1.00	0.85	0.94
	μ	0.64	0.86	0.60	0.79
No. of records with yielding		2	2	0	0

Table 5.15 Capacity design force for roof diaphragm

Parameter	Category of CBF		
	SBF	NDBF	DBF
Force modification factor, R	1.5	2.0	3.0
Base shear for building (kN)	1932	1449	966
$V_p = v\ I\ S_p\ W_p$ (kN)	1409	1409	1409
Brace selection ($F_Y = 350$ MPa)			
Factored base shear for each CBF (kN)	1082	812	541
Brace x-section required (mm^2)	4290	3218	2145
Allowable slenderness ratio	300	300	102
Minimum radius of gyration required (mm)	25.0	25.0	73.5
Square HSS brace selected (class H)	152x8	102x10	203x10
Brace x-section provided (mm^2)	4430	3280	7150
Tensile capacity of a brace with $\phi = 1.0$ (kN)	1551	1148	2503
Post-buckling capacity of brace with $\phi = 1.0$ (kN)	128	39	339
Lateral load capacity of the pair of CBFs (kN)	2688	1901	4551
Capacity design force for roof diaphragm (kN)	2688	1901	4551
Shear strength required of roof diaphragm (kN)	1343	950	2275
Ratio of capacity design force to base shear	1.39	1.31	4.71

Note: Allowable slenderness ratio for braces in a DBF $= 1900 / \sqrt{F_Y} = 102$

Table 5.16 Dynamic response with the capacity design in zone 5 (Victoria)

Response parameter	Response level	Cladding absent A-set	Cladding absent V-set
Number of records		12	7
CBF drift (%)	maximum	0.73	0.72
	$\mu+1\sigma$	0.49	0.60
	μ	0.29	0.44
Roof drift (%)	maximum	0.94	1.03
	$\mu+1\sigma$	0.74	0.89
	μ	0.51	0.71
Column response ratio	maximum	0.78	0.78
	$\mu+1\sigma$	0.73	0.83
	μ	0.50	0.69
Brace response ratio	maximum	1.00	1.00
	$\mu+1\sigma$	0.93	1.07
	μ	0.62	0.88
Ductility demand	maximum	1.99	1.98
No. of records with yielding		3	4
No. of records with buckling		8	7
Cladding response ratio	maximum	-	-
Roof diaphragm			
Bending response ratio	maximum	0.63	0.63
	$\mu+1\sigma$	0.53	0.57
	μ	0.41	0.50
No. of records with yielding		-	-
Shear force response ratio	maximum	1.00	0.86
	$\mu+1\sigma$	0.88	0.88
	μ	0.65	0.79
No. of records with yielding		1	-
Slip in link (mm)	maximum	0	-
Base shear response ratio	maximum	1.00	1.00
	$\mu+1\sigma$	0.95	1.05
	μ	0.69	0.91
No. of records with yielding		3	4

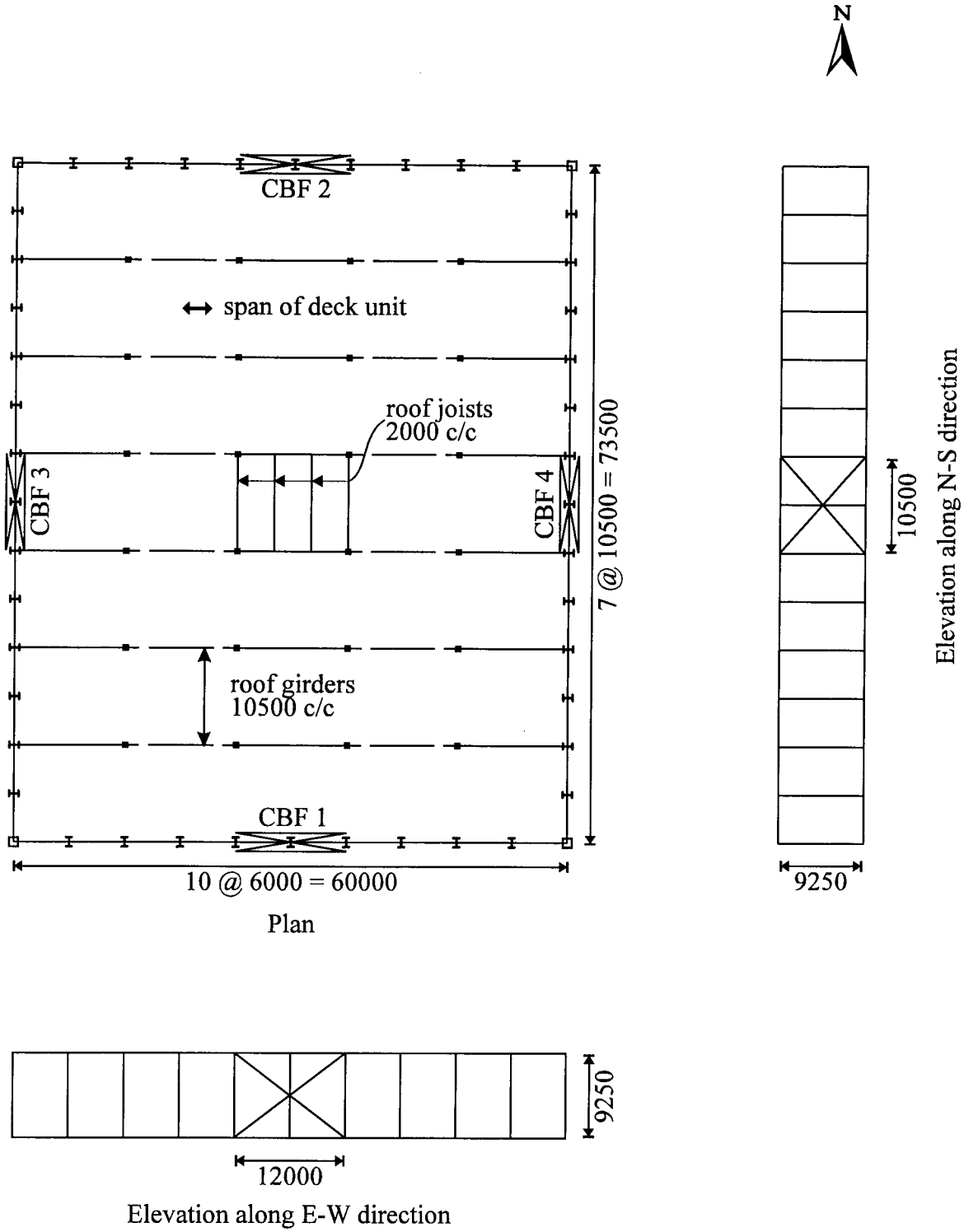

Figure 5.1 Layout of single-storey building

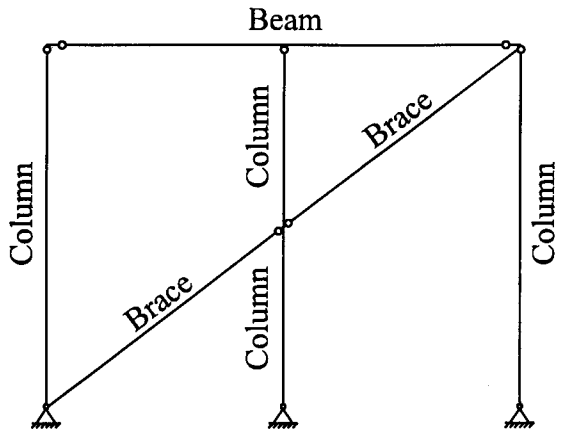

Figure 5.2 Model for design of the CBF

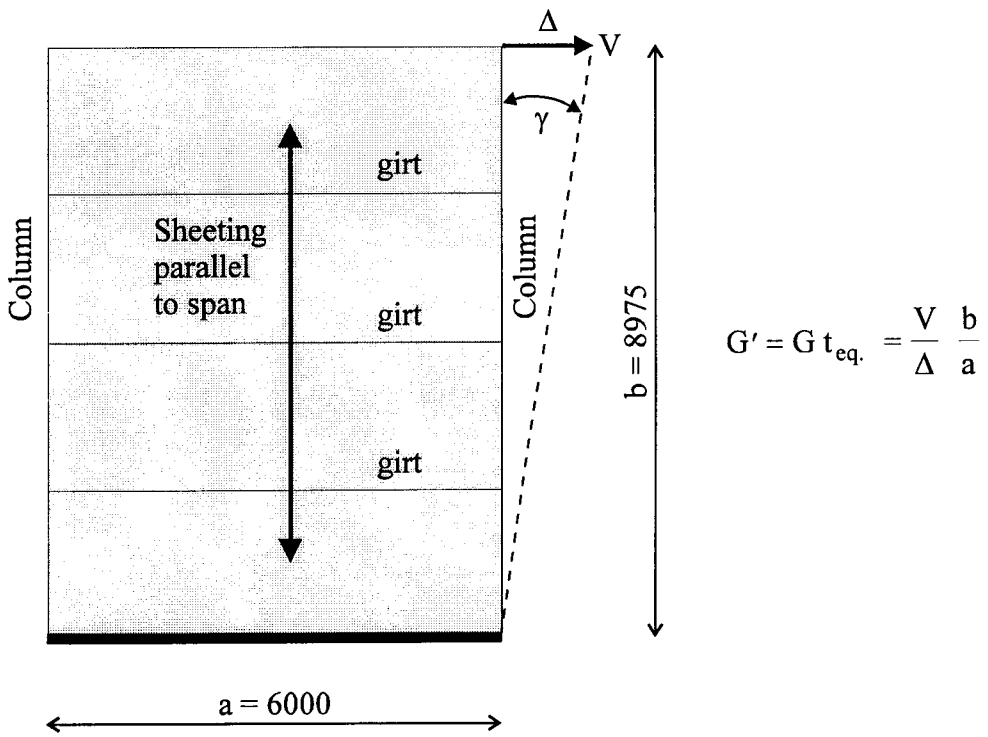

Figure 5.3 Typical cladding panel

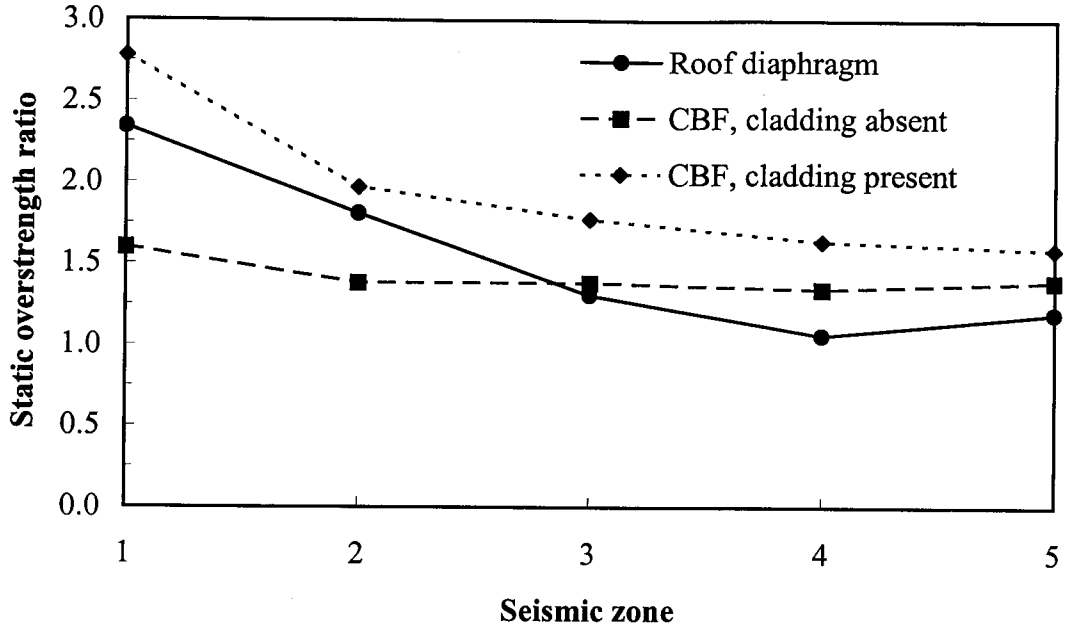

Figure 5.4 Static overstrength ratio for diaphragm and CBF

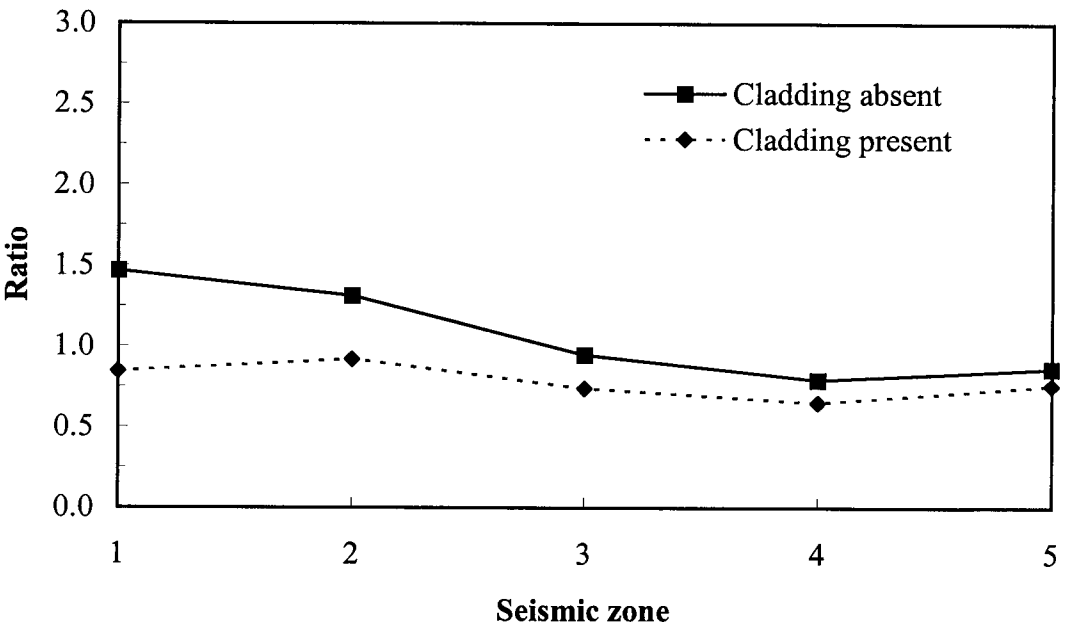

Figure 5.5 Ratio of diaphragm strength to CBF strength

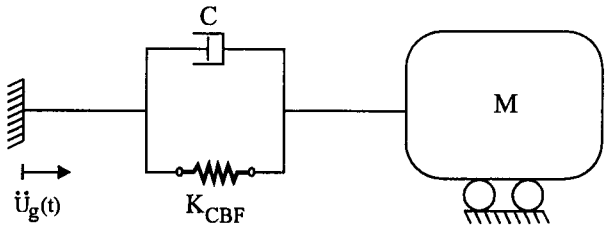

Figure 5.6 Single degree of freedom elastic model (SDOFE)

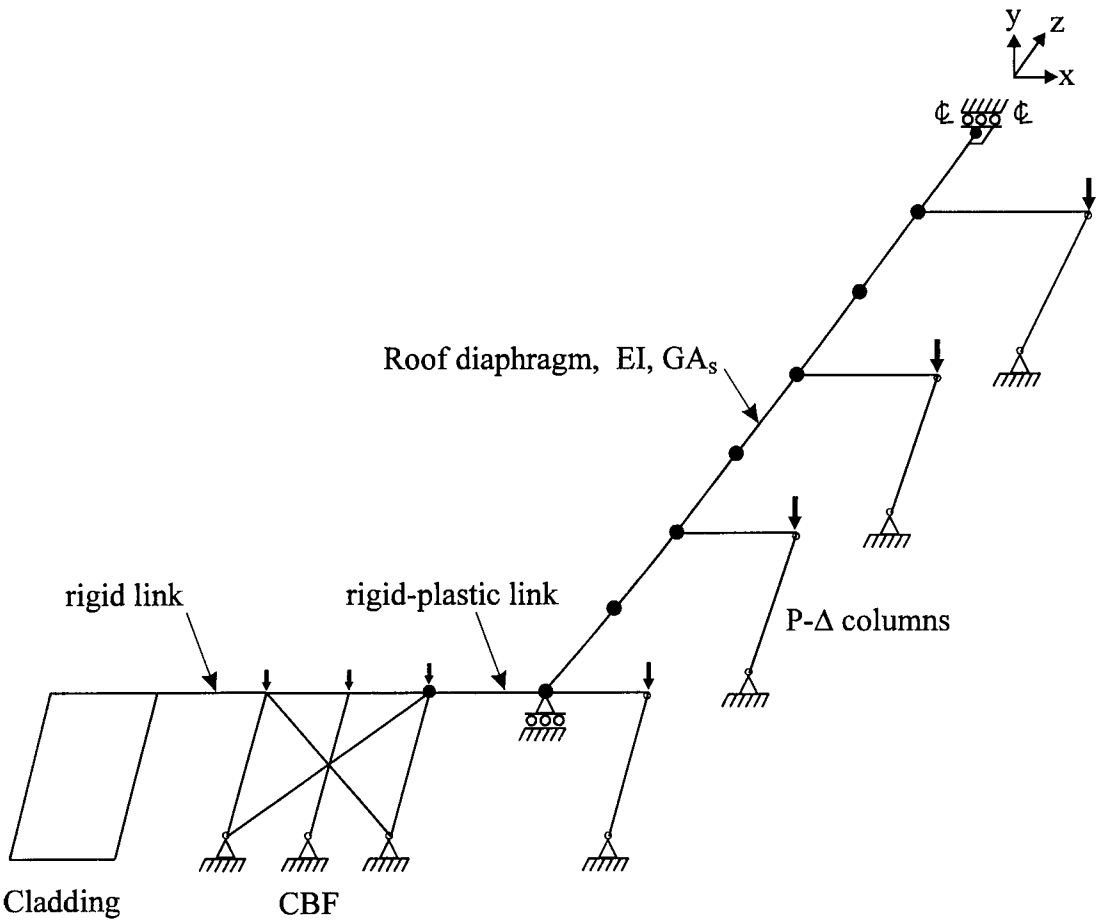

Figure 5.7 Multi-degree of freedom nonlinear model (MDOFN)

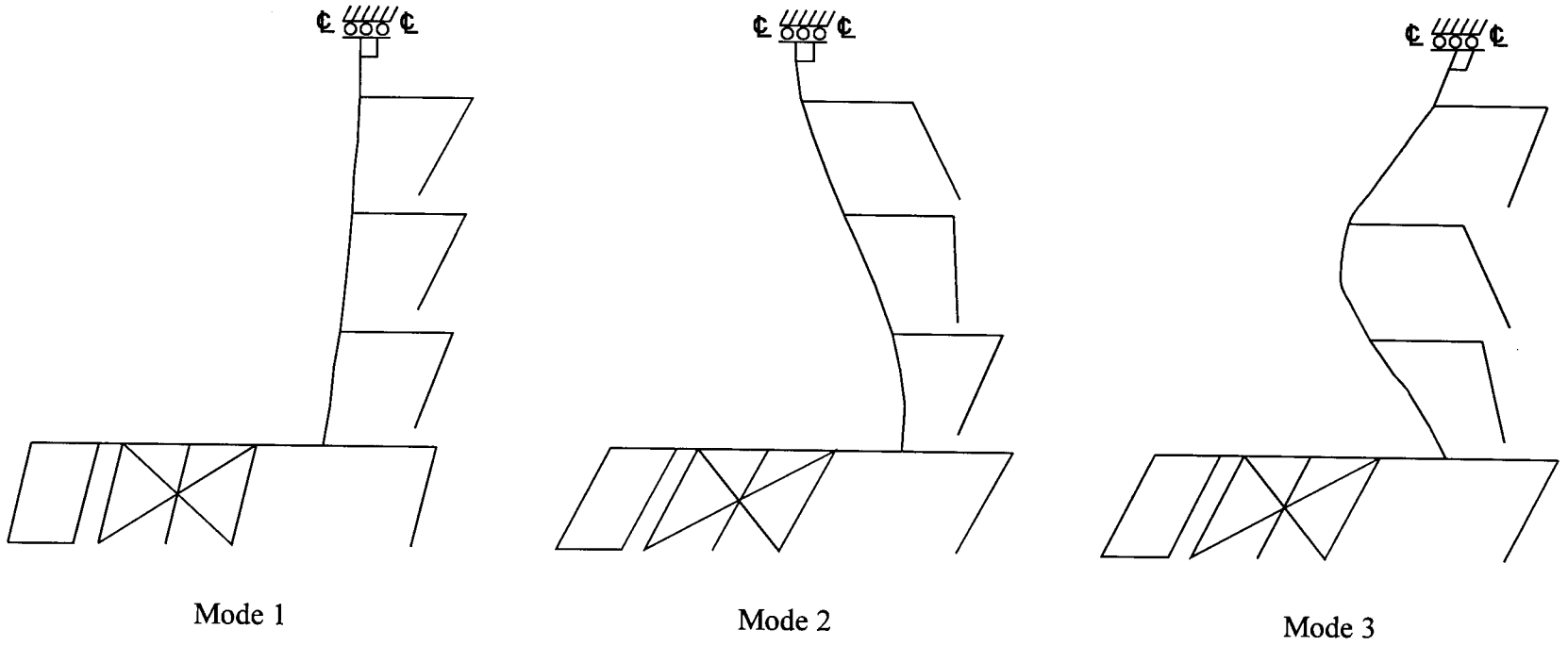

Figure 5.8 Mode shapes with the MDOFN model

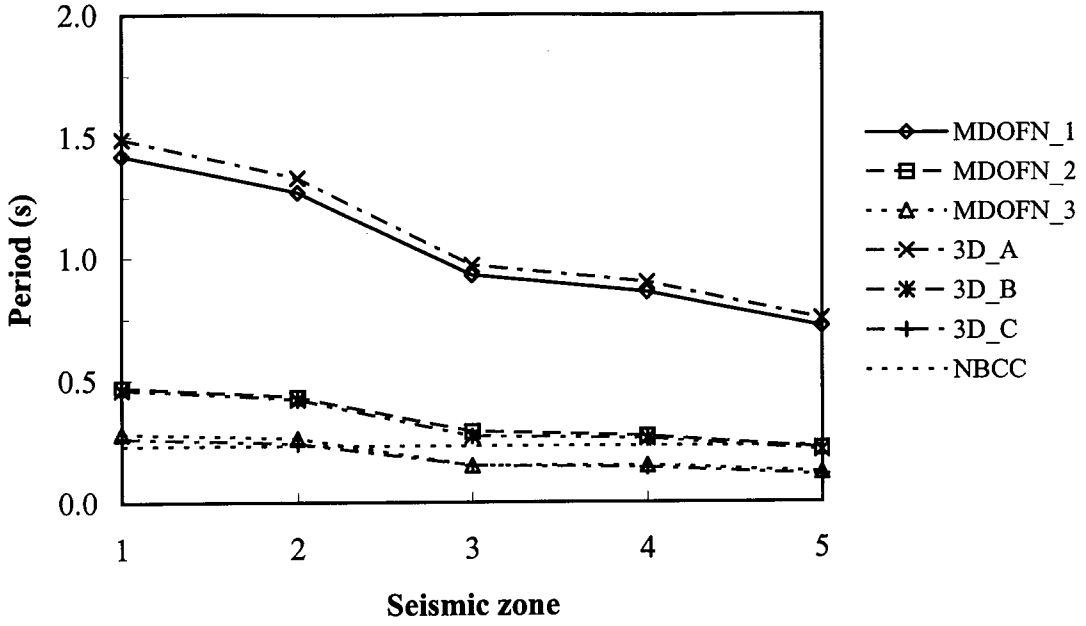

Figure 5.9 Comparison of periods: MDOFN model vs. 3-D model

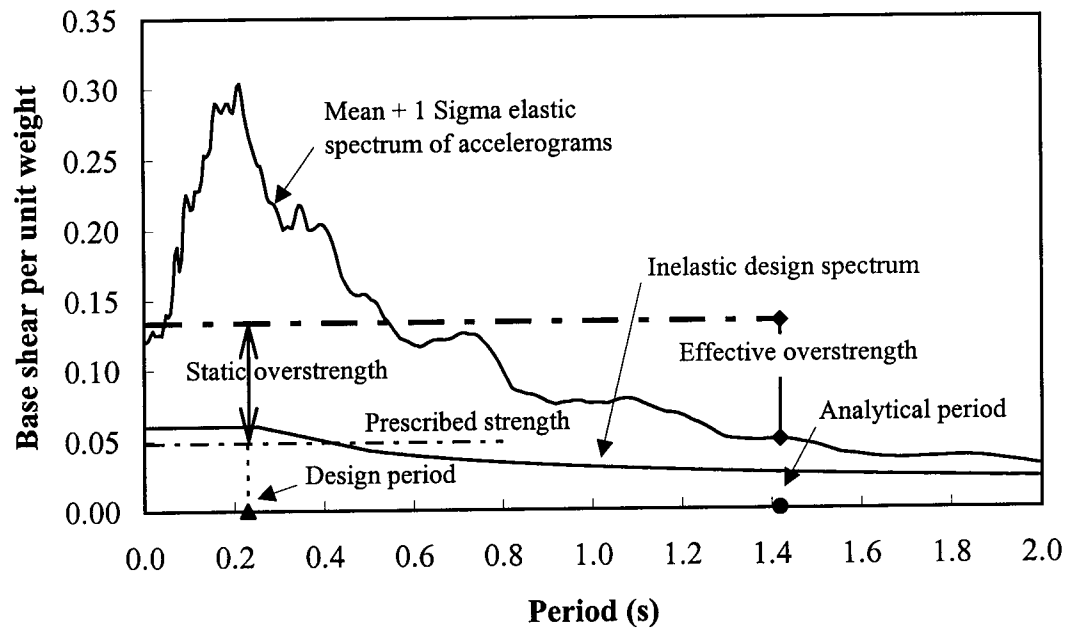

Figure 5.10 Static and effective overstrength

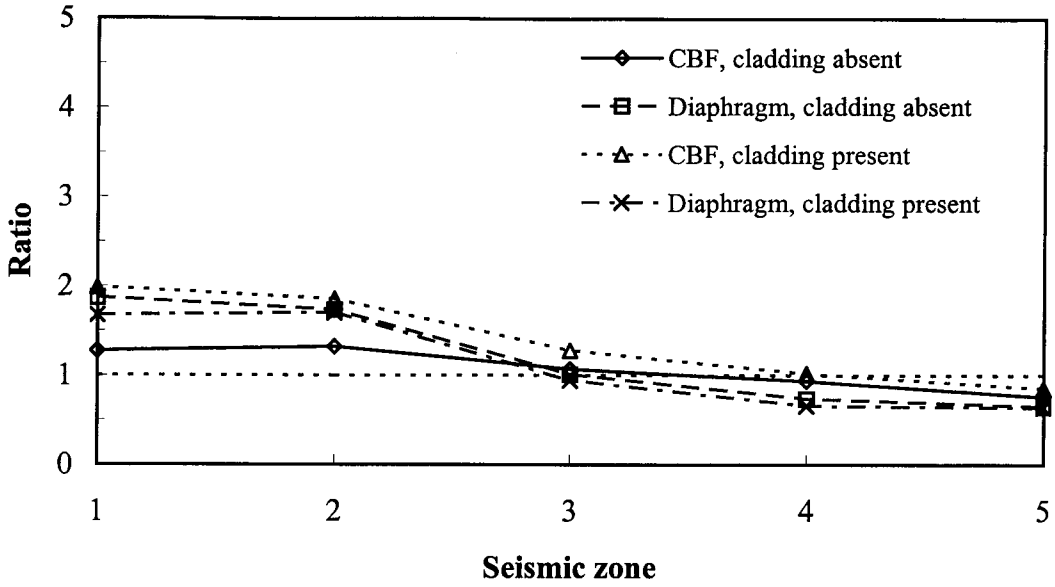

Figure 5.11 Effective overstrength ratio - acceleration set of records

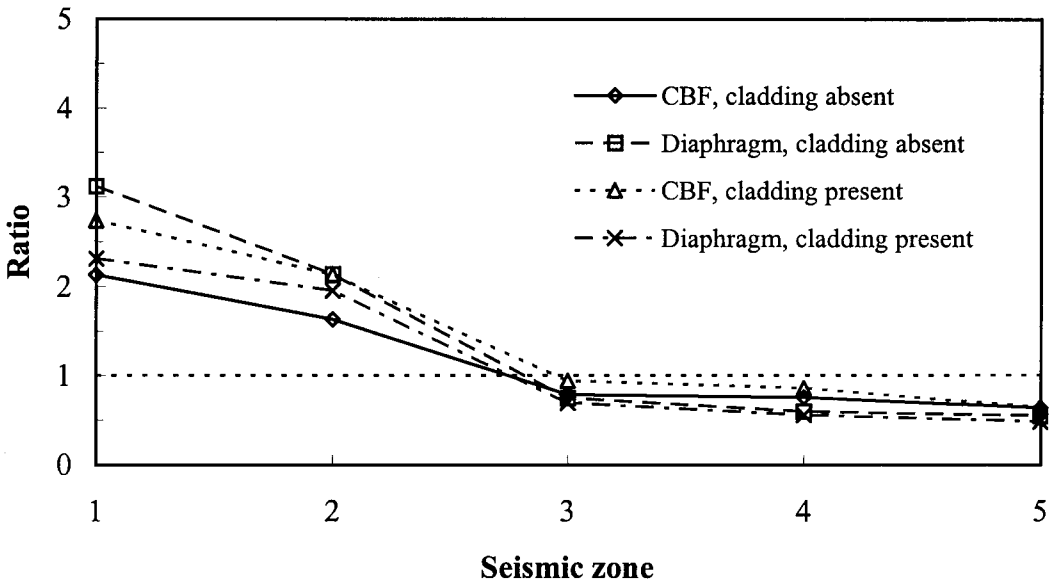

Figure 5.12 Effective overstrength ratio - velocity set of records

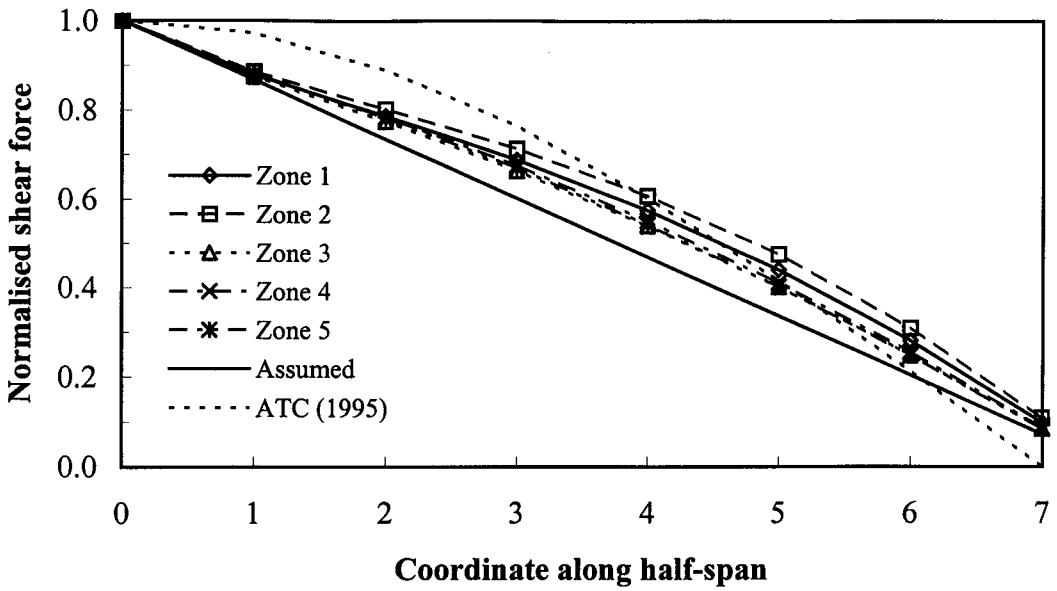

Figure 5.13 Distribution of shear force along diaphragm from response spectrum analysis (MDOFN model, cladding absent)

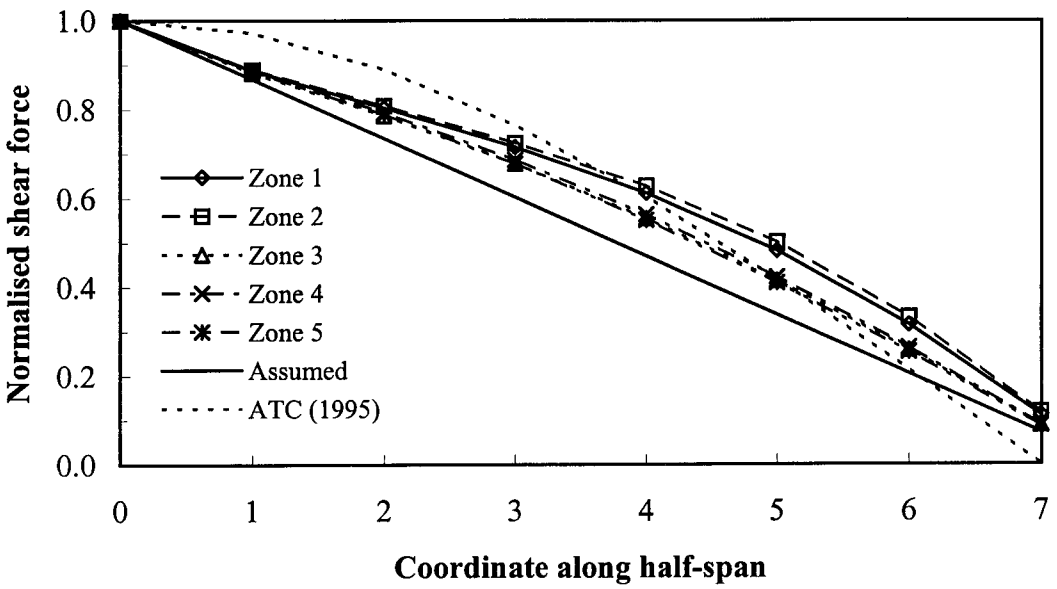

Figure 5.14 Distribution of shear force along diaphragm from response spectrum analysis (MDOFN model, cladding present)

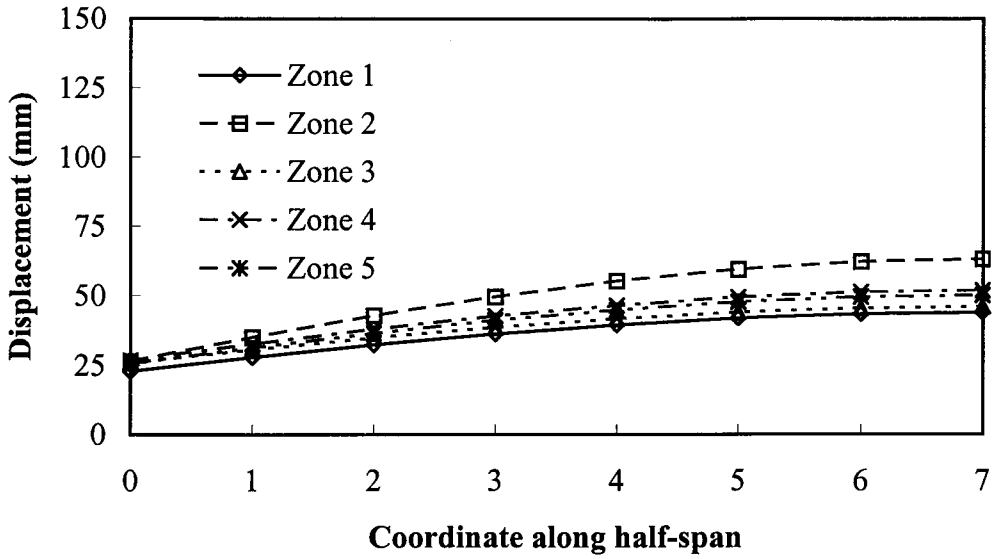

Figure 5.15 Drift under prescribed lateral force from nonlinear static analysis, cladding absent

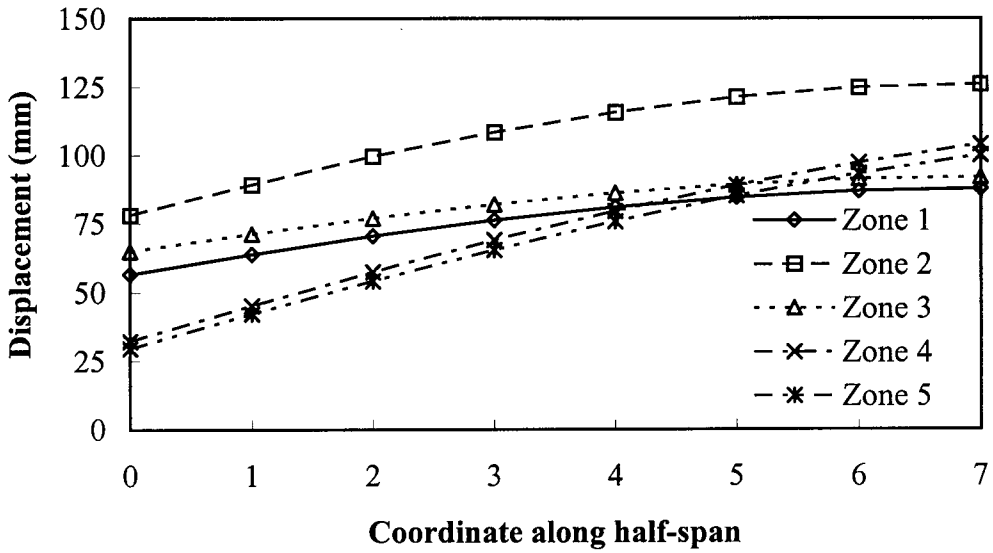

Figure 5.16 Displaced shape of diaphragm at target displacement from static pushover analysis, cladding absent

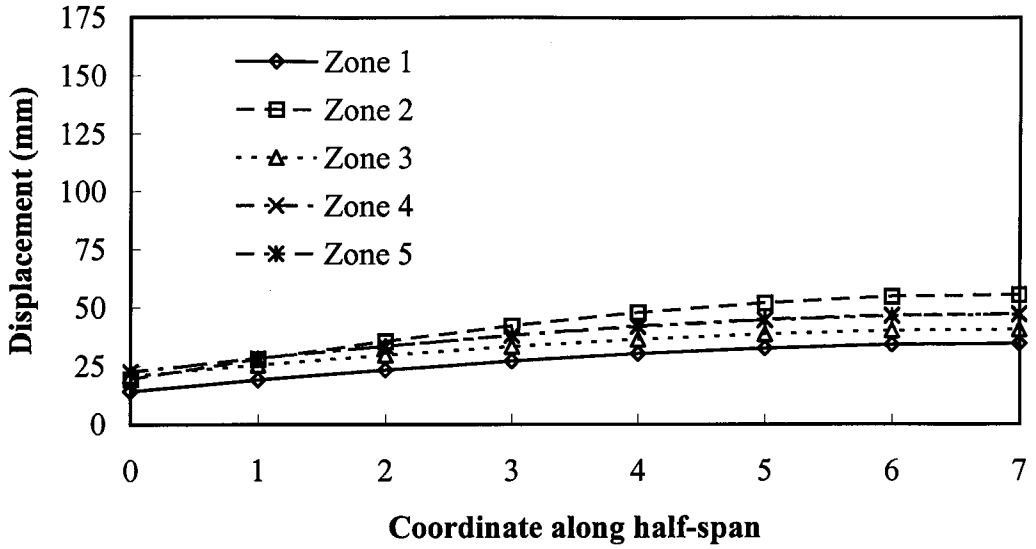

Figure 5.17 Drift under prescribed lateral force from nonlinear static analysis, cladding present

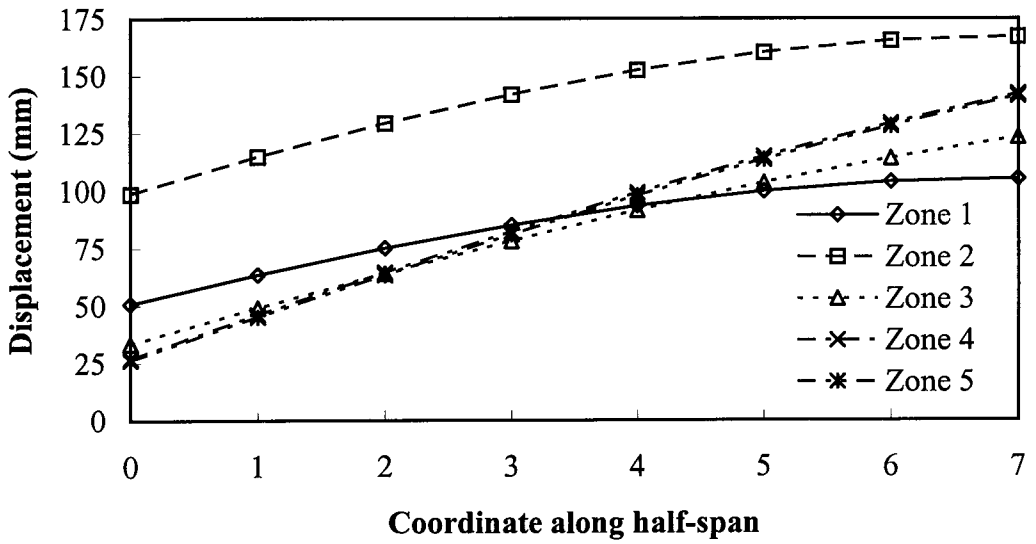

Figure 5.18 Displaced shape of diaphragm at target displacement from static pushover analysis, cladding present

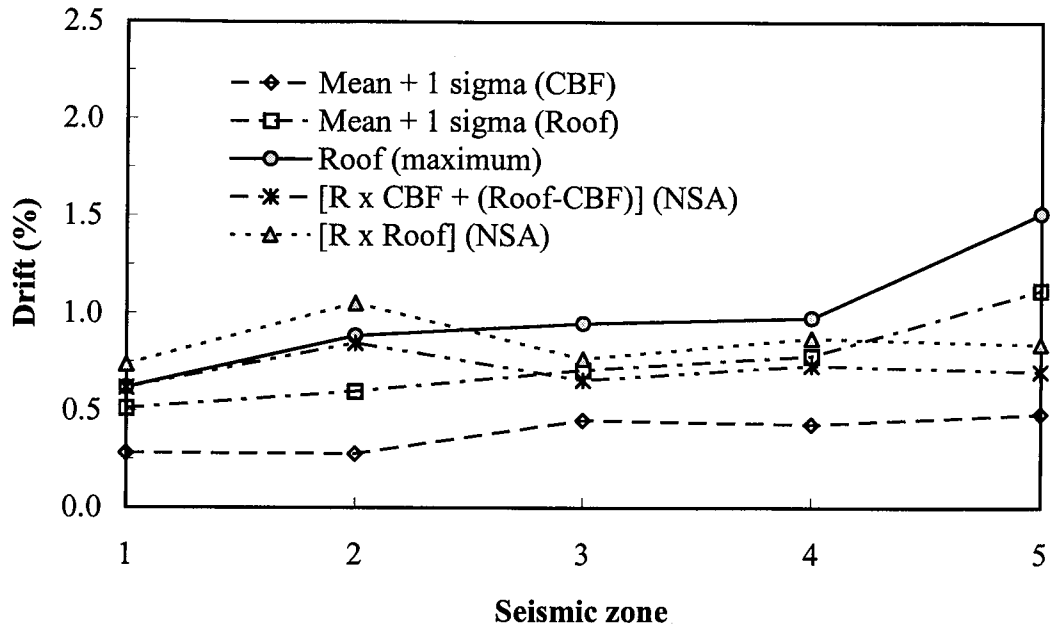

Figure 5.19 Estimate of lateral drift with cladding absent

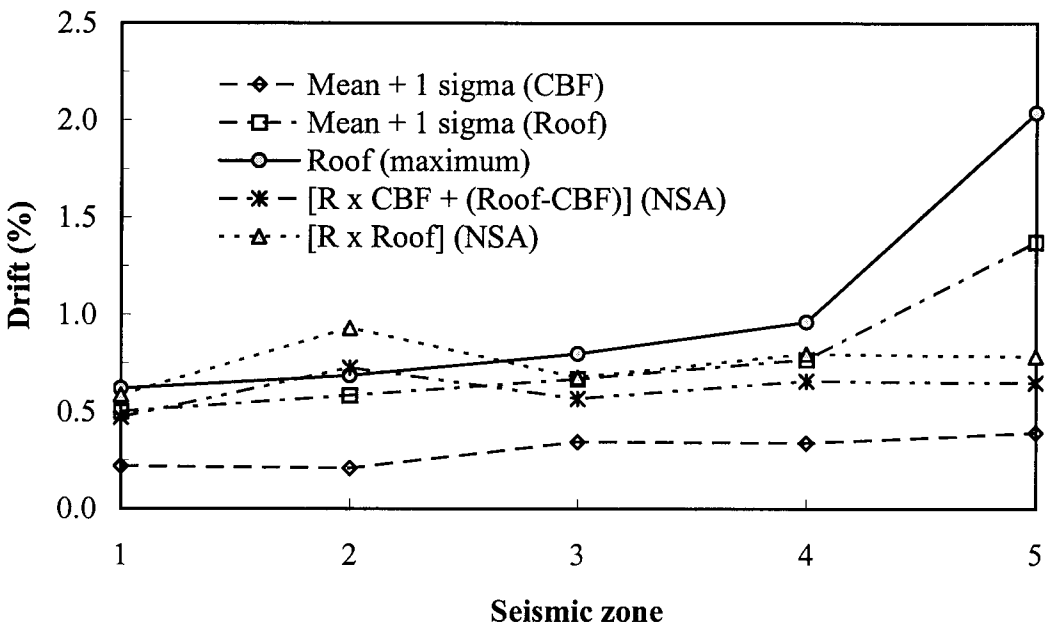

Figure 5.20 Estimate of lateral drift with cladding present

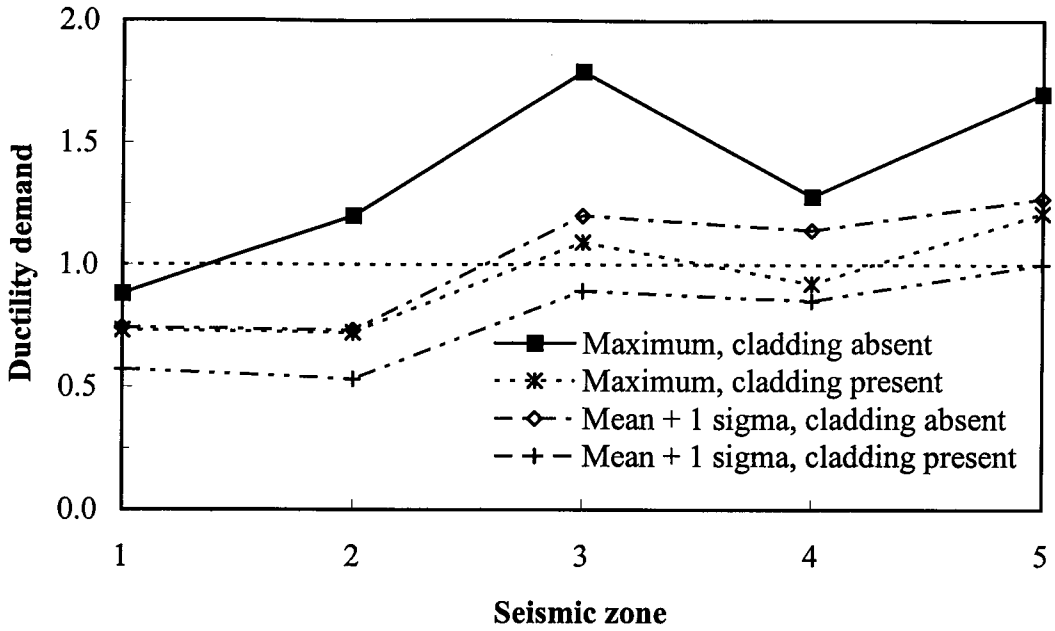

Figure 5.21 Brace ductility demand in tension

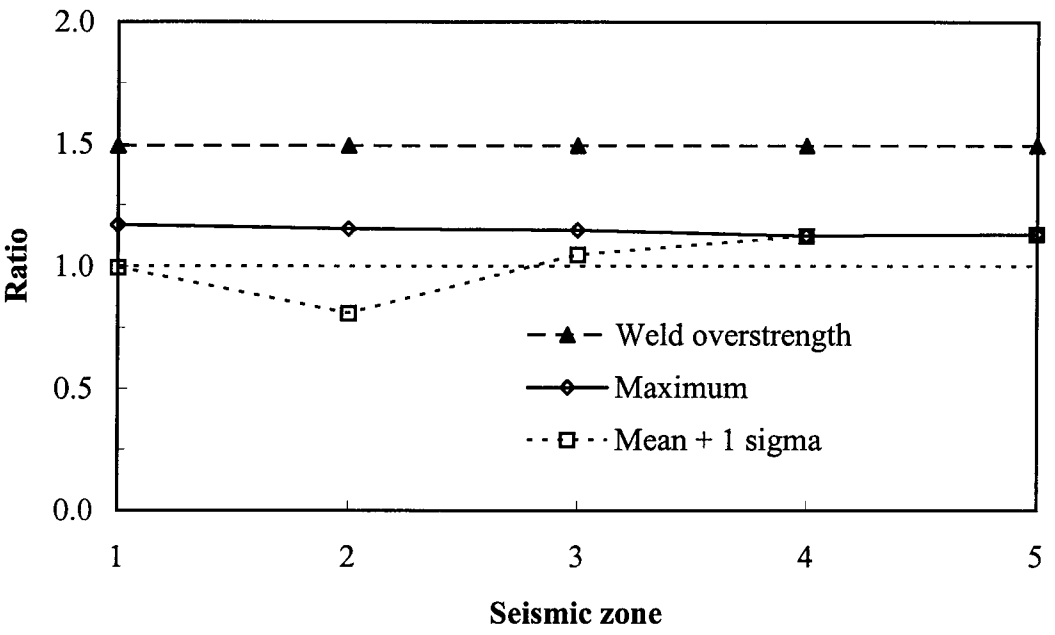

Figure 5.22 Ratio of brace response force to connection design force

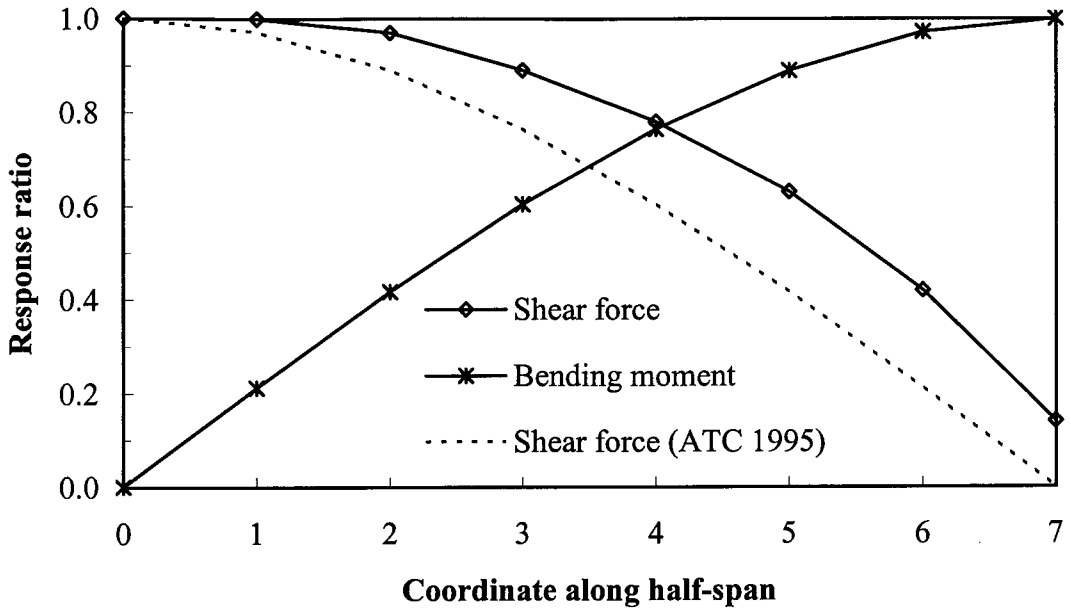

Figure 5.23 Envelope of shear force and bending moment along half-span of diaphragm

6. ASSESSMENT OF THE EFFECT OF OVERSTRENGTH

6.1 Introduction

The design of members and connections in the lateral load path is primarily governed by load combinations that include the code prescribed earthquake load. However, in some situations, member selection may be governed by architectural considerations, drift control, stringent local buckling requirements for seismic design, or other considerations. Members in the lateral load path may also have to resist significant gravity loads. These factors may result in an oversize of the lateral load resisting elements. Consequently, the lateral stiffness and possibly the base shear capacity of the structure may become significantly greater than the design value. There have been instances when the nominal yield capacity of a brace is typically 5 to 10 times the prescribed seismic load. Such oversupply is not of concern for elements that primarily resist gravity loads. However, it is of significant concern for elements in the lateral load path especially when the brace members are designed as ductile or nominally ductile members that are expected to absorb energy through yielding. Connections are then needed for this to be so.

Seismic detailing standards and guidelines differ in considering the effect of oversupply. CSA Standard S16.1-94 (CSA 1994), ATC (1995), and HERA (Feeney and Clifton 1995) specify that structures in high seismic zones should have connections capable of transferring member yield loads. Earlier standards, CSA (1989), SEAOC (1990), AISC (1992), and even the latest Uniform Building Code (ICBO 1997) permit lower connection design loads in the case of overdesigned braces, but the degree of overstrength for this to be acceptable is unclear (Redwood *et al.* 1991). Designers are concerned about the cost of the connections for these overstrong members as well as the treatment of the forces that they can transmit. They may use lower connection design loads if justifiable.

In this study, the effect of brace overstrength on the seismic response of a single-storey steel building with concentrically braced frames (CBFs) and a roof diaphragm that acts structurally is assessed by comparing the dynamic response of the building without overstrength to that of one with significant overstrength. Four structural

idealizations that differ in modelling of the roof diaphragm and the CBF are used for time history dynamic analysis. The objectives of this study are:

(a) Investigate the feasibility of time history dynamic analyses in justifying connection design loads for overdesigned braces that are less than the member yield load.

(b) Investigate the effect of different modelling assumptions on analytical results.

(c) Identify the importance of various modelling refinements.

(d) Compare results by the 'equivalent static' approach with more advanced techniques.

(e) Discuss implications in seismic design and rehabilitation analysis.

Although the structure used as the basis for this study is itself overstrong with respect to the NBCC (ACNBC 1995a) design requirement, this strength-to-demand ratio is not the focus of this study.

6.2 Description of the building

The single-storey building described in Chapter 5 is used in this study. The stiffness and strength contributions of the exterior cladding are neglected.

6.3 Design of the building

The building is assumed to be located in Vancouver (zone 4). The design methodology is described in section 5.3. Details of the building design are listed under zone 4 in Table 5.3. The brace cross section provided is a class 1 section with an area that exceeds that required by 1% only. This is referred to as the 'normal' design. It qualifies as a nominally ductile braced frame when the connections are detailed appropriately. Assuming a resistance factor, ϕ, of 1.0 to obtain the most likely strength of the member, the 'normal' braces have a tensile capacity of 1036 kN and a compressive capacity of 170 kN. The brace connections are designed to transfer the brace yield load of $A_{gn} F_Y$, where the subscript 'n' refers to the normal design.

6.4 Overstrong design

Consider a building with overstrong braces instead of the 'normal' ones required to resist the base shear. While not recommended because of the extra load that the connections may have to carry, this situation may arise when some other considerations

govern the brace design. For instance, the brace may be used to provide lateral support to a masonry wall. In this study, the brace size is arbitrarily increased to 4 times that required for seismic design. Thus, a HSS 305 x 203 x 13 with a cross sectional area of 11 800 mm^2 is used instead of the HSS 152 x 102 x 6 given in Table 5.3 with an area of 2960 mm^2. This design is referred to as the 'overstrong' design. The brace connections for the overstrong design are assumed capable of transferring the brace yield load of $A_{go} F_Y$, where the subscript 'o' designates the overstrong design. The implications of not providing this connection capacity are discussed later. The size (and hence capacity) of the other members is left unchanged. The effect of brace overstrength is assessed by comparing the dynamic response of the normal design with that of the overstrong one.

6.5 Structural models and assumptions

The dynamic response of the building is obtained for earthquake ground motion in the E-W direction only. Four different structural idealizations are used to model the building that differ in how the distributed mass and flexibility of the roof diaphragm and the strength of its connection to the CBF are modelled. All 4 idealizations are used for time history dynamic analyses. The models include; (a) single degree of freedom elastic model (SDOFE), (b) single degree of freedom nonlinear model (SDOFN), (c) two degree of freedom nonlinear model (2DOFN), and (d) multi-degree of freedom nonlinear model (MDOFN). The stiffness and strength contributions of the exterior cladding are neglected in all the models.

The SDOFE model, shown in Fig. 6.1(a), is described in section 5.6. The SDOFN model shown in Fig. 6.1(b) is a pin-connected truss with the lateral displacement of the nodes at the top of the CBF constrained to be equal so that there is only one lateral degree of freedom. Diaphragm flexibility is neglected. The diaphragm mass, M_d, and the associated weight are placed on a dummy column that is used to model the P-Δ effect. A rigid link connects the diaphragm to the CBF. The SDOFN idealization permits modelling of the nonlinear seismic behaviour of the CBF. The strength and stiffness of the braces are explicitly considered in the analysis. The columns are assumed to be elastic. This model however does not limit the force in the diaphragm shear connection and forces in excess of the connection capacity may be transferred to the CBF.

The 2DOFN model is derived from the SDOFN model by replacing the rigid link between the roof diaphragm and the CBF with a rigid-plastic link. This idealization may not represent the actual behaviour of such connections (Mazzolani *et al.* 1996). The tension and compression yield level of this link are set equal to the strength of the diaphragm shear connection. The maximum force that can be transferred from the diaphragm to the CBF is thus limited by the capacity of this link. This idealization permits an investigation of the effect of different strength levels of the CBF relative to the diaphragm shear strength.

The MDOFN model, shown in Fig. 6.1(c), is also described in section 5.6.

6.6 Free vibration analysis

Table 6.1 gives the periods from free vibration analysis with each model for the normal and the overstrong design and the fundamental period determined by NBCC procedures. For the nonlinear models, the period given is the initial elastic period. The calculation of the period assumes that the stiffness contribution is from the tension diagonal only. The increased stiffness due to overstrong braces causes a significant reduction in the period of the SDOFE, SDOFN, and the 2DOFN models. With the MDOFN model, the reduction in period is not as significant because an increase in brace cross section stiffens the CBF only while the roof diaphragm remains unchanged. There is a significant difference between the calculated fundamental periods for both the normal and the overstrong designs that are considerably greater than the NBCC estimate. Results from a three dimensional dynamic analysis of the building are also reported. The periods show good agreement with those obtained by the MDOFN model.

6.7 Nonlinear dynamic time history analysis

Dynamic response of the SDOFE model to earthquake excitation is computed by the constant-average acceleration method. Response of the other models is obtained with DRAIN-2D (Kannan and Powell 1973). The damping ratio is specified as 5% for the SDOFE model, and 3% for the SDOFN and the 2DOFN models. It is specified as 3% and 5% for the first and second mode of the MDOFN model, respectively.

Braces of the CBF are modelled with the EL9 buckling element described in Appendix C. Connections of the CBF are not modelled. A comparison of the peak brace force developed with the assumed connection capacity indicates the adequacy of the connection.

The earthquake accelerograms for time history analysis are given in Tables 4.7 and 4.8. Figure 6.2 shows the 5% damped elastic acceleration response spectra for the acceleration set of records scaled to a PHA of 0.2 g and the NBCC elastic design spectrum. The mean spectrum of the accelerograms is significantly lower than the NBCC spectrum while the mean + 1 sigma spectrum and even the maximum spectrum for longer periods agree fairly well. Figure 6.3 shows similar spectra for the velocity set of records scaled to a PHV of 0.2 m/s and the NBCC spectrum. The mean spectrum agrees well for periods up to 0.5 s. Thereafter, the maximum and the mean + 1 sigma spectrum agree fairly well.

6.8 Response of structural models

The results of time history dynamic analyses for the normal design and the overstrong design are presented for each structural model in Tables 6.2 through 6.5 and are discussed below.

6.8.1 SDOFE model

The response of the SDOFE model is obtained from the 5% damped elastic acceleration response spectra shown in Figs. 6.2 and 6.3. Because the spectral ordinates are proportional to the base shear that the system attracts, a comparison of spectral ordinates for the normal design (T equal to 0.73 s) and the overstrong design (T equal to 0.39 s) gives the increase in seismic demand due to overstrength. Table 6.2 gives the spectral ordinates for the maximum, mean + 1 sigma, and mean response levels for each design where the overstrength amplification factor is the ratio of the spectral ordinate of the overstrong design to that of the normal design. The response is seen to increase by a factor ranging between 1.5 and 1.7 for the acceleration set and between 1.7 and 2.1 for the velocity set depending on the response level selected. The brace axial force in the normal design will be amplified by the same amount. Although the brace

cross section for the normal design, A_{gn}, was increased 4 times to arrive at the overstrong design, A_{go}, the peak brace force has only doubled. Hence, providing brace connections in the overstrong design to transfer the brace yield load (i.e. $4\ A_{gn}\ F_Y$) appears to be conservative based on this simple model.

The base shear for the normal design corresponds to a spectral acceleration of 0.48 g as shown on Figs. 6.2 and 6.3. This ordinate represents the strength level of the normal design and is obtained by multiplying the ordinate of the NBCC curve for period equal to 0.23 s by the factor of 0.8 (as the analytical period is greater than the NBCC estimate of 0.23 s). For the normal design (T equal to 0.73 s), all spectral ordinates are less than the strength level provided. Now, consider the overstrong design (T equal to 0.39 s). The mean + 1 sigma and the maximum spectral ordinates of 0.57 to 0.87 exceed the strength level of the normal design. This implies that connection overload is possible if the overstrong braces were provided with connections that could only transfer the brace yield load corresponding to the normal design ($A_{gn}\ F_Y$). Because the roof diaphragm is provided with strength corresponding to the normal design, overload of the diaphragm shear connection is also possible.

Thus, by examining the response of the SDOFE model, one may conclude that the brace connections in the overstrong design will have to transfer a force greater than the brace yield load for the normal design ($A_{gn}\ F_Y$) but less than the brace yield load for the overstrong design ($4\ A_{gn}\ F_Y$). This model also suggests the possible overload of the diaphragm shear connection.

An estimate of the structural drift is obtained by using the relation $S_a = \omega^2\ S_d$ where S_a is the spectral acceleration, ω is the circular frequency, and S_d is the spectral displacement. Thus, the maximum drift ratio, the drift divided by the effective storey height expressed as a percentage, for the acceleration set is 0.62% for the normal design and 0.26% for the overstrong design. The corresponding ratios for the velocity set are 0.62% and 0.37%. These drift calculations assume a centerline height of 9 m for the CBF. Oversupply in stiffness is seen to reduce the structural drift but increase the seismic demand.

6.8.2 SDOFN model

This model accounts for the nonlinear seismic response of the CBF. It, however, neglects the distributed mass and flexibility of the roof diaphragm and the limited strength of the diaphragm shear connection. Results based on this model are presented in Table 6.3. The column and brace responses are the ratio of the maximum axial force in these elements to their nominal capacity. The 'number of records with yielding' indicates the number of accelerograms within the set in which yielding occurred. The base shear response is the ratio of the base shear developed to the base shear capacity of the structure. The calculation of base shear capacity assumes nominal tensile resistance of the tension diagonal and only 25% of the nominal compressive resistance of the compression diagonal and is consistent with the behaviour of the EL9 buckling element assumed in analysis. Thus, the base shear capacity of the CBF is 830 kN + 0.25 x 136 kN = 864 kN for the normal design and 3307 kN + 0.25 x 1939 kN = 3792 kN for the overstrong design.

For the normal design the drift is well within the 2% limit; the column response has a maximum value of 0.9; braces yield in 2 out of 12 records and 3 out of 8 records in the acceleration and velocity set, respectively; and the peak ductility demand in tension is 1.5. The base shear capacity is attained in the same records that cause brace yielding.

The overstrong design shows significantly reduced drift. Columns are overloaded in both the acceleration and velocity sets. The peak column response of 2.68 in the velocity set was precipitated by buckling of the compression diagonal throwing more load on the overstrong tension brace. The overstrong braces do not yield in tension. Buckling of the compression brace was limited to only one record. Multiplying the peak brace response for the overstrong design by the brace capacity ($4\ A_{gn}\ F_Y$), gives peak axial forces of $2.24\ A_{gn}\ F_Y$ and $3.20\ A_{gn}\ F_Y$ for the acceleration and velocity sets, respectively. This implies that brace connections for the overstrong design could be severely overloaded if they were provided with a capacity less than $3.2\ A_{gn}\ F_Y$. Because both Figs. 6.2 and 6.3 show that the mean + 1 sigma response level for the period range from 0.39 s to 0.95 s matches well with the NBCC spectrum, it is considered appropriate to examine the response at this level. This gives axial forces of $1.56\ A_{gn}\ F_Y$ and

2.28 $A_{gn} F_Y$ for the acceleration and velocity sets, respectively. Also, the base shear response shows no yielding in either set.

About 82% of the mass of this model is attributed to the roof diaphragm and the remainder to the end frames that consist of the CBF and the exterior cladding. Hence, assuming the same percentage of base shear to be generated at the roof suggests that overload of the diaphragm shear connection is possible for both the normal and the overstrong design. For example, for the normal design, acceleration set, the peak base shear ratio is 1.0. Therefore, 0.82 x 1.0 x 864 kN (base shear capacity) is equal to 708 kN, and is greater than the diaphragm shear connection strength of 681 kN. Hence, the shear connection is likely to yield.

In summary, the columns of the CBF are severely overloaded due to overstrength of the braces. The columns were modelled with elastic beam-column elements in the analysis. Hence, they appear to be able to carry compressive forces greater than their calculated capacity without undergoing large displacements that may effect the entire CBF. The columns are pin-ended and do not contribute any lateral stiffness to the model. Hence, if the analyses were carried out with revised column sections of greater compressive capacity, the drifts and brace forces would not be significantly different. Brace connections weaker than the brace capacity may also be severely overloaded. The diaphragm shear connection is overloaded as well. One would expect this to limit the load transferred to the CBF. As this model cannot account for such an effect, it is investigated with the 2DOFN model.

6.8.3 2DOFN model

The 2DOFN model is similar to the SDOFN model except that it considers the strength of the diaphragm shear connection as described in section 6.5. Table 6.4 presents the results obtained with this model. The link response is the ratio of the maximum link force to the diaphragm shear connection capacity. Thus, a link response of 1.0 indicates that the shear connection capacity has been reached.

The response of the normal design in both the acceleration and velocity sets is almost identical to that obtained with the SDOFN model (Table 6.3) except that the peak brace ductility demand is seen to reduce marginally because of 'yielding' of the link in a

total of 7 records. The drift of the CBF and the roof, expressed as percentage drift, are almost identical because of limited inelastic deformation in the link and because the maximum deformations in the CBF and the link do not occur simultaneously.

The response of the overstrong design shows significantly reduced drift for the CBF and the diaphragm, as compared to the normal design, even when for the latter the link extensions of 18 mm and 36 mm are considered. The link extension however causes a significant difference between the drift of the CBF and the diaphragm. The column response for the overstrong design is reduced from the normal design. The braces do not yield in tension or buckle in compression. Multiplying the peak brace response by the brace capacity of 4 $A_{gn} F_Y$ gives peak axial forces of 0.76 $A_{gn} F_Y$ and 0.96 $A_{gn} F_Y$ for the acceleration and velocity set, respectively, because of the limited force that the diaphragm link can transfer. These values are less than the peak force of $A_{gn} F_Y$ (yield) obtained for the normal design in both sets. The link response is increased significantly for the overstrong design as compared to the normal design. The number of records in which yielding occurs increases from 3 to 10 for the acceleration set and from 4 to 7 for the velocity set. The peak inelastic extension shows a significant increase as well.

In summary, the effect of overstrength based on this model is to concentrate the ductility demand on the diaphragm shear connection. This in turn reduces the force transferred to the CBF and consequently the brace and column axial loads and the base shear are reduced. The peak brace force is 0.96 $A_{gn} F_Y$. An overstrong brace with a weak diaphragm shear connection would seem to be adequate because the ductility demand is concentrated at the diaphragm shear connection. Moreover, the brace connection force is also limited, but the diaphragm shear connection is severely deformed inelastically.

6.8.4 MDOFN model

The MDOFN model is an extension of the 2DOFN model and accounts for the distributed mass, flexibility, and strength of the roof diaphragm. The free vibration analysis reported in Table 6.1 gives a longer period for this model due to the effect of diaphragm flexibility. The response spectra shown in Figs. 6.2 and 6.3 have lower

spectral ordinates with increasing period. Thus, one may expect the response of both designs with this model to be lower than the corresponding ones with models that assume a rigid diaphragm. Table 6.5 presents the response with the MDOFN model. The results for both the acceleration and velocity sets for the normal design are identical to those reported in Table 5.13.

The response of the normal design for both sets is similar to that obtained with the 2DOFN model. However, some differences are observed as deduced by comparing Tables 6.4 and 6.5 for the normal design. The maximum roof drift, at the mid-span of the roof, increases due to flexibility of the diaphragm from 0.52% to 0.93% for the acceleration set and from 0.48% to 0.97% for the velocity set. Table 6.5 shows that the diaphragm attains its bending capacity in a few records. While the link response is similar, peak deformations are seen to increase significantly.

Table 6.5 shows that the response of the overstrong design exhibits significantly less drift for the CBF as compared to the normal design, but the roof drift does not reduce as much. The column and brace responses are reduced, again because of the relatively weak link between the roof diaphragm and the CBF. Multiplying the peak brace response by the brace capacity ($4\ A_{gn}\ F_Y$) gives a peak brace force of $0.52\ A_{gn}\ F_Y$ that is about half of that obtained for the normal design. The bending response of the diaphragm and the link response also increase with yielding being attained in more records. However, the inelastic extension of the link is reduced as compared to the normal design.

In summary, the effect of overstrength based on this model is similar to that for the 2DOFN model. Ductility demand is concentrated at the weakest element in the load path. The peak brace force is $0.52\ A_{gn}\ F_Y$. Hence, overstrong braces with weak connections between them and the roof diaphragm would be adequate as the limited shear connection strength of the diaphragm limits the load transferred to the CBF.

6.9 Influence of model on response

Table 6.6 presents values of the peak response obtained for the overstrong design with each model. The SDOFE and the SDOFN model give higher estimates of drift for the CBF but lower estimates for the roof drift as compared to the 2DOFN and the MDOFN model. The peak response of the columns and braces is heavily dependent on

the model. These elements are overloaded in the SDOFE and the SDOFN model that are not that realistic. The 2DOFN and the MDOFN model show this not to be the case. These models account for the limited shear connection strength of the diaphragm. This happens to be the weakest element in the lateral load path. Hence, ductility demand is concentrated at this weak link as is evident from the link response. Consequently, the lateral force on the CBF reduces and the column and brace responses reduce.

The behaviour of the 2DOFN and the MDOFN model is analogous to the soft storey effect in a multi-storey building (Chopra 1995). For this single-storey building, the roof diaphragm connection represents the soft storey while the overstrong CBF represents the strong storey. Thus, the ductility demand is expected to concentrate at the discontinuity in strength level, i.e., at the diaphragm shear connection. This damage pattern has been observed in past earthquakes when relatively flexible steel roofs were anchored to stiff walls. In this case the weak shear connection would suffer damage in the modelled earthquakes and the roof diaphragm would require repair.

Among the 4 models considered, the MDOFN model, considered to be by far the most realistic, gives minimum peak forces for the columns and braces. It also generates the least base shear due to the combined effect of diaphragm flexibility and the weak diaphragm shear connection.

6.10 Implications in design and rehabilitation analyses

When the braces of the lateral load resisting system (LLRS) are significantly stronger than required to resist the seismic load, a designer should be concerned about the adequacy of the brace connections to transfer the brace forces. CSA Standard S16.1-94 (CSA 1994) requires all brace connections in high seismic zones to transfer the brace yield forces, based on the premise that no other failure occurs in the load path to the LLRS. The designer, however, may adopt lower connection design loads if they are justifiable. One possible method of justifying lower design loads is by performing time history dynamic analyses of an appropriate model of the structure under a set of relevant earthquake accelerograms and obtaining the peak brace loads, as has been performed here. The response obtained from such analyses depends on the assumptions made in the model. A clear visualization of the lateral load path and consideration of the strength and

stiffness of all elements in the load path to the LLRS is essential to arrive at a model that is capable of representing the behaviour of the structure realistically. For the system studied here, a check on strength levels indicates that the diaphragm shear connection is the weak link. Hence, strengthening of the columns or brace connection is considered to be unnecessary under these circumstances. The more important issue is an assessment of the consequences of yielding in the diaphragm shear connection and damage to the diaphragm. If inelastic action that limited the forces transferred did not occur in the load path to the CBF, the brace connections would have to be designed for the brace yield load or an appropriate brace load found by time history analyses. In lieu of designing for the appropriate brace load, CSA Standard S16.1-94 (CSA 1994) justifiably requires the brace connections [and the remainder of the load path] to be designed for the brace yield load.

6.11 Equivalent static lateral force procedure

The base shear prescribed by the equivalent static lateral force procedure of the NBCC is given by [2.8] and [2.9], and other factors being equal, depends on S, the seismic response factor. The period of the CBF, from [2.10], is 0.23 s for both the normal and the overstrong design. The value of S, shown in Fig. 2.2, is constant for periods less than 0.25 s. Hence, on first glance a designer may misinterpret this to infer that the seismic demand is the same for both systems. However, the response spectra shown in Figs. 6.2 and 6.3 indicate that this is not the case because the period is changed. Léger and Romano (1992) have suggested that the NBCC spectrum is unconservative in the short period range. Given this situation, the only rational design approach is to assess the strength of all elements in the lateral load path and determine the weak link. If all lateral loads can be transferred to the CBF, the designer would logically have to provide brace connections to transfer brace yield loads. If some other element is the weak link, while the brace loads are likely reduced, the designer must assess the consequences of failure of this link.

The amplification factor approach may be used with a SDOFE model in conjunction with a set of appropriate response (not design) spectra. As this approach is likely to give high amplification factors should the building with overstrong braces have its fundamental period in the short period range, an explicit check on strength level is still

necessary. This would indicate whether the structure is likely to respond inelastically or not. Such action would reduce the seismic demand on the system but concentrate the ductility demand at the weak link, assuming one exists.

6.12 Conclusions

The effect of brace overstrength on the seismic response of a single-storey concentrically braced steel-framed building has been investigated by carrying out time history dynamic analyses with 4 different structural models of the building. Based on the results of this investigation, the following conclusions can be drawn:

(a) Overstrength in certain elements of the LLRS will also be accompanied by an increase in lateral stiffness. The effect of both the overstrength and increased lateral stiffness should be considered in seismic design and rehabilitation analyses.

(b) Oversupply in stiffness reduces the period of the structure. This usually results in an increase in the seismic demand on the structure.

(c) The relative strength of components in the lateral load path is of utmost importance. The effect of making a certain element in the load path stronger than required is likely to make some other element in the load path the 'weak link.' In a severe event, the ductility demand will concentrate at this 'weak link.' Hence, a hierarchy in the provision of strength to components in the load path is important.

(d) Time history dynamic analyses may be used to assess the adequacy of structures with significant overstrength in the LLRS. The models chosen for such an analysis must be based on a clear visualization of the lateral load path and must account for the strength and stiffness of various elements in the load path. This helps the designer identify where the seismic demand is concentrated and appropriate measures can then be taken.

(e) Use of an elastic model (SDOFE) or a limited inelastic model (SDOFN) gives an indication of the increased seismic demand due to overstrength. However, the designer should explicitly verify that the strength of any element in the load path is not exceeded. This shows where ductility demands are concentrated and may render unnecessary the strengthening of a non-critical component in the lateral load path.

(f) Nonlinear models (2DOFN and MDOFN) that account for the strength and stiffness of various elements in the load path, represent the behaviour of the structure more

appropriately and give a better assessment of the effect of overstrength. In the example considered, inelastic action in the idealized rigid-plastic roof diaphragm connection limited the force on the CBF. Designers should not consider providing a weak link between the roof diaphragm and the CBF to avoid ductile detailing of the braces or reduced brace connection forces or both, until the hysteresis behaviour of the link is established experimentally. Only certain type of connections may be able to sustain inelastic loading cycles. Further experimental work is necessary to investigate the seismic response of roof diaphragm assemblies.

Table 6.1 Periods from free vibration analysis in the E-W direction

Model	Calculated period (s)				NBCC estimate (s)
	Normal design		Overstrong design		
	Mode 1	Mode 2	Mode 1	Mode 2	
SDOFE SDOFN 2DOFN	0.73	-	0.39	-	0.23
MDOFN	0.91	0.28	0.68	0.22	0.23
3-D Model	0.95	0.27	0.73	0.23	0.23

Table 6.2 Response of the SDOFE model

Response level	Normal design	Overstrong design	Overstrength Amplification factor
	Sa (g), acceleration set		
maximum	0.41	0.62	1.51
$\mu + 1\,\sigma$	0.36	0.57	1.58
μ	0.23	0.39	1.70
	Sa (g), velocity set		
maximum	0.41	0.87	2.12
$\mu + 1\,\sigma$	0.38	0.74	1.95
μ	0.28	0.48	1.71

Table 6.3 Response parameters of the SDOFN model

Response parameter	Response level	Acceleration set Design		Velocity set Design	
		Normal	Overstrong	Normal	Overstrong
Number of records		12	12	8	8
Drift (%)	maximum	0.56	0.27	0.48	0.38
	$\mu + 1\,\sigma$	0.43	0.19	0.46	0.27
	μ	0.28	0.13	0.34	0.16
Column response ratio	maximum	0.90	1.90	0.90	2.68
	$\mu + 1\,\sigma$	0.89	1.34	0.90	1.94
	μ	0.63	0.94	0.73	1.19
Brace response ratio	maximum	1.00	0.56	1.00	0.80
	$\mu + 1\,\sigma$	1.00	0.39	1.00	0.57
	μ	0.68	0.27	0.80	0.34
Ductility demand	maximum	1.52	0.56	1.30	0.79
No. of records with yielding		2	0	3	0
No. of records with buckling		10	0	8	1
Base shear response ratio	maximum	1.00	0.71	1.00	0.75
	$\mu + 1\,\sigma$	0.99	0.49	1.00	0.63
	μ	0.70	0.34	0.82	0.41
No. of records with yielding		2	0	3	0

Table 6.4 Response parameters of the 2DOFN model

Response parameter	Response level	Acceleration set Design		Velocity set Design	
		Normal	Overstrong	Normal	Overstrong
Number of records		12	12	8	8
CBF drift (%)	maximum	0.52	0.09	0.46	0.11
	$\mu+1\sigma$	0.42	0.09	0.44	0.10
	μ	0.27	0.08	0.33	0.08
Roof drift (%)	maximum	0.52	0.26	0.48	0.42
	$\mu+1\sigma$	0.42	0.20	0.45	0.28
	μ	0.27	0.15	0.34	0.16
Column response ratio	maximum	0.90	0.68	0.90	0.84
	$\mu+1\sigma$	0.89	0.68	0.90	0.73
	μ	0.63	0.59	0.73	0.59
Brace response ratio	maximum	1.00	0.19	1.00	0.24
	$\mu+1\sigma$	1.00	0.19	1.00	0.20
	μ	0.67	0.16	0.80	0.16
Ductility demand	maximum	1.41	0.19	1.26	0.24
No. of records with yielding		2	0	3	0
No. of records with buckling		10	0	8	0
Roof diaphragm response					
Link response	maximum	1.00	1.00	1.00	1.00
	$\mu+1\sigma$	1.03	1.05	1.02	1.06
	μ	0.75	0.97	0.85	0.97
Extension (mm)	maximum	7	18	7	36
No. of records with yielding		3	10	4	7
Base shear response ratio	maximum	1.00	0.24	1.00	0.30
	$\mu+1\sigma$	0.98	0.24	1.00	0.26
	μ	0.70	0.20	0.82	0.21
No. of records with yielding		2	0	3	0

Table 6.5 Response parameters of the MDOFN model

Response parameter	Response level	Acceleration set Design		Velocity set Design	
		Normal	Overstrong	Normal	Overstrong
Number of records		12	12	8	8
CBF drift (%)	maximum	0.43	0.06	0.47	0.06
	$\mu+1\sigma$	0.38	0.07	0.43	0.06
	μ	0.25	0.05	0.33	0.05
Roof drift (%)	maximum	0.93	0.68	0.97	0.76
	$\mu+1\sigma$	0.74	0.58	0.78	0.72
	μ	0.49	0.38	0.59	0.50
Column response ratio	maximum	0.90	0.50	0.90	0.50
	$\mu+1\sigma$	0.86	0.51	0.90	0.49
	μ	0.59	0.39	0.75	0.42
Brace response ratio	maximum	1.00	0.13	1.00	0.13
	$\mu+1\sigma$	0.96	0.13	1.01	0.13
	μ	0.63	0.10	0.82	0.10
Ductility demand	maximum	1.17	0.13	1.28	0.13
No. of records with yielding		3	0	3	0
No. of records with buckling		10	0	8	0
Roof diaphragm response					
Bending response ratio	maximum	1.00	1.00	1.00	1.00
	$\mu+1\sigma$	0.97	1.12	1.03	1.03
	μ	0.72	0.82	0.86	0.90
No. of records with yielding		3	7	3	4
Link response	maximum	1.00	1.00	1.00	1.00
	$\mu+1\sigma$	1.00	1.14	1.02	1.03
	μ	0.73	0.84	0.86	0.91
Extension (mm)	maximum	25	8	18	14
No. of records with yielding		4	9	3	4
Base shear response ratio	maximum	1.00	0.17	1.00	0.17
	$\mu+1\sigma$	0.95	0.18	1.01	0.17
	μ	0.66	0.13	0.83	0.14
No. of records with yielding		3	0	3	0

Table 6.6 Peak response parameters of overstrong design with different models

Response parameter	Model SDOFE	SDOFN	2DOFN	MDOFN
Total number of records	20	20	20	20
CBF drift (%)	0.37	0.38	0.11	0.06
Roof drift (%)	0.37	0.38	0.42	0.76
CBF response				
Column response ratio	2.12*	2.68	0.84	0.50
Brace force (x A_{gn} F_Y)	2.12*	3.20	0.96	0.52
Peak brace ductility demand	-	0.79	0.24	0.13
Roof diaphragm				
Bending response ratio	-	-	-	1.00
No. of records with yielding	-	-	-	11
Link response	2.12*	-	1.00	1.00
Maximum extension (mm)	-	-	36	14
No. of records with yielding	-	-	17	13
Base shear response ratio	-	0.75	0.30	0.17

* assumed equal to peak amplification factor in Table 6.2

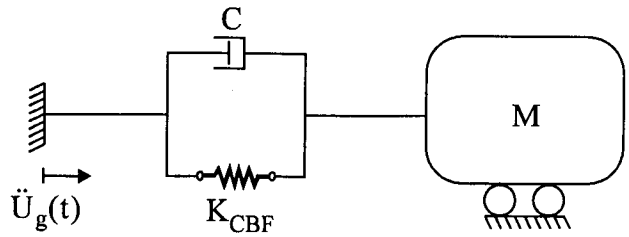

(a) Single degree of freedom elastic model (SDOFE)

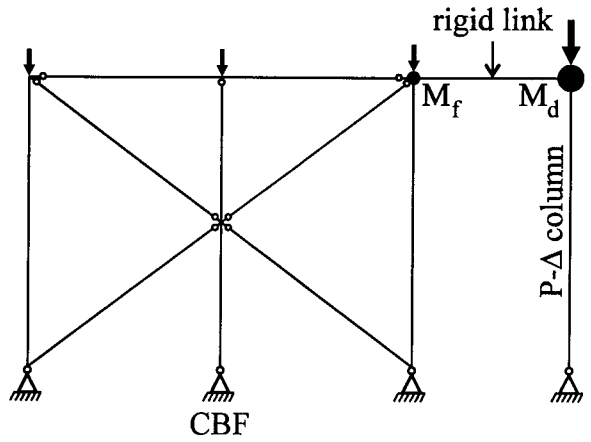

(b) Single degree of freedom nonlinear model (SDOFN)

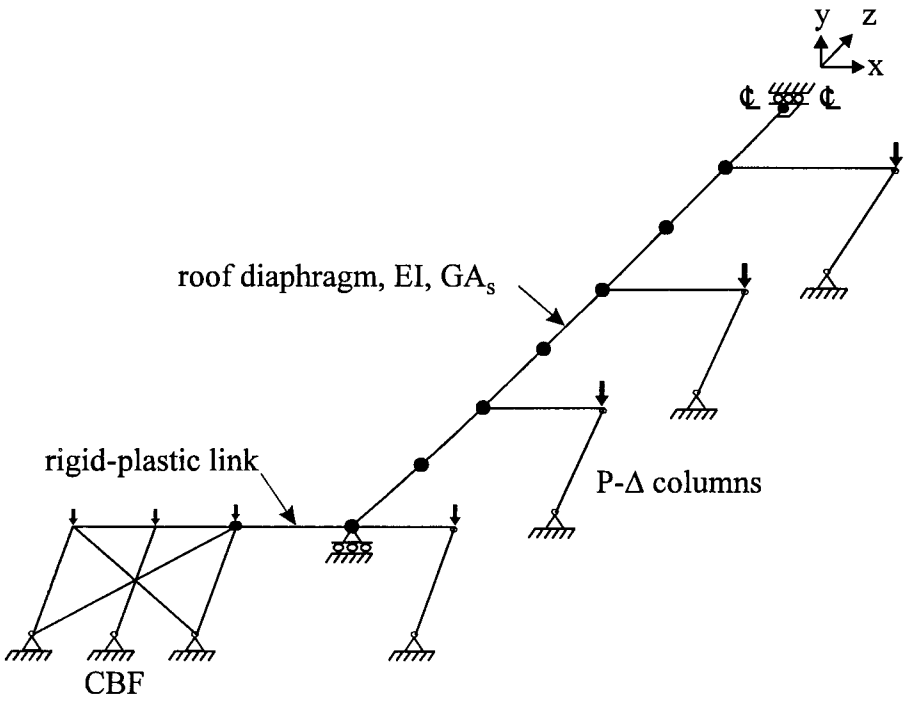

(c) Multi-degree of freedom nonlinear model (MDOFN)

Figure 6.1 Analytical models for time history dynamic analysis

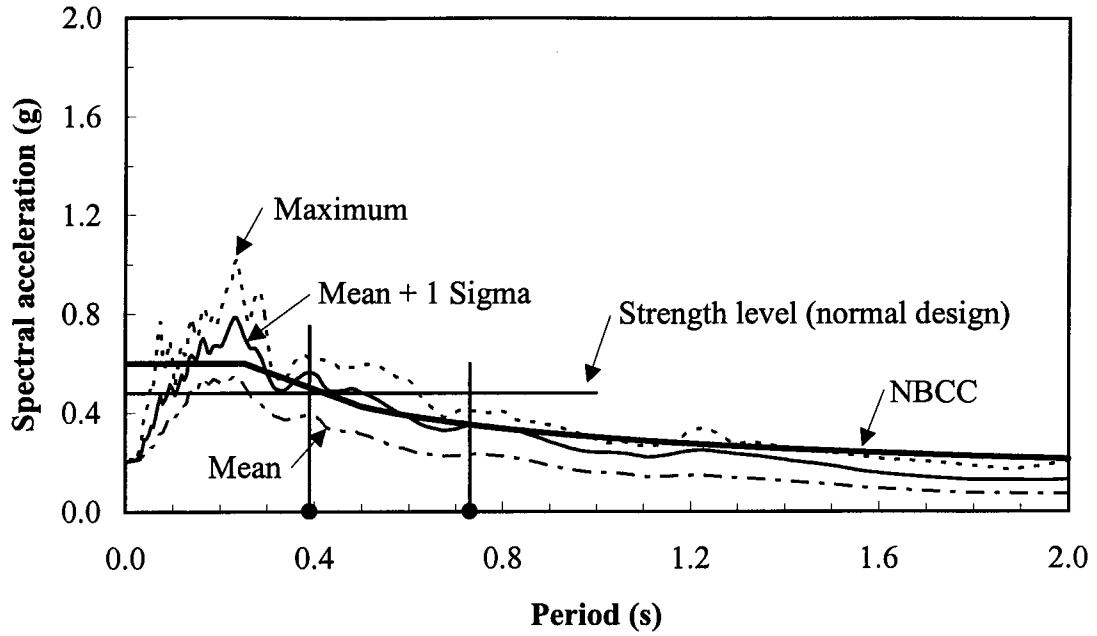

Figure 6.2 Response spectra of acceleration set of records for zone 4

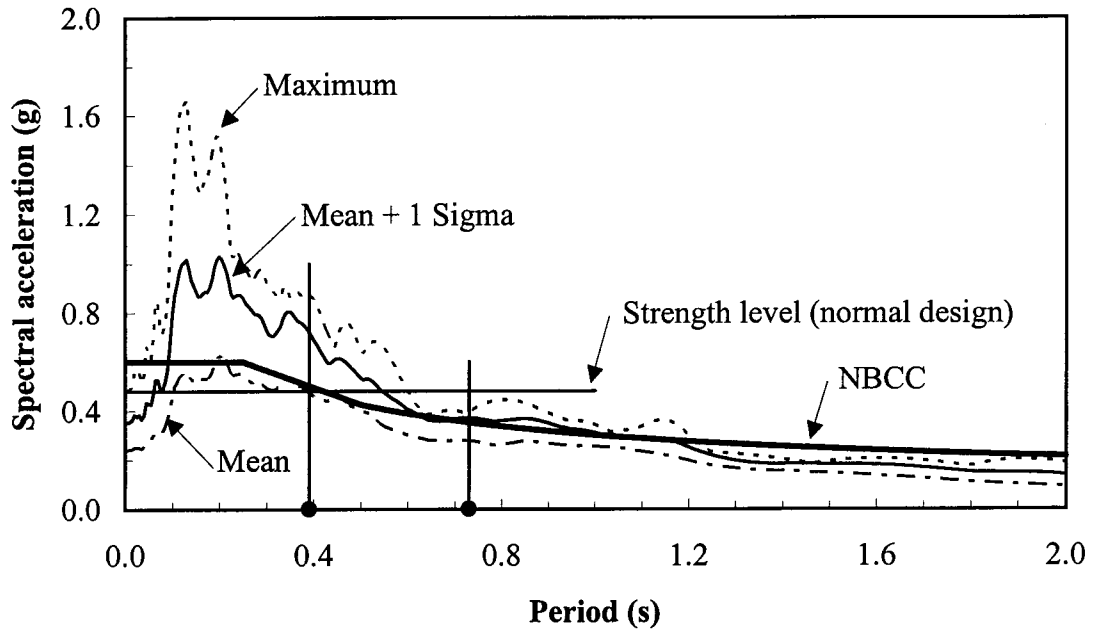

Figure 6.3 Response spectra of velocity set of records for zone 4

7. CASE STUDY II: TWO-STOREY BUILDING

7.1 Introduction

Analytical studies are performed on a two-storey steel building which uses concentrically braced frames (CBFs) as the lateral load resisting system (LLRS) and has a flexible roof diaphragm and a rigid floor diaphragm. The building is designed according to the provisions of the NBCC (ACNBC 1995a) and CSA Standard S16.1-94 (CSA 1994) for five seismic zones of Canada. Structural models are developed for static and dynamic analyses of the building that consider the nonlinear behaviour of the CBF, the stiffness and strength contribution of the partitions, and the shear strength of the roof diaphragm. The influence of roof diaphragm flexibility on the fundamental period is investigated. The distribution of lateral force over the building height is determined from response spectrum analysis and is compared with the distribution recommended by the NBCC. The seismic response of the building is obtained with nonlinear static and nonlinear dynamic time history analyses and assessed against the acceptance criteria given in section 4.7. Recommendations are made for the seismic design and analysis of such buildings.

7.2 Description of the building

The building is adapted from the "Low rise office building design aid" published by the Canadian Institute of Steel Construction (Chien 1991). The original three-storey asymmetric building layout is simplified to a two-storey symmetric layout shown in Fig. 7.1. The built-up roofing system is carried by a 38 mm (1.5 inch) metal deck supported by open web steel joists and steel girder framing. The floor system described by Chien (1991) has a 75 mm (3 inch) metal deck topped with a 75 mm thick concrete cover slab. The vertical LLRS consists of two CBFs of 9000 mm width in each principal direction. The cladding is of precast concrete panels that are supported by the exterior framing. Interior partitions are assumed to be of gypsum wallboard of 12.5 mm (1/2 inch) thickness attached on either side of metal studs that are anchored to the floor at the bottom and the floor (or roof) at the top.

7.3 Design of the building

The building is designed for the 5 locations listed in Table 5.1. The dead load, inclusive of structural steel, is taken as 1.05 kPa and 4.80 kPa for the roof and the floor, respectively. The dead load of the cladding is taken as 11 kN/m and 8 kN/m for storey 1 and storey 2, respectively. The floor live load is specified as 2.40 kPa subject to the live load reduction factor specified in the NBCC (ACNBC 1995a).

Many aspects of the seismic design carry over from the design of the single-storey building given in section 5.3. The seismic design assumes a strength braced frame (SBF) with tension-only bracing. Hence, a force modification factor, R, of 1.5 is used. The base shear specified by the NBCC is given by [2.8]. The importance factor, I, and the foundation factor, F, are both assumed equal to 1.0. The effective seismic weight, W, assumed to be the same at all five locations, is 16 800 kN, with a weight of 4100 kN at the roof and 12 800 kN at the floor, as given in Table 7.1 where the figures have not been rounded off. For the CBF, the height, h_n, is 8.1 m, and the width, D_s, is 9.0 m, giving a period of 0.24 s from [2.10] in both directions at all five locations. From Fig. 2.2, the S factor for a period of 0.24 s is 3.0, resulting in the same base shear in both directions. The period of the building computed analytically, as verified by subsequent analyses, is greater than 0.24 s in all the zones. Hence, the base shear is taken as 0.80 times that from [2.8] and is reported in line 1 of Table 7.2. The base shear, V, is distributed as a lateral force at each level given by

$$[7.1] \qquad F_x = V \frac{W_x h_x}{\sum_{i=1}^{n} W_i h_i}$$

where W_x is the effective weight and h_x is the height to level 'x.' Thus, about 38% of the base shear is applied at the roof level and the remainder at the floor. One half the lateral force from [7.1] is applied on each CBF and the torsion provision of the NBCC is then applied. The CBFs in the N-S and E-W direction are assumed to have equal lateral stiffness and the floor and roof diaphragms are assumed rigid. The base shear for the CBF is increased by about 17% in the N-S direction and by about 22% in the E-W direction due to the NBCC torsion provision.

Structural design of the CBF is carried out with SODA (Acronym Software 1994). A two-dimensional model is used as shown in Fig. 7.2. All columns of the building are continuous through the floor. The floor beam is simply supported at its ends and is continuous over the central column. The roof beam is simply supported for the entire 9 m span. The top flanges of the roof and floor beams are assumed to be braced laterally at all load points. The bottom flanges of both beams are assumed to be unbraced laterally between vertical supports. The pin-ended braces are constrained to be hollow structural sections (HSS) with the effective slenderness ratio, KL/r, limited to 300. The load combinations considered in design are;

(a) $1.25\ D + 1.5\ L$,

(b) $1.25\ D + 0.7\ (1.5\ L \pm 1.5\ W)$, and

(c) $1.0\ D + 0.5\ L \pm 1.0\ E$

where D, L, W, and E are the specified dead load, live load (including snow), wind load, and earthquake load, respectively. For load combination (c), the lateral force at the roof level is distributed between nodes N3 and N6 in Fig. 7.2 in proportion to the tributary areas. For example, with the lateral force acting from north to south, 58% of the lateral force at the roof level is applied at node N3 and the remainder at node N6. This ensures that the roof beam is subjected to an appropriate compressive load for design. Similarly, about 46% of the lateral force at the floor is applied at node N2 and the remainder at node N5. The lateral force due to wind does not govern the design of the CBF in any of the five zones. Once a preliminary design is obtained, a P-Δ analysis of the CBF is carried out under lateral drifts that are amplified by the force modification factor, R (ACNBC 1995a). The lateral forces are increased to account for the P-Δ effect and the adequacy of the preliminary design is checked. The factored base shear for each CBF in the N-S direction is given in line 2 of Table 7.2, and includes the increments due to torsion and the P-Δ effect. Without these increments, the base shear for each of the two CBFs would have been one half of that given in line 1. Lines 3 and 4 give the lateral force on the floor and the roof, respectively. The members of the CBFs in the N-S direction are also given in Table 7.2 along with the governing load combination for design. The brace cross-section provided in storey 1 is within 1.07 times of that required,

while that provided in storey 2 is within 1.11 times of that required. The floor beam in zone 4 was revised from a W410x60 to a W610x84 because a plastic hinge formed in this member in nonlinear dynamic time history analyses due to the combined action of seismic axial and gravity loads. Due to a similar occurrence in zone 5, the floor beam was revised from a W360x64 to a W610x125. The capacity design approach (Feeney and Clifton 1995) was used to arrive at the revised member section, and is discussed in section 7.4. The current design approach in CSA Standard S16.1-94 (CSA 1994), except for DBFs, does not require a capacity design approach and therefore would not have detected this failure.

The lateral force at the roof level from [7.1] is amplified by 1.17 for the torsion increment and is then distributed uniformly along the roof diaphragm that is assumed to be continuous over the CBFs in the N-S direction, as shown in Fig. 7.3. The diaphragm is designed for the resulting distribution of shear force and bending moment. The design methodology is described in section 5.3. Design parameters of the diaphragm in each of the five zones are given in Table 7.3.

In this study, the CBF is analysed for earthquake forces acting in the N-S direction only. For the sake of completeness, the CBF design parameters affecting the lateral stiffness in the E-W direction are given in Table 7.4. The cross-sectional area of the braces provided in both storeys is not significantly different from that provided for CBFs in the N-S direction, as given in lines 7 and 12 of Table 7.2, resulting in about the same stiffness in both directions.

7.4 Capacity design of the floor beam

As discussed in the previous section, the floor beam in zones 4 and 5 was subjected to an axial force in time history dynamic analyses that exceeded its compressive resistance. The revised compressive load for beam design was determined by considering equilibrium of the CBF in a state wherein the braces are assumed to have yielded in tension and buckled in compression.

Consider the building in a displaced configuration similar to the first mode shape, as shown in Fig. 7.4(a). Assuming rigid floor and roof diaphragms, the compatibility of deformations requires one of the brace diagonals to be in tension and the other in

compression. Figure 7.4(b) shows the forces at joint N9 located at mid-span of the floor beam where the brace diagonals and the central column intersect. Brace axial forces T_1 and T_2 act along the tension diagonal while forces C_1 and C_2 act along the compression diagonal. Axial force, F_1, and shear force, V_1, act on the segment of the floor beam to the right of joint N9, while forces F_2 and V_2 act on the segment to the left. Similarly, F_3 and V_3 are the axial force and shear force in the central column, respectively. The equilibrium of forces in the X and Y direction gives

[7.2] $$(F_1 + F_2) = (T_1 + C_1)\cos\theta_1 - (T_2 + C_2)\cos\theta_2 - V_3$$

[7.3] $$F_3 = (T_1 - C_1)\sin\theta_1 - (T_2 - C_2)\sin\theta_2 + (V_1 + V_2)$$

The compressive load for design of the floor beam is determined from [7.2]. Because the central column is pin-ended, the shear force, V_3, exists only due to the P-Δ effect and may be ignored. The upper bound for forces T_1 and T_2 is the yield capacity of the brace, P_{yp}. Similarly, the upper bound for forces C_1 and C_2 is the compressive resistance of the brace in its first cycle, P_{yn}. To avoid excessive conservatism in design, C_1 and C_2 may also be assumed equal to the reduced compressive resistance of the brace, P_{ync}. Forces F_1 and F_2 may be assumed proportional to the tributary area of the floor that generates the lateral force. Similarly, the capacity based axial compression in the central column, F_3, may be found from [7.3].

If the displaced configuration in Fig. 7.4(a) is assumed similar to the second mode shape, the sign of the term '$T_2 + C_2$' in [7.2] changes, and [7.3] is unchanged. This results in a larger, more conservative estimate of the axial force in the floor beam.

7.5 Stiffness and strength contribution of the partitions

The building is enclosed on all sides by an exterior cladding of precast concrete panels that are typically fastened to the exterior framing by proprietary connections. These connections usually accommodate some differential movement between the top of the panels and the framing to allow for thermal expansion. Although such panels are known to contribute to the lateral stiffness to the building (Palsson *et al.* 1984), this contribution is not considered here. It is likely that the stiffness and strength are

controlled by the connections of the panels to the frame. Experimental data on the behaviour of such connections under lateral load is lacking. However, the contribution of steel cladding was considered for the single-storey building in section 5.4. Also, the contribution of the interior partitions is considered as discussed in the following.

Interior partitions are of 12.5 mm thick gypsum wallboard attached on either side of metal studs that are anchored to the floor at the bottom and the floor (or roof) at the top. The stiffness and strength of such partitions have been investigated by Freeman (1977) and Rihal (1986). Based on these studies and suggestions from Cohen[1], the effective lateral stiffness of an idealized panel is assumed as

$$\frac{V}{\Delta} = \frac{G\,t\,L}{h} \qquad [7.4]$$

The effective shear modulus of the partitions, G, is assumed equal to 30 MPa (Freeman 1977). The gypsum wallboard has an effective thickness, t, of 25.4 mm. The partitions are assumed to be present along all lines with framing in the plan shown in Fig. 7.1. Thus, the total length of partitions in the N-S direction is 288 m (equal to 8 x 36 m). The height of the partitions, h, is assumed equal to the storey height. With this data, [7.4] gives a lateral stiffness of 52 kN/mm for partitions in storey 1 and 56 kN/mm for partitions in storey 2. The lateral deformation of the partitions at yield and at failure is assumed as 0.3% and 0.9% of the storey height, respectively. Thus, the partitions contribute a shear strength of 658 kN to each storey. These contributions of stiffness and strength are assumed to be the same for all five zones. Two bounding cases are considered: the first assumes that the partitions are 'absent' and do not provide any stiffness and strength; the second assumes that they are 'present' and are effective. In both cases, a dead load allowance of 1.2 kPa is included for the partitions in the floor dead load of 4.8 kPa.

7.6 Estimate of static overstrength

The static overstrength ratio, ρ_o, was defined in section 5.5 as the ratio of the strength provided by the LLRS to that prescribed by the NBCC in [2.8]. Table 7.5 gives

---

[1] Cohen, J.M. 1996. Personal communication.

the strength of the roof diaphragm and the CBF, and gives the static overstrength ratios for both. The factored base shear for the CBF, line 4 of Table 7.5, is one half of the base shear in line 1 of Table 7.2. Similarly, the factored storey shear for storey 2, line 9 of Table 7.5, is one half of the force at the roof (equal to 0.5 x 0.38 x base shear in line 1 of Table 7.2). These overstrength ratios are also shown in Fig. 7.5.

The value of ρ_o for the diaphragm is greatest in zone 1 and reduces thereafter. For the CBF with partitions absent, the value of ρ_o for storey 1 is almost constant for zones 1, 2, and 3. It increases in zones 4 and 5 because the contribution of the compression diagonal increases due to reduction in the brace KL/r ratio. For storey 2, it follows a similar trend except that it reduces in zone 5 due to an increase in the brace KL/r ratio. With partitions effective, the strength of both storeys is augmented by the shear strength of the partitions, resulting in an increase in ρ_o.

7.7 Structural models and assumptions

Static and dynamic analyses of the building are performed for earthquake ground motion in the N-S direction only. Three different structural idealizations are used to model the building. The models include: (a) a two-degree of freedom elastic model (2DOFE), (b) a two-dimensional, multi-degree of freedom nonlinear model (MDOFN), and (c) a three-dimensional model (3-D).

The 2DOFE model is used for free vibration analysis only. The roof and floor diaphragms are assumed to be rigid and are represented by single masses as shown in Fig. 7.6. Lateral stiffnesses K_1 and K_2 are provided by the tension diagonal of the CBFs, the partitions, and all the columns in the building. The columns contribute to lateral stiffness predominantly in the second mode. They are continuous through the floor and therefore would have to bend to accommodate this mode shape.

The two-dimensional model used for design of the CBF is enhanced to obtain the MDOFN model, shown in Fig. 7.7. This planar model, representing one of the two symmetric CBFs, is used with all the response analysis procedures mentioned in section 4.4. The MDOFN model accounts for the nonlinear seismic behaviour of the CBF, the contribution of the partitions, and the limited strength of the roof diaphragm.

However, flexibility of the roof diaphragm is neglected. This assumption is considered valid because (a) the CBFs are located at about the third points, (b) the mass at the roof level is only about 1/4 of the total effective mass, and (c) the rigid floor constrains all deflections at the floor level to be the same. Consequently, the effect of roof diaphragm flexibility is decreased. The braces are modelled with truss elements. The beams and columns are modelled with beam-column elements with appropriate end conditions. The moment of inertia of each "exterior" column of the braced bay is increased to account for the contribution of the gravity columns to the lateral stiffness, and is given in Table 7.6. The partitions are modelled with plane stress elements that are placed within the braced bay in Fig. 7.7. Thus, one half of the partitions in a storey are lumped together in the plane of each CBF. The total mass at each level is lumped into two masses based on the tributary area on each side of the CBF. These masses and the appropriate weights are placed on dummy columns used to model the P-Δ effect. Although relatively simple, the dummy columns as shown for the second storey introduce two approximations. The P-Δ effect is over emphasized because the total deflection and not just that of the second storey is used. Secondly, the gravity loads acting on the first storey columns do not include those from the roof. These approximations could be removed by simply placing the second storey dummy columns on top of the first storey columns. The dummy columns are attached to the CBF with rigid-plastic links. The strength of these links at the roof level is set equal to the shear capacity of an appropriate length of the diaphragm. For example, the strength of rigid-plastic link element number 3, in Fig. 7.7, is set equal to 2 times the shear strength of the diaphragm between C-1 and C-2, in Fig. 7.1, because the lateral shears are generated from roof masses on the two sides. The factor of 2 represents the maximum force that can be transferred from this segment of the diaphragm to the CBF. The strength of the links at the floor level is set to a high value. The axial force developed in these links in the time history analyses may be compared to the design force for the floor beam-exterior column connections.

The 3-D model is used for free vibration analysis only. The CBF is modelled with truss elements. The remaining framework is modelled with beam-column elements with appropriate end conditions. The roof diaphragm and the partitions are modelled with plane stress elements of appropriate thickness. Translational masses are distributed

in the plane of the roof diaphragm in both horizontal directions. Thus, the flexibility of the roof diaphragm is considered. The floor diaphragm is assumed to be rigid and the mass is simply lumped at that level.

Table 7.6 summarises the modelling details used in each zone. The strengths of the braces are used in nonlinear static and dynamic analyses with the MDOFN model.

7.8 Free vibration analysis

Table 7.7 summarises the fundamental period obtained from a free vibration analysis with each model in the N-S direction. The design period specified by the NBCC is also given for comparison. All the models assume stiffness contribution from the tension diagonal only. The effect of stiffness contribution of the partitions is assessed by comparing the periods obtained with the partitions absent and present. The effect reduces with increase in the seismic zone as the stiffness provided by the CBFs increases proportionately. The periods obtained by the 2DOFE, MDOFN, and the 3-D model are in good agreement and suggest that flexibility of the roof diaphragm does not influence the fundamental period significantly. Hence, the MDOFN model that neglects the flexibility of the roof diaphragm is considered to be adequate for analysis of this building. The period by all these models is significantly greater than the NBCC estimate. Additional analyses with the 3-D model assuming both diagonals and the partitions to be effective, gives periods ranging from 0.65 s in zone 1 to 0.33 s in zone 5.

7.9 Effective overstrength

The effective overstrength ratio was defined in section 5.10. Figures 7.8 and 7.9 give the effective overstrength ratio for both storeys of the CBF and the roof diaphragm. Yielding may occur in some earthquakes if the ratio is less than 1.0. For storey 1, the presence of the partitions does not change the ratio much. For storey 2, there is a significant increase in the ratio with the partitions present, that reduces with increase in the seismic zone. The ratio for the roof diaphragm decreases with the presence of the partitions because of an increase in the spectral ordinates due to a reduction in period. The figures suggest that yielding may occur in all zones.

7.10 Response spectrum analysis

Figure 7.10 shows the distribution of lateral force at the roof and the floor from a response spectrum analysis (RSA) with the partitions absent, and the distribution used in design from [7.1]. The lateral force is normalised with respect to the base shear developed. The force applied at the roof is greater marginally than that from the RSA in all zones, except zone 1. The reverse occurs for the floor. Figure 7.11 shows similar data for the case with partitions present. The lateral force at the roof from the RSA reduces marginally from that in Fig. 7.10 and the reverse occurs for the floor. The distribution of lateral force by [7.1] is appropriate for such buildings with rigid diaphragms and agrees well with that from the RSA.

7.11 Nonlinear static analysis

A nonlinear static analysis of the building is performed with the MDOFN model to assess the behaviour under the prescribed lateral force and under large displacements that might occur in the design earthquake. A bilinear elasto-plastic model is used for the braces in each storey with the tensile and compressive capacity assumed equal to P_{yp} and P_{ync}, respectively, given in Table 7.6.

Figure 7.12 shows the drift under the prescribed lateral force given on lines 3 and 4 in Table 7.2, for the case with partitions absent. The compression diagonal buckles in all zones. The drift in zones 4 and 5 is reduced from that in the other zones because of the significant compressive capacity of the braces. The average drift for all five zones from an elastic analysis with SODA assuming a tension-only bracing, is 16 mm at the floor and 29 mm at the roof, with a coefficient of variation of 0.04 for both. The drift at the roof is amplified by an arbitrary factor of 2.0 and is used as a target displacement for static 'pushover analysis.' The lateral force distribution obtained from response spectrum analysis is applied on the structure. Figure 7.13 shows the displaced shape at the target displacement. The tension diagonal of the CBF yields at a base shear of 579 kN, 1250 kN, 1970 kN, 3180 kN, and 4730 kN in zones 1, 2, 3, 4, and 5, respectively. In the pushover analysis of the CBF in zone 5, the original floor beam section (W360x64) developed a plastic hinge due to combined axial load and moment. Results reported for zone 5 are with the revised section (W610x125).

Figures 7.14 and 7.15 show the results for the case with partitions present. The drifts in Fig. 7.14 are less than those in Fig. 7.12 because of the additional stiffness from the partitions. The compression diagonal buckles in all zones. In the static 'pushover analysis,' a yield mechanism is formed in storey 1 at a base shear of 990 kN, 1330 kN, 2010 kN, 3220 kN, and 4960 kN in zones 1, 2, 3, 4, and 5, respectively.

In some of the static 'pushover analyses,' rigid-plastic links number 3 and 4, shown in Fig. 7.7, yielded before the braces in storey 2. This suggests that in a severe earthquake, the shear strength of the roof diaphragm may be attained before brace yield in storey 2. An appropriate measure may be to strengthen the diaphragm so that the braces yield first. This was not carried out because it is not mandatory in the current design philosophy which is not capacity based.

7.12 Nonlinear dynamic time history analyses

Some relevant parameters for the MDOFN model of the building are given in Table 7.6. The braces of the CBF are modelled with the EL9 buckling element described in Appendix C. Rayleigh damping is used with the constants chosen to obtain 3% and 5% damping in the first and second mode, respectively. The P-Δ effect is considered in all analyses. Earthquake accelerograms for analysis in each seismic zone are given in Tables 4.1 to 4.10. The time history dynamic response of the structure is evaluated at the response levels given in Table 7.8. The rationale used to select these levels is explained in section 5.13. The dynamic response of the building in zones 1 to 5 is reported in Tables 7.9 to 7.13, respectively. Most of the response parameters have been discussed in Chapter 5. The beam response ratio is the interaction ratio of the beam in tension or in compression. The shear force response ratio of the roof diaphragm is the greater of the ratio of the force developed in links 3 or 4 to their capacity discussed in section 7.7. Similarly, the 'slip in link' defines the maximum inelastic extension in these links. The dynamic response in each zone is discussed in the following sections.

7.12.1 Response in zone 1 (Kamloops)

Table 7.9 presents the summary of dynamic response in zone 1. The response of the acceleration set is evaluated at the $\mu + 1\ \sigma$ level. For the case with partitions absent,

the $\mu + 1\ \sigma$ roof drift of 0.37% is less than the 1% limit in Table 4.13. The $\mu + 1\ \sigma$ interstorey drift for both storeys exceeds 0.35% and is indicative of brace yielding. The columns and beams respond elastically. The brace response in both storeys is predominantly elastic with yielding occurring in only 1 of the 8 records. The braces buckle extensively due to their low compressive capacity. The roof diaphragm response is elastic. The storey shear capacity is attained in the same records that cause brace yielding.

With partitions present, the $\mu + 1\ \sigma$ drift of the roof reduces from 0.37% to 0.28%. The interstorey drift of both storeys decreases. The response ratio of the exterior column reduces, while that of the central column, floor beam, and roof beam, increases. The brace response reduces in both storeys. The partitions respond elastically. The response of the roof diaphragm increases. The storey shear response ratio also reduces because of load sharing by the partitions.

The response of the velocity set is also evaluated at the $\mu + 1\ \sigma$ level. With the partitions absent, the response is qualitatively similar to that of the acceleration set with the exception that no brace yielding occurs. With the partitions present, the change in response is similar to that observed for the acceleration set.

In summary, the response in zone 1 is predominantly elastic. The slender braces buckle extensively in compression and yield in tension in only 1 of the 8 records of the acceleration set but do not yield in any of the records of the velocity set. The maximum ductility demand in tension is 1.11 for braces in storey 1 and 1.34 for braces in storey 2. Damage may initiate in some of the non-structural partitions as the interstorey drift exceeds 0.25% at the $\mu + 1\ \sigma$ level of response.

7.12.2 Response in zone 2 (Princeton)

Table 7.10 presents the summary of dynamic response in zone 2. The $\mu + 1\ \sigma$ response level is used to evaluate the response of both the acceleration set and the velocity set. For the acceleration set with partitions absent, the $\mu + 1\ \sigma$ drift of the roof is 0.43%. The $\mu + 1\ \sigma$ interstorey drift for both storeys exceeds 0.35% indicative of brace yielding. The columns and beams respond elastically. The braces in both storeys yield in 3 of the 12 records. The shear capacity of the diaphragm is attained in 6 of the 12 records

with a maximum slip of 3 mm in the rigid-plastic link. With the partitions present, the change in response is similar to that observed in zone 1. Partitions in storey 1 yield in 3 of the 12 records.

For the velocity set, the response is qualitatively similar to that of the acceleration set with some exceptions. With partitions present, the interstorey drift is seen to increase for storey 1 while it reduces for storey 2 and the roof. The brace response increases in storey 1 while that in storey 2 reduces. Partitions in storey 1 yield in 6 of the 12 records while those in storey 2 remain elastic. The storey shear response ratio increases for storey 1 and reduces for storey 2.

In summary, some inelastic action is evident in the response of the braces and the roof diaphragm. The maximum brace ductility demand is 1.57 in storey 1 and 1.34 in storey 2. Damage to non-structural partitions may initiate in both storeys as the $\mu + 1\ \sigma$ drift exceeds 0.25%.

7.12.3 Response in zone 3 (Hope)

Table 7.11 presents the summary of dynamic response in zone 3. The $\mu + 1\ \sigma$ level is used to evaluate the response of the acceleration set. With the partitions absent, the $\mu + 1\ \sigma$ drift of the roof is 0.34% and the interstorey drift in storey 1 exceeds 0.35% indicating brace yield. The response of the exterior column is elastic. However, the central column is overloaded in compression. This column is modelled with an elastic beam-column element and hence appears to be able to carry a compressive force greater than its calculated capacity. No large deformation effect occurs in the analysis because no yielding occurs. The overload suggests that the column section needs revision. This was not done because an increase in the column size would only increase its axial stiffness in the analysis. This column does not contribute any lateral stiffness because it is pinned at both ends. Thus, all other results would have been almost the same if the column section were revised and the dynamic analyses repeated. The column design philosophy is reviewed for zones 4 and 5 to prevent such a failure. The beam response is elastic. Braces yield in 2 of the 12 records in storey 1 while those in storey 2 respond elastically. The response of the roof diaphragm is also elastic.

With partitions present, the drifts, column responses, and brace responses reduce while those of the beams increase. Partitions yield in 4 of the 12 records in storey 1 while those in storey 2 remain elastic. The roof diaphragm response is elastic.

For the velocity set, the response is evaluated at the μ level and is qualitatively similar to that of the acceleration set. Braces in storey 1 yield in 4 of the 9 records while those in storey 2 respond elastically. Partitions yield in 5 of the 9 records in storey 1 only. The shear force response ratio for the roof diaphragm shows yield in 1 of the 9 records with a maximum slip of 2 mm only.

In summary, some inelastic action occurs in the braces and limited inelastic action in the roof diaphragm. The maximum brace ductility demand in storey 1 is 1.5 while that in storey 2 is marginally less than 1.0. Damage may initiate in non-structural partitions as the interstorey drift exceeds 0.25%. The response ratio of the central column exceeds 1.0 at the $\mu + 1\ \sigma$ level for all four cases. This requires a review of the column design philosophy to ensure that the central column does not fail. Although the column overload may be transferred, at least in part, to the floor beam and the upper tension diagonal, column failures, in general, should be avoided because such failures can be disastrous (Osteraas and Krawinkler 1989).

7.12.4 Response in zone 4 (Vancouver)

The floor beam in this zone is designed by the capacity design approach described in section 7.4. The compressive capacity of the central column is also checked with [7.3]. Table 7.12 presents the response in zone 4. The response is evaluated at the $\mu + 1\ \sigma$ level for the acceleration set. With the partitions absent, the $\mu + 1\ \sigma$ drift of the roof is 0.45% and the interstorey drift of both storeys exceeds 0.35%. The exterior columns, central column, and the beams respond elastically. Braces in storey 1 yield in 2 of the 12 records while those in storey 2 respond elastically. The shear capacity of the diaphragm is exceeded in 10 of the 12 records with a maximum extension of 31 mm in the rigid-plastic link. The storey shear response ratio also shows inelastic response in storey 1. With partitions present, the drifts and the response of the exterior columns, reduce. The response of the central column and the beams increases. The brace response in storey 1 is almost unchanged while that in storey 2 reduces significantly, largely due to the limited

instance of brace buckling in this storey. Partitions in storey 1 yield in 7 of the 12 records while those in storey 2 respond elastically. The diaphragm response is almost unchanged.

For the velocity set, the response is evaluated at the μ level and is qualitatively similar to that of the acceleration set.

In summary, limited inelastic action occurs in the braces while significant inelastic action occurs in the roof diaphragm. The capacity design approach protects the floor beam and it responds elastically with a maximum response ratio of 0.93 in compression. The maximum brace ductility demand is 1.50 in storey 1 and 1.25 in storey 2. Partitions yield in storey 1 only.

7.12.5 Response in zone 5 (Victoria)

Table 7.13 presents the response in zone 5. The capacity design approach was used to revise the floor beam design. The compressive capacity of the central column was also checked with [7.3]. The response is evaluated at the $\mu + 1\,\sigma$ level for the acceleration set. With partitions absent, the $\mu + 1\,\sigma$ drift of the roof is 0.63%. The interstorey drift at storey 2 is 0.91% suggesting severe inelastic action in the braces and partitions. The response of the columns and beams is elastic. The braces in storey 1 respond elastically while those in storey 2 show extensive yielding in 9 of the 12 records. The roof diaphragm also attains its shear capacity in 9 of the 12 records.

With partitions present, the drift at the roof and the interstorey drift at storey 2 reduces while that in storey 1 increases. The response of the columns reduces while that of the beams increases. The brace response in storey 1 increases with yielding occurring in 3 of the 12 records while that in storey 2 reduces marginally. Partitions yield extensively in both storeys. The roof diaphragm also responds inelastically with yielding in 9 of the 12 records.

For the velocity set, the response is evaluated at the μ level. While the response is qualitatively similar to that of the acceleration set, several points may be noted. For the case with partitions absent, the interstorey drift in storey 2 is large. The response ratio for the floor beam in compression attains a value of 1.03 suggesting that the section is just adequate. The brace ductility demand in storey 2 has a value of 3.1 at the $\mu + 1\,\sigma$ level and reduces significantly with partitions present.

In summary, there is limited inelastic action in the braces in storey 1 with a maximum ductility demand of 1.6. There is severe inelastic action in the braces in storey 2 with a maximum ductility demand of 4.1. The partitions in both storeys yield in a few records. The roof diaphragm response also shows extensive yielding. The interstorey drift exceeds 0.25% at the μ level for all cases indicating damage to non-structural partitions. The interstorey drift exceeds 0.75% at the $\mu + 1\,\sigma$ level in storey 2 for the case of partitions absent and could cause failure of non-structural partitions.

7.13 Evaluation of the capacity design approach

As discussed in section 7.4, the capacity design approach was used to determine the axial compression for design of the floor beam in zones 4 and 5. Table 7.14 gives the axial compression for design of the floor beam, F_1, and the central column, F_3, determined from [7.2] and [7.3], respectively. The tensile (T_1 & T_2) and compressive forces (C_1 & C_2) in the braces are taken equal to P_{yp} and P_{ync}, respectively. The maximum response ratio of the floor beam in compression is 0.93 in zone 4, and 1.03 in zone 5. This suggests that the capacity provided by this approach is just adequate to ensure elastic response of the floor beam. Note that a more conservative design force could be adopted in zone 5 by selecting a lower value for the forces T_2 and C_2 in [7.2]. The capacity of the central column is checked against the force F_3 from [7.3]. Table 7.15 gives a comparison of the axial compression from the capacity design approach, that is, force F_1 for the floor beam and force F_3 for the central column from Table 7.14, with the factored load assumed in the design of the floor beam and the central column. The latter is obtained from the three load combinations given in section 7.3. The ratio for the floor beam is particularly high in zones 4 and 5 with values of 1.8 and 2.1, respectively. This explains the failure of the floor beam with the originally selected W410x60 section in zone 4 and the W360x64 section in zone 5, as mentioned in section 7.3. For the central column, although the factored load is greater than F_3 in all the zones, the column is overloaded in compression in zone 3. This may also be explained with the help of [7.3]. An examination of the response in zone 3 reported in Table 7.11, shows that braces in

storey 1 yield in tension and buckle in compression while those in storey 2 remain elastic. Referring to the details for zone 3 in Table 7.6 and substituting T_1 equal to 2338 kN, C_1 equal to 249 kN, T_2 less than 966 kN, and C_2 equal to 491 kN in [7.3], results in values for F_3 that exceed the value of 1085 kN given in Table 7.14. Hence, it may be prudent to adopt a conservative estimate from [7.3] for design of the central column.

Table 7.16 gives the axial force for design of the connections between the floor beam and the exterior columns of the CBF. Element numbers 1 and 2 refer to the rigid-plastic links at the floor level of the MDOFN model shown in Fig. 7.7. The response force is the greater of the $\mu + 1\ \sigma$ response among the acceleration and velocity sets for the case with partitions absent. The factored load for elements 1 and 2 is the axial force that the connections would typically be designed for; the two loads add up to the lateral force at the floor in line 3 of Table 7.2. The ratio of the response force to factored load ranges from 1.04 to 2.24 for element 1, and from 1.11 to 2.54 for element 2. This suggests that the connections may be inadequate in zones 4 and 5 where the ratio is particularly high. The 'capacity force' in Table 7.16 is the axial force for design of the connections from the capacity design approach [in which all diagonal members are considered to have reached their tensile or compressive capacities simultaneously] and is equal to the force F_1 or F_2 in Table 7.14. The ratio of the response force to the capacity design force suggests that overload of the connections can be controlled by use of this approach. For braces reaching their capacities in the displaced shape of the first mode, the ratios of the forces do not exceed the resistances when the connection overstrength ratio ($1/\phi$, see section 5.16) is considered.

7.14 Estimate of lateral drift

Figure 7.16 shows the maximum and the $\mu + 1\ \sigma$ drift of the roof and the floor from time history dynamic analyses with partitions absent, and the NBCC drift estimate from [2.15]. The maximum roof drift includes the greater of the inelastic extension of the two rigid-plastic links at the roof level. The drifts at both response levels are the greater of those obtained for the acceleration set and the velocity set in each zone. The NBCC drift estimate is obtained by multiplying the drift from nonlinear static analysis (NSA) of

the building under the prescribed lateral force, by the force modification factor, R. The NBCC drift provides a reasonable estimate of the maximum roof drift in zones 1, 2, and 3. However, the maximum roof drift is significantly greater in zones 4 and 5 because of inelastic action in the rigid-plastic links. The same observation is valid for the $\mu + 1\ \sigma$ roof drift. The average roof drift in all zones from a linear elastic analysis neglecting the compression diagonal is 0.36%. Using [2.15], a drift of 0.54% is obtained that is greater than the $\mu + 1\ \sigma$ drift in zones 1 to 4. Although the maximum and the $\mu + 1\ \sigma$ roof drifts exceed the NBCC estimate in zones 4 and 5, they are still within the ATC (1995) limit of 1% and the NBCC limit of 2%. The NBCC estimate of the floor drift is in reasonable agreement with those from dynamic analyses in zones 1, 2, and 3, and is significantly lower in zones 4 and 5. The amplified floor drift from a linear elastic analysis neglecting the compression diagonal is 0.30% and provides a good estimate of the maximum floor drift in all zones.

With partitions present, the maximum and the $\mu + 1\ \sigma$ drifts of the roof and the floor shown in Fig. 7.17, reduce from those in Fig. 7.16, except for the maximum drift in zone 5. The drifts from dynamic analyses are greater than the corresponding NBCC drift estimates in all zones.

The NBCC drift from [2.15] may provide a better estimate of the maximum roof drift if there is no inelastic action in the rigid-plastic links. Such a design requires use of the capacity design approach to ensure that braces in storey 2 yield before the rigid-plastic links.

7.15 Brace ductility demand in tension

Figure 7.18 shows the maximum and the $\mu + 1\ \sigma$ brace ductility demands in tension at both storeys for the case with partitions absent. In zones 1 to 4, the maximum demand in both storeys does not exceed the 'rule of thumb' limit of 1.5. The demand at both response levels is significantly greater than 1.5 in zone 5 only.

Figure 7.19 shows similar data for the case with partitions present. The demand at both response levels is within the limit of 1.5 in all zones, except zone 5 where the maximum demand is 1.6. Comparison of Figs. 7.18 and 7.19 shows that the presence of the partitions does not influence the demand in storey 1 as significantly as in storey 2.

The static overstrength ratios shown in Fig. 7.5 suggest that the presence of the partitions provides a significant increase in strength at storey 2, resulting in a reduced ductility demand.

An examination of the time history output for the braces reveals that the maximum number of tension yield excursions in a brace in a given earthquake record is limited to 3 for braces in storey 1 and 5 in storey 2. The maximum strain rate in the braces just before yield in storey 1 and storey 2 is 35×10^{-3}/s and 86×10^{-3}/s, respectively. The braces are class 1 sections and should be capable of satisfying the ductility demands observed.

7.16 Design of CBF connections

Figure 7.20 shows the ratio of the brace response force at the $\mu + 1\ \sigma$ and the μ response levels to the design force for brace connections for the case with partitions absent. For a tension-only CBF, the connection design force is assumed equal to the force in the tension braces to resist the lateral force given in lines 3 and 4 of Table 7.2. The ratio of the $\mu + 1\ \sigma$ brace force to the connection design force exceeds 1.0 for both storeys in all zones. The ratio of the mean brace force to the connection design force is lower with a minimum value of 0.72 for storey 1 and 0.67 for storey 2.

Figure 7.21 shows similar data for the case with partitions present. The ratio of the $\mu + 1\ \sigma$ brace force to the connection design force for storey 1 is 0.97 in zone 1 and exceeds 1.0 in zones 2 to 5. For storey 2, this ratio has a minimum of 0.75 in zone 1. The ratio of the mean brace force to the connection design force has a minimum value of 0.69 for storey 1 and 0.53 for storey 2.

Assuming the $\mu + 1\ \sigma$ response level as representative in all zones, the brace connections should develop the tensile strength of the brace.

7.17 Conclusions and recommendations

Based on the analytical studies performed with the two-storey building in five seismic zones, conclusions and recommendations for seismic design of such buildings are developed as follows:

7.17.1 Estimate of period

A comparison of the fundamental period obtained with models that neglect the flexibility of the roof diaphragm and the three-dimensional model that considers it, suggests that roof diaphragm flexibility has little influence on the fundamental period of this building. Hence, models that assume a rigid roof diaphragm are adequate for free vibration and response spectrum analysis of such buildings as discussed in section 7.7. The stiffness from non-structural partitions and cladding can reduce the period of the building significantly. This effect is pronounced in the low seismic zones and reduces in high seismic zones as the stiffness provided by the CBF increases proportionately. The empirical estimate of the period of braced frames in the NBCC gives periods that are significantly smaller than those obtained with various analytical models considered in this study and results in the provision of greater base shear capacity to the structure.

7.17.2 Distribution of lateral force along height

The NBCC distributes the lateral force along the building height by [7.1] that assumes the building to be responding primarily in the first mode with a mode shape that is linear. This distribution is found to be appropriate for such buildings and agrees with that obtained from response spectrum analysis.

7.17.3 Use of the capacity design approach

The capacity design approach is recommended in zones 3, 4, and 5, even though the roof diaphragm responds inelastically in zone 2. The inelastic response of the roof diaphragm observed in zone 2, and for that matter in zones 4 and 5, if considered unsatisfactory, may be avoided by ensuring that the roof diaphragm has greater shear strength than the bracing in storey 2. The failure of the initial selection for the floor beam in zones 4 and 5 and of the central column in zone 3 was explained by this approach and shows its effectiveness. Most structural analysis and design programs perform a linear elastic structural analysis and consider the strength of the individual members for member selection and design only. This traditional design approach neglects the relative strength of elements in the lateral load path that is of primary concern in seismic design. In a

large earthquake, the force that the connections, beams, and columns of the CBF are likely to be subjected to is limited by the actual strength of the bracing.

7.17.4 Use of various analytical procedures in seismic design

A linear elastic static analysis of the structure is adequate for implementing the equivalent lateral force procedure of the NBCC. All designs in this study were performed with a linear elastic structural analysis and design program, SODA (Acronym Software 1994), using a tension-only CBF in all seismic zones. Based on the results from dynamic analyses, this design method is adequate in low seismic zones. However, in moderate to high zones, a check on the relative strength of components along the lateral load path is necessary to determine the weakest link that will yield in a severe earthquake. The compressive resistance of the braces increases with seismic zone and is significant in zones 3, 4, and 5. This results in overstrength in the system and the adequacy of the beams and columns of the CBF should be checked to avoid failure of these elements.

The nonlinear static analysis (NSA) was able to predict possible yielding in the rigid-plastic links at the roof level and the failure of the W360x64 section originally selected for the floor beam in zone 5. However, the failure of the W410x60 section for the floor beam in zone 4 was not detected by this procedure. Similarly, overload of the central column in zone 3 was also not detected. Although the NSA procedure is a static procedure and does not give information on the dynamic demands, it is a useful extension of the conventional static analysis in that it gives an indication of the inelastic behaviour. It is therefore recommended for design office use.

7.17.5 Anticipated deformations of the structure

The NBCC drift provides a reasonable estimate of the drift in zones 1 to 3 only. In zones 4 and 5, the observed drifts are greater because of inelastic response. Although inelastic action occurred in the rigid-plastic links at the roof level, the maximum drift was still within the ATC (1995) limit of 1%. The NBCC drift limit of 2% seems to be rather large for this building. The allowable interstorey drift may be determined more meaningfully by considering the geometry and material properties of the braced frame and determining the ductility demand on the braces for various assumed drifts.

7.17.6 Design of brace members

The compressive resistance of the compression diagonal is significant in moderate and high seismic zones and should be considered while evaluating the adequacy of the beams and columns of the CBF. The HSS braces provided in this study were within 11% of the design requirement. Oversized brace members should be avoided because it is difficult to arrive at a suitable design load for the connections, beams, and columns of the CBF. Use of class 1 sections for the braces is recommended because they are likely to sustain the observed ductility demands and inelastic cycles better than other sections.

7.17.7 Design of connections

Brace connections should develop the tensile strength of the member, preferably in all zones. Because the braces provided are within 11% of the design requirement, this is not an expensive proposition and results in better design practice. The connections should also develop the compressive resistance of the braces in zones 3, 4, and 5.

7.17.8 Design of non-structural components

All partitions in this study were lumped in the plane of the bracing. From the geometry and material properties of the CBF, the braces yield at an interstorey drift of 0.35% in both storeys. Studies on partitions by Freeman (1977) and Rihal (1986) suggest that damage initiates in gypsum wallboard partitions at an interstorey drift of about 0.25% to 0.30% and failure occurs at about 0.75%. Thus, the coupling of these flexible elements with the stiff CBFs protects them from excessive drift and damage. This concept may be used in low and moderate seismic zones where earthquakes are less frequent. The ICBO (1997) gives stiffness and strength estimates for typical partitions that may be used in design. In high seismic zones where moderate earthquake events are expected to occur frequently, isolation of the non-structural elements from the LLRS may be an alternative to avoiding damage and repair.

Table 7.1 Estimate of effective seismic weight

Item	Roof		Floor	
	Intensity	Load (kN)	Intensity	Load (kN)
Dead load	1.05 kPa	2381	4.80 kPa	10886
Live load including snow	0.40 kPa	896		
Dead load of cladding	4.0 kN/m	792	9.5 kN/m	1881
Total		**4069**		**12767**

Table 7.2 CBF design parameters in the N-S direction

Line	Parameter	Zone 1	Zone 2	Zone 3	Zone 4	Zone 5
1	base shear (kN)	808	1616	2425	3233	4849
		CBF design				
2	factored base shear (kN)	529	1004	1480	1953	2898
3	lateral force at floor (kN)	341	603	889	1225	1811
4	lateral force at roof (kN)	188	401	591	728	1087
		Design of brace member				
	Storey - 1					
5	x-section required (mm^2)	2297	4360	6427	8481	12585
6	square HSS used (class 1)	102 x 6	152 x 8	152 x 13	254 x 10	305 x 11
7	x-section provided (mm^2)	2320	4430	6680	9090	12800
8	ratio (provided/required)	1.01	1.02	1.04	1.07	1.02
9	KL/r ratio	160	105	110	62	52
	Storey - 2					
10	x-section required (mm^2)	790	1685	2483	3058	4566
11	square HSS used (class 1)	64 x 4	102 x 5	152 x 5	178 x 5	127 x 11
12	x-section provided (mm^2)	872	1790	2760	3250	4840
13	ratio (provided/required)	1.10	1.06	1.11	1.06	1.06
14	KL/r ratio	247	152	99	85	128
15	Exterior columns	W410x67	W410x67	W610x84	W610x84	W610x101
16	governing load case	(a)	(c)	(c)	(c)	(c)
17	Central column	W200x42	W200x46	W200x52	W250x73	W310x79
18	governing load case	(c)	(c)	(c)	(c)*	(c)*
19	Floor beam	W410x60	W410x60	W410x60	W610x84	W610x125
20	governing load case	(a)	(a)	(a)	(c)*	(c)*
21	Roof beam	W530x82	W530x82	W530x82	W530x82	W530x82
22	governing load case	(a)	(a)	(a)	(a)	(a)

* revised sections

Table 7.3 Roof diaphragm design parameters

Parameter	Zone 1	Zone 2	Zone 3	Zone 4	Zone 5
factored shear force (kN)	103	224	333	411	616
shear strength (kN)	189	227	427	427	821
shear stiffness, G′ (kN/mm)	2.41	2.48	4.17	4.17	18.52
profile depth (mm)	38	38	38	38	38
profile thickness (mm)	0.76	0.76	0.91	0.91	1.22
# of sheet/purlin fasteners per sheet	4	4	4	4	7
seam fastener spacing (mm)	600	300	150	150	300
sheet length	sheets assumed 3 span continuous over the purlins				

Table 7.4 CBF design parameters in the E-W direction

Parameter	Zone 1	Zone 2	Zone 3	Zone 4	Zone 5
base shear for building (kN)	808	1616	2425	3233	4849
CBF design					
factored base shear (kN)	556	1052	1550	2047	3041
lateral force at floor (kN)	358	631	931	1284	1903
lateral force at roof (kN)	198	421	619	763	1138
Design of braces					
Storey - 1					
square HSS used (class 1)	89 x 8	127 x 10	152 x 13	254 x 10	305 x 13
x-section provided (mm^2)	2410	4240	6680	9090	14400
Storey - 2					
square HSS used (class 1)	64 x 4	76 x 6	152 x 5	102 x 10	152 x 10
x-section provided (mm^2)	872	1670	2760	3280	5210

Table 7.5 Static overstrength ratio for roof diaphragm and CBF

Line	Parameter	Zone 1	Zone 2	Zone 3	Zone 4	Zone 5
	Roof diaphragm					
1	factored shear force (kN)	103	224	333	411	616
2	shear strength (kN)	189	227	427	427	821
3	overstrength ratio	1.83	1.01	1.28	1.04	1.33
	CBF: Storey-1					
4	factored base shear (kN)	404	808	1212	1617	2425
	strength provided					
5	(a) partitions absent (kN)	625	1264	1891	3303	5044
6	overstrength ratio	1.55	1.56	1.56	2.04	2.08
7	(b) partitions present (kN)	955	1593	2221	3632	5373
8	overstrength ratio	2.36	1.97	1.83	2.25	2.22
	CBF: Storey - 2					
9	factored storey shear (kN)	154	336	499	616	923
	strength provided					
10	(a) partitions absent (kN)	236	502	823	1144	1385
11	overstrength ratio	1.53	1.49	1.65	1.86	1.50
12	(b) partitions present (kN)	565	831	1152	1473	1714
13	overstrength ratio	3.67	2.47	2.31	2.39	1.86

Table 7.6 Modelling details for CBFs

Parameter	Zone 1	Zone 2	Zone 3	Zone 4	Zone 5
Exterior columns					
moment of inertia (mm^4)	1.41E+09	1.41E+09	1.67E+09	1.67E+09	1.83E+09
CBF: Storey-1					
tension yield force, P_{yp} (kN)	812	1551	2338	3182	4480
compressive capacity, P_{yn} (kN)	174	710	997	2672	4032
reduction factor for P_{ync}	0.25	0.25	0.25	0.50	0.60
post-buckling capacity, P_{ync} (kN)	44	178	249	1336	2419
base shear capacity (kN)	625	1263	1891	3303	5044
Storey - 2					
tension yield force, P_{yp} (kN)	305	627	966	1138	1694
compressive capacity, P_{yn} (kN)	28	149	491	752	553
reduction factor for P_{ync}	0.25	0.25	0.25	0.50	0.25
post-buckling capacity, P_{ync} (kN)	7	37	123	376	138
storey shear capacity (kN)	236	502	823	1144	1385

Table 7.7 Fundamental period from free vibration analyses in the N-S direction

Line	Model description	Zone 1	Zone 2	Zone 3	Zone 4	Zone 5
				Period (s)		
1	NBCC empirical estimate	0.24	0.24	0.24	0.24	0.24
	2DOFE model					
2	partitions absent	1.12	0.78	0.63	0.55	0.46
3	partitions present	0.81	0.65	0.56	0.50	0.43
	MDOFN model					
4	partitions absent	1.07	0.78	0.64	0.56	0.47
5	partitions present	0.80	0.66	0.57	0.51	0.44
	Three-dimensional model					
6	partitions absent	1.11	0.83	0.68	0.61	0.48
7	partitions present	0.80	0.66	0.57	0.51	0.43

Note: All models assume a tension-only bracing system

Table 7.8 Response level for evaluating the time history dynamic response

Acclerogram set	Zone 1	Zone 2	Zone 3	Zone 4	Zone 5
Acceleration set	$\mu + 1\,\sigma$	$\mu + 1\,\sigma$	$\mu + 1\,\sigma$	$\mu + 1\,\sigma$	$\mu + 1\,\sigma$
Velocity set	$\mu + 1\,\sigma$	$\mu + 1\,\sigma$	μ	μ	μ

Table 7.9 Summary of dynamic response in zone 1 (Kamloops)

Response parameter	Response level	Partitions absent		Partitions present	
		A-set	V-set	A-set	V-set
Number of records		8	9	8	9
Roof drift (%)	$\mu+1\sigma$	0.37	0.31	0.28	0.26
Interstorey drift at storey-1 (%)	maximum	0.42	0.37	0.45	0.33
	$\mu+1\sigma$	0.37	0.31	0.35	0.31
	μ	0.23	0.24	0.21	0.23
Interstorey drift at storey-2 (%)	maximum	0.49	0.34	0.24	0.23
	$\mu+1\sigma$	0.39	0.32	0.21	0.20
	μ	0.25	0.26	0.14	0.16
Column response ratio					
Exterior column (storey-1)	maximum	0.70	0.68	0.64	0.64
	$\mu+1\sigma$	0.68	0.67	0.62	0.62
	μ	0.62	0.64	0.58	0.59
Central column	maximum	0.87	0.84	0.92	0.84
	$\mu+1\sigma$	0.82	0.75	0.83	0.80
	μ	0.63	0.66	0.62	0.69
Beam response ratio					
Floor beam - tension	maximum	0.45	0.44	0.48	0.48
- compression	maximum	0.40	0.40	0.45	0.44
Roof beam - tension	maximum	0.26	0.26	0.28	0.28
- compression	maximum	0.24	0.23	0.27	0.27
Brace response ratio					
Storey-1	maximum	1.00	0.95	1.00	0.87
	$\mu+1\sigma$	0.92	0.81	0.85	0.81
	μ	0.56	0.63	0.50	0.61
Ductility demand	maximum	1.05	0.90	1.11	0.80
	$\mu+1\sigma$	0.90	0.75	0.85	0.74
No. of records with yielding		1	0	1	0
Strain rate (s^{-1})	maximum	6.96E-03	-	1.02E-02	-
No. of records with buckling		7	9	7	9

continued

Table 7.9 Summary of dynamic response in zone 1 (concluded)

Response parameter	Response level	Partitions absent		Partitions present	
		A-set	V-set	A-set	V-set
Number of records		8	9	8	9
Brace response ratio					
Storey-2	maximum	1.00	0.93	0.71	0.68
	$\mu+1\sigma$	0.97	0.87	0.64	0.60
	μ	0.64	0.73	0.41	0.48
Ductility demand	maximum	1.34	0.90	0.67	0.63
	$\mu+1\sigma$	1.06	0.84	0.60	0.56
No. of records with yielding		1	0	0	0
Strain rate (s^{-1})	maximum	1.56E-02	-	-	-
No. of records with buckling		8	9	8	9
Partition response ratio					
Storey-1	$\mu+1\sigma$	-	-	0.94	0.95
No. of records with yielding		-	-	2	3
Storey-2	$\mu+1\sigma$	-	-	0.69	0.66
No. of records with yielding		-	-	0	0
Roof diaphragm response					
Shear force response ratio	maximum	0.78	0.71	0.91	0.92
	$\mu+1\sigma$	0.71	0.70	0.81	0.80
	μ	0.50	0.58	0.58	0.67
No. of records with yielding		0	0	0	0
Slip in link (mm)	maximum	-	-	-	-
Storey shear response ratio					
Storey-1	maximum	1.00	0.96	1.00	0.92
	$\mu+1\sigma$	0.93	0.82	0.89	0.86
	μ	0.62	0.67	0.58	0.67
No. of records with yielding		1	0	1	0
Storey-2	maximum	1.00	0.93	0.76	0.72
	$\mu+1\sigma$	0.97	0.87	0.67	0.64
	μ	0.65	0.74	0.45	0.51
No. of records with yielding		1	0	0	0

Table 7.10 Summary of dynamic response in zone 2 (Princeton)

Response parameter	Response level	Partitions absent		Partitions present	
		A-set	V-set	A-set	V-set
Number of records		12	12	12	12
Roof drift (%)	$\mu+1\sigma$	0.43	0.44	0.33	0.37
Interstorey drift at storey-1 (%)	maximum	0.62	0.55	0.59	0.55
	$\mu+1\sigma$	0.47	0.40	0.40	0.42
	μ	0.27	0.28	0.23	0.29
Interstorey drift at storey-2 (%)	maximum	0.46	0.51	0.24	0.27
	$\mu+1\sigma$	0.40	0.45	0.21	0.26
	μ	0.26	0.34	0.14	0.20
Column response ratio					
Exterior column (storey-1)	maximum	0.89	0.89	0.79	0.79
	$\mu+1\sigma$	0.84	0.87	0.74	0.78
	μ	0.72	0.78	0.65	0.70
Central column	maximum	0.87	0.84	0.90	0.93
	$\mu+1\sigma$	0.74	0.76	0.74	0.86
	μ	0.46	0.56	0.45	0.62
Beam response ratio					
Floor beam - tension	maximum	0.59	0.61	0.63	0.65
- compression	maximum	0.61	0.62	0.68	0.65
Roof beam - tension	maximum	0.27	0.27	0.28	0.30
- compression	maximum	0.28	0.28	0.30	0.30
Brace response ratio					
Storey-1	maximum	1.00	1.00	1.00	1.00
	$\mu+1\sigma$	0.87	0.92	0.83	0.96
	μ	0.55	0.67	0.52	0.69
Ductility demand	maximum	1.57	1.38	1.47	1.36
	$\mu+1\sigma$	1.17	0.98	0.97	1.03
No. of records with yielding		3	1	2	2
Strain rate (s^{-1})	maximum	1.59E-02	1.91E-02	1.64E-02	2.08E-02
No. of records with buckling		6	10	6	10

continued

Table 7.10 Summary of dynamic response in zone 2 (concluded)

Response parameter	Response level	Partitions absent		Partitions present	
		A-set	V-set	A-set	V-set
Number of records		12	12	12	12
Brace response ratio					
Storey-2	maximum	1.00	1.00	0.78	0.83
	$\mu+1\sigma$	0.92	1.05	0.65	0.77
	μ	0.60	0.80	0.41	0.56
Ductility demand	maximum	1.24	1.34	0.71	0.79
	$\mu+1\sigma$	1.01	1.11	0.57	0.69
No. of records with yielding		3	2	0	0
Strain rate (s^{-1})	maximum	1.41E-02	1.60E-02	-	-
No. of records with buckling		11	12	9	11
Partition response ratio					
Storey-1	$\mu+1\sigma$	-	-	0.91	1.07
No. of records with yielding		-	-	3	6
Storey-2	$\mu+1\sigma$	-	-	0.69	0.88
No. of records with yielding		-	-	0	0
Roof diaphragm response					
Shear force response ratio	maximum	1.00	1.00	1.00	1.00
	$\mu+1\sigma$	1.03	1.10	1.01	1.11
	μ	0.76	0.89	0.78	0.91
No. of records with yielding		6	7	5	9
Slip in link (mm)	maximum	3	17	6	14
Storey shear response ratio					
Storey-1	maximum	1.00	1.00	1.00	1.00
	$\mu+1\sigma$	0.95	0.98	0.90	1.01
	μ	0.68	0.77	0.64	0.77
No. of records with yielding		3	1	2	2
Storey-2	maximum	1.00	1.00	0.80	0.87
	$\mu+1\sigma$	0.96	1.08	0.67	0.81
	μ	0.68	0.86	0.47	0.62
No. of records with yielding		3	2	0	0

Table 7.11 Summary of dynamic response in zone 3 (Hope)

Response parameter	Response level	Partitions absent		Partitions present	
		A-set	V-set	A-set	V-set
Number of records		12	9	12	9
Roof drift (%)	$\mu+1\sigma$	0.34	0.40	0.29	0.36
Interstorey drift at storey-1 (%)	maximum	0.52	0.63	0.42	0.61
	$\mu+1\sigma$	0.44	0.53	0.38	0.49
	μ	0.33	0.35	0.29	0.31
Interstorey drift at storey-2 (%)	maximum	0.24	0.38	0.18	0.22
	$\mu+1\sigma$	0.23	0.30	0.18	0.21
	μ	0.19	0.20	0.15	0.15
Column response ratio					
Exterior column (storey-1)	maximum	0.61	0.72	0.57	0.61
	$\mu+1\sigma$	0.60	0.65	0.56	0.59
	μ	0.54	0.54	0.51	0.50
Central column	maximum	1.21	1.21	1.19	1.22
	$\mu+1\sigma$	1.23	1.23	1.14	1.21
	μ	0.93	0.81	0.86	0.78
Beam response ratio					
Floor beam - tension	maximum	0.67	0.67	0.70	0.71
- compression	maximum	0.71	0.81	0.75	0.82
Roof beam - tension	maximum	0.27	0.27	0.29	0.29
- compression	maximum	0.24	0.31	0.28	0.29
Brace response ratio					
Storey-1	maximum	1.00	1.00	0.98	1.00
	$\mu+1\sigma$	1.00	1.04	0.92	1.02
	μ	0.77	0.71	0.71	0.67
Ductility demand	maximum	1.18	1.50	0.91	1.45
	$\mu+1\sigma$	0.96	1.23	0.83	1.12
No. of records with yielding		2	4	0	4
Strain rate (s^{-1})	maximum	1.78E-02	2.25E-02	-	2.60E-02
No. of records with buckling		10	7	10	7

continued

Table 7.11 Summary of dynamic response in zone 3 (concluded)

Response parameter	Response level	Partitions absent		Partitions present	
		A-set	V-set	A-set	V-set
Number of records		12	9	12	9
Brace response ratio					
Storey-2	maximum	0.78	0.98	0.63	0.70
	$\mu+1\sigma$	0.72	0.85	0.58	0.67
	μ	0.57	0.56	0.45	0.44
Ductility demand	maximum	0.78	0.98	0.63	0.70
	$\mu+1\sigma$	0.72	0.85	0.58	0.67
No. of records with yielding		0	0	0	0
Strain rate (s^{-1})	maximum	-	-	-	-
No. of records with buckling		0	2	0	0
Partition response ratio					
Storey-1	$\mu+1\sigma$	-	-	1.06	1.06
No. of records with yielding		-	-	4	5
Storey-2	$\mu+1\sigma$	-	-	0.59	0.71
No. of records with yielding		-	-	0	0
Roof diaphragm response					
Shear force response ratio	maximum	0.80	1.00	0.86	1.00
	$\mu+1\sigma$	0.79	0.92	0.83	0.94
	μ	0.69	0.67	0.69	0.66
No. of records with yielding		0	1	0	1
Slip in link (mm)	maximum	-	1	-	2
Storey shear response ratio					
Storey-1	maximum	1.00	1.00	0.99	1.00
	$\mu+1\sigma$	1.01	1.03	0.94	1.01
	μ	0.83	0.77	0.77	0.73
No. of records with yielding		2	4	0	4
Storey-2	maximum	0.81	0.98	0.62	0.73
	$\mu+1\sigma$	0.74	0.88	0.59	0.70
	μ	0.62	0.62	0.49	0.49
No. of records with yielding		0	0	0	0

Table 7.12 Summary of dynamic response in zone 4 (Vancouver)

Response parameter	Response level	Partitions absent		Partitions present	
		A-set	V-set	A-set	V-set
Number of records		12	8	12	8
Roof drift (%)	$\mu+1\sigma$	0.45	0.55	0.40	0.42
Interstorey drift at storey-1 (%)	maximum	0.41	0.58	0.39	0.60
	$\mu+1\sigma$	0.39	0.44	0.39	0.47
	μ	0.27	0.31	0.27	0.31
Interstorey drift at storey-2 (%)	maximum	0.40	0.54	0.27	0.29
	$\mu+1\sigma$	0.36	0.46	0.27	0.28
	μ	0.27	0.32	0.20	0.21
Column response ratio					
Exterior column (storey-1)	maximum	0.72	0.73	0.63	0.64
	$\mu+1\sigma$	0.70	0.72	0.62	0.63
	μ	0.60	0.62	0.54	0.55
Central column	maximum	0.60	0.65	0.59	0.68
	$\mu+1\sigma$	0.40	0.51	0.43	0.50
	μ	0.25	0.28	0.27	0.27
Beam response ratio					
Floor beam - tension	maximum	0.69	0.80	0.74	0.79
- compression	maximum	0.84	0.84	0.89	0.93
Roof beam - tension	maximum	0.30	0.29	0.33	0.33
- compression	maximum	0.28	0.29	0.28	0.28
Brace response ratio					
Storey-1	maximum	1.00	1.00	1.00	1.00
	$\mu+1\sigma$	1.02	0.98	1.00	0.98
	μ	0.71	0.74	0.70	0.72
Ductility demand	maximum	1.07	1.50	1.02	1.50
	$\mu+1\sigma$	1.02	1.16	1.01	1.21
No. of records with yielding		2	2	2	3
Strain rate (s^{-1})	maximum	2.32E-02	2.35E-02	2.06E-02	3.47E-02
No. of records with buckling		7	4	7	3

continued

Table 7.12 Summary of dynamic response in zone 4 (concluded)

Response parameter	Response level	Partitions absent		Partitions present	
		A-set	V-set	A-set	V-set
Number of records		12	8	12	8
Brace response ratio					
Storey-2	maximum	0.99	1.00	0.63	0.78
	$\mu+1\sigma$	0.88	0.95	0.63	0.71
	μ	0.63	0.68	0.46	0.51
Ductility demand	maximum	0.95	1.25	0.63	0.78
	$\mu+1\sigma$	0.85	1.08	0.63	0.71
No. of records with yielding		0	2	0	0
Strain rate (s^{-1})	maximum	-	3.34E-02	-	-
No. of records with buckling		7	6	1	2
Partition response ratio					
Storey-1	$\mu+1\sigma$	-	-	1.08	1.03
No. of records with yielding		-	-	7	3
Storey-2	$\mu+1\sigma$	-	-	0.89	0.93
No. of records with yielding		-	-	0	0
Roof diaphragm response					
Shear force response ratio	maximum	1.00	1.00	1.00	1.00
	$\mu+1\sigma$	1.11	1.08	1.11	1.07
	μ	0.92	0.89	0.89	0.91
No. of records with yielding		10	6	9	6
Slip in link (mm)	maximum	31	30	24	24
Storey shear response ratio					
Storey-1	maximum	1.00	1.00	1.00	1.00
	$\mu+1\sigma$	1.04	1.01	1.03	1.01
	μ	0.75	0.79	0.74	0.77
No. of records with yielding		2	2	2	3
Storey-2	maximum	0.99	1.00	0.80	0.85
	$\mu+1\sigma$	0.94	1.02	0.79	0.84
	μ	0.72	0.77	0.59	0.63
No. of records with yielding		0	2	0	0

Table 7.13 Summary of dynamic response in zone 5 (Victoria)

Response parameter	Response level	Partitions absent		Partitions present	
		A-set	V-set	A-set	V-set
Number of records		12	7	12	7
Roof drift (%)	$\mu+1\sigma$	0.63	0.78	0.59	0.77
Interstorey drift at storey-1 (%)	maximum	0.31	0.42	0.36	0.60
	$\mu+1\sigma$	0.30	0.37	0.36	0.49
	μ	0.25	0.30	0.28	0.36
Interstorey drift at storey-2 (%)	maximum	1.08	1.61	0.75	0.69
	$\mu+1\sigma$	0.91	1.23	0.66	0.66
	μ	0.63	0.80	0.47	0.51
Column response ratio					
Exterior column (storey-1)	maximum	0.79	0.79	0.79	0.79
	$\mu+1\sigma$	0.83	0.81	0.81	0.78
	μ	0.72	0.75	0.67	0.71
Central column	maximum	0.19	0.29	0.20	0.36
	$\mu+1\sigma$	0.20	0.24	0.19	0.30
	μ	0.16	0.18	0.15	0.20
Beam response ratio					
Floor beam - tension	maximum	0.69	0.75	0.74	0.75
- compression	maximum	0.79	1.03	0.89	0.88
Roof beam - tension	maximum	0.38	0.37	0.38	0.39
- compression	maximum	0.49	0.48	0.51	0.51
Brace response ratio					
Storey-1	maximum	0.95	1.00	1.00	1.00
	$\mu+1\sigma$	0.92	0.98	1.04	0.99
	μ	0.73	0.84	0.81	0.86
Ductility demand	maximum	0.95	1.24	1.09	1.61
	$\mu+1\sigma$	0.92	1.08	1.06	1.35
No. of records with yielding		0	2	3	3
Strain rate (s^{-1})	maximum	-	2.80E-02	2.81E-02	3.18E-02
No. of records with buckling		0	3	5	3

continued

Table 7.13 Summary of dynamic response in zone 5 (concluded)

Response parameter	Response level	Partitions absent		Partitions present	
		A-set	V-set	A-set	V-set
Number of records		12	7	12	7
Brace response ratio					
Storey-2	maximum	1.00	1.00	1.00	1.00
	$\mu+1\sigma$	1.10	1.04	1.10	1.03
	μ	0.89	0.93	0.83	0.89
Ductility demand	maximum	2.64	4.13	1.70	1.61
	$\mu+1\sigma$	2.13	3.05	1.42	1.51
No. of records with yielding		9	5	7	4
Strain rate (s^{-1})	maximum	5.78E-02	8.62E-02	4.85E-02	4.03E-02
No. of records with buckling		12	7	10	7
Partition response ratio					
Storey-1	$\mu+1\sigma$	-	-	1.08	1.01
No. of records with yielding		-	-	8	3
Storey-2	$\mu+1\sigma$	-	-	1.11	1.00
No. of records with yielding		-	-	9	7
Roof diaphragm response					
Shear force response ratio	maximum	1.00	1.00	1.00	1.00
	$\mu+1\sigma$	1.08	1.03	1.08	1.03
	μ	0.90	0.96	0.90	0.96
No. of records with yielding		9	4	9	5
Slip in link (mm)	maximum	28	27	34	54
Storey shear response ratio					
Storey-1	maximum	0.94	1.00	1.00	1.00
	$\mu+1\sigma$	0.91	0.98	1.04	1.00
	μ	0.74	0.85	0.83	0.87
No. of records with yielding		0	2	3	3
Storey-2	maximum	1.00	1.00	1.00	1.00
	$\mu+1\sigma$	1.07	1.04	1.08	1.02
	μ	0.92	0.94	0.87	0.92
No. of records with yielding		9	5	7	4

Table 7.14 Capacity design force for floor beam and central column

Zone	Storey-1		Storey-2		Capacity design force		
	P_{yp}	P_{ync}	P_{yp}	P_{ync}	F_1	F_2	F_3
	kN	kN	kN	kN	kN	kN	kN
1	812	44	305	7	211	179	541
2	1551	178	627	37	413	349	762
3	2338	249	966	123	579	490	1085
4	3182	1336	1138	376	1169	989	973
5	4480	2419	1694	138	1982	1677	599

Table 7.15 Comparison of capacity design force to factored load for floor beam and central column

Zone	Floor beam			Central column		
	a	b		c	d	
	F_1	Factored load	Ratio a / b	F_3	Factored load	Ratio c / d
	kN	kN		kN	kN	
1	211	178	1.19	541	587	0.92
2	413	320	1.29	762	843	0.90
3	579	459	1.26	1085	1088	1.00
4	1169	651	1.80	973	1418	0.69
5	1982	961	2.06	599	1949	0.31

Table 7.16 Connection forces at the floor level

Zone	Element number	a Response force	b Factored load	Ratio a / b	c Capacity force	Ratio a / c
		kN	kN		kN	
1	1	162	156	1.04	179	0.91
	2	205	185	1.11	211	0.97
2	1	377	276	1.37	349	1.08
	2	499	327	1.53	413	1.21
3	1	619	407	1.52	490	1.27
	2	782	481	1.63	579	1.35
4	1	1225	561	2.18	989	1.24
	2	1609	663	2.43	1169	1.38
5	1	1863	830	2.24	1677	1.11
	2	2493	981	2.54	1982	1.26

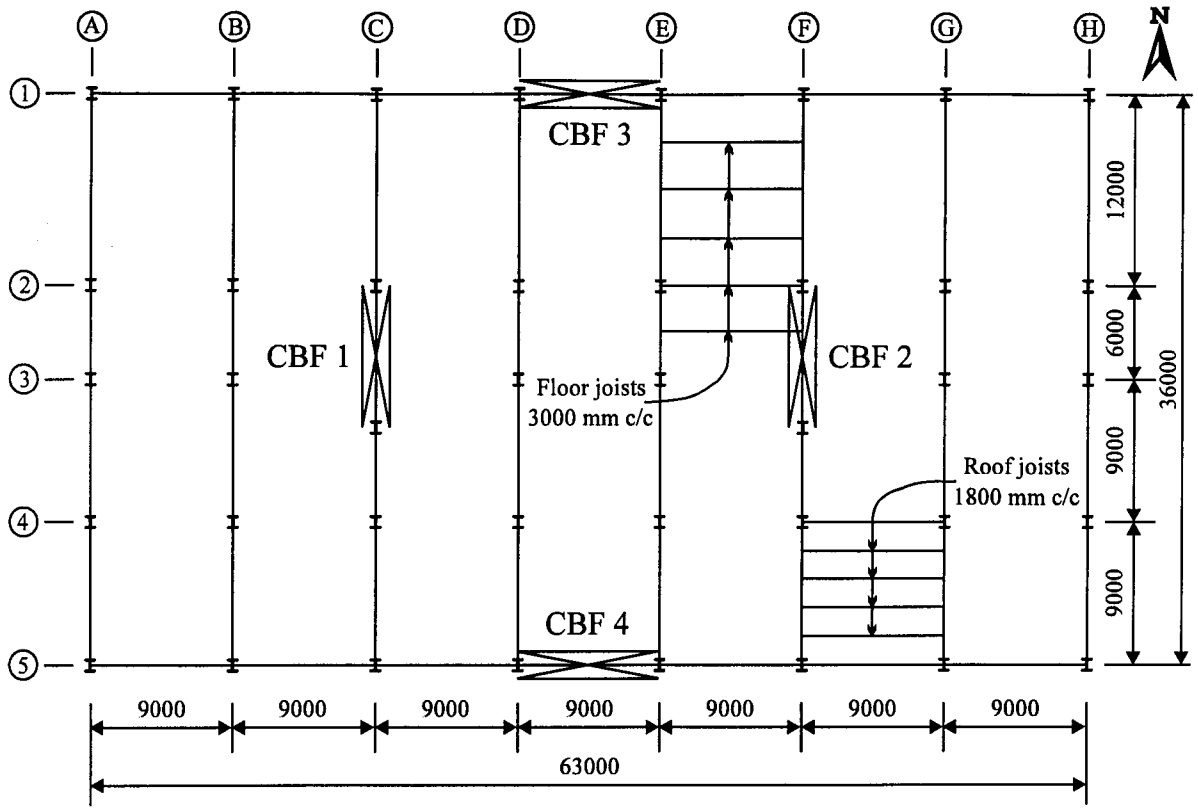

Plan

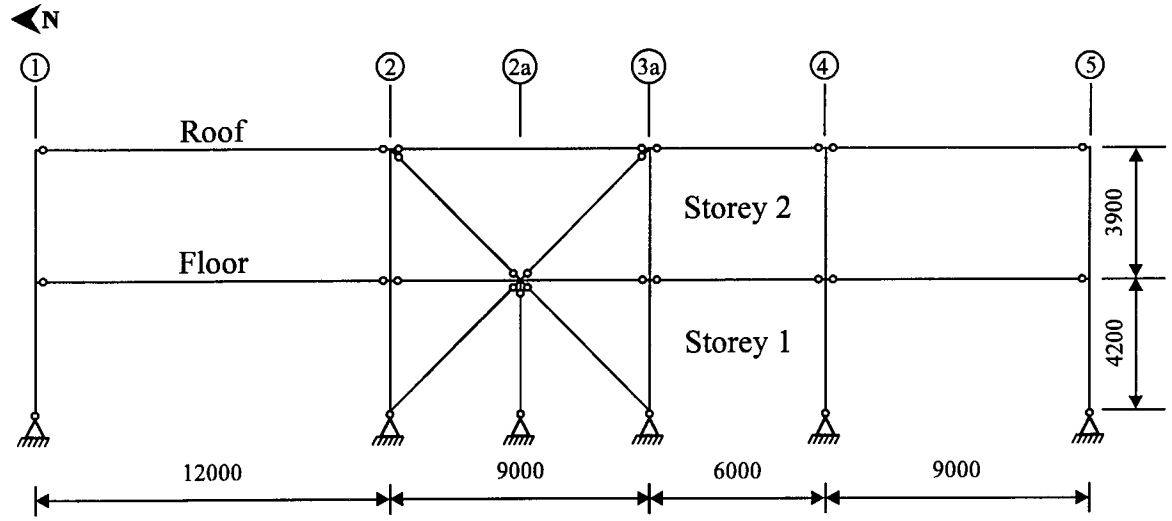

Elevation along lines C and F

Figure 7.1 Layout of two-storey building

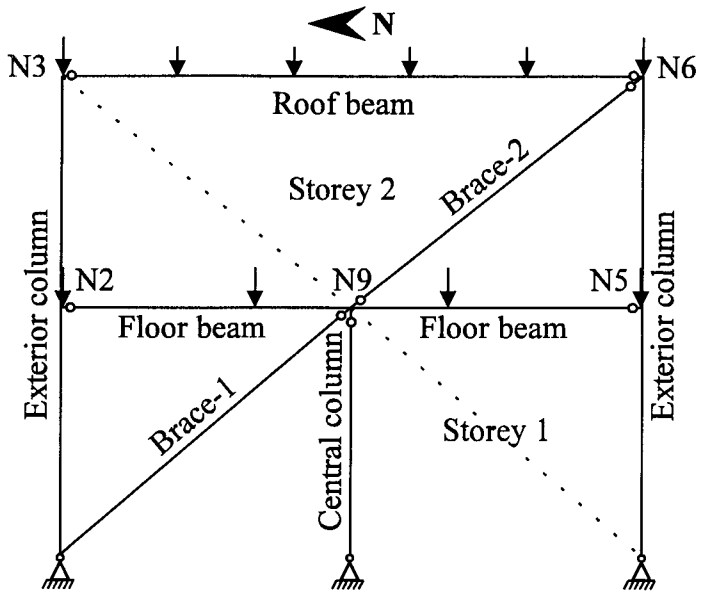

Figure 7.2 Model for design of the CBF

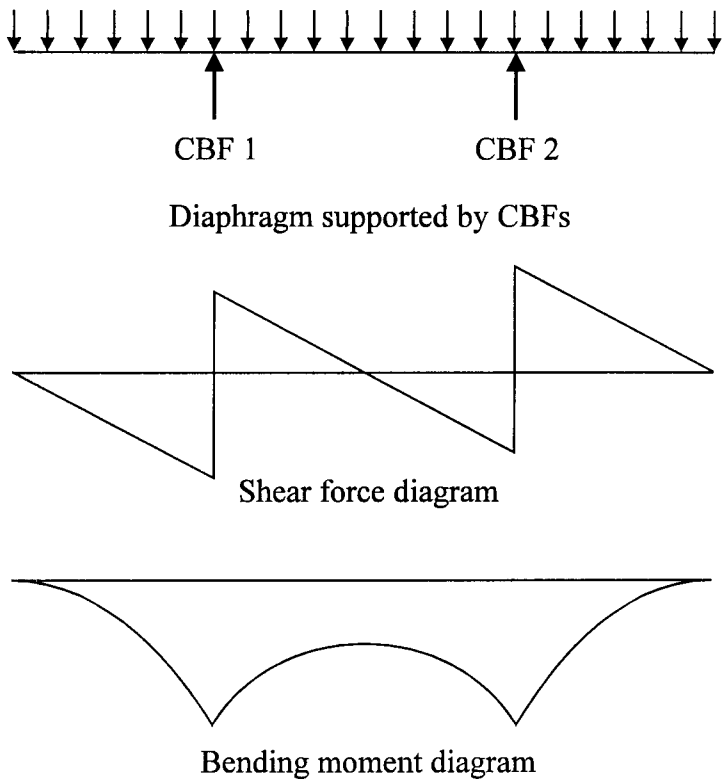

Figure 7.3 Model for design of the roof diaphragm

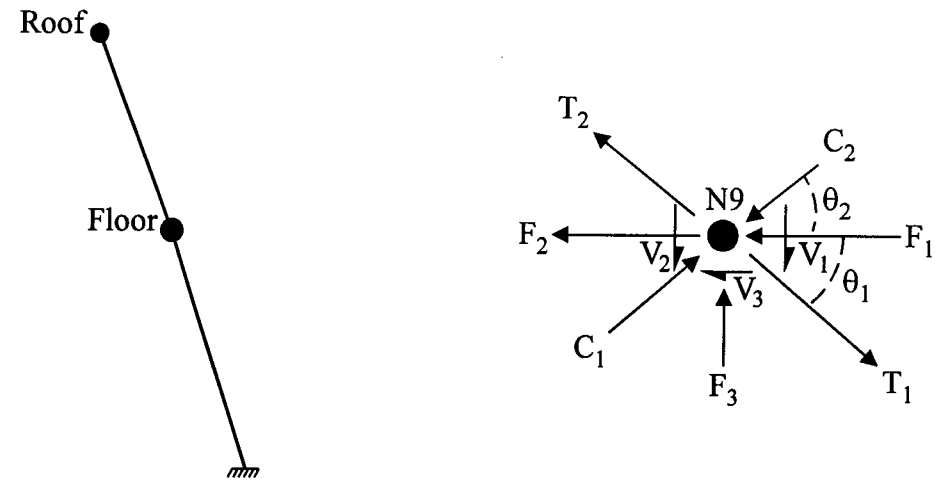

(a) Displaced shape

(b) Equilibrium of joint N9

Figure 7.4 Capacity design of floor beam

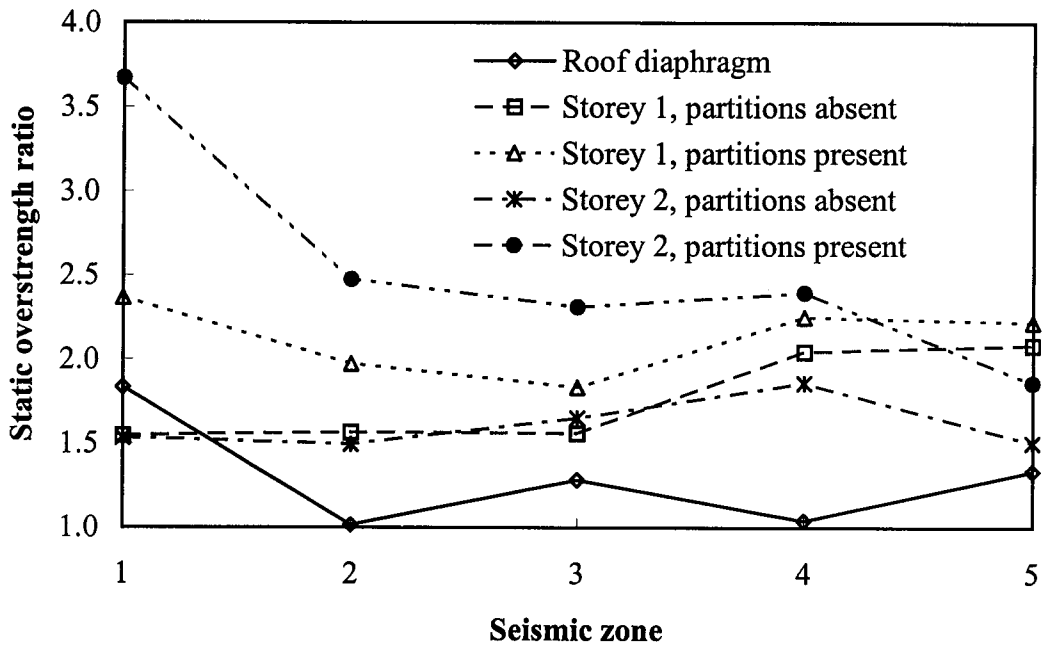

Figure 7.5 Static overstrength ratio for diaphragm and CBF

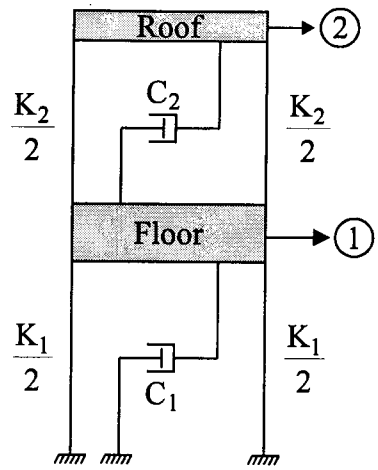

Figure 7.6 Two-degree of freedom elastic model (2DOFE)

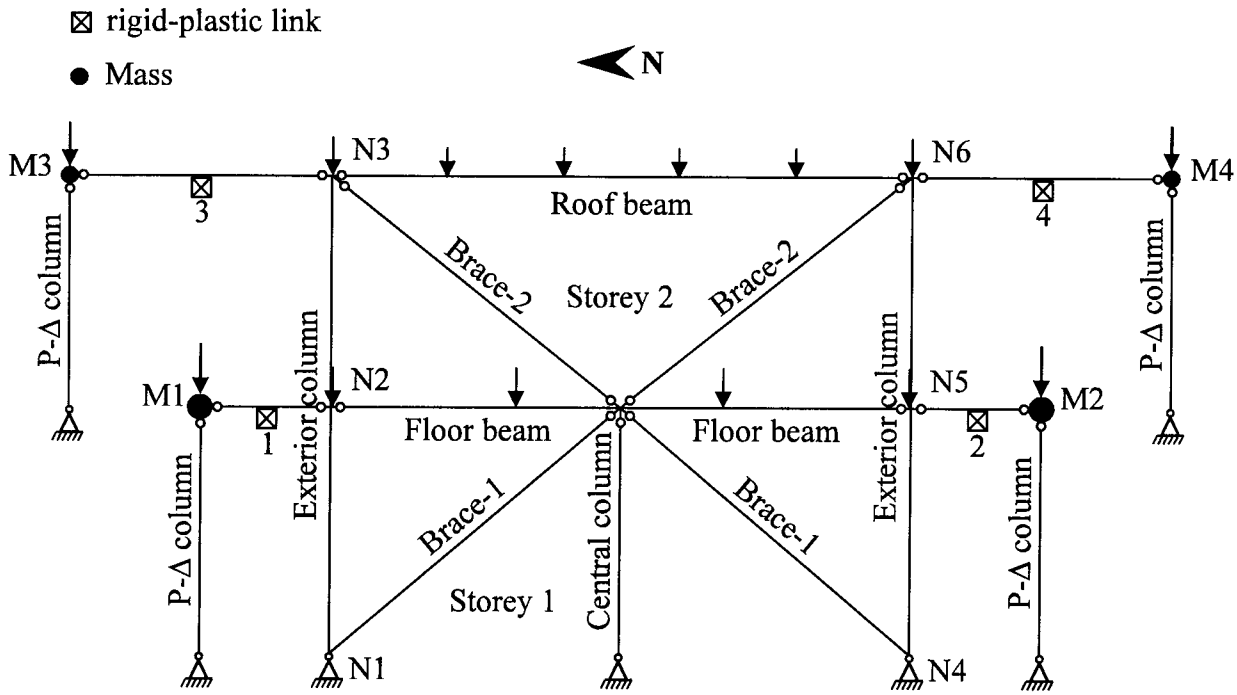

Figure 7.7 Multi-degree of freedom nonlinear model (MDOFN)

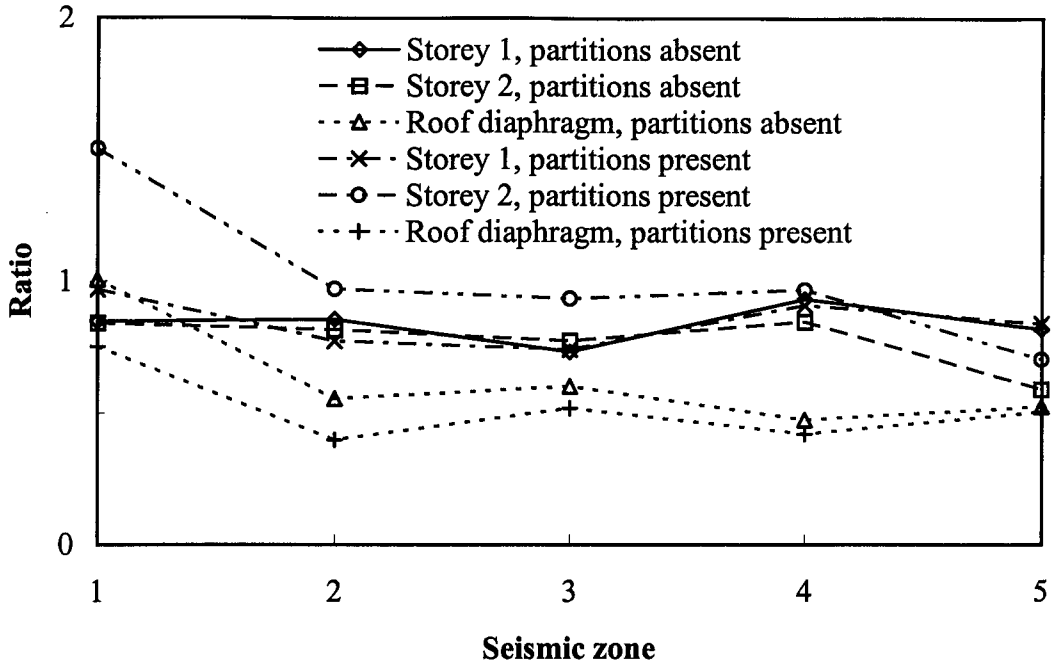

Figure 7.8 Effective overstrength ratio from acceleration set of records

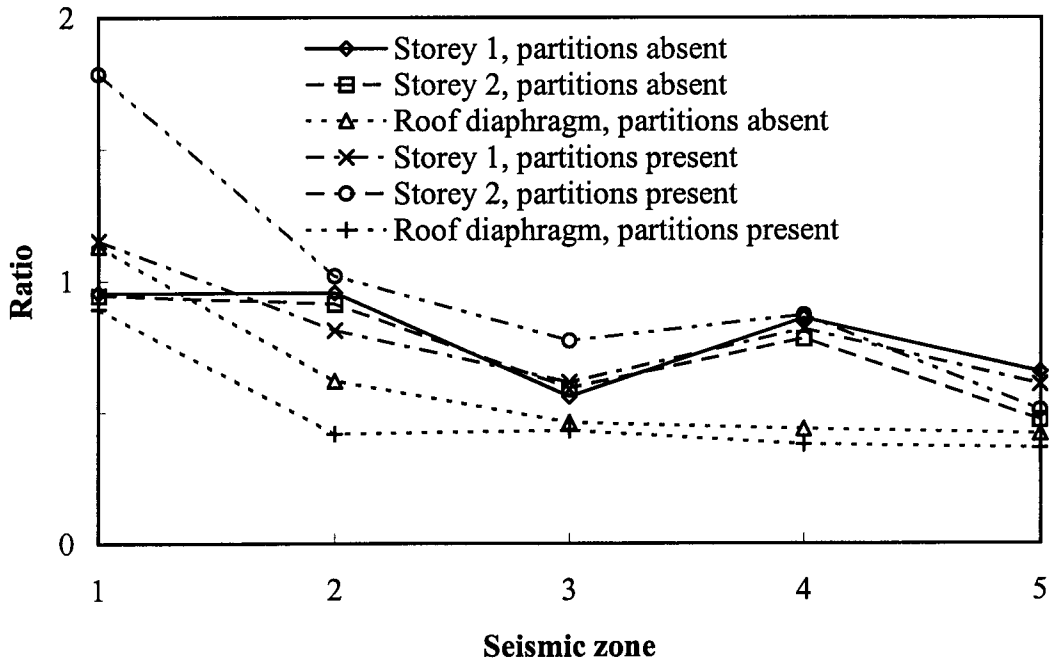

Figure 7.9 Effective overstrength ratio from velocity set of records

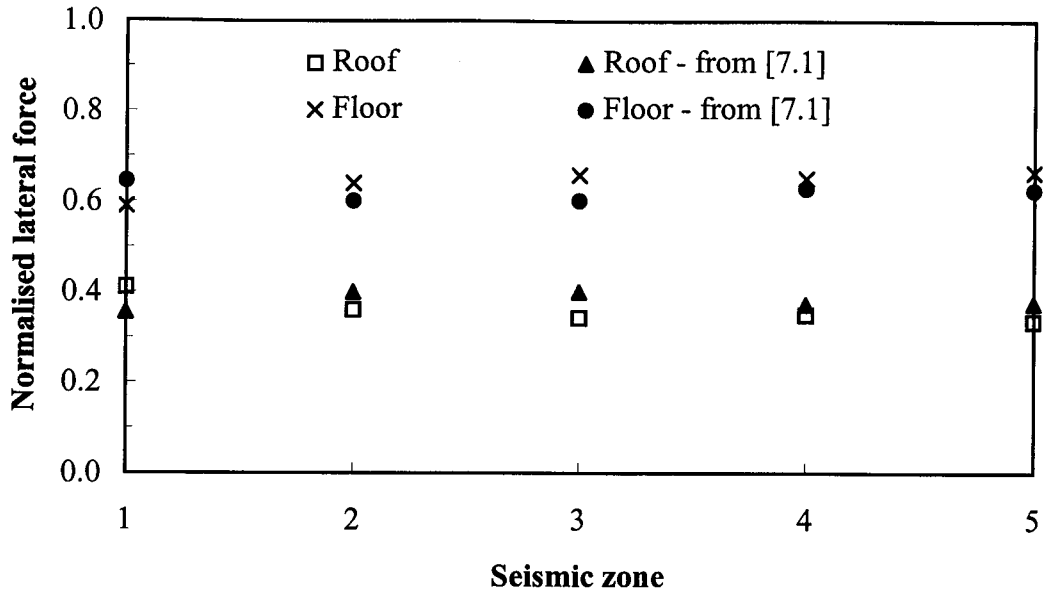

Figure 7.10 Distribution of lateral force from response spectrum analysis, partitions absent

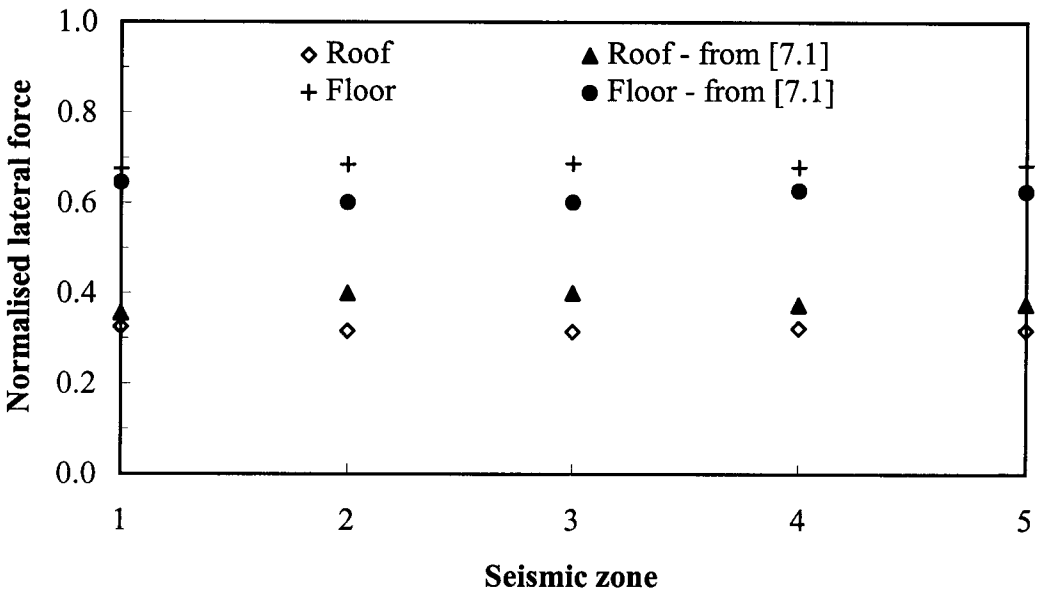

Figure 7.11 Distribution of lateral force from response spectrum analysis, partitions present

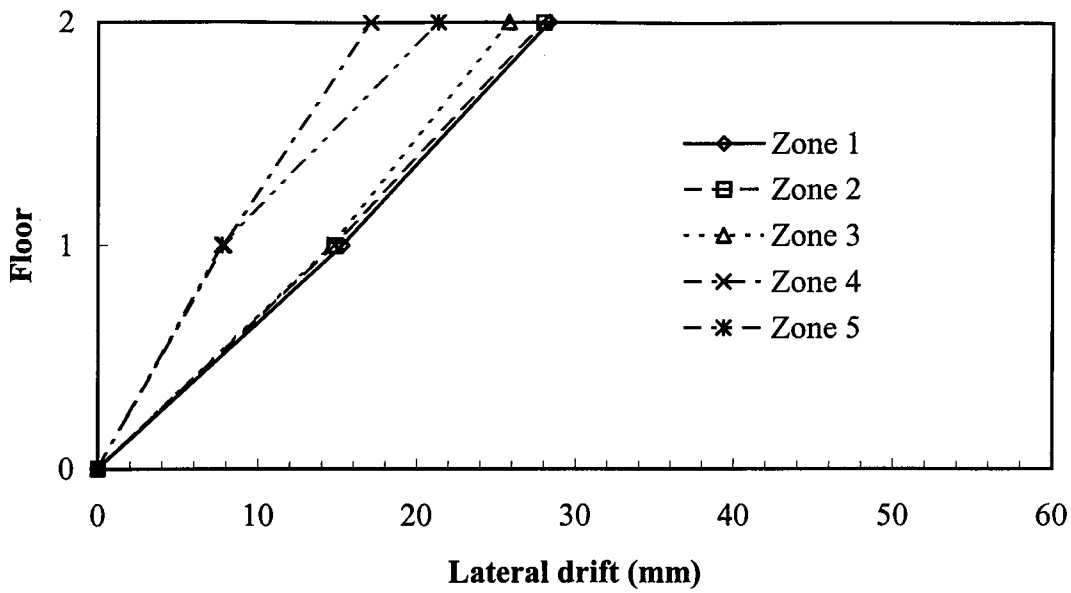

Figure 7.12 Drift under prescribed lateral force from nonlinear static analysis, partitions absent

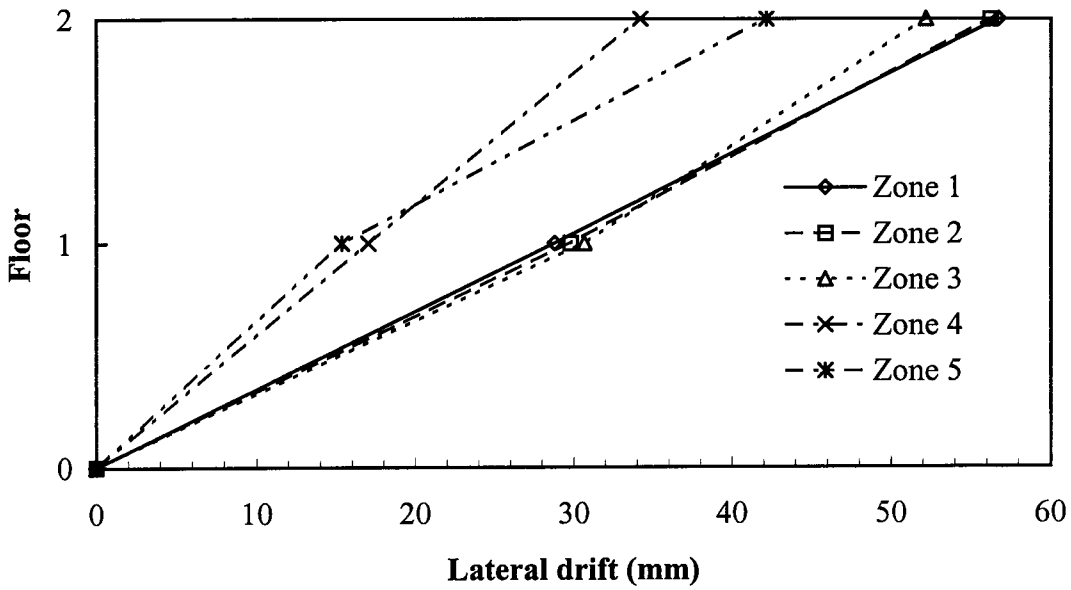

Figure 7.13 Displaced shape at target displacement from static pushover analysis, partitions absent

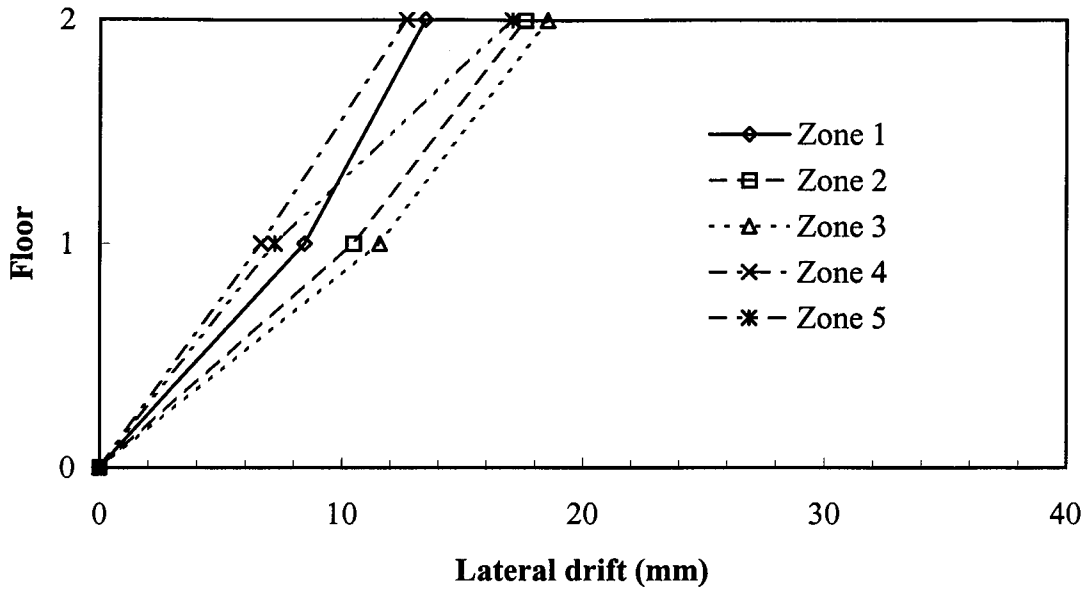

Figure 7.14 Drift under prescribed lateral force from nonlinear static analysis, partitions present

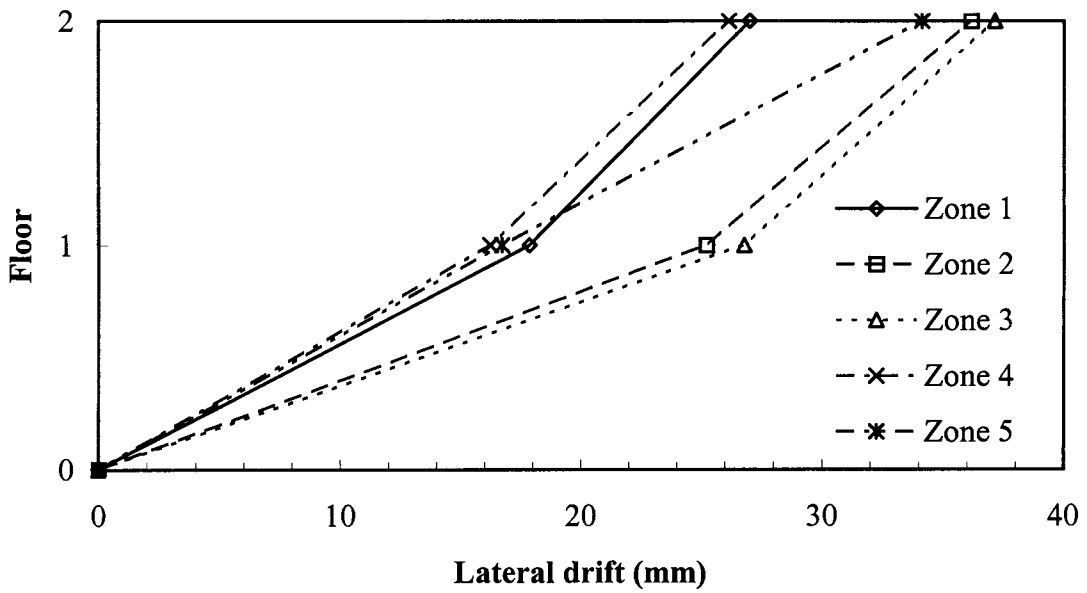

Figure 7.15 Displaced shape at target displacement from static pushover analysis, partitions present

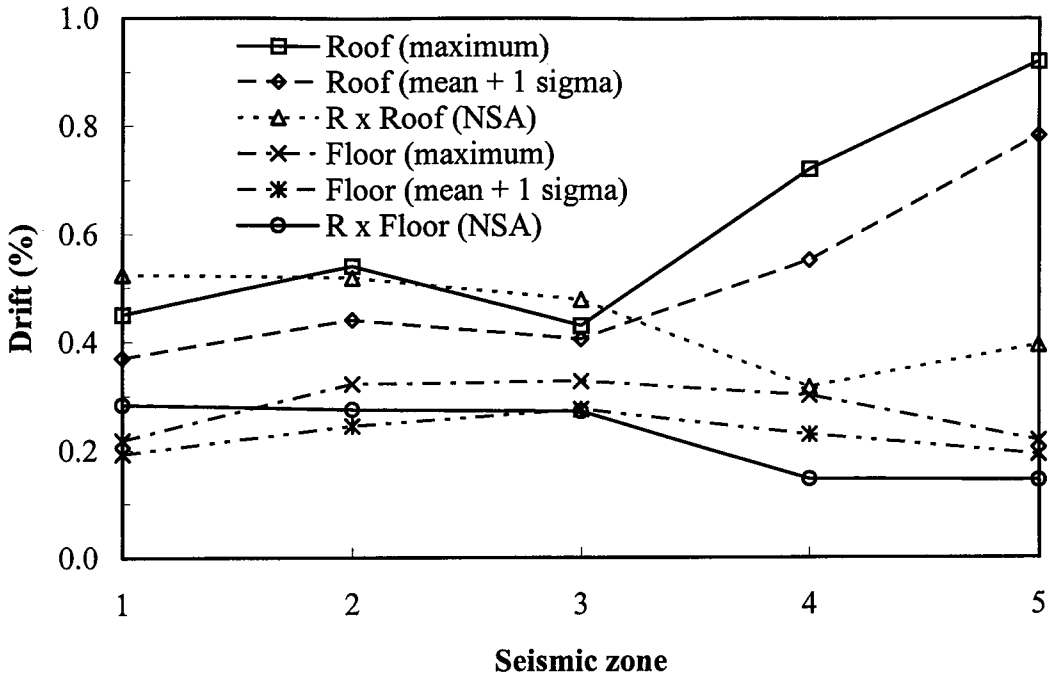

Figure 7.16 Estimate of lateral drift with partitions absent

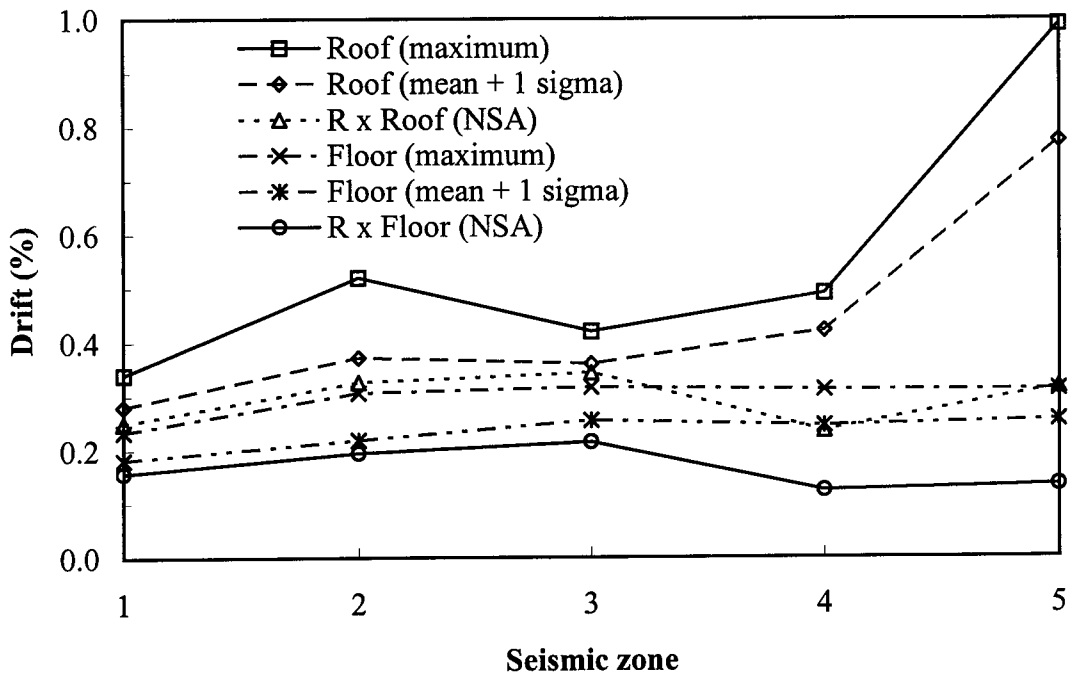

Figure 7.17 Estimate of lateral drift with partitions present

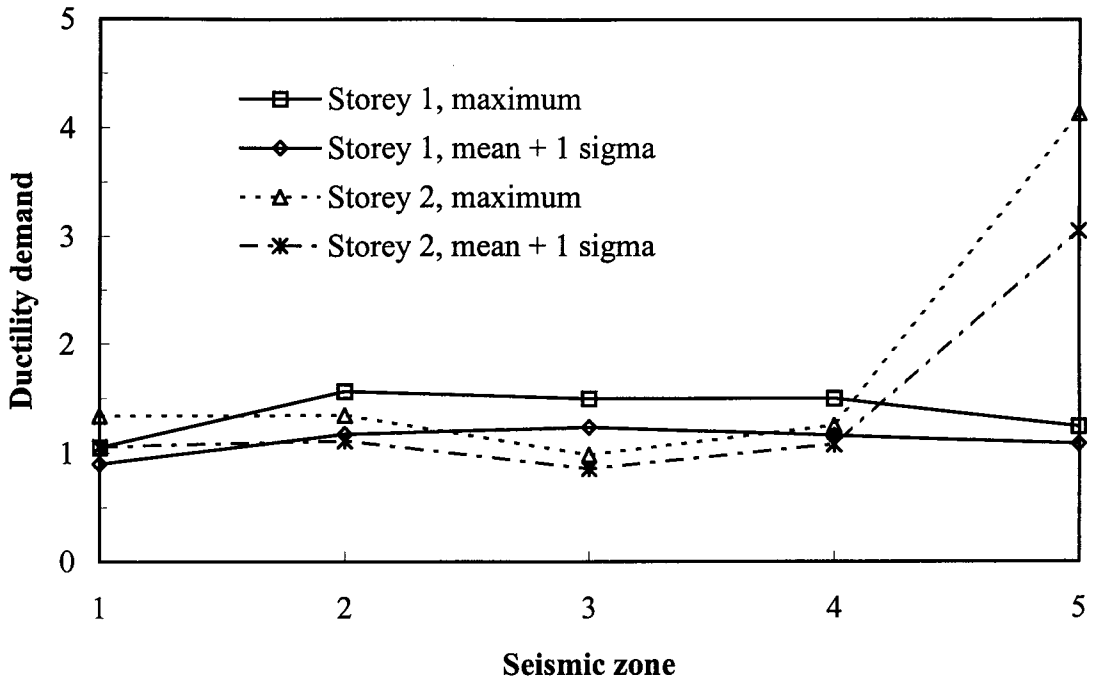

Figure 7.18 Brace ductility demand with partitions absent

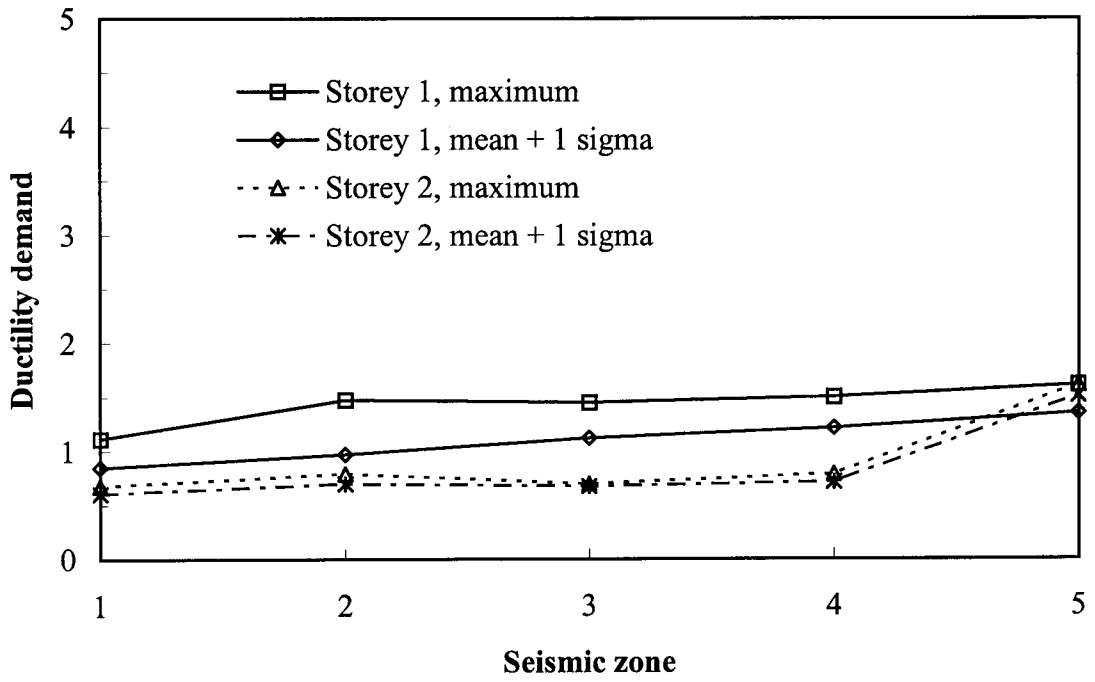

Figure 7.19 Brace ductility demand with partitions present

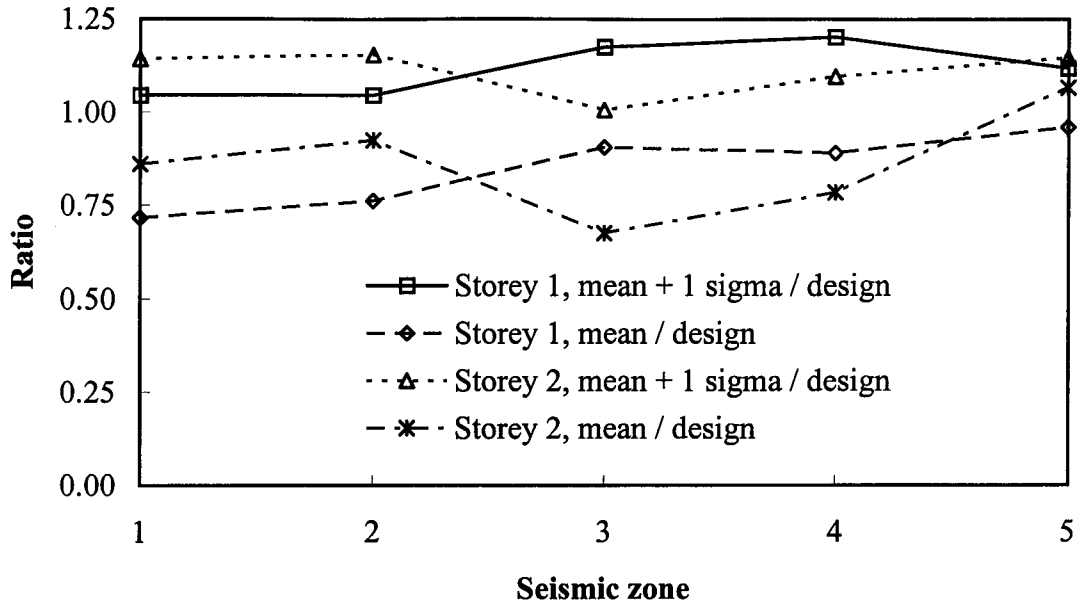

Figure 7.20 Ratio of brace response force to connection design force, partitions absent

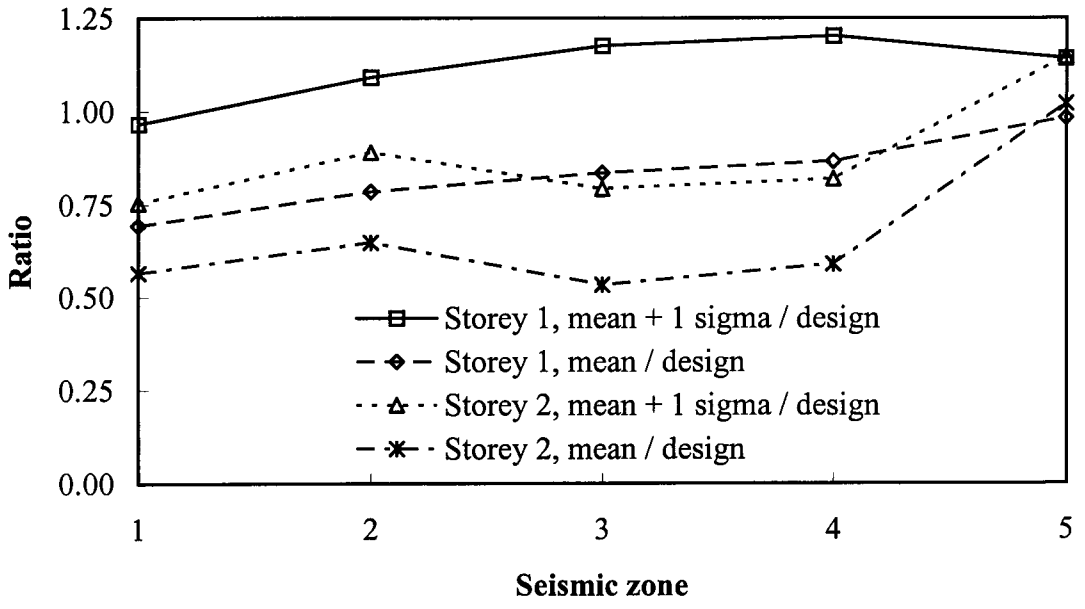

Figure 7.21 Ratio of brace response force to connection design force, partitions present

8. DISPLACEMENT-BASED SEISMIC DESIGN METHOD

8.1 Introduction

The spectral acceleration-based design method is used by the NBCC (ACNBC 1995a) and by other codes (e.g. ICBO 1997, FEMA 1994) for the seismic design of structures. The conceptual basis of this method and its limitations are reviewed. An alternative seismic design method that uses displacements as the basis for the design procedure is then described. Its conceptual basis and application to single degree of freedom (SDOF) and multi-degree of freedom (MDOF) structures are presented. The advantages of this method over the spectral acceleration-based method are also discussed.

8.2 Spectral acceleration-based design method

Consider the design of a structure that may be represented by a SDOF system of mass, M, period, T_e, and damping ratio, ξ. The period, T_e, is established by empirical equations that are derived from experiments on similar real structures. Figure 8.1 shows the design acceleration response spectra specified by the NBCC (ACNBC 1995a) for seismic zones with Z_a equal to Z_v. The acceleration of the mass is obtained by determining the elastic spectral acceleration, $(S_a/g)_e$, corresponding to the specified period, T_e. The elastic base shear that the SDOF system attracts is given by

[8.1] $$V_e = M\,g\,(S_a / g)_e$$

If the SDOF system is provided with strength V_i that is less than V_e (keeping the initial period equal to T_e), the system will respond inelastically as shown in Fig. 8.2. Hence, seismic codes reduce the elastic design acceleration spectrum by the force modification factor, R, to arrive at the inelastic design acceleration spectrum as shown in Fig. 8.1. The inelastic base shear is given by

[8.2] $$V_i = \left(\frac{V_e}{R}\right) = M\,g\,(S_a / g)_i$$

The SDOF system with a base shear capacity of V_i will respond inelastically in the design earthquake. Hence, the objective of inelastic seismic design is achieved.

8.3 Limitations of the spectral acceleration-based design method

The spectral acceleration-based design method has a number of limitations as discussed below.

(a) The method requires an estimate of the fundamental period, T_e, to start the design process. This period cannot be obtained from mechanics at the start of the process as the design is not yet available. Therefore, seismic codes use empirical expressions, derived from experimental data, that involve a general description of the structural system and its geometry only. The period from these expressions is intentionally less than the measured ones to give a conservative design (FEMA 1994, ATC 1995).

(b) The force modification factor, R, is intended to be a simple means of arriving at an inelastic design. Seismic codes specify values for the factor, R, depending upon the material of construction and the type of structural system used. However, these values appear to be arbitrary and are difficult to justify. There is no consistent method of establishing these values from experiments or analysis of structural systems.

(c) It is difficult to predict the displacement response of the resulting inelastic system over the entire range of periods of the acceleration spectrum. A typical acceleration response spectrum may be considered to consist of 4 distinct zones. At very short periods, the structure is essentially rigid and both the elastic and the inelastic systems are subjected to the peak ground acceleration (PGA). The inelastic system will fail if its strength is less than that of the elastic one. In the acceleration sensitive region of the spectrum (typically $T < 0.5$ s), the displacement of the inelastic system is greater than that of the elastic one of the same initial period (i.e. stiffness). In the velocity sensitive region of the spectrum (typically $0.5 \text{ s} < T < 3.0$ s), the displacements of the inelastic and elastic systems are similar. At very long periods, there is no structural response to ground motion. In the spectral acceleration-based method, the strength of the elastic system, V_e, is reduced by the force modification factor, R, to arrive at the inelastic system with strength V_i. Because the strength and stiffness of a structure are inter-related, provision of less strength results in less stiffness and consequently the period increases from T_e to T_i as shown in Fig. 8.1. This lengthening in the period further complicates the issue.

Thus, the relationship between the peak displacement response of the inelastic system of strength V_i and the elastic system of strength V_e, is complex.

(d) The spectral acceleration-based approach treats displacements in a somewhat cursory manner. Displacements are not considered at the beginning of the design process, but are checked at the end of the process only. Damage to both non-structural and structural elements is deformation sensitive and a member or structure may be deemed unsatisfactory if it deforms excessively. This is a serviceability limit state. Similarly, collapse does not occur merely due to forces exceeding the strength of a structure, but may be due to the instability caused by the associated deformations. These limit states are governed by deformations. It may also be easier to define failure of a structural element as a limit on deformation rather than as a limit on the force.

Therefore, it seems rational to examine a seismic design method wherein displacements are considered at the start of the design process. A designer then focuses attention on several limit states and provides the structural system that best suits the requirements. For example, a serviceability limit state on deformations could be applied to moderate earthquakes that are likely to occur relatively frequently in the life of the structure, by imposing drift limits so that non-structural damage does not occur. To prevent collapse in a major earthquake, the ductility demand on the structural elements has to be controlled. This in turn requires control on the overall deformation of the structure. This may be achieved more rationally with a displacement-based design method rather than an acceleration-based one.

8.4 Displacement-based design method for a SDOF system

The method presented here is based on Priestley (1993). The central concept is that a structure is designed for a specified target displacement. The method is illustrated by reference to a single-storey, single-bay concentrically braced frame (CBF) that is modelled as a SDOF system as shown in Fig. 8.3. A set of elastic displacement response spectra for different levels of equivalent viscous damping is required, as shown in Fig. 8.4. They are generated by integrating numerically the equation of motion of an elastic SDOF system subjected to earthquake ground acceleration. These curves typically

converge to the peak ground displacement at large periods. The design procedure for a SDOF system is summarised as follows:

(a) Estimate the yield displacement of the structure, Δ_y. For the CBF shown in Fig. 8.3, this displacement is the lateral drift at the roof level that yields the brace and is a function of the geometry and material properties (E, F_Y) only.

(b) Select an appropriate maximum inelastic displacement, Δ_{in}. This selection depends on the deformation capacity of the structural elements. A larger value may be selected for structures that are detailed for ductile response. For a CBF with nominal ductility, Δ_{in} may be taken as 1.0 Δ_y, i.e. the ductility demand is 2.0.

(c) The maximum displacement of the SDOF system, Δ_{max}, is the sum of the yield displacement, Δ_y, and the maximum inelastic displacement, Δ_{in}. For the CBF, the maximum displacement is thus explicitly related to the brace ductility demand assumed in step (b).

(d) Select an appropriate value of effective structural damping, ξ_{eff}. This value depends on the ductility level implied in step (b).

(e) The effective period, T_{eff}, is determined corresponding to the maximum displacement, Δ_{max}, from the elastic displacement response spectrum for the selected damping, ξ_{eff}, as shown in Fig. 8.4.

(f) The effective stiffness of the equivalent SDOF system, K_{eff}, is given by

[8.3] $$K_{eff} = \frac{4\pi^2 m_{eff}}{T_{eff}^2}$$

where m_{eff} is the mass of the SDOF system.

(g) The base shear capacity to be provided, as shown in Fig. 8.5, is

[8.4] $$V_b = K_{eff} \Delta_{max}$$

(h) Select structural elements that will provide the required lateral stiffness, K_{eff}, and base shear capacity, V_b. Once the member selection is done, the initial design of the structure is completed and it can now be analysed. The elastic stiffness and a revised estimate of the yield displacement are obtained.

(i) Revision is necessary if the members selected in step (h) provide significantly different stiffness and strength than required. The brace ductility demand, maximum displacement, and effective damping are revised and steps (e) to (h) are repeated until a stable and satisfactory solution is obtained.

8.5 Basis of the displacement-based design method

A fundamental question that arises is *"how does the displacement-based design method make use of elastic displacement response spectra and arrive at a design wherein the structure will respond inelastically in the design earthquake ?"* This objective is achieved by recourse to the *Substitute Structure Approach.* In this procedure, an inelastic SDOF system is modelled as an equivalent linear elastic analogue (Gulkan and Sozen 1974) having the 'substitute' properties of; (a) effective stiffness, K_{eff}, (b) effective damping, ξ_{eff}, and (c) effective period, T_{eff}. One estimates the maximum displacement of the inelastic SDOF system by using the substitute properties along with an elastic displacement response spectrum.

To understand the basis of the substitute structure approach, consider the response of an inelastic SDOF system with an initial period (before inelastic action occurs) of T_e, and damping ratio, ξ. Let Δ_y be the yield displacement of this system and let Δ_{max} be the maximum displacement that is somehow known. Considering Fig. 8.6 (Bonacci 1994), there are several ways to reach the maximum displacement, Δ_{max}, starting from the point 'o' at T_e and Δ_y on the elastic displacement response spectra. One may select any of the following alternatives; (i) with the same period, T_e, select a lower damping ratio to reach point 'a', (ii) with the same damping ratio, select a longer period, T_1, to reach point 'b', (iii) select both a longer period, T_2, and a larger damping ratio to reach point 'c', and (iv) select a shorter period, T_3, and a lower damping ratio to reach point 'd'. The first and last alternatives are unrealistic because inelastically responding structures exhibit both greater damping and a longer period due to softening. Gulkan and Sozen (1974) conducted dynamic tests on SDOF concrete frames and deduced guidelines for selecting the substitute period and damping. The substitute period was determined experimentally

by taking the ratio of the maximum displacement to the maximum absolute acceleration and using the relation $S_a = \omega^2 S_d$, where S_a is the spectral acceleration, S_d is the spectral displacement, and ω is the circular frequency. The substitute damping was evaluated by assuming that the energy input to the SDOF system during the earthquake excitation was totally dissipated by a linear viscous dashpot. Shibata and Sozen (1976) extended this approach to the design of reinforced concrete frames modelled as MDOF systems.

For design purpose, the lengthened period (substitute period) is taken to correspond to the assumed maximum displacement, Δ_{max}, from an elastic design displacement spectrum as shown in Fig. 8.6. The substitute damping, ξ_{eff}, depends on the ductility demand imposed on the structural elements under the assumed maximum displacement. Guidelines for selecting ξ_{eff} for reinforced concrete structures are given by Gulkan and Sozen (1974) and Shibata and Sozen (1976). Little information is available on effective damping values for steel structures responding inelastically. Newmark and Hall (1982) recommend a damping ratio between 5% and 7% for steel structures with welded connections and between 10% and 15% for steel structures with bolted connections.

Once the substitute period, T_{eff}, is determined for a desired maximum displacement, Δ_{max}, the effective stiffness of the SDOF system is found from

$$[8.3] \qquad K_{eff} = \frac{4\pi^2 m_{eff}}{T_{eff}^2}$$

which is a secant stiffness to the maximum displacement, Δ_{max}, as shown in Fig. 8.5. [If the period, T_e, corresponding to the yield displacement, Δ_y, is used in [8.3], the elastic stiffness, K_e, is obtained.] The inelastic base shear for the SDOF system is given by

$$[8.4] \qquad V_b = K_{eff}\, \Delta_{max}$$

An additional issue that needs to be addressed is *the decrease in base shear with an increased value of the assumed maximum displacement, Δ_{max}.* This is illustrated in Fig. 8.7(a) with reference to the SDOF system shown in Fig. 8.7(b) where Δ_1 and Δ_2 are

two values of the assumed maximum displacement, Δ_{max}, that are both greater than the yield displacement, Δ_y.

Consider the design of the SDOF system for a maximum displacement equal to Δ_i. The effective period, T_i, is determined from an elastic displacement response spectrum corresponding to the assumed maximum displacement, Δ_i, and effective damping, ξ_{eff}. The effective stiffness, K_{eff}, is obtained from [8.3]. The inelastic base shear is obtained from [8.4]. Let K_e be the elastic stiffness obtained from [8.3] for period, T_e, that corresponds to the yield displacement, Δ_y. Assuming the mass, M, to remain constant, the ratio of the stiffness, K_{eff} to K_e, is obtained as

$$[8.5] \qquad \frac{(K_{eff})_i}{K_e} = \left(\frac{T_e}{T_i}\right)^2$$

where T_i is the period corresponding to the assumed maximum displacement, Δ_i. Figure 8.8 shows a design displacement spectrum wherein the spectral displacement is assumed to increase linearly with period. This linearization is considered acceptable for the range of periods within which the fundamental period of most low-rise to moderate-rise buildings, lies. Using the assumed linear relation between period and spectral displacement, [8.5] simplifies to

$$[8.6] \qquad \frac{(K_{eff})_i}{K_e} = \left(\frac{\Delta_y}{\Delta_i}\right)^2$$

Using [8.4], the ratio of inelastic to elastic base shear is obtained as

$$[8.7] \qquad \frac{V_i}{V_e} = \frac{\Delta_y}{\Delta_i}$$

Thus, for the linearized design displacement spectrum shown in Fig. 8.8, the base shear decreases in inverse proportion to the ratio of the assumed maximum displacement, Δ_{max}, to the yield displacement, Δ_y.

8.6 Displacement-based design method for a MDOF system

Consider a MDOF system with n degrees of freedom as shown in Fig. 8.9. The displacement-based design method can be applied to this system by first transforming it

to an equivalent SDOF system, as outlined by Calvi and Kingsley (1995), and then using the procedure outlined in section 8.4 for a SDOF system. The MDOF system is forced to behave like a SDOF system by permitting displacements of only a single pre-determined (assumed) shape. The transformation is based on the following assumptions:

(a) The MDOF system has a harmonic response in this assumed displaced shape,

(b) The base shear developed by the MDOF system and its SDOF equivalent are the same, and

(c) The work done by the lateral earthquake force on both systems is the same.

Let the assumed displacement vector of this MDOF system be represented by

$$[8.8] \qquad \langle \delta \rangle = \langle \delta(h,t) \rangle = \langle \delta_1(t), \delta_2(t), \ldots, \delta_n(t) \rangle^T$$

This vector may be expressed as

$$[8.9] \qquad \langle \delta(h,t) \rangle = \langle \Phi(h) \rangle Z(t)$$

where $\Phi(h)$ is a spatial (shape) function and $Z(t)$ is a temporal function. Assuming harmonic response, [8.9] is written as

$$[8.10] \qquad \langle \delta(h,t) \rangle = Z_o \sin(\omega t) \langle \Phi(h) \rangle$$

This expresses the first assumption that the shape of the MDOF system does not change with time; only the amplitude of motion varies harmonically. Differentiating [8.10] twice with respect to time gives the acceleration vector

$$[8.11] \qquad \langle a(h,t) \rangle = - Z_o \omega^2 \sin(\omega t) \langle \Phi(h) \rangle = - \omega^2 \langle \delta(h,t) \rangle$$

Thus, the acceleration at each DOF, a_i, is proportional to the assumed displacement, δ_i.

Let the effective properties of the equivalent SDOF system be mass, m_{eff}, stiffness, K_{eff}, damping, ξ_{eff}, and let δ_{eff} and V_b be the effective displacement and base shear, respectively, where these properties are to be derived from those of the MDOF system. The displacement of the MDOF system may be expressed in terms of the effective displacement of the SDOF system by

$$[8.12] \qquad \langle \delta(h,t) \rangle = \delta_{eff} \langle c(h,t) \rangle$$

where $\langle c(h,t) \rangle$ is the normalized profile of the assumed displaced shape. As acceleration is proportional to the assumed displacement, the acceleration of the MDOF system may be expressed in terms of the acceleration of the SDOF system, a_{eff}

[8.13] $$a_i = c_i \, a_{eff}$$

The lateral force at the 'i' th DOF is given by

[8.14] $$F_i = m_i \, a_i$$

The sum of the lateral forces on the MDOF system is equal to the base shear, V_b. Thus,

[8.15] $$V_b = \sum_{i=1}^{n} F_i = \sum_{i=1}^{n} m_i \, a_i = \left\{ \sum_{i=1}^{n} m_i \, c_i \right\} a_{eff} = m_{eff} \, a_{eff}$$

From the above equation, the effective mass of the SDOF system is defined as

[8.16] $$m_{eff} = \sum_{i=1}^{n} m_i \, c_i$$

The lateral force, F_i, at each DOF from [8.14] may be expressed in terms of the base shear, V_b, by manipulating [8.12], [8.13] and [8.15] to give

[8.17] $$F_i = \frac{m_i \, \delta_i}{\sum_{j=1}^{n} m_j \, \delta_j} V_b$$

The effective displacement, δ_{eff}, is found by equating the work done by the lateral force on each system

[8.18] $$V_b \, \delta_{eff} = \sum_{i=1}^{n} F_i \, \delta_i$$

Solving [8.18] for δ_{eff} and substituting for F_i from [8.17] results in

[8.19] $$\delta_{eff} = \frac{\sum_{i=1}^{n} m_i \, \delta_i^2}{\sum_{i=1}^{n} m_i \, \delta_i}$$

The effective stiffness, K_{eff}, of the SDOF system is given by

[8.20] $$K_{eff} = \frac{V_b}{\delta_{eff}}$$

Thus equations [8.19], [8.16], and [8.20] define the effective displacement, mass, and stiffness, respectively, of the equivalent SDOF system.

8.7 Design procedure for a MDOF system

The design procedure for a generalised MDOF system consists of the following basic steps; (i) assume a desired displaced shape of the MDOF system, (ii) transform it into an equivalent SDOF system, (iii) obtain the base shear for the SDOF system, (iv) transform back to the MDOF system to obtain the forces at each mass, and (v) design the MDOF system for the above forces and compare its displaced shape with the desired one.

The detailed procedure is as follows.

(a) Select an initial desired displaced shape for the structure, δ_i. For a multi-storey CBF, the desired drift at each floor level will have to be specified. The brace ductility demand can be calculated from the assumed storey drift because it depends only on the geometry and material properties of the frame.

(b) Select the effective damping, ξ_{eff}, for the structure. This depends on the ductility implied with the desired displaced shape, δ_i.

(c) Transform the MDOF system into an equivalent SDOF system. Determine the effective displacement, δ_{eff}, from [8.19].

(d) Obtain the assumed displaced profile, c_i, from [8.12].

(e) Obtain the effective mass, m_{eff}, from [8.16].

(f) Determine the effective period of the SDOF system, T_{eff}, from an elastic design displacement spectrum for displacement, δ_{eff}, and damping, ξ_{eff}.

(g) Obtain the effective stiffness, K_{eff}, from [8.3].

(h) Obtain the base shear, V_b, from [8.20].

(i) Obtain the lateral forces on the MDOF system from [8.17].

(j) Design the lateral load resisting system (LLRS) for the above forces and the appropriate gravity load. Material standards are used at this stage to select member

details that have adequate deformation capacity as implied in the desired displaced shape in step (a).

(k) Once the appropriate members are selected, a design is now available for analysis. A nonlinear static analysis of the structure under the lateral earthquake force profile is recommended. This analysis will approximately account for the redistribution of internal forces when the structure is loaded into the inelastic range. The objectives of this analysis are to check the displaced shape against the desired one assumed in step (a) and to assess the strength and deformation demands on the structural elements.

Following this analysis procedure, one of two cases may obtain. In the first case, the lateral force profile is applied and the load factor is incremented until the lateral force is attained. Inelastic action may occur at some locations in the structure. [For direct-acting bracing, the use of a small strain-hardening modulus is required]. In the second case, the lateral forces in the assumed profile are applied until the desired deformation is reached at a specified location, e.g., the roof level. Inelastic action does take place in the structure. Obviously, nonlinear dynamic time history analyses give a better assessment of the drift and the ductility demands.

(l) If the displaced shape and the associated deformation demands on the structural elements from the nonlinear static analysis are significantly different from those assumed, the stiffness distribution should be revised to obtain the desired result. If detailing restrictions make it unfeasible to obtain the desired result, the desired shape itself must be revised and the process repeated from step (a) onwards.

8.8 Torsional effects

The effects of torsion have not been addressed by Priestley (1993). Considering accidental torsion, one method would be to simply reduce the assumed displaced shape by an arbitrary amount to allow for the torsional displacements. This parallels the current NBCC procedure of applying an arbitrary torsional moment. Based on the CBFs investigated herein, the effect of the NBCC accidental torsional moment was determined to increase the base shear by a factor ranging from 1.08 to 1.22. Therefore, an appropriate figure within this range would be the first estimate of the reduction in

displacement to account for accidental torsion. Further study is required to address this issue.

For buildings in which the center of mass and the center of rigidity are not coincident, the approach is as follows.

(a) Insofar as possible, modify the frame stiffnesses to minimise the structural eccentricity defined as the distance measured perpendicular to the direction of seismic loading between the centre of mass and the centre of rigidity at the level being considered.

(b) The residual structural eccentricity results in a torsional moment and attendant shear forces that are distributed on the basis of equilibrium to the resisting frames.

(c) The adequacy of the frames is checked and they are modified as required and iterations performed as necessary.

8.9 Displaced shape for buildings modelled as a MDOF system

An important step in this design method is the selection of an initial displaced shape. One might intuitively select a displaced profile that matches the expected shape of the first mode. The displaced profile given by

$$[8.21] \qquad \Phi(h) = \left(\frac{h}{h_n}\right)^{\alpha}$$

is a versatile one for buildings that are fairly regular in elevation and plan, where h_n is the height of the building and α is a positive exponent. Figure 8.10 shows a plot of [8.21] for various values of the exponent α. A value of α greater than 1.0 results in a shape that is similar to the first mode of a cantilever flexural beam. Buildings that are relatively slender have a first mode shape similar to this. A value of α less than 1.0 results in a shape similar to the first mode of a cantilever shear beam. Multi-storey moment-resisting frames show this mode shape.

In any event, iterations on the initial shape selected can be performed until the desired level of matching is attained.

8.10 Advantages of the displacement-based design method

In comparing the spectral acceleration-based design method with the displacement-based design method, the following are found to be true for the latter.

(a) Displacements play a major role at the preliminary design stage itself resulting in good control over the entire design process. The designer can select displacement criteria for the serviceability and collapse limit states and thus achieve better damage control.

(b) Strength and stiffness of the LLRS are the end product of the design process. They are chosen to satisfy the desired deformation criteria.

(c) Empirical equations for estimating the fundamental period of the structure for preliminary design of the LLRS are not required. Instead, an acceptable deformation criterion is imposed at the start of the design process that is equivalent to providing initial stiffness to keep the desired deformation in control.

(d) The choice of a displaced shape at the start of the design process forces the engineer to consider the configuration of the LLRS and the drift tolerance for the non-structural elements. The displaced shape may often be explicitly linked to the member ductility demand, as observed in the CBF where the brace ductility is a function of geometry and material properties only. The allowable drift for non-structural elements could be obtained from laboratory tests and used directly in design.

(e) An empirical and somewhat arbitrary force modification factor, R, as used in the spectral acceleration-based design method, is not needed. Instead, a target maximum allowable deformation is chosen and the structure is provided with (reduced) strength and stiffness to attain this deformation. The inelastic component of this deformation is related to the member ductility demand.

8.11 Closure

The displacement-based design method, as outlined in sections 8.4 and 8.6, has been applied to the seismic design of RC bridge columns (Kowalsky *et al.* 1995) and MDOF bridge structures (Calvi and Kingsley 1995), respectively. It was reported to work well with both structures. It is applied to the design of an 8-storey building and a 2-storey building in the following chapters.

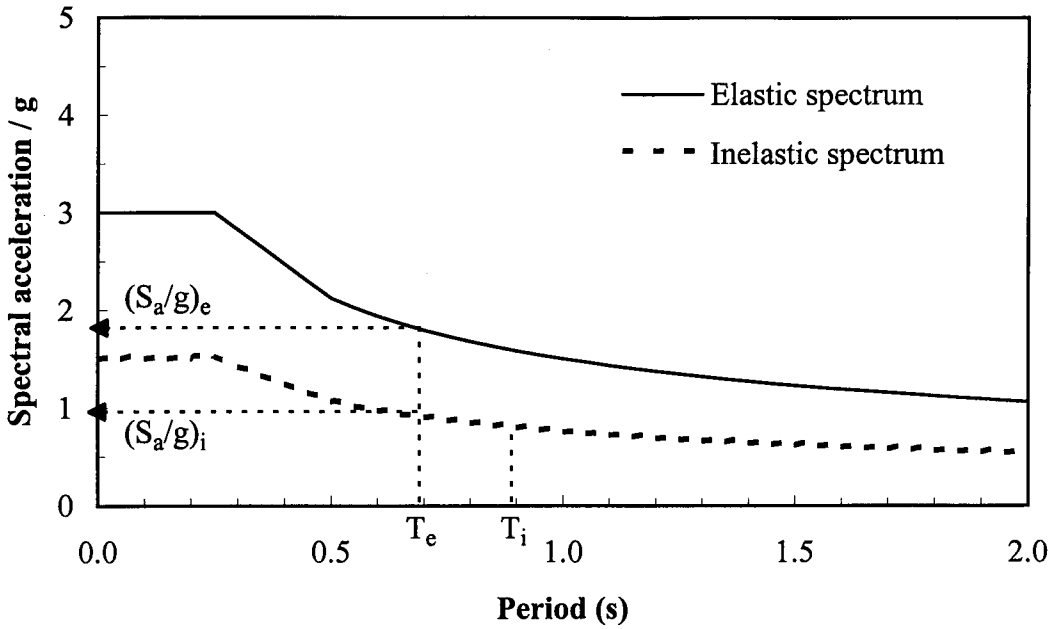

Figure 8.1 Design acceleration response spectra

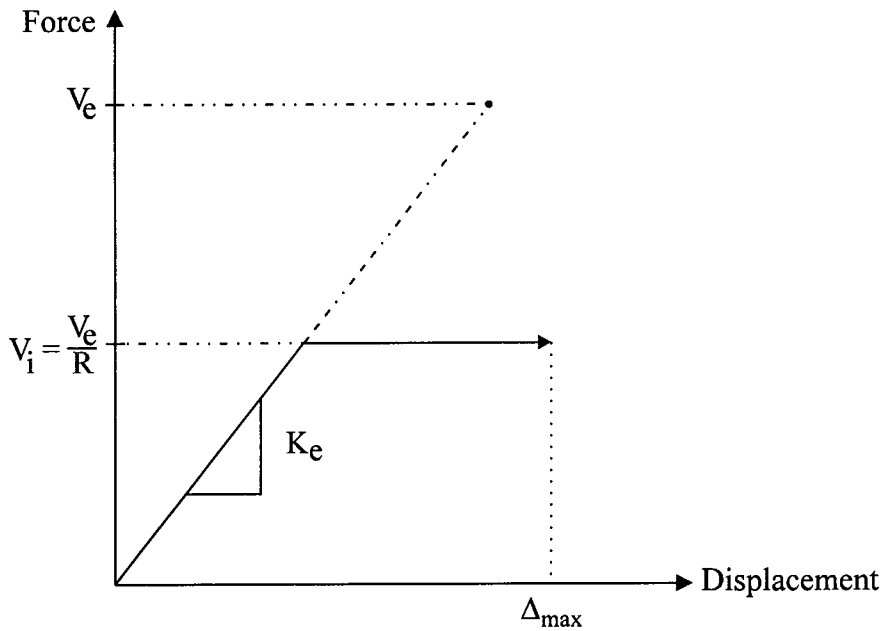

Figure 8.2 Inelastic response of a SDOF system

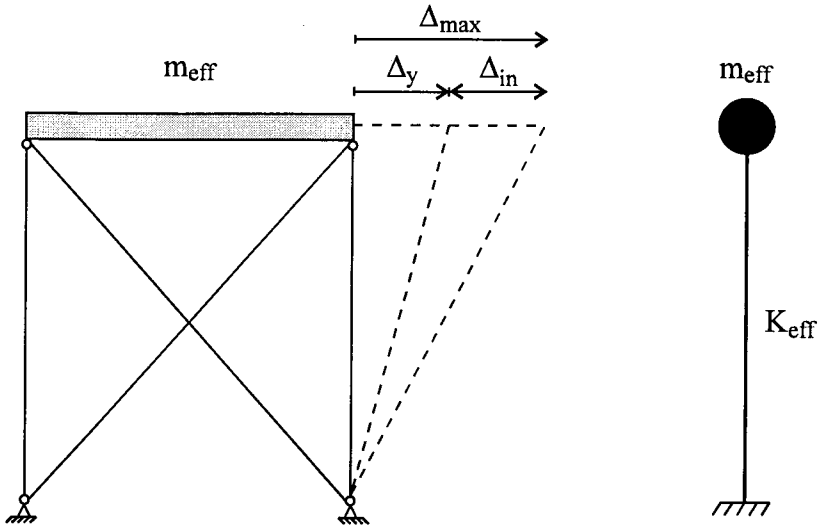

Figure 8.3 SDOF model of a CBF

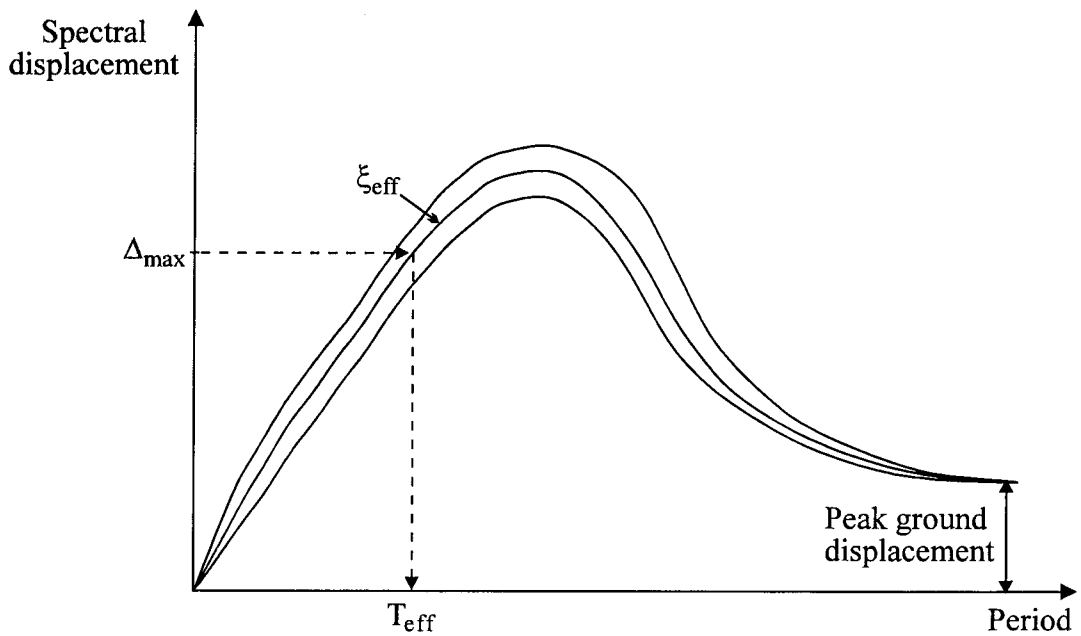

Figure 8.4 Design displacement response spectra

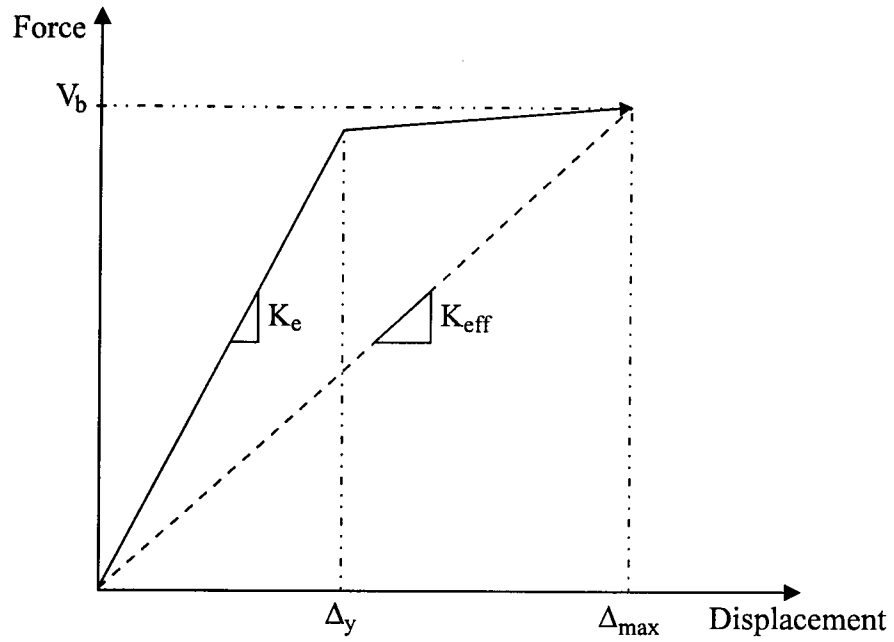

Figure 8.5 Substitute structure approach

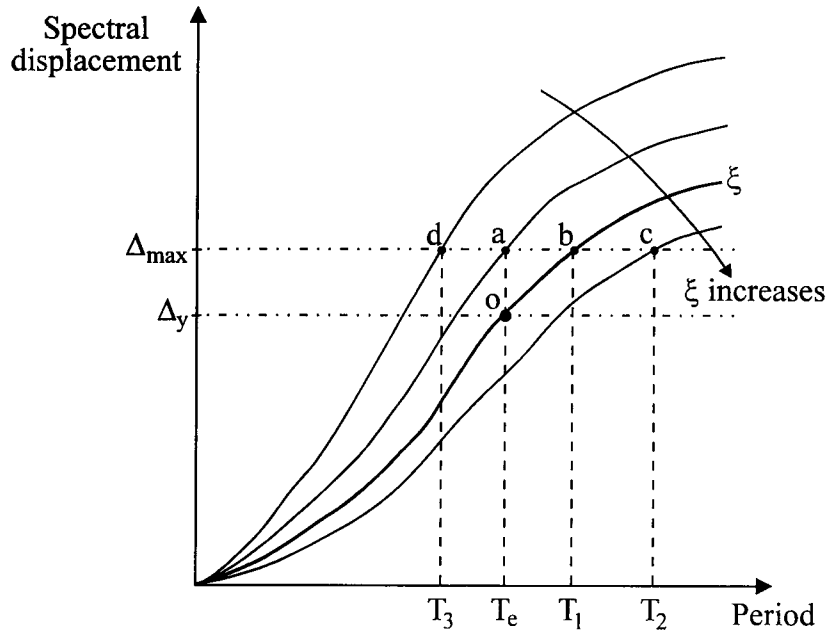

Figure 8.6 Substitute properties for elastic response spectra

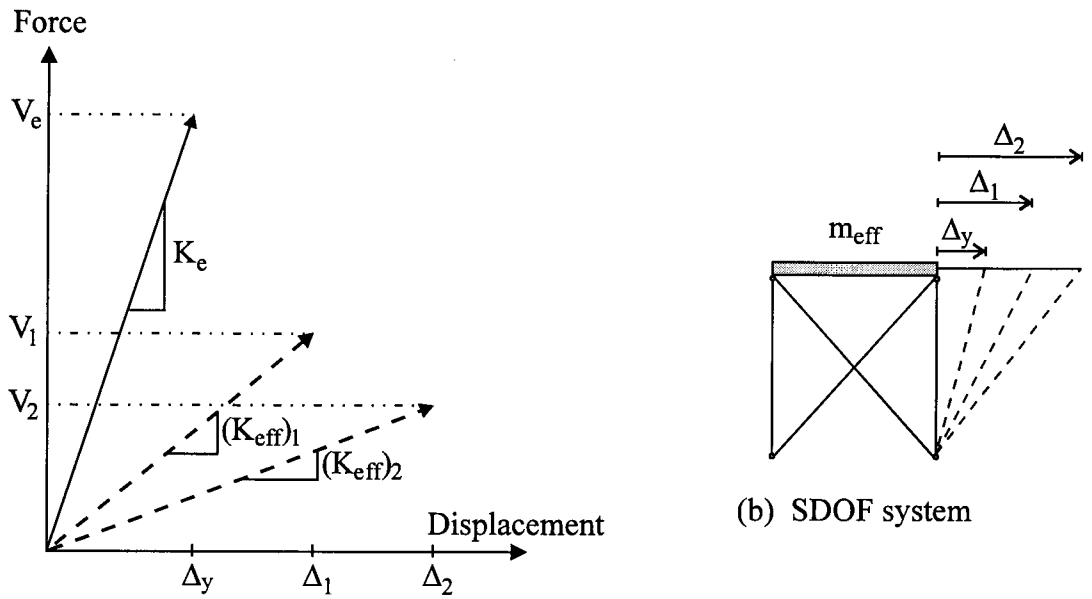

(a) Base shear vs. effective displacement

(b) SDOF system

Figure 8.7 Reduction in base shear with displacement

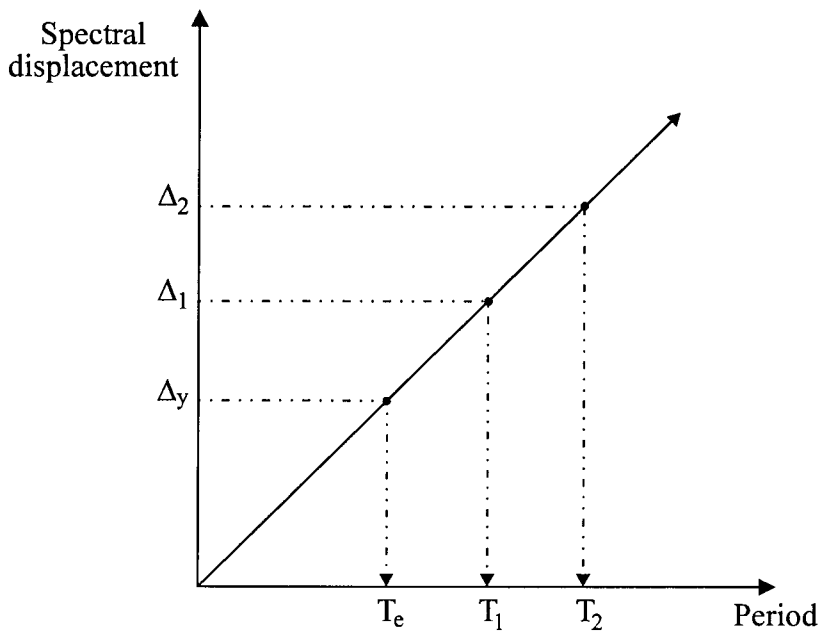

Figure 8.8 Linearized design displacement spectrum

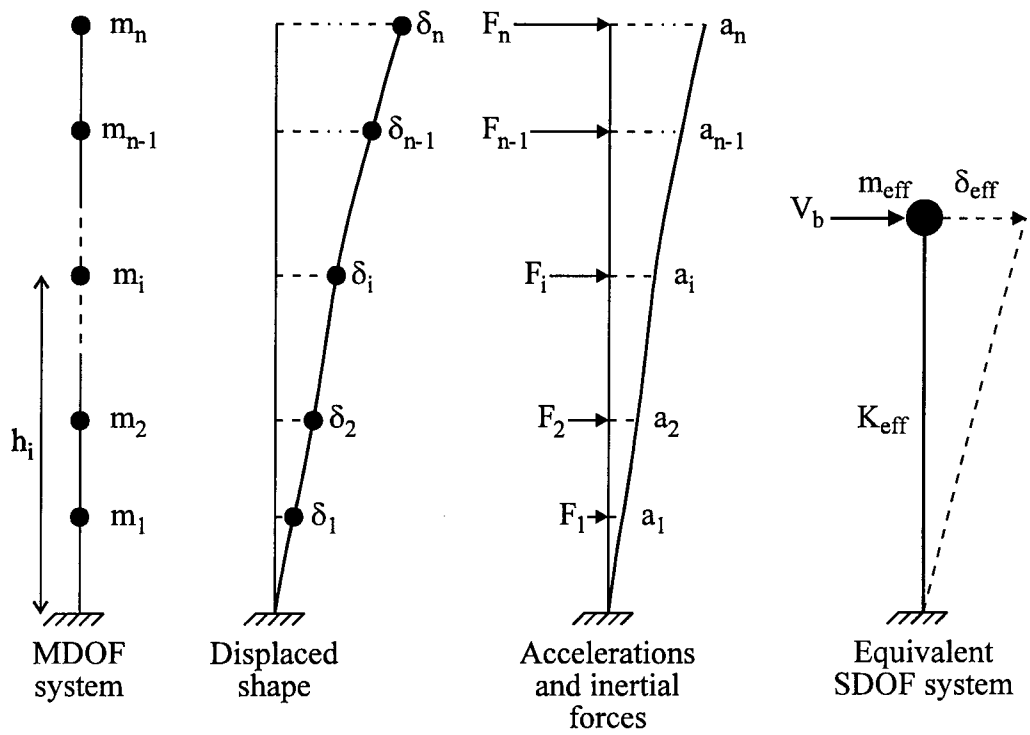

Figure 8.9 Multi-degree of freedom system

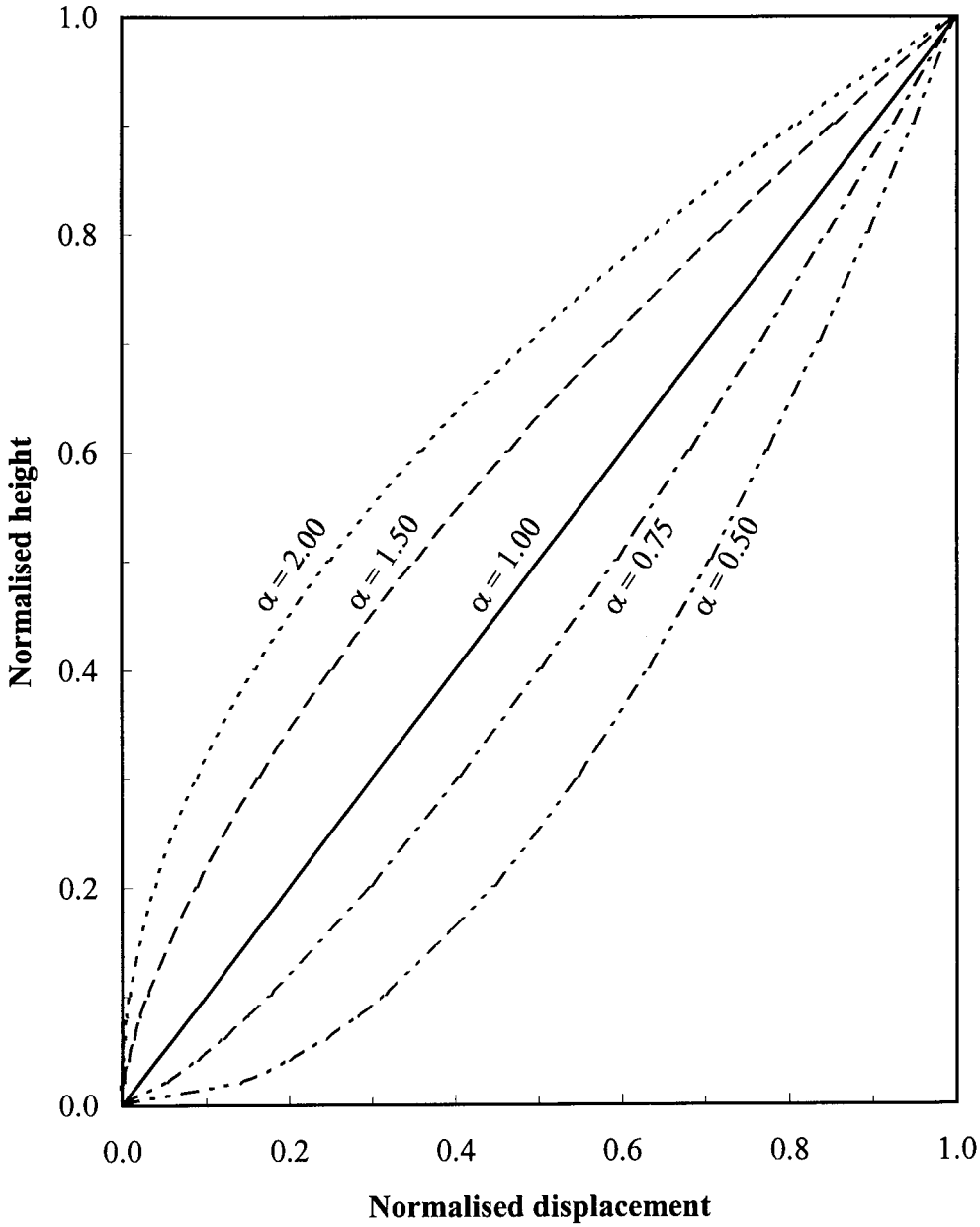

Figure 8.10 Initial displaced shape for buildings

9. EVALUATION OF THE DISPLACEMENT-BASED SEISMIC DESIGN METHOD - I

9.1 Introduction

The displacement-based seismic design method is evaluated by applying it to the design of an 8-storey building located in Victoria, BC (zone 5). The building uses concentrically braced frames (CBFs) as one of the lateral load resisting systems (LLRS). The required displacement response spectra are developed from the scaled earthquake accelerograms selected for this zone. The CBF is designed for several assumed displaced shapes. Structural models of the CBF are then developed to analyse its seismic response. A nonlinear analysis under static lateral earthquake force, a free vibration analysis, and nonlinear dynamic time history analyses are performed with these models to study the behaviour of the CBF and evaluate its performance.

A total of 6 design examples are considered. For simplicity and to focus attention on the displacement-based design method itself, a number of assumptions are made in the first design and analysis example as follows:

(a) The columns of the CBF are modelled to respond elastically in the nonlinear analyses by providing them with excess strength either by increasing their cross-sectional area beyond the design requirement or increasing the yield stress. Alternatively, well-established capacity design principles could be adopted to ensure that inelastic action is restricted to the diagonal braces only (Redwood and Channagiri 1991, Feeney and Clifton 1995).

(b) The diagonal braces are assumed to have the same capacity in tension and compression. A bilinear hysteresis behaviour is assumed and the degradation in brace compressive resistance due to cyclic buckling is neglected. In a realistic design situation, the storey strength is developed by the tension and compression diagonal of the CBF. Hence, tensile resistance of the brace and its reduced compressive resistance (to account for cyclic buckling) are added together to provide the required storey strength (CSA 1994). This usually results in an oversupply of strength to the storey.

(c) The P-Δ effect due to the gravity load moving through the lateral drift is ignored in analysis and design.

These assumptions drive the structure away from a realistic one. In later examples, all these simplifying assumptions are discarded.

9.2 Displacement response spectra

A pre-requisite to the application of this method is the availability of appropriate displacement response spectra (DRS). These spectra are developed herein by integrating numerically the equation of motion of a 5 % damped elastic SDOF system subjected to the earthquake accelerograms in Tables 4.9 and 4.10.

Figure 9.1 shows the maximum, mean + 1 sigma ($\mu + 1\ \sigma$), and the mean DRS for the 12 records of the acceleration set and Fig. 9.2 shows the corresponding ones for the 7 records of the velocity set. Also shown in both figures is the DRS obtained by converting the NBCC (ACNBC 1995a) elastic design acceleration spectrum (S factor curve) for locations with Z_a equal to Z_v. The period selected for generating the DRS, ranging from zero to 1.5 seconds, is one within which the fundamental period of this 8-storey building is expected to lie.

In this work, the $\mu + 1\ \sigma$ DRS is used for design. It is proposed that the period corresponding to the target spectral displacement be obtained from the DRS of the acceleration and the velocity sets separately and the mean of the two periods then be used for design. The DRS of the velocity set shown in Fig. 9.2 has a prominent local peak at a period of about 0.68 s. This could result in having two or more periods with the same target displacement. In such an event, the smallest period is selected for design. The $\mu + 1\ \sigma$ DRS shown in Figs. 9.1 and 9.2 has a spectral displacement of about 130 mm at a period of 1.5 s. Hence, in the following design examples, the initial displaced shape is chosen so that the effective displacement, δ_{eff}, from [8.19] does not exceed this value. This limitation need not exist in a realistic design situation wherein appropriate smoothed DRS would typically be used with displacements specified well into the long period range (Calvi and Kingsley 1995).

9.3 Description of the building

The building considered in this study is adapted from Chien (1987). It has also been used by Redwood and Channagiri (1991) and Redwood *et al.* (1991) for studying

the seismic response of CBFs designed by the spectral acceleration-based approach of the NBCC (ACNBC 1990). The building is rectangular in plan as shown in Fig. 9.3. Lateral load resistance in the East-West direction is provided by two CBFs that lie within the building core, while that in the North-South direction is provided by two moment resisting frames that lie along the exterior line of columns. Each CBF is 8000 mm wide and 29 700 mm high. The columns of the CBF are assumed to be in single storey lifts and are pinned at both ends. Loads from out-of-plane beams framing into the columns of the braced bay are assumed to be applied concentrically. The two braces in each storey are assumed to be identical.

Gravity loads are as described by Redwood and Channagiri (1991). A concentric dead load of 262 kN is applied at each column level. The beams spanning east-west have uniformly distributed dead and live loads of 16.5 kN/m and 10.8 kN/m, respectively. The concentrated live load from adjacent floor areas, taking the live load reduction factor of the NBCC for floors into account, is 60 kN at each floor and 101 kN at the roof. The effective seismic weight of the building, including 25% of the roof snow, is 54 200 kN, with a load of 7030 kN at the roof and 6740 kN at each floor.

9.4 Design of the building

In this work, only the seismic design of the CBF for earthquake load acting in the East-West direction is addressed. The two CBFs are identical because the building is symmetric in plan. Hence, they are lumped together and designed and analysed as a single frame. Accidental torsion is neglected for simplicity but could be included. At the start of the design process, only the approximate weight at each floor and the geometry of the CBF are known. Columns and braces are taken to be of grade 350W steel with a yield strength of 350 MPa. The braces in the first storey have a length of 6020 mm while those in all other storeys have a length of 5380 mm. From geometry of the CBF shown in Fig. 9.3, the storey drift required to yield the brace is

$$[9.1] \qquad \Delta = \frac{\Delta_Y}{\cos\theta} = \frac{F_Y L_b}{E \cos\theta}$$

where Δ_Y is the yield elongation of the brace, L_b is the brace length, F_Y is the yield stress (equal to 350 MPa), E is the elastic modulus, and θ is the angle of inclination of

the brace with the horizontal. Equation [9.1] gives a storey drift of 15.9 mm to yield the braces in the first storey and 12.7 mm for all other storeys.

9.5 Example 1

In this example, an initial displaced shape is assumed wherein the braces at all storeys are assumed to just reach yield. The brace ductility is defined as the maximum extension of the brace divided by its yield elongation. As all braces are assumed to attain a ductility of 1.0, this is referred to as the '$\mu = 1.0$' profile. The storey drifts required to yield the braces are added together to give the desired displaced shape. The design procedure for a MDOF system outlined in section 8.7, is implemented as shown in Table 9.1. The effective displacement of the SDOF system, δ_{eff}, from [8.19] is 75 mm and the effective mass, m_{eff}, from [8.16] is 4.48 kN s^2/mm. The latter is about 81% of the total building mass. The effective damping, ξ_{eff}, is taken as 5% of critical. The period corresponding to the effective displacement, δ_{eff}, obtained from the DRS of both the acceleration and the velocity sets (Figs. 9.1 and 9.2), is 0.75 s for the acceleration set and 0.60 s for the velocity set. The mean of the two periods, T_{eff} (equal to 0.68 s), is used for design. The effective stiffness, K_{eff}, from [8.3] is 389 kN/mm, and the base shear, V_b, from [8.20] is 28 940 kN. The static lateral force at each floor, F_i, from [8.17] and the static lateral force profile are given in Table 9.1. The sum of the static lateral forces from the roof to the 'i' th storey gives the storey strength, Q_i, which the braces of that storey have to develop. The cumulative storey shear strength is obtained by summing the individual storey strengths, Q_i, and is an approximate measure of the volume of steel required for the CBF.

9.5.1 Structural design

The CBF is designed for the static lateral forces given in Table 9.1 and the tributary gravity loads. The lateral load is resisted by the braces only. As discussed in section 9.1, the braces are assumed to have the same capacity in tension and compression. The columns at each storey are designed to resist the gravity load and the axial compression induced by the static lateral earthquake force. The column cross-section

thus obtained is increased by an arbitrary factor of 1.5 to ensure that the column remains elastic in the nonlinear analyses. The cross-sectional area of the braces and columns used at each storey are given in Table 9.2. Note that these properties are for the pair of CBFs lumped together.

9.5.2 Structural models and assumptions

The CBF is modelled as a two-dimensional truss. Thus, the columns and braces are assumed to have pinned ends. The floor diaphragms are assumed to be rigid in-plane. Hence, only one lateral degree of freedom (DOF) is specified at each floor at which the translational mass is lumped. Rotational inertia of the floors is neglected. Two models of the CBF are developed to investigate the effect of column shortening. In the first model, column shortening is prevented by constraining all vertical DOFs to be zero. In the second model, column shortening is allowed by removing the above constraint. Lateral stiffness at each storey is provided by the braces only. The P-Δ effect arising due to the gravity loads moving through the lateral drift is not modelled in this example for simplicity but is considered subsequently.

For nonlinear static analysis, the columns and braces are modelled with the Type-01 inelastic bar element of DRAIN-2DX (Powell 1993). This is a simple truss element with bi-linear behaviour in tension and compression. A strain-hardening modulus equal to 1% of the initial elastic modulus is specified for the braces only. For nonlinear dynamic analyses, Rayleigh damping is assumed with the coefficients specified to give 5% damping in the first and the last (eighth) mode. Columns are pinned at both ends and are modelled with the beam-column element of DRAIN-2D (Kannan and Powell 1973). Braces are modelled with the inelastic truss element with the same capacity specified in tension and compression. The hysteresis behaviour assumed is elasto-plastic with no strain-hardening.

9.5.3 Nonlinear static analysis

A nonlinear static analysis of the CBF is carried out with the program DRAIN-2DX. The objective of this analysis is to check the deformed shape of the CBF under the static lateral earthquake force given in Table 9.1 and compare it with the

assumed displaced shape. If the two shapes are in reasonable agreement, no revision of member stiffness or displaced shape is necessary.

Figure 9.4(a) shows the comparison between the assumed displaced shape and that from static analysis for the case with column shortening neglected. The two shapes match, as expected, because the displaced shape is obtained from the brace extensions at yielding, and no revision is necessary. Figure 9.5(a) shows similar comparison for the case with column shortening considered. The CBF has significantly greater lateral flexibility due to the finite axial stiffness of the columns. As the two shapes differ appreciably, revision of the member stiffness or of the assumed displaced shape is recommended. In example 1, none of the above are revised and the brace and column details given in Table 9.2, are used for dynamic analysis. Example 2 is an iteration with a revised displaced shape.

9.5.4 Free vibration analysis

The periods and mode shapes of the 8-storey CBF are obtained from free vibration analysis with the program DRAIN-2DX. The periods of both models, with and without column shortening considered, are given in Table 9.3. When column shortening is neglected, the period of the first mode is 0.68 s, and is equal to the design period, T_{eff}. This period increases to 0.91 s on considering column shortening. The period of the second and higher modes is also greater than the corresponding ones obtained when column shortening is neglected. The effective mass participating in each mode as a percentage of the total mass, as given by DRAIN-2DX, is shown in Figs. 9.4(b) and 9.5(b) for the two models. When column shortening is neglected, about 81% of the total mass participates in the first mode. Column shortening increases the contribution of the second mode significantly.

9.5.5 Nonlinear dynamic time history analyses

Nonlinear dynamic time history analyses of the structural models is carried out with the program DRAIN-2D. Each model is subjected to a total of 19 scaled earthquake records; 12 of the acceleration set and 7 of the velocity set. All analyses are carried out with a time step of 0.001s. From each analysis, the following information is collected:

(a) peak drift attained at each floor, and

(b) peak brace ductility demand in tension and in compression at each storey.

The $\mu + 1\,\sigma$ sigma value of the above peak responses is compared with the assumed values. This is consistent with the $\mu + 1\,\sigma$ DRS that was used for design. As the response spectrum is used for design directly, any difference obtained between a response quantity and its expected value may not be attributed to the difference between the design and the response spectra.

Figure 9.4(a) shows the lateral drift from dynamic analysis for the model with column shortening neglected. The displaced shape is in excellent agreement with the assumed shape but it is noted that the drift of the different floors from dynamic analysis do not occur simultaneously in the time history. Hence, the ductility demand on the braces cannot be obtained by calculating the storey drift from Fig. 9.4(a). The ductility demand on the braces, shown in Fig. 9.4(c), is obtained from the program output for the brace elements. The assumed ductility demand for the '$\mu = 1.0$' profile is 1.0 at each storey, that is, the braces are assumed to just reach yield. The ductility demand compares well with the assumed demand for storeys 1 to 6. The dynamic values exceed the assumed ones at storeys 7 and 8 with a ductility demand of 1.9 at storey 8.

Figure 9.5(a) shows the lateral drift from dynamic analysis for the model with column shortening considered. These drifts show better agreement with the assumed shape than that obtained from nonlinear static analysis. The ductility demand on the braces is less than the assumed demand for storeys 1 to 6 and greater for storeys 7 and 8, as shown in Fig. 9.5(c). The demand at storey 8 is 2.7.

9.5.6 Effect of column shortening

Column shortening makes a frame more flexible. This causes the period of the first mode to become greater than the design period, T_{eff}. Assuming that the dynamic response is predominantly in the first mode, the result of lengthening of the period is that the frame may undergo a greater displacement. This can be explained conceptually with the help of a DRS shown in Fig. 9.6. Let δ_{eff} be the target displacement for design of a SDOF system. The design period, T_{eff}, and the strength and stiffness required correspond

to this target displacement. Let T_1 be the period of the SDOF system after it has been designed. As T_1 is greater than T_{eff}, the maximum displacement, Δ_{max}, is greater than the target displacement, δ_{eff}.

The effect of additional flexibility due to column shortening is evident on comparing the results of static, free vibration, and dynamic time history analyses with the two models for example 1. In static analysis, the CBF shows significantly greater lateral drift than the assumed displaced shape, as may be deduced by comparing Figs. 9.4(a) and 9.5(a). In free vibration analysis, a lengthening of periods is observed as indicated in Table 9.3. The results from dynamic analysis suggest that greater flexibility results in an increased ductility demand in the upper two storeys of this CBF, as may be deduced by comparing Figs. 9.4(c) and 9.5(c).

The additional flexibility due to column shortening may be taken into account in the design stage itself. One approach is to use a period from the DRS that is less than that of the equivalent SDOF system, T_{eff}, thus providing an excess stiffness that counter-balances the reduction in stiffness due to column shortening. This technique may also be used to account for the reduction in lateral stiffness due to the P-Δ effect. Alternatively, column shortening may also be accounted for directly in a manner similar to that for the braces. The lateral drift of the n th floor, Δ_{nc}, due to shortening and elongation of all the columns of the CBF below it is

$$[9.2] \qquad \Delta_{nc} = \sum_{i=1}^{n} \frac{C_i h_i^2}{A_i E D_s} + \sum_{i=1}^{n-1} \frac{T_i h_i^2}{A_i E D_s}$$

where D_s is the width of the CBF, E is the modulus of elasticity, h_i is the storey height, A_i is the area of cross-section of the column, and C_i and T_i are the compressive and tensile axial forces in the columns of the i th storey. The axial stress, C_i/A_i and T_i/A_i, may be assumed equal to 0.7 F_Y to obtain an initial estimate of the floor drift, Δ_{nc}.

9.5.7 Conclusions from example 1

The displacement-based design approach works well for this example. The displaced shape from dynamic analysis and the brace ductility demands are in good

agreement with the assumed values. The increased ductility demand in the upper storeys of the CBF is due to the contribution of higher modes to the overall response. For this example, the assumed displaced shape is one in which the lateral drift increases linearly with height. This may not be a good shape because the building has a first mode shape that resembles the fundamental mode of a cantilever flexural beam. This shape is used in the next example.

9.6 Example 2

In this example, the initial displaced profile is similar to the first mode shape of the CBF with column shortening taken from example 1. The assumed displaced shape is chosen so that the effective displacement, δ_{eff}, from [8.19] is 1.5 times that of example 1. The assumed brace ductility demand at each storey and other relevant calculations are presented in Table 9.4. The properties of the equivalent SDOF system are; mass, m_{eff}, of 4 kN s^2/mm; effective displacement, δ_{eff}, of 112 mm; period, T_{eff}, of 1.16 s; stiffness, K_{eff}, of 117 kN/mm; and base shear, V_b, of 13 040 kN.

With a greater effective displacement of 112 mm as compared to 75 mm for example 1, the effective period increases and results in a reduced effective stiffness and a reduced base shear which is only about 45% of that in example 1. The reduction in base shear with increasing effective displacement, δ_{eff}, depends upon the shape of the DRS as explained in section 8.5. Braces are provided to develop the storey strength given in Table 9.4. The columns are assumed to be the same as in example 1. Nonlinear static analysis, free vibration analysis, and nonlinear dynamic time history analyses are performed on a model of this CBF. The modelling details and procedure are similar to example 1. Column shortening is considered in all the analyses for this example.

The displaced shape from static analysis agrees well with the assumed shape, as shown in Fig. 9.7(a). Part of this is attributed to the fact that the columns are the same as in the previous example; hence, the columns in the model have extra axial stiffness. Figure 9.7(b) gives the periods from a free vibration analysis. The period of the first mode, when column shortening is considered is 1.15 s, and obviously is less if column shortening is neglected (equal to 0.98 s). The design period is 1.16 s with column

shortening neglected. About 76% of the total mass participates in the first mode. The floor drift from dynamic analyses is given in Fig. 9.7(a). It is in good agreement with the assumed shape except at the top storey. The ductility demand on the braces is given in Fig. 9.7(c). The demand from dynamic analyses matches the assumed demand well for storeys 1 to 6, thereafter, it is significantly greater and reaches a demand of 6.6 at storey 8. Figure 9.7(d) shows the base shear capacity and the cumulative storey strength that is approximately proportional to the volume of steel required for the CBF. When compared with the corresponding values for example 1 given in Figs. 9.4(d) and 9.5(d), the design of example 2 is more economical. This occurs at the expense of a slightly increased ductility demand at storeys 1 to 6 and significantly greater demand at storeys 7 and 8.

9.6.1 Conclusions from example 2

This example demonstrates how a displaced shape with a greater effective displacement, δ_{eff}, results in a decrease in base shear. The displaced shape and ductility demand from dynamic analyses agree well with the assumed values for all storeys except the upper two. The increased demand is due to the effect of higher modes that are obviously not accounted for in the design process that replaces the MDOF system with an equivalent SDOF system.

9.7 Example 3

The initial displaced shape for this example is a linear one with the braces at all storeys assumed to extend to 1.5 Δ_Y, where Δ_Y is the yield elongation of the brace. This is referred to as the '$\mu = 1.5$' profile. Table 9.5 gives the assumed displaced shape. Table 9.6 lists the effective properties of the equivalent SDOF model and compares them with those obtained in example 2. Note that the effective displacement, δ_{eff}, from [8.19] is chosen to be the same in both examples. Thus, the design period obtained from the DRS is also the same. The effective mass, m_{eff}, is greater than that in example 2 and is equal to that obtained in example 1. This is due to the particular displaced shape as is evident from [8.16]. The difference in effective stiffness and base shear is attributed to the difference in effective mass only.

The static lateral forces are given in Table 9.5. Braces are provided to develop the necessary storey strength. The columns are assumed to be the same as in example 2 (and example 1) and the effect of column shortening is considered in all analyses.

The displaced shape from nonlinear static analysis agrees well with the assumed shape for storeys 1 to 6 and is greater at storeys 7 and 8, as shown in Fig. 9.8(a). The member stiffness and assumed displaced shape are not revised. The periods from free vibration analysis shown in Fig. 9.8(b), are not significantly different from those obtained in example 2. The drift from dynamic analysis is less than that assumed for floors 1 to 7, as shown in Fig. 9.8(a). It is greater at the roof. The ductility demand from dynamic analyses, shown in Fig. 9.8(c), is controlled well up to storey number 6, but is significantly greater than the assumed demand for storeys 7 and 8 with a value of 8.3 at the latter. These ductilities are greater than the ones obtained for example 2 where a nonlinear displaced profile was assumed.

9.7.1 Conclusions from example 3

The non-uniform displaced shape assumed in example 2 is a better initial shape as compared to the linear one assumed in example 3. Both examples have the same effective displacement, δ_{eff}, and the base shear in example 3 is 1.12 times greater than that in example 2. A comparison of static lateral forces for examples 2 and 3, given in Tables 9.4 and 9.5, respectively, shows that lower storey strength is provided at storeys 7 and 8 in example 3. Hence, example 3 shows greater ductility demand in these storeys. This suggests that a displaced shape similar to example 2 but with greater displacement at the upper two storeys will control the ductility demand on these storeys more effectively. This idea is explored in the next example.

9.8 Example 4

In this example, some additional issues are considered in design and analysis. These include the P-Δ effect and the effect of strain-hardening in the braces. The initial displaced shape is based on an assumed ductility demand that increases along the height of the CBF with a large demand assumed at the upper two storeys, as given in Table 9.7. The properties of the equivalent SDOF system are; mass, m_{eff}, of 3.85 kN s^2/mm;

effective displacement, δ_{eff}, of 128 mm; period, T_{eff}, of 1.31 s; stiffness, K_{eff}, of 88 kN/mm; and base shear, V_b, of 11 260 kN. The effective displacement, δ_{eff}, is the largest among the designs considered and results in the least base shear.

The P-Δ effect is accounted for approximately in the design stage itself. The method used is specified in Appendix J of the CSA Standard S16.1-94 (CSA 1994). The cumulative gravity load, ΣP_i, and the assumed storey drift, δ_i, are known at each floor. Hence, the sway force due to the P-Δ effect, H_i, can be calculated as shown in Fig. 9.9. This force is added to the lateral force at each floor and the resultant is reported in Table 9.7. The P-Δ effect increases the base shear by only 1.02 times for this assumed displaced shape. Braces are provided to develop the necessary storey strength. Columns are provided to resist the gravity load and the axial compression induced by the static lateral earthquake force. The column shortening effect is considered in all the analyses and the cross-sectional area is not increased by the arbitrary factor of 1.5 that was used in the examples 1, 2, and 3. Thus this example models the frame quite realistically.

Nonlinear static analysis of the CBF gives greater displacements than assumed as shown in Fig. 9.10(a). The greater displacements are attributed to the effects of axial deformation of the columns. No iterations are performed to make the two shapes match. The periods from free vibration analysis are shown in Fig. 9.10(b). The period of the first mode is 1.51 s when column shortening is included in the elastic analysis. If column shortening is not considered, this period reduces to 1.04 s. The design period, T_{eff}, assuming inelastic behaviour but neglecting column shortening is 1.31 s. About 71% of the total mass participates in the first mode.

For dynamic analyses, the P-Δ effect is modelled by adding a stack of dummy columns to the model with appropriate gravity load. Two dynamic analyses are performed. In dynamic analysis 1, the brace behaviour assumed is elasto-plastic with no strain-hardening. In dynamic analysis 2, the braces are assumed to have a strain-hardening modulus equal to 5% of the initial elastic modulus. [In retrospect, this assumption may be unconservative. However, the increase in the yield strength due to the strain rate under dynamic loading has not been considered].

Nonlinear dynamic time history analyses were performed with the structural models. In some of the 19 scaled earthquakes, the columns attained their yield load in the upper three storeys of the CBF. [It is recognized that most columns cannot reach their yield load and would in practice, under factored loads, be loaded for intermediate lengths to, say 0.7 times the yield load. In this example, this could be accommodated by providing larger columns.] Here, the resistance of these columns that yielded was increased by specifying a greater yield strength (thereby not affecting the axial stiffness) and the analysis repeated. The floor drifts shown in Fig. 9.10(a) show good agreement with the assumed displaced shape and are significantly lower than those from nonlinear static analysis. Strain-hardening has no noticeable effect on the floor drift. The ductility demand on the braces is given in Fig. 9.10(c). The demand from analysis with no strain-hardening is lower than the assumed demand for storeys 1 to 7 and greater at storey 8 with a value of 4.5. Analysis with strain-hardening results in a ductility demand that is lower than the assumed demand at all storeys, with a value of 3.3 at storey 8. Strain-hardening is seen to reduce the ductility demand at the upper 2 storeys where significant yielding occurs in the braces. Had column deformations been considered to match the drifts from nonlinear static analysis to those assumed, the brace sizes would have to be increased, and consequently, the brace ductility demand would decrease even further.

9.8.1 Conclusions from example 4

This example demonstrates how the P-Δ effect may be accounted for approximately in the design stage itself. An assumed displaced shape with large storey drift in the upper storeys results in increased lateral force towards the top of the CBF and appears to control the ductility demand better. Strain-hardening reduces the ductility demand obtained from dynamic analysis. Hence, if strain-hardening had been considered in all previous examples, the ductility demand in the upper storeys would have been lower than that obtained.

9.9 Control of ductility demand in the upper storeys, examples 5 & 6

It is evident from the result of examples 1, 2, and 3, that the ductility demand from dynamic analysis significantly exceeds the assumed demand in storeys 7 and 8. One method of controlling the ductility demand was explored in example 4 where a large storey drift was assumed at the upper 2 storeys thereby increasing the lateral force on the respective floors. This in turn leads to the provision of greater strength and stiffness for the upper storeys and thereby controls the ductility demand. An alternative method is used in the spectral acceleration-based approach of the NBCC to account for the effect of higher modes in buildings that have a fundamental period greater than 0.7 s. This consists of applying an appropriate fraction of the base shear (see equation 2.11) as a concentrated force at the roof and distributing the remainder along the building height. A similar approach is investigated herein.

In example 1, a linear displaced shape was assumed wherein the ductility demand at each storey was 1.0. The resulting static lateral forces are given in Table 9.1. In example 5, this lateral force distribution is modified so that 15% of the base shear is applied at the roof and the remaining 85% is distributed along the building height as given by [8.17]. This lateral force distribution was determined iteratively in order to reduce the ductility demand in the upper storeys to the target value. The lateral force profile for both examples is compared in Fig. 9.11(a) where the 'normalised force' is the static lateral force divided by the base shear. The profile for both examples is linear up to storey 7; thereafter, the profile for example 5 increases due to the additional force applied at the roof. Figure 9.11(b) shows the increase in the cumulative storey strength due to this modification. Although the base shear for both examples is the same (equal to 28 900 kN), there is a 6% increase in the cumulative storey strength at the bottom storey for example 5. The increase in volume of steel required may be considered approximately proportional to this. The floor drifts from dynamic analyses for examples 1 and 5 are compared in Fig. 9.11(c). They are similar except for a reduced drift at storey 8 for example 5. The ductility demand from dynamic analyses is compared in Fig. 9.11(d). For example 5, the ductility demand at storeys 7 and 8 is significantly less than that for example 1 and the demand at all storeys is close to the target demand of

1.0. The adjustment in the lateral force profile decreases the demand in the upper storeys significantly and increases it slightly at the bottom storey.

In example 3, a linear displaced shape was assumed with a ductility demand of 1.5 at each storey. In example 6, the lateral force profile of example 3 is adjusted in a manner similar to that described for example 5. The lateral force profile for examples 3 and 6 are compared in Fig. 9.12(a). These profiles are identical to those obtained for example 1 and 5, respectively. The increase in cumulative storey strength at the first storey is about 6%. The floor drift from dynamic analysis is shown in Fig. 9.12(c). Example 6 has significantly reduced drift at the roof while the drift at floors 1 to 6 is seen to increase marginally from those of example 3. Figure 9.12(d) compares the ductility demand from dynamic analysis. A very significant reduction in demand is observed at storeys 7 and 8. There is an increase in demand at all lower storeys.

Thus examples 5 and 6 demonstrate that one method of controlling the ductility demand in the upper storeys of the CBF is to adjust the static lateral force profile by putting more force on the upper storeys. This increases the strength and stiffness of these storeys, while keeping the base shear the same, and thus controls the ductility demand. The 15% of the base shear applied as a concentrated force at the roof with the remainder distributed along the building height was determined arbitrarily. Further study is required to judge if this percentage is adequate for tall CBFs.

9.10 Conclusions from the study on the 8-storey CBF

The displacement-based seismic design method has been applied to the design of an 8-storey CBF located in Victoria, BC. The method is shown to work well and is considered to be a viable alternative to the spectral acceleration-based design method. The design process is quite straightforward and rational. Based on the 6 design examples considered in this study, conclusions are presented in the following sections. Observations are also made pertaining to the DRS, the selection of an initial displaced shape, and allowance for column shortening and the P-Δ effect in preliminary design.

9.10.1 Design displacement spectra

There is a need to develop appropriate design displacement spectra for each seismic zone. Typically, smoothed design displacement spectra would be specified in building codes. In this study, the $\mu + 1\,\sigma$ DRS of a set of accelerograms was used for design purpose. For the 8-storey CBF and the displacement limits chosen, a DRS with periods up to 1.5 s was adequate. As noted earlier, a local peak is present in the DRS of the velocity set shown in Fig. 9.2. This results in two or more periods for spectral displacements between 80 to 100 mm. This did not affect any of the design examples considered as the effective displacement happened to lie outside this range. Typically, one would expect a monotonically increasing DRS curve as was approximately obtained for the acceleration set shown in Fig. 9.1. The presence of any plateau in the DRS will result in a number of periods satisfying the same displacement criteria. In such a case, the shortest period may be used.

9.10.2 Initial displaced shape

The selection of an appropriate initial displaced shape is very important in this design approach as it affects the base shear, the static lateral force profile, and the member design requirements.

A linear displaced shape was assumed in examples 1 and 3 while a nonlinear displaced shape was assumed in examples 2 and 4. The effective displacement of the displaced shape, δ_{eff}, from [8.19], determines the base shear [8.20]. Figure 9.13 shows the base shear for various effective displacements considered in this study. A greater effective displacement results in a lower base shear. As noted earlier, the reduction in base shear is a function of the shape of the DRS used. Figure 9.14 shows the normalised static lateral force profile, obtained by dividing the static lateral force at the floors by the base shear, for each example. This profile also depends upon the initial displaced shape. A greater amplitude of displacement assumed at a particular co-ordinate in the structure will increase the lateral force there. In example 4, a combined effect is seen where the base shear reduces due to a relatively large effective displacement (equal to 128 mm) and the static lateral force profile is biased towards the top due to the large displacement assumed towards the top of the CBF.

To obtain an initial displaced shape, storey drifts are required. In the CBF, the storey drift is explicitly linked to the brace ductility demand [when column flexibility is neglected.] Hence, selection of an initial displaced shape is equivalent to specifying how much elastic or inelastic action is expected in the braces at each storey. Braces and their connections may then be detailed for this to be so.

An initial displaced shape with a profile that matches the first mode shape, taking into account brace elongation and column shortening, is a good first choice. MDOF systems will typically respond elastically in the first mode before developing inelastic action. Displaced shapes with inelastic drift implied in them may also be developed based on the first mode shape, as was done in example 2.

9.10.3 Allowance for other effects

Other effects such as column shortening and P-Δ effects may be accounted for approximately in the preliminary design stage itself. To anticipate the effect of column shortening, one may select a shorter period from the DRS. Additional lateral forces due to the P-Δ effect may also be calculated based on the assumed displaced shape and the gravity loads.

9.10.4 Results of dynamic analysis

The initial displaced shape was revised for example 2 only. In all other examples, the initial displaced shape was used even though it did not match that from static nonlinear analyses well. The latter typically suggested a more flexible structure than assumed due to the combined effect of column flexibility and inelastic action in the braces under the static lateral forces.

The variation of floor drift with height and brace ductility demand depends on the relative stiffness and relative yield strengths of the storeys. The displaced shape from dynamic analysis agrees well with the assumed shape for most of the design examples. For tall CBFs better agreement is obtained for nonlinear displaced shapes than linear ones. The brace ductility demand determined from time history dynamic analyses also agrees fairly well with the assumed demand for storeys 1 to 6. Greater demands are observed in the upper 2 storeys of the CBF due to the influence of higher modes. The

ductility demand on these storeys may be controlled by providing them with greater strength. Two methods were explored for providing this extra strength. The first method, assuming an initial displaced shape with large displacements towards the upper storeys of the CBF, was used in example 4. This results in a greater lateral force being applied on these storeys. The second method adjusted the lateral force profile without changing the base shear so that 15% of the base shear was applied at the roof and the remainder distributed over the height by [8.17]. This method was used in examples 5 and 6. Both methods were effective in controlling the ductility demand in the upper storeys.

Another major issue is whether target floor displacements or storey ductility demands should be given more importance. A problem with the target floor displacements is that they do not occur simultaneously in the time history. Hence, if the roof attains its target displacement but the floor immediately below does not, the resulting storey drift and brace ductility demand will be greater than that assumed. Damage to structural and non-structural elements in any storey is proportional to the storey drift. For the CBF, storey drift is explicitly related to the brace ductility demand. Hence, damage control can best be achieved by restricting the brace ductility demand to acceptable limits.

9.11 Recommendations for further work

The displacement-based design method implemented here is based on fundamental principles. No calibration factors such as the U factor nor the force modification factor, R, of the NBCC (ACNBC 1995a) are used. No attempt is made to compare this approach to the spectral acceleration-based approach of the NBCC. Further studies with this method should address the following issues:

(a) appropriate DRS for design,

(b) hysteretic damping in steel structures for use with the substitute structure approach,

(c) selection of appropriate displacement limits for structural elements, non-structural elements, and structures,

(d) use of realistic brace members in design and analysis. Real braces have an asymmetric response in tension and compression that was not considered here. Cyclic buckling of the braces also results in a reduction in compressive resistance with number of cycles.

(e) methods to account for the effect of higher modes in tall CBFs,

(f) the use of other LLRS such as moment resisting frames, eccentrically braced frames, and steel plate shear walls, and,

(g) the application of the method to low-rise buildings.

Table 9.1 Design parameters for example 1

Storey #	Storey height	Height to floor H	Weight W	Storey drift for brace yield δy_i	Assumed displaced shape δ_i	$m_i \delta_i$	$m_i \delta_i^2$	Assumed displaced profile c_i	$m_i c_i$	Static lateral force F_i	Static lateral force profile F_i/V_b	Storey strength Q_i	Cumulative storey strength
	(m)	(m)	(kN)	(mm)	(mm)	(kN s^2)	(kN s^2 mm)		(kN s^2/mm)	(kN)		(kN)	(kN)
8	3.6	29.7	7028	12.67	104.55	75	7831	1.40	1.01	6490	0.22	6490	6490
7	3.6	26.1	6740	12.67	91.88	63	5800	1.23	0.85	5470	0.19	11960	18449
6	3.6	22.5	6740	12.67	79.21	54	4311	1.06	0.73	4715	0.16	16675	35124
5	3.6	18.9	6740	12.67	66.54	46	3042	0.89	0.61	3961	0.14	20636	55760
4	3.6	15.3	6740	12.67	53.87	37	1994	0.72	0.50	3207	0.11	23843	79604
3	3.6	11.7	6740	12.67	41.20	28	1166	0.55	0.38	2453	0.08	26296	105899
2	3.6	8.1	6740	12.67	28.53	20	559	0.38	0.26	1698	0.06	27994	133893
1	4.5	4.5	6740	15.86	15.86	11	173	0.21	0.15	944	0.03	28938	162831
Σ			54208			334	24875		4.48	28938	1.00		

Notes

1. $m_{eff} = \Sigma m_i c_i = 4.48$ kN s^2/mm
2. $\delta_{eff} = \Sigma m_i \delta_i^2 / \Sigma m_i \delta_i = 24875 / 334 = 75$ mm

Table 9.2 Example 1 - Brace and column areas

Storey	cross-section provided (mm^2) Brace	Column
8	12475	14450
7	22985	39270
6	32050	73185
5	39660	114740
4	45825	162480
3	50540	214955
2	53805	270700
1	62225	342220

Table 9.3 Example 1 - Periods from free vibration analysis

Mode	Period (s) Column shortening (a) Neglected	(b) Considered	ratio (b/a)
1	0.68	0.91	1.35
2	0.27	0.33	1.18
3	0.17	0.19	1.10
4	0.13	0.13	1.07
5	0.10	0.10	1.02
6	0.08	0.08	1.03
7	0.07	0.07	1.01
8	0.06	0.06	1.00

Table 9.4 Design parameters for example 2

Storey #	Storey height (m)	Height to floor H (m)	Weight W (kN)	Storey drift for brace yield δy_i (mm)	Assumed brace ductility demand	Assumed displaced shape δ_i (mm)	$m_i \delta_i$ (kN s^2)	$m_i \delta_i^2$ (kN s^2 mm)	Assumed displaced profile c_i	$m_i c_i$ (kN s^2/mm)	Static lateral force F_i (kN)	Static lateral force profile F_i/V_b	Storey strength Q_i (kN)	Cumulative storey strength (kN)
8	3.6	29.7	7028	12.67	2.26	163.82	117	19226	1.47	1.05	3428	0.26	3428	3428
7	3.6	26.1	6740	12.67	1.98	135.18	93	12554	1.21	0.83	2713	0.21	6142	9570
6	3.6	22.5	6740	12.67	1.98	110.07	76	8324	0.99	0.68	2209	0.17	8351	17921
5	3.6	18.9	6740	12.67	1.63	84.97	58	4960	0.76	0.52	1705	0.13	10056	27977
4	3.6	15.3	6740	12.67	1.62	64.38	44	2847	0.58	0.40	1292	0.10	11348	39325
3	3.6	11.7	6740	12.67	1.23	43.79	30	1318	0.39	0.27	879	0.07	12227	51552
2	3.6	8.1	6740	12.67	1.23	28.15	19	544	0.25	0.17	565	0.04	12792	64344
1	4.5	4.5	6740	15.86	0.79	12.50	9	107	0.11	0.08	251	0.02	13043	77387
Σ			54208				446	49881		4.00	13043	1.00		

Notes

1. $m_{eff} = \Sigma\, m_i\, c_i = 4.00$ kN s^2/mm
2. $\delta_{eff} = \Sigma\, m_i\, \delta_i^2 \,/\, \Sigma\, m_i\, \delta_i = 49881 / 446 = 112$ mm

Table 9.5 Design parameters for example 3

Storey #	Assumed displaced shape δ_i (mm)	Static lateral force (kN)	Static lateral force profile
8	156.82	3282	0.22
7	137.82	2766	0.19
6	118.81	2385	0.16
5	99.81	2003	0.14
4	80.80	1622	0.11
3	61.80	1240	0.08
2	42.79	859	0.06
1	23.79	477	0.03
Σ	V_b =	14635 kN	1.00

Table 9.6 Comparison between effective properties of examples 2 and 3

Effective property	Example 2	Example 3	Ratio
Displacement, δ_{eff} (mm)	111.72	111.72	1.00
Period, T_{eff} (s)	1.16	1.16	1.00
Mass, m_{eff} (kN s^2/mm)	4.00	4.48	1.12
Stiffness, K_{eff} (kN/mm)	117	131	1.12
Base shear, V_b (kN)	13043	14635	1.12

Table 9.7 Design parameters for example 4

Storey #	Storey height (m)	Height to floor H (m)	Weight W (kN)	Storey drift for brace yield δy_i (mm)	Assumed brace ductility demand	Assumed displaced shape δ_i (mm)	$m_i \delta_i$ (kN s^2)	$m_i \delta_i^2$ (kN s^2 mm)	Assumed displaced profile c_i	$m_i c_i$ (kN s^2/mm)	Static lateral force (incl. P-Δ) F_i (kN)	Static lateral force profile F_i/V_b	Storey strength Q_i (kN)	Cumulative storey strength (kN)
8	3.6	29.7	7028	12.67	4.00	199.57	143	28535	1.56	1.12	3376	0.29	3376	3376
7	3.6	26.1	6740	12.67	3.00	148.89	102	15232	1.17	0.80	2391	0.21	5766	9142
6	3.6	22.5	6740	12.67	2.00	110.88	76	8448	0.87	0.60	1745	0.15	7511	16653
5	3.6	18.9	6740	12.67	1.50	85.54	59	5028	0.67	0.46	1346	0.12	8858	25511
4	3.6	15.3	6740	12.67	1.50	66.54	46	3042	0.52	0.36	1083	0.09	9941	35452
3	3.6	11.7	6740	12.67	1.25	47.53	33	1552	0.37	0.26	748	0.07	10689	46141
2	3.6	8.1	6740	12.67	1.25	31.70	22	690	0.25	0.17	529	0.05	11218	57359
1	4.5	4.5	6740	15.86	1.00	15.86	11	173	0.12	0.09	232	0.02	11450	68809
Σ			54208				491	62699		3.85	11450	1.00		

Notes

1. $m_{eff} = \Sigma\, m_i\, c_i = 3.85$ kN s^2/mm
2. $\delta_{eff} = \Sigma\, m_i\, \delta_i^2 / \Sigma\, m_i\, \delta_i = 62699 / 491 = 128$ mm

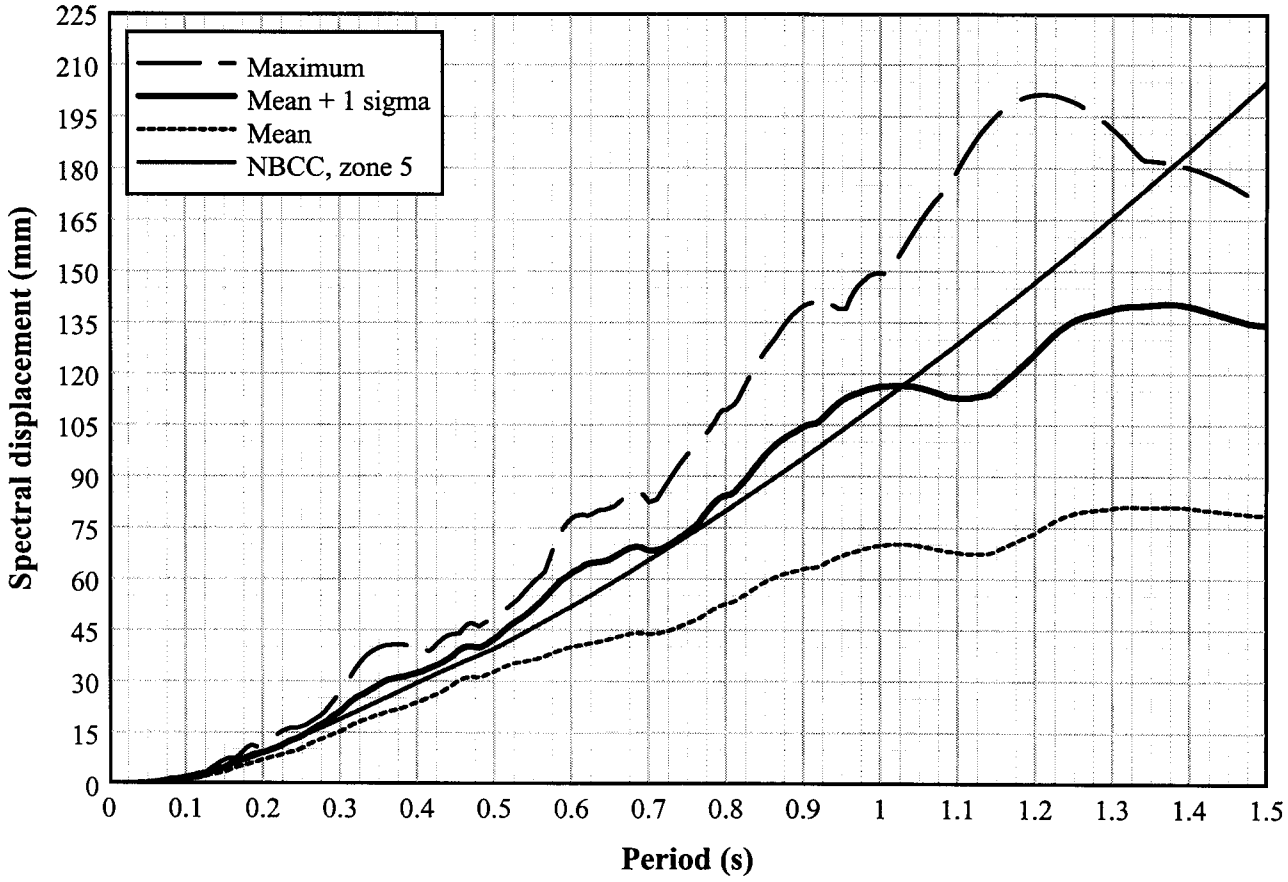

Figure 9.1 Displacement response spectra (from acceleration set of records for zone 5)

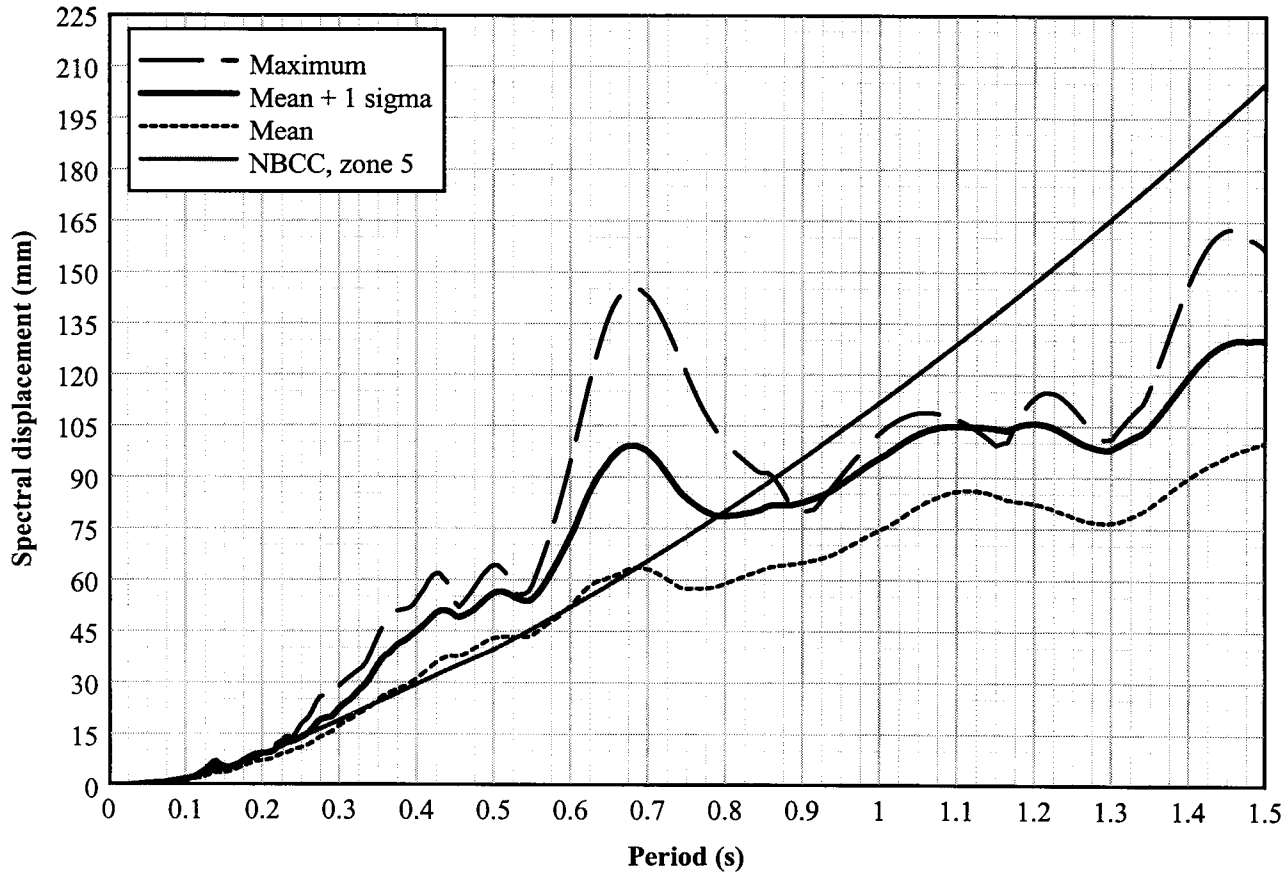

Figure 9.2 Displacement response spectra (from velocity set of records for zone 5)

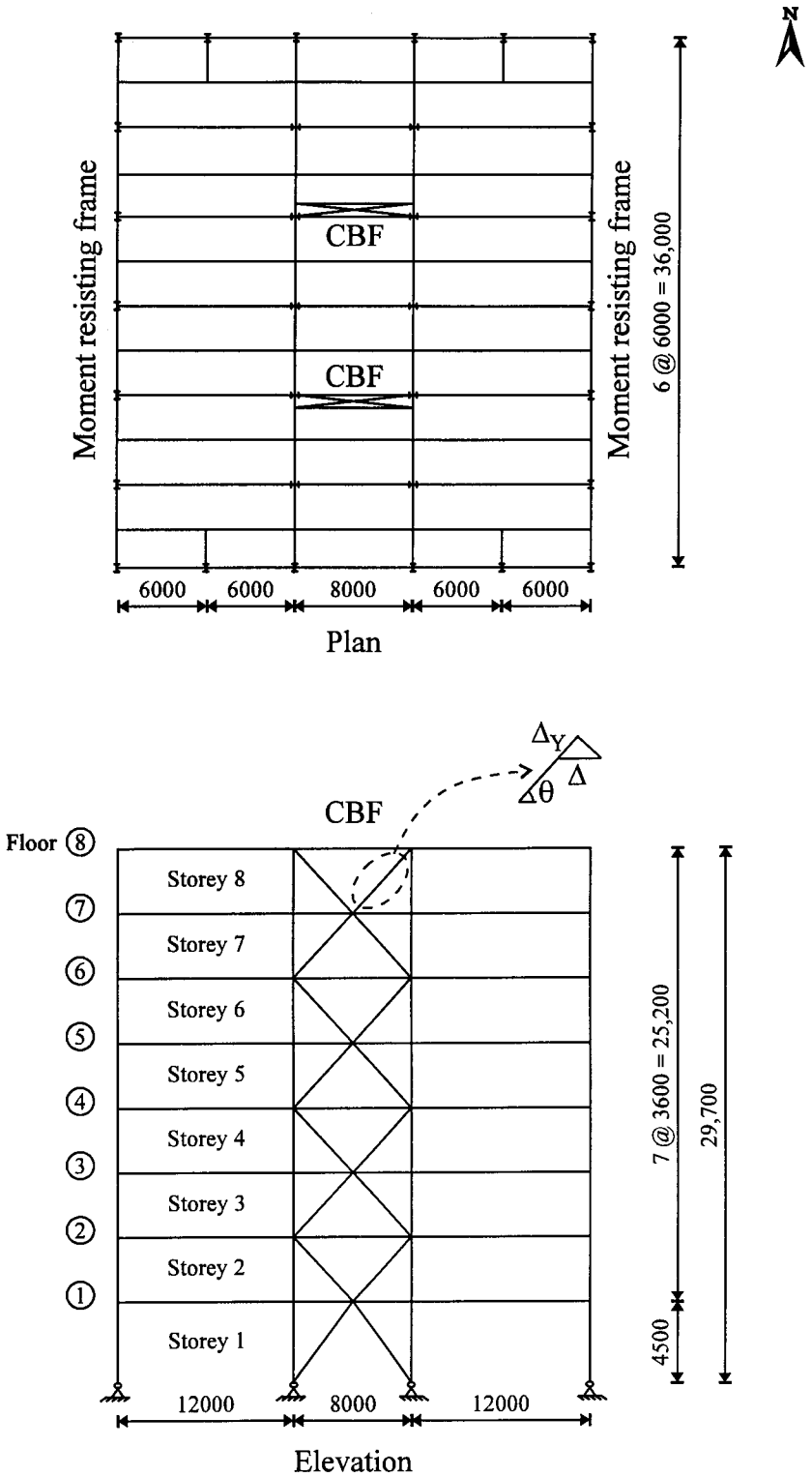

Figure 9.3 Layout of 8-storey building

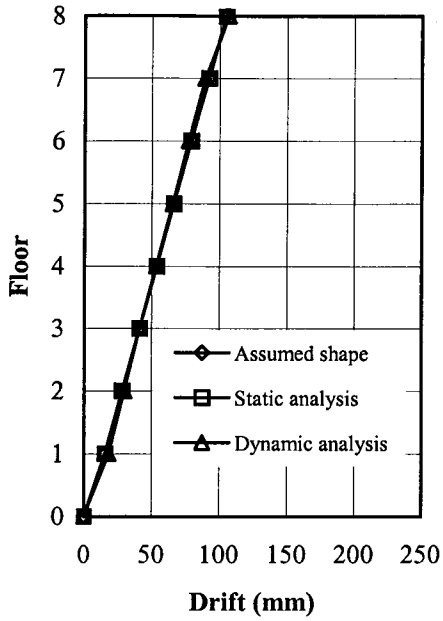

(a) Floor drift

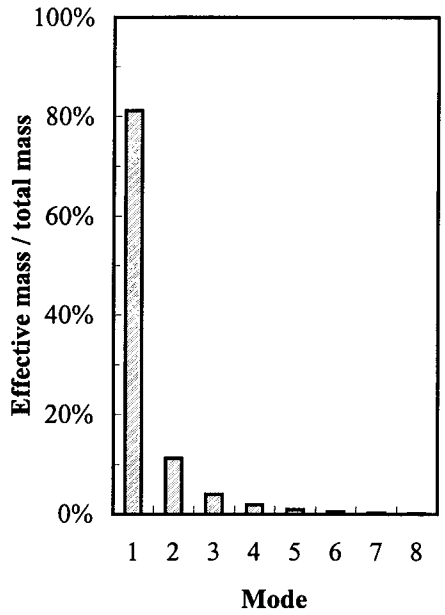

(b) Effective modal mass

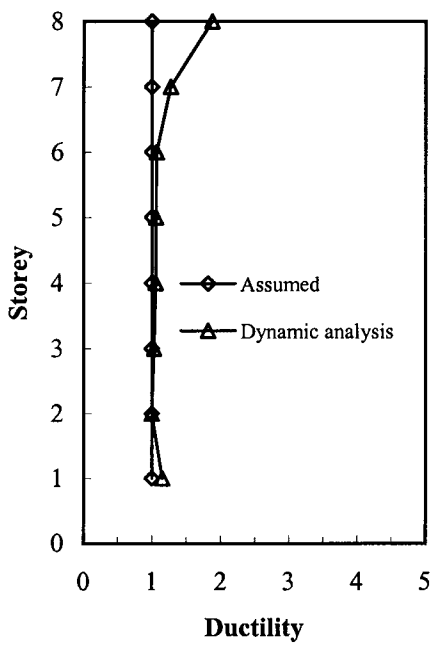

(c) Ductility demand

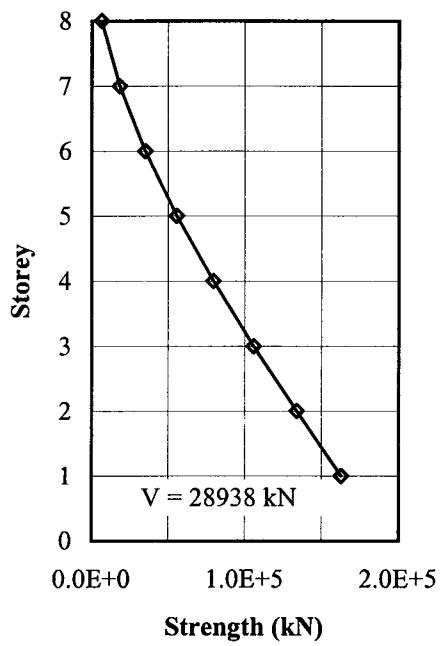

(d) Cumulative storey strength

Figure 9.4 Results for example 1: column shortening neglected

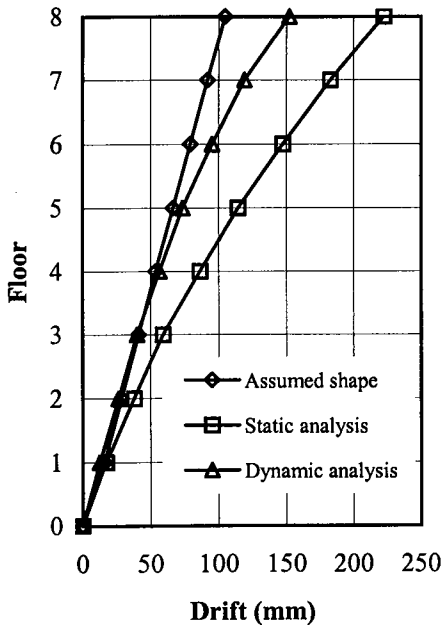

(a) Floor drift

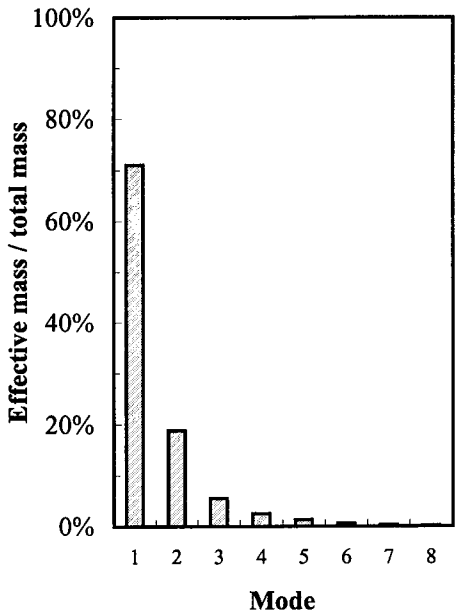

(b) Effective modal mass

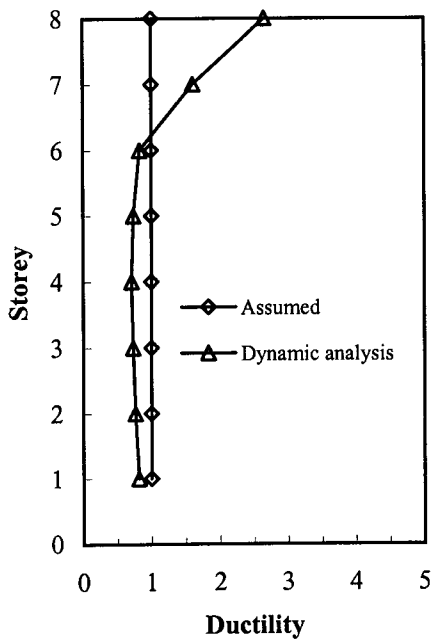

(c) Ductility demand

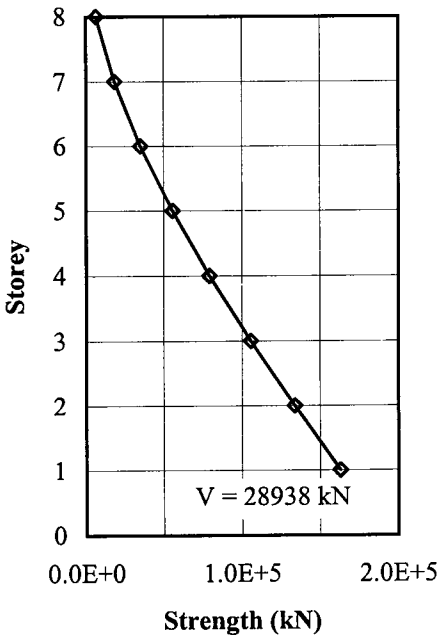

(d) Cumulative storey strength

Figure 9.5 Results for example 1: column shortening considered

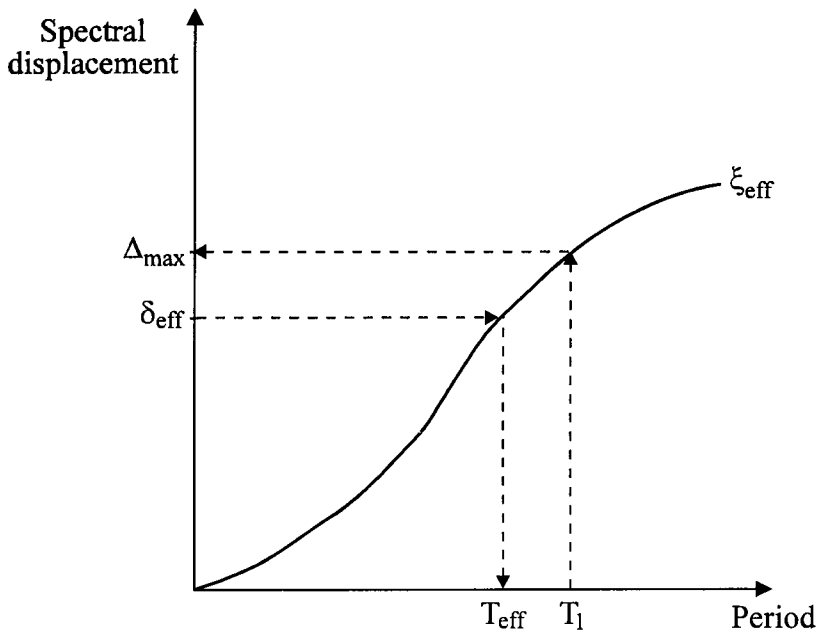

Figure 9.6 Effect of lengthening in period on displacement

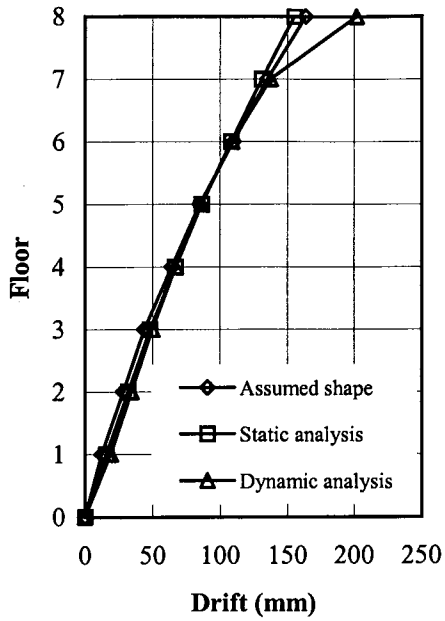

(a) Floor drift

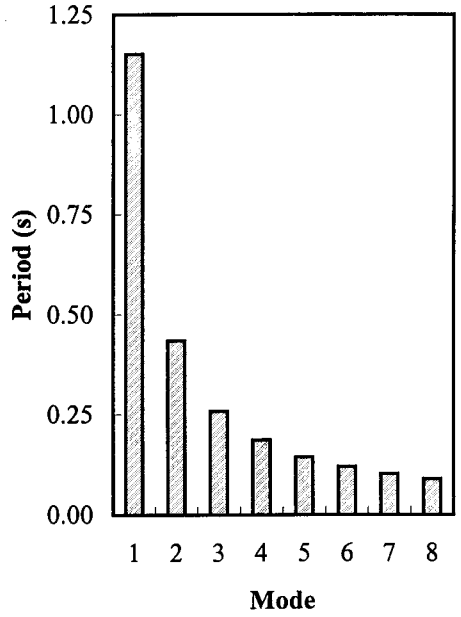

(b) Periods

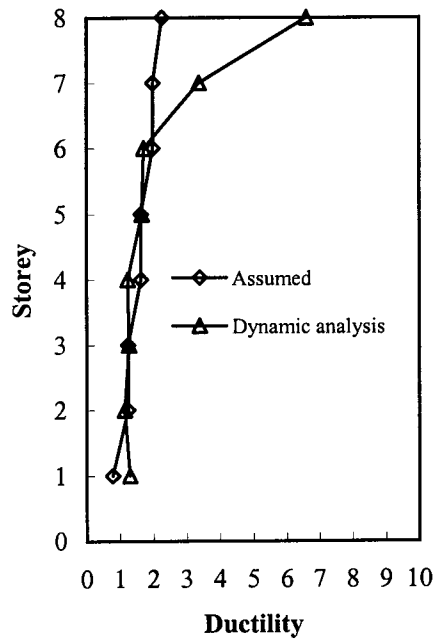

(c) Ductility demand

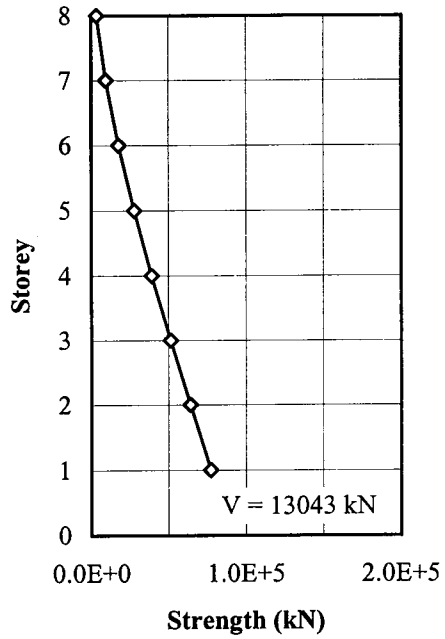

(d) Cumulative storey strength

Figure 9.7 Results for example 2

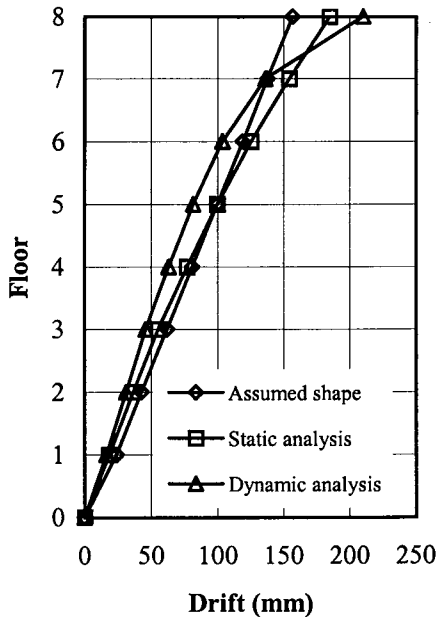

(a) Floor drift

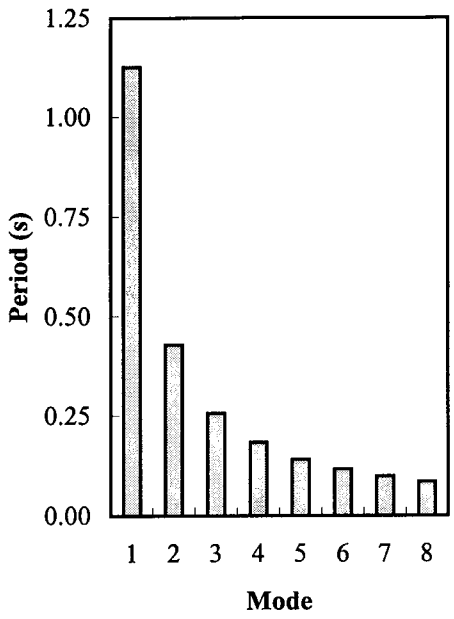

(b) Periods

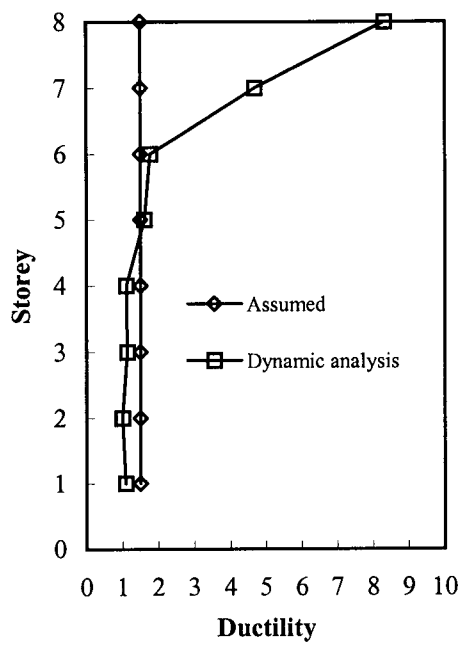

(c) Ductility demand

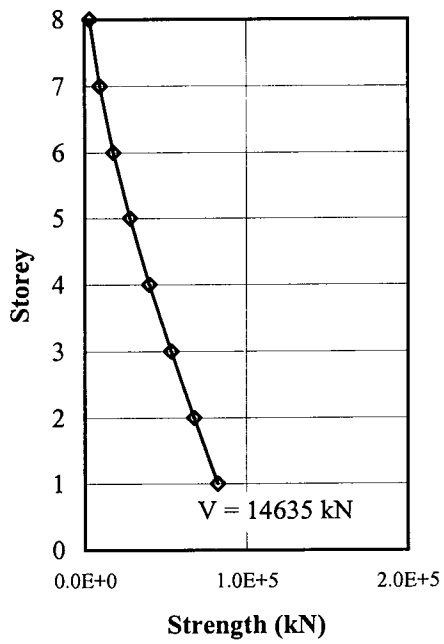

(d) Cumulative storey strength

Figure 9.8 Results for example 3

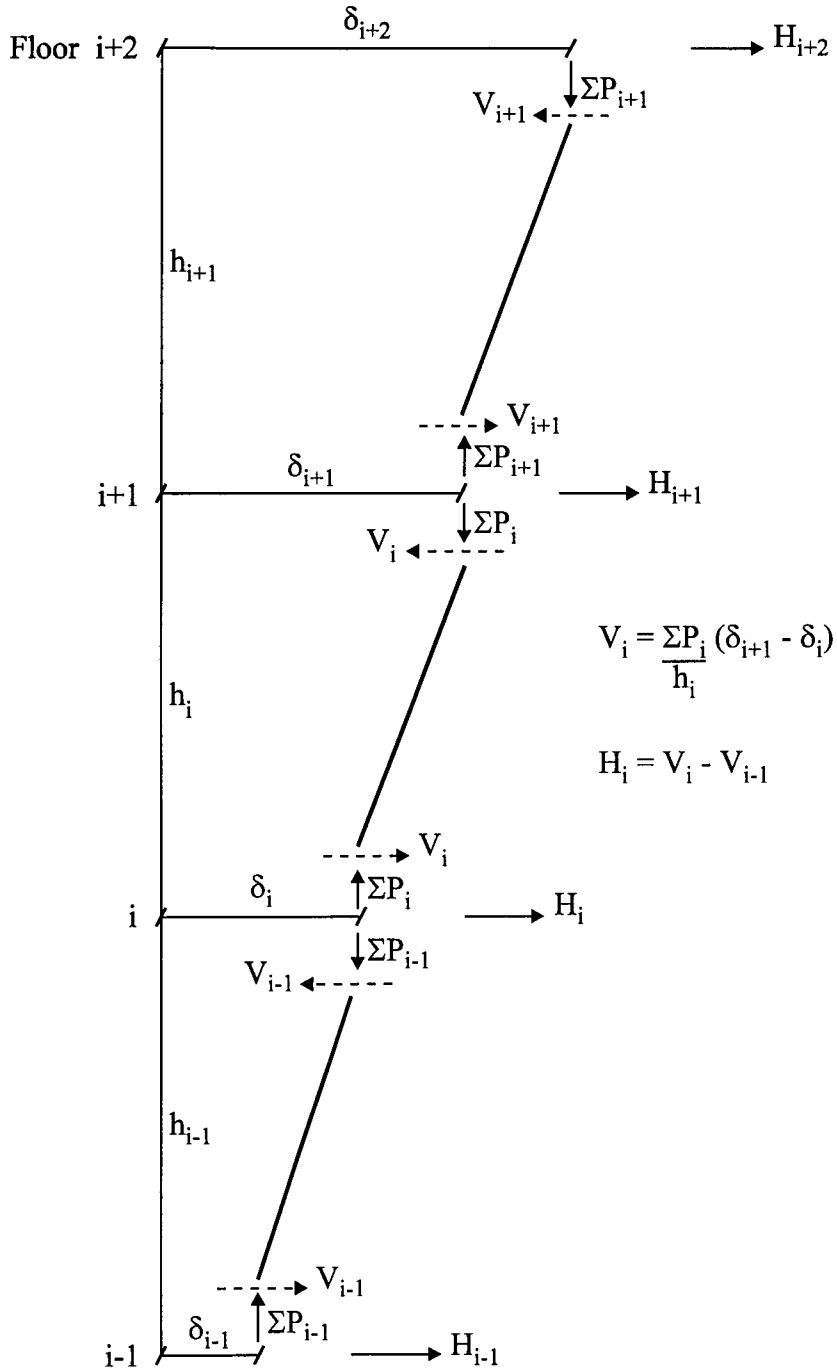

Figure 9.9 Sway force due to the P-Δ effect

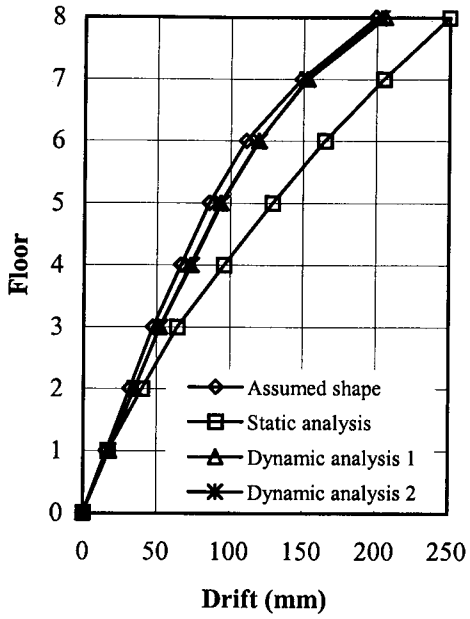

(a) Floor drift

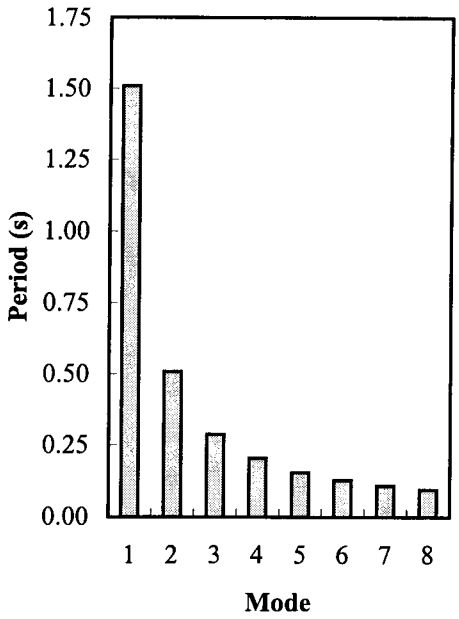

(b) Periods

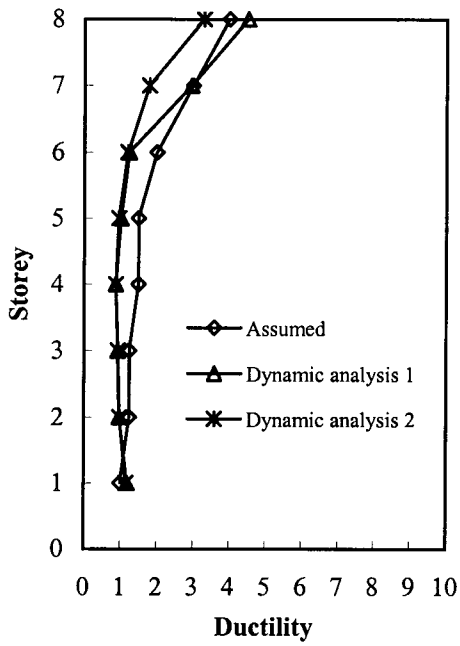

(c) Ductility demand

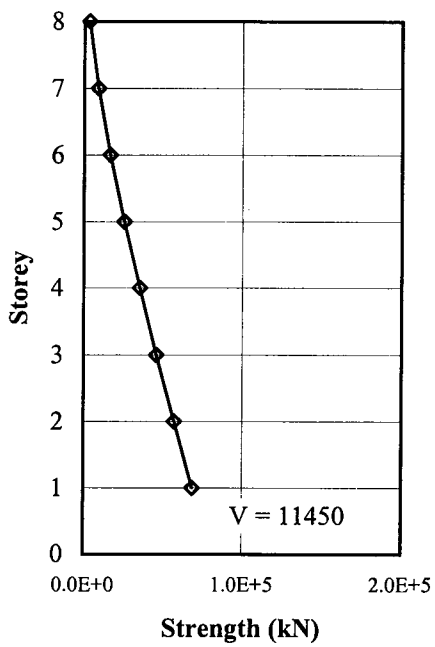

(d) Cumulative storey strength

Figure 9.10 Results for example 4

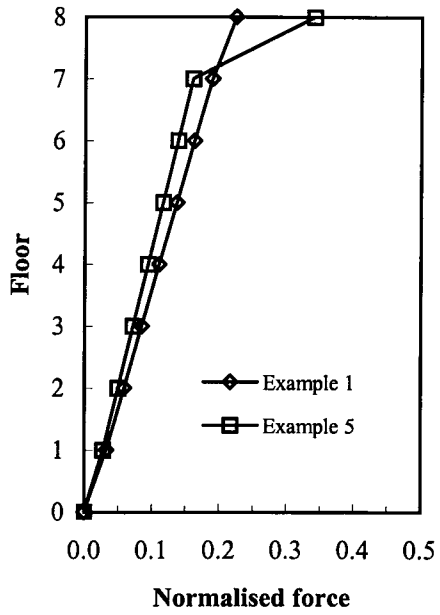

(a) Lateral force profile

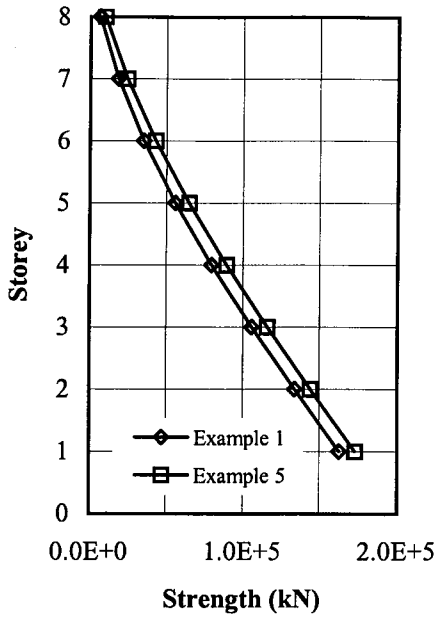

(b) Cumulative storey strength

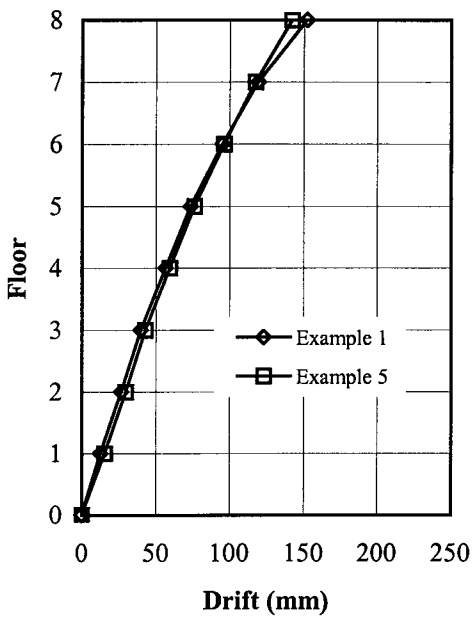

(c) Floor drift

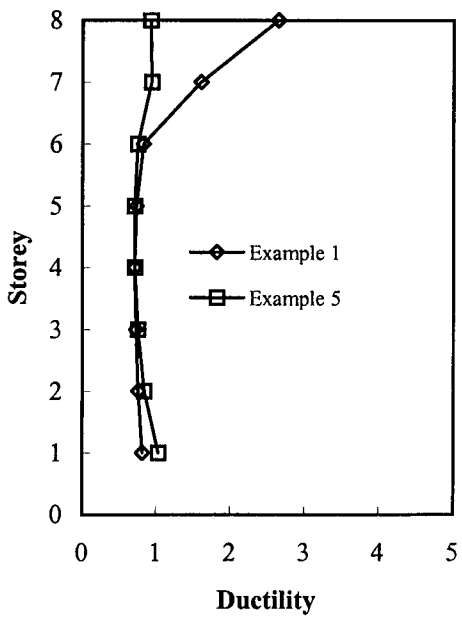

(d) Ductility demand

Figure 9.11 Comparison of results, example 1 vs. example 5

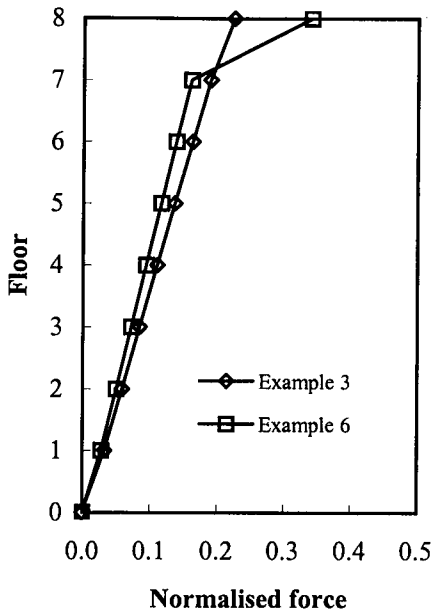

(a) Lateral force profile

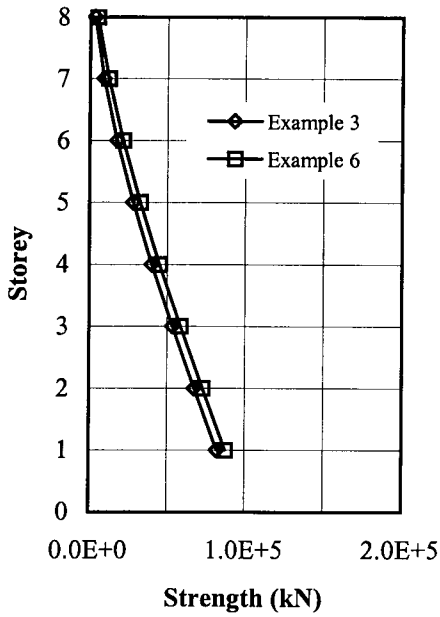

(b) Cumulative storey strength

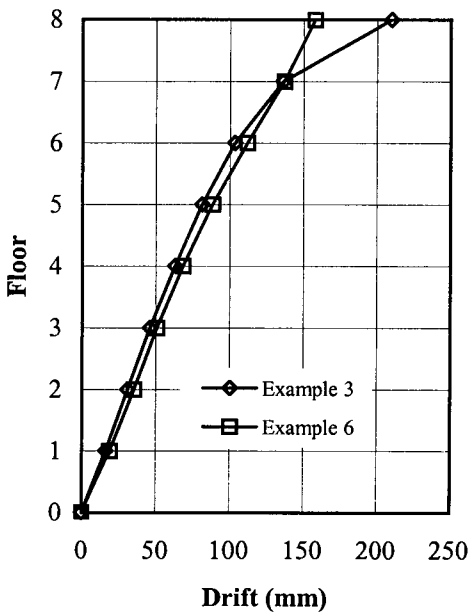

(c) Floor drift

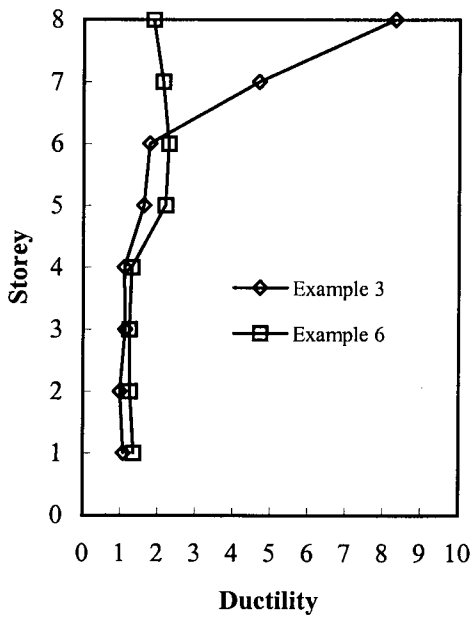

(d) Ductility demand

Figure 9.12 Comparison of results, example 3 vs. example 6

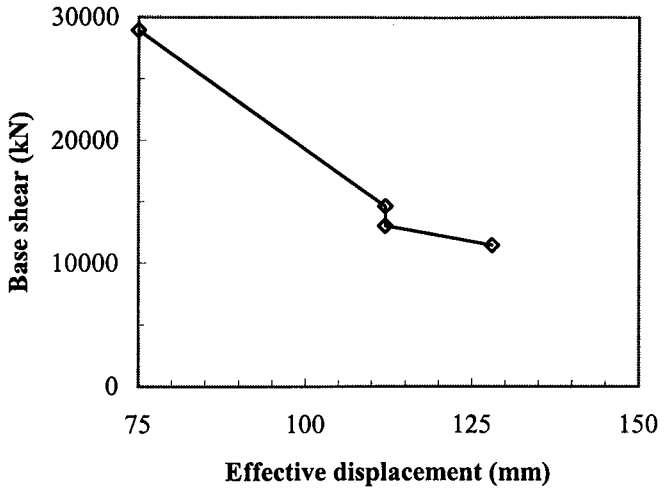

Figure 9.13 Reduction in base shear with effective displacement

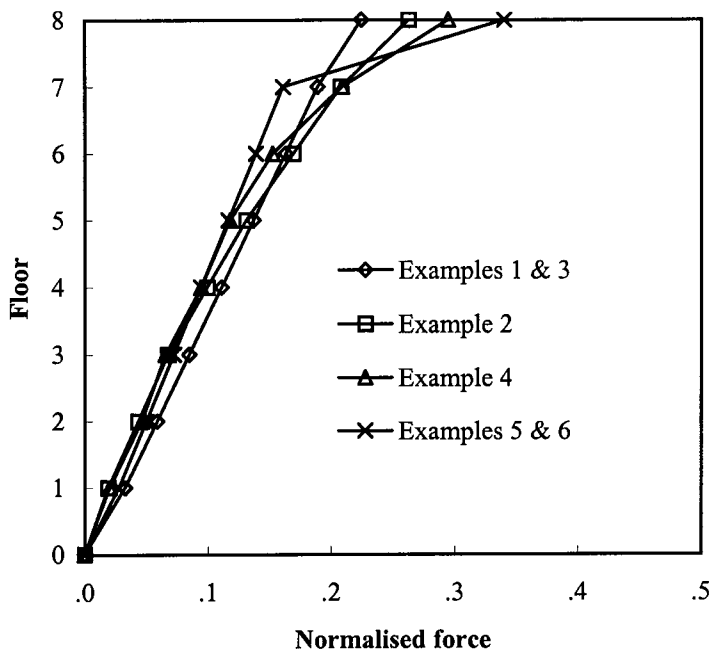

Figure 9.14 Static lateral force profiles

10. EVALUATION OF THE DISPLACEMENT-BASED SEISMIC DESIGN METHOD - II

10.1 Introduction

The displacement-based seismic design method is applied to the design of a two-storey building located in Vancouver, BC (zone 4). The methodology used for evaluation of the design procedure is similar to that in Chapter 9. The design process adopted here differs from that of Chapter 9 as follows: (a) the design is carried out with the displacement response spectrum derived from the NBCC acceleration response spectrum, (b) industry standard sections are used for the columns, beams, and braces of the concentrically braced frame (CBF), (c) column shortening and the P-Δ effect are considered in design and analysis, and (d) in the nonlinear dynamic time history analyses, the hysteresis model developed by Jain *et al.* (1980) is used for the braces.

Two design examples, with an assumed linear displaced shape in both, are considered. The first example attempts to obtain an elastic response in both storeys of the building and the second example investigates inelastic response. The structural design and the dynamic response of the CBF in the second example are compared with those obtained from the spectral acceleration-based approach.

An equivalent nonlinear single degree of freedom (SDOF) model is also developed to estimate the seismic response of the CBF. This model is suitable for parametric studies on low-rise CBFs designed by this method.

10.2 Displacement response spectrum for design

Figure 10.1 shows the displacement response spectrum (DRS) obtained from [2.5] by converting the NBCC (ACNBC 1995a) elastic design acceleration spectrum for Vancouver. The latter is the product of the zonal velocity ratio, v (equal to 0.20), and the S factor curve for Z_a equal to Z_v, shown in Fig. 2.2. Also shown in Fig. 10.1 are the 5% damped mean + 1 sigma ($\mu + 1\ \sigma$) DRS and the mean DRS for the 20 accelerograms selected for zone 4 in Tables 4.7 and 4.8. The $\mu + 1\ \sigma$ DRS of the accelerograms agrees well with the NBCC DRS for the range of periods shown in Fig. 10.1. Thus, the response

from time history dynamic analyses is evaluated at the $\mu + 1\ \sigma$ level and the NBCC DRS is used for design.

10.3 Description of the building

The two-storey building shown in Fig. 7.1 is used here. The description of the building and the specified loads are given in sections 7.2 and 7.3.

10.4 Design of the building

In this work, only the CBFs along the North-South direction are designed. Accidental torsion is neglected for simplicity but could be included in design. Only the braces are assumed to provide lateral stiffness and strength to the CBF and the contributions of the exterior cladding and interior partitions are ignored. For both design and analysis, the columns are assumed to be in single storey lifts although in an actual structure two storey lifts would likely be used.

At the start of the design process, the known quantities are the approximate weight at the roof and the floor, given in Table 7.1, and the geometry and material properties of the CBF. Columns and beams are assumed to be of grade 300W steel with a yield strength of 300 MPa, while the braces are assumed to be of grade 350W steel with a yield strength of 350 MPa. The braces in the first storey have a length of 6155 mm while those in the second storey have a length of 5955 mm. From geometry of the CBF shown in Fig. 7.1, the storey drift required to yield the brace is

$$[10.1] \qquad \Delta = \frac{\Delta_Y}{\cos\theta} = \frac{F_Y L_b}{E \cos\theta}$$

where Δ_Y is the yield elongation of the brace, L_b is the brace length, F_Y is the yield stress (equal to 350 MPa), E is the elastic modulus, and θ is the angle of inclination of the brace with the horizontal. Equation [10.1] gives a storey drift of 14.7 mm to yield the braces in the first storey and 13.8 mm for the second storey.

10.5 Example 1

In this example, the initial displaced shape is assumed wherein the braces at both storeys just reach the yield level. The brace ductility is defined as the maximum

extension of the brace divided by the yield elongation. The storey drifts required to yield the braces are added together to give the desired displaced shape. The design procedure for a MDOF system outlined in section 8.7, is implemented as shown in Table 10.1. The effective displacement of the SDOF system, δ_{eff}, from [8.19] is 20 mm and the effective mass, m_{eff}, from [8.16] is 1.55 kN s^2/mm. The latter is about 90% of the effective seismic mass. The effective damping, ξ_{eff}, is assumed to be 5% of critical. From the NBCC DRS in Fig. 10.1, an effective period, T_{eff}, of 0.40 s is obtained corresponding to the effective displacement, δ_{eff}. The effective stiffness, K_{eff}, from [8.3] is 382 kN/mm, and the base shear, V_b, from [8.20] is 7640 kN. The static lateral force at each floor level is obtained from [8.17]. An approximate P-Δ analysis is carried out as explained in section 9.8. The revised static lateral force and the force profile are given in Table 10.1. Each CBF is designed for one half of the static lateral force, F_i.

10.5.1 Structural design

A two-dimensional model is used for design of the CBF, as described in section 7.3 and shown in Fig. 7.2. The compression brace in each storey is designed to resist at least 30% of the storey shear force. The capacity design approach is used to determine an appropriate compressive force for design of the floor beam and the central column from equations [7.2] and [7.3], respectively, and thus restrict inelastic action to the braces. A similar check is performed for the exterior columns of the CBF. The members selected are given in Table 10.2.

10.5.2 Structural models and assumptions

A two-dimensional, multi-degree of freedom model of the CBF is used for free vibration analysis, nonlinear static analysis, and nonlinear dynamic time history analyses. The model is similar to the MDOFN model described in section 7.7 and shown in Fig. 7.7. Partitions are neglected in this study. The flexibility of the roof diaphragm is neglected, as described in section 7.7. The strength of the roof diaphragm is also ignored and the rigid-plastic links that connect the roof and floor masses to the CBF are assumed to be strong enough to transfer whatever inertia forces are developed at the masses.

10.5.3 Structural analyses

A free vibration analysis gives periods of 0.38 s and 0.23 s for the first and second mode, respectively. The analysis assumes that both the tension and compression brace are effective in each storey. When column shortening is neglected, the periods of the first and second modes are 0.37 s and 0.21 s, respectively, indicating that column shortening has no significant influence on the dynamic behaviour of this low-rise CBF.

Nonlinear static analysis of the CBF under the prescribed lateral force gives a drift of 13.2 mm at the floor and 25.5 mm at the roof level. These drifts are compared with the assumed displaced shape in Fig. 10.2(a).

Nonlinear dynamic time history analyses are performed with the accelerograms given in Tables 4.7 and 4.8. Braces of the CBF are modelled with the EL9 element of DRAIN-2D (Jain *et al.* 1980). The following information is obtained from each analysis: (a) peak drift attained at the roof and the floor, and (b) peak brace ductility demand in tension at each storey. As discussed in section 10.2, the $\mu + 1\,\sigma$ value of the above peak responses is compared with the assumed value. Figure 10.2(a) shows the floor drifts from the dynamic analysis and compares them with the assumed drifts. Figure 10.2(b) compares the brace ductility demands from dynamic analysis with those assumed in Table 10.1.

10.5.4 Conclusions from example 1

The displacement-based design approach works reasonably well for this realistic design example. An elastic response is anticipated as the braces are assumed to extend just up to yield. The response obtained from dynamic analyses is largely so with the drifts and the brace ductility demands marginally greater than the assumed values. This would be expected because, at the fundamental period of 0.38 s, the $\mu + 1\,\sigma$ DRS of the accelerograms in Fig. 10.1 has a greater spectral ordinate as compared to the NBCC DRS which was used for design.

10.6 Example 2

In this example, the CBF is designed to respond inelastically by assuming an initial displaced shape wherein the braces at both storeys extend to $2.0\,\Delta_Y$. Table 10.3

gives the relevant design parameters. The effective displacement from [8.19] is 40 mm, the effective mass from [8.16] is 1.55 kN s^2/mm, the effective period, T_{eff}, from the NBCC DRS in Fig. 10.1 is 0.66 s for the target displacement of 40 mm, the effective stiffness from [8.3] is 140 kN/mm, and the base shear from [8.20] is 5600 kN. The effective mass and the static lateral force profile are the same as in example 1 because of an identical displaced profile for both examples. The members selected for this CBF are given in Table 10.4.

10.6.1 Structural analyses

A free vibration analysis gives periods of 0.44 s and 0.26 s for the first and second mode, respectively. The period of the first mode is less than the effective period of 0.66 s because the former is based on the initial elastic stiffness of the CBF while the latter is based on the lesser secant stiffness corresponding to the assumed spectral displacement of 40 mm.

A linear static analysis of the CBF under the prescribed lateral force in Table 10.3 gives drifts of 13.4 mm and 22.2 mm at the floor and roof, respectively. A static pushover analysis with the lateral force profile in Table 10.3 suggests that the ductility demand is localised at the braces in storey 1 with those in storey 2 remaining elastic. The drifts from the above analyses are compared with the assumed drift in Fig. 10.3(a).

The drifts and brace ductility demands from nonlinear dynamic time history analyses are shown in Figs. 10.3(a) and 10.3(b), respectively. The drift of the floor and the brace ductility demand at storey 1 are in reasonable agreement with the assumed values. However, the response of the braces in storey 2 is predominantly elastic and both the interstorey drift and the ductility demand are significantly less than the assumed value.

10.6.2 Conclusions from example 2

In this example, the assumed displaced shape implies a ductility demand of 2.0 in the braces at both storeys. The effective displacement is (2 times) greater than that in example 1 and consequently the design base shear reduces from 7640 kN to 5600 kN.

The brace ductility demand in storey 1 increases from that in example 1 while it reduces in storey 2.

The structural design and the dynamic response of example 2 may be compared with that obtained by the spectral acceleration-based approach in Chapter 7, wherein the same building was designed at Vancouver (zone 4) with a force modification factor, R, of 1.5. Table 10.5 compares the design and response of the CBF by the two design approaches. The methods prescribe different base shears for the CBF. The acceleration-based design method uses an assumed period, an assumed R value of 1.5, and incorporates the calibration factor, U (equal to 0.6). None of these impinge on the base shear used in the displacement-based method. The structural design is almost the same with differences only in the brace section used in storey 1 and the column sections. Apart from the difference between the force modification factor, R, which could be considered related to the ductility demand, it is considered that the difference in the brace size arises because the acceleration-based design assumes tension-only bracing whereas the displacement-based design assumes tension-compression bracing.

The dynamic response of the spectral acceleration-based design reported in Table 10.5 is the average of the $\mu + 1\ \sigma$ response of the A-set and the V-set for the case with partitions absent in Table 7.12. The displacement-based design gives a smaller roof drift even though some members of the CBF are smaller. The ductility demand is localised in storey 1. This greater ductility demand for the displacement-based design is associated with the smaller brace provided (HSS 254x254x8 vs. HSS 254x254x10). As well, the exterior column provided is smaller.

10.7 Studies with an equivalent SDOF model

An equivalent nonlinear SDOF model is developed to substitute for the MDOF model of the two-storey CBF in nonlinear dynamic time history analysis. The equivalent SDOF model is suitable for parametric studies to investigate the inelastic seismic response of low-rise CBFs designed by the displacement-based method.

10.7.1 Development of the SDOF model

The conceptual development of this model requires an investigation of the force-deformation behaviour of a single-storey, single-bay CBF, as shown in Fig. 10.4(a). Let Δ_Y be the brace elongation at yield and let Δ_1 be the corresponding lateral drift at the roof level. If the geometry and the material properties are assumed constant, both Δ_Y and Δ_1 are also constant and are independent of the area of cross-section of the brace (and hence independent of the base shear). Consider the design of this CBF with the displacement-based method for three values of effective displacement, δ_{eff}, equal to Δ_1, $2\,\Delta_1$, and $3\,\Delta_1$. Figure 10.4(b) shows the force-deformation relationship for the resulting SDOF systems. Let T_1, T_2, and T_3 be the effective periods (T_{eff}), K_1, K_2, and K_3 be the effective stiffnesses (secant stiffness, K_{eff}), and F_1, F_2, and F_3 be the design base shears corresponding to the assumed effective displacements Δ_1, $2\,\Delta_1$, and $3\,\Delta_1$, respectively. The stiffnesses K_{1e}, K_{2e}, and K_{3e} represent the initial elastic stiffness up to the yield deformation, Δ_1. Let T_{1e}, T_{2e}, and T_{3e} be the periods of the SDOF system corresponding to these initial elastic stiffnesses.

Consider the SDOF system with the base shear capacity of F_1. The initial elastic stiffness, K_{1e}, is equal to the secant stiffness, K_1, because the effective displacement, δ_{eff}, is assumed equal to the yield displacement, Δ_1. Thus the period T_{1e} is equal to T_1.

For the design in example 1, the braces in both storeys are assumed to extend up to yield. The effective displacement, δ_{eff}, of 20 mm may be considered analogous to the yield displacement, Δ_1. The periods T_{1e} and T_1 are both equal to 0.40 s. The period of the first mode of the MDOF model in example 1 is 0.38 s.

Now consider the SDOF system with the base shear capacity of F_2, as shown in Fig. 10.4(c). The initial elastic stiffness, K_{2e}, is given by

$$[10.2] \qquad K_{2e} = K_2 \frac{\delta_e}{\Delta_1}$$

As stiffness is inversely proportional to the square of the period, the initial elastic period, T_{2e}, is related to the effective period, T_2, by

[10.3] $$T_{2e} = T_2 \sqrt{\frac{\Delta_1}{\delta_e}}$$

In example 2, the effective displacement, δ_{eff}, is assumed equal to 2 Δ_1 (40 mm) and the effective period, T_2, from the NBCC DRS in Fig. 10.1 is 0.66 s. Equation [10.3] gives the period T_{2e} as 0.47 s. The period of the first mode of the MDOF model in example 2 is 0.44 s.

Because the period of the SDOF system is equal to the period of the first mode of the MDOF model, the former may be used instead of the latter in time history dynamic analysis to obtain the seismic response of the two-storey CBF. The yield deformation of the SDOF system is taken equal to the effective displacement of the profile wherein the braces at both storeys are assumed to extend up to yield (that is, a ductility of 1.0). The mass of the SDOF system is assumed equal to the effective mass of the MDOF system, m_{eff}. The base shear capacity and the initial elastic period of both systems are the same.

10.7.2 Response with the SDOF model

Two SDOF models are developed corresponding to the displaced shapes investigated in examples 1 and 2. Each model has a mass of 1.55 kN s^2/mm and a yield displacement of 20 mm (δ_{eff} in example 1). The base shear capacity is equal to that of the corresponding CBF, namely, 7710 kN and 5740 kN from Tables 10.1 and 10.3, respectively. The inelastic seismic response of the SDOF model to the accelerograms for zone 4 is obtained with the computer program NONSPEC (Mahin and Lin 1983). Elasto-plastic hysteresis behaviour is assumed with no strain-hardening. The dynamic analyses are carried out with a time step of 0.001 s.

The equivalent SDOF model gives ductility demands of 1.16 and 1.39 at the $\mu + 1\ \sigma$ level of response for examples 1 and 2, respectively. These ductility demands are marginally less than the demand of 1.21 and 1.63 obtained at storey 1 with the MDOF model. Hence, the equivalent SDOF model may be used to estimate the ductility demand in low-rise CBFs.

10.8 Conclusions

The displacement-based seismic design method has been applied to the design of a two-storey CBF located in Vancouver, BC. Based on the design examples considered in this study, the following conclusions are drawn:

(a) This study shows how a displacement response spectrum may be specified in the NBCC and used for design purposes.

(b) The target drifts and brace ductility demands are marginally exceeded in example 1 while they are within the assumed values in example 2. The method controls the deformation demand on the system reasonably well.

(c) A comparison of the structural designs by the acceleration-based and the displacement-based design methods shows minor differences in the members provided. A comparison of the dynamic response of the designs does not show any major differences. Hence, the displacement-based design method is a viable alternative.

(d) The equivalent nonlinear SDOF model developed may be used to carry out parametric studies on low-rise CBFs and calibrate the displacement-based design procedure.

Table 10.1 Design parameters for example 1

Storey #	Storey height (m)	Height to floor H (m)	Weight W (kN)	Storey drift for brace yield δy_i (mm)	Assumed brace ductility demand	Assumed displaced shape δ_i (mm)	$m_i \delta_i$ (kN s^2)	$m_i \delta_i^2$ (kN s^2 mm)	Assumed displaced profile c_i	$m_i c_i$ (kN s^2/mm)	Static lateral force (kN)	Static lateral force (incl. P-Δ) F_i (kN)	Static lateral force profile F_i/V_b
2	3.9	8.1	4069	13.8	1.0	28.5	11.83	338	1.43	0.59	2903	2918	0.38
1	4.2	4.2	12767	14.7	1.0	14.7	19.18	283	0.74	0.96	4737	4791	0.62
Σ			16836				31	620		1.55	7640	7709	1.00

Notes 1. $m_{eff} = \Sigma m_i c_i = 1.55$ kN s^2/mm 2. $\delta_{eff} = \Sigma m_i \delta_i^2 / \Sigma m_i \delta_i = 620 / 31 = 20$ mm

Table 10.2 Members selected for CBF in example 1

Columns	Exterior column	W200x86
	Central column	W200x59
Beams	Floor beam	W610x84
	Roof beam	W530x82
Braces	Storey 1	HSS 254x254x11
	Storey 2	HSS 152x152x8

Table 10.3 Design parameters for example 2

Storey #	Storey height (m)	Height to floor H (m)	Weight W (kN)	Storey drift for brace yield δy_i (mm)	Assumed brace ductility demand	Assumed displaced shape δ_i (mm)	$m_i \delta_i$ (kN s^2)	$m_i \delta_i^2$ (kN s^2 mm)	Assumed displaced profile c_i	$m_i c_i$ (kN s^2/mm)	Static lateral force (kN)	Static lateral force (incl. P-Δ) F_i (kN)	Static lateral force profile F_i/V_b
2	3.9	8.1	4069	13.8	2.0	57.1	23.66	1350	1.43	0.59	2128	2157	0.38
1	4.2	4.2	12767	14.7	2.0	29.5	38.35	1130	0.74	0.96	3472	3584	0.62
Σ			16836				62	2480		1.55	5600	5741	1.00

Notes 1. $m_{eff} = \Sigma m_i c_i = 1.55$ kN s^2/mm 2. $\delta_{eff} = \Sigma m_i \delta_i^2 / \Sigma m_i \delta_i = 2480 / 62 = 40$ mm

Table 10.4 Members selected for CBF in example 2

Columns	Exterior column	W250x67
	Central column	W200x52
Beams	Floor beam	W610x84
	Roof beam	W530x82
Braces	Storey 1	HSS 254x254x8
	Storey 2	HSS 178x178x5

Table 10.5 Comparison of CBF design and response for Vancouver (zone 4)

Parameter	Design method	
	Acceleration-based	Displacement-based
Base shear for building (kN)	3233	5600
CBF design		
factored base shear (kN)	1953	2871
lateral force at floor (kN)	1225	1792
lateral force at roof (kN)	728	1079
Brace section provided		
storey-1	HSS 254x254x10	HSS 254x254x8
storey-2	HSS 178x178x5	HSS 178x178x5
Column section provided		
exterior column	W610x84	W250x67
central column	W250x73	W200x52
Beam section provided		
floor beam	W610x84	W610x84
roof beam	W530x82	W530x82
Period (T-C bracing)		
Mode 1 (s)	0.41	0.44
Mode 2 (s)	0.22	0.26
$\mu + 1\,\sigma$ roof drift (mm)	41	35
Brace ductility demand		
storey-1	1.09	1.63
storey-2	0.97	0.69

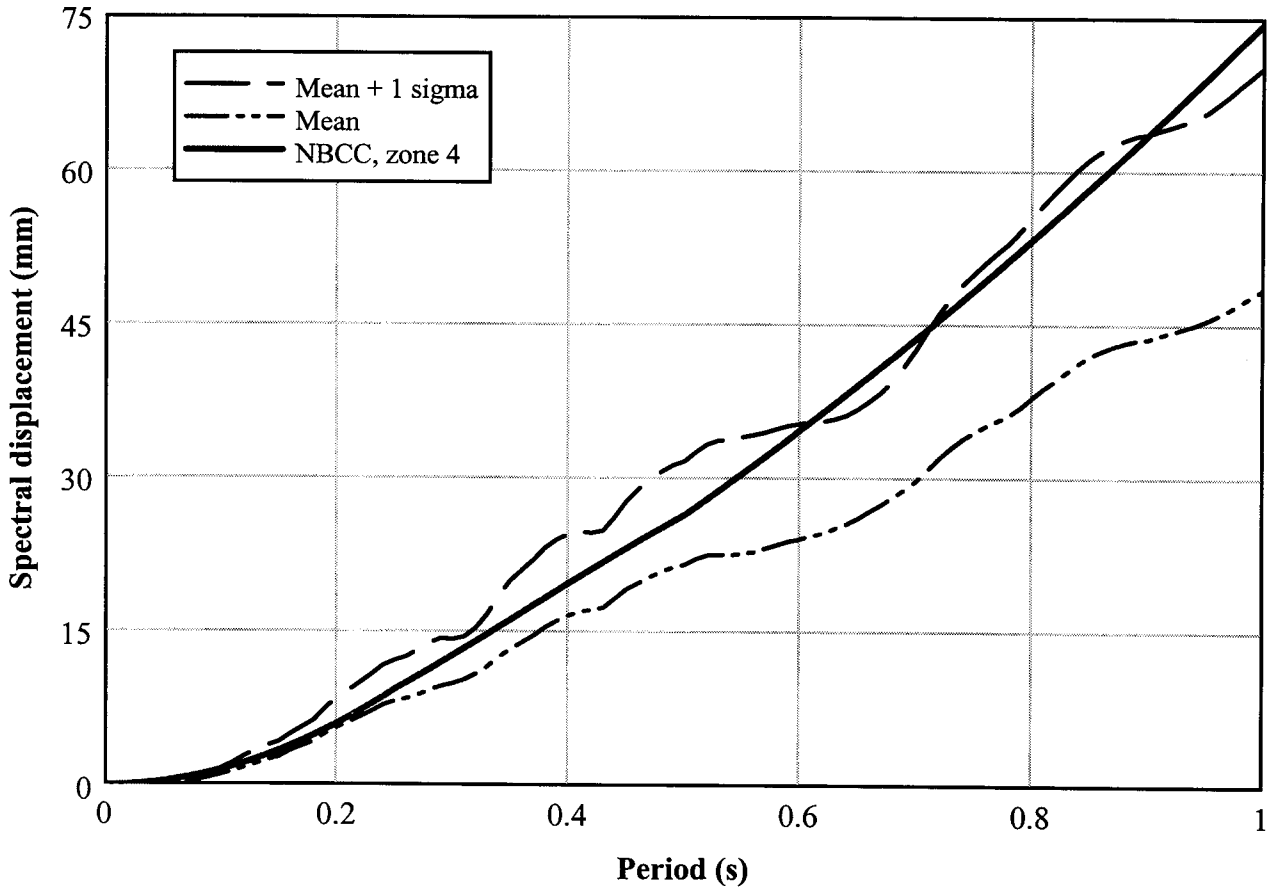

Figure 10.1 Displacement response spectra for zone 4

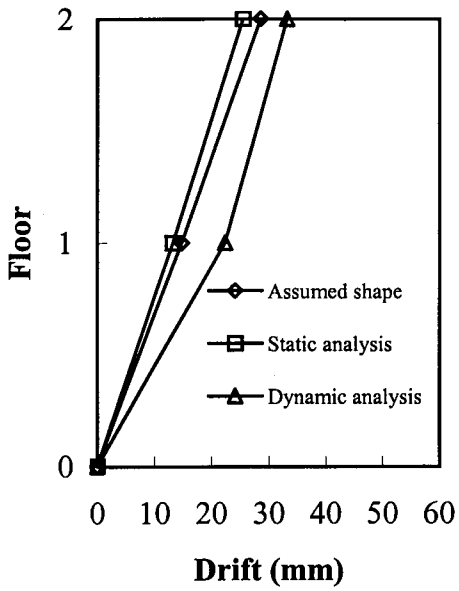

(a) Floor drift

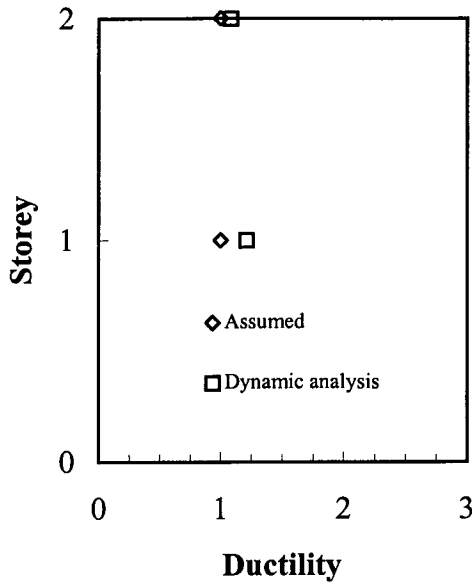

(b) Brace ductility demand

Fig. 10.2 Results for example 1

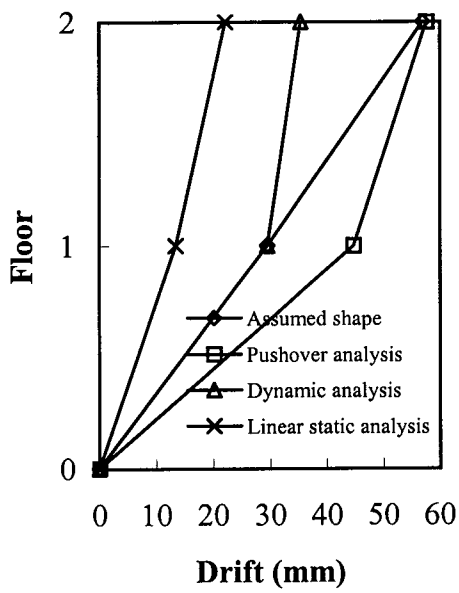

(a) Floor drift

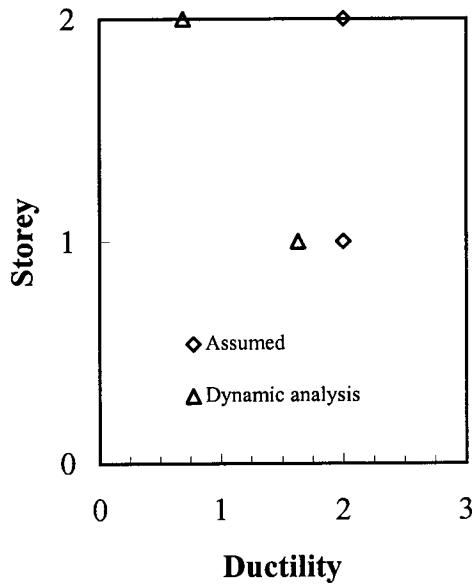

(b) Brace ductility demand

Fig. 10.3 Results for example 2

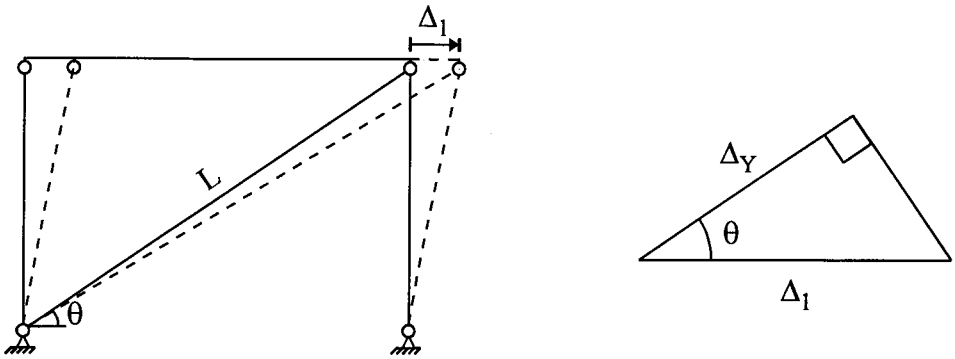

(a) Single-storey CBF and geometry of brace deformation

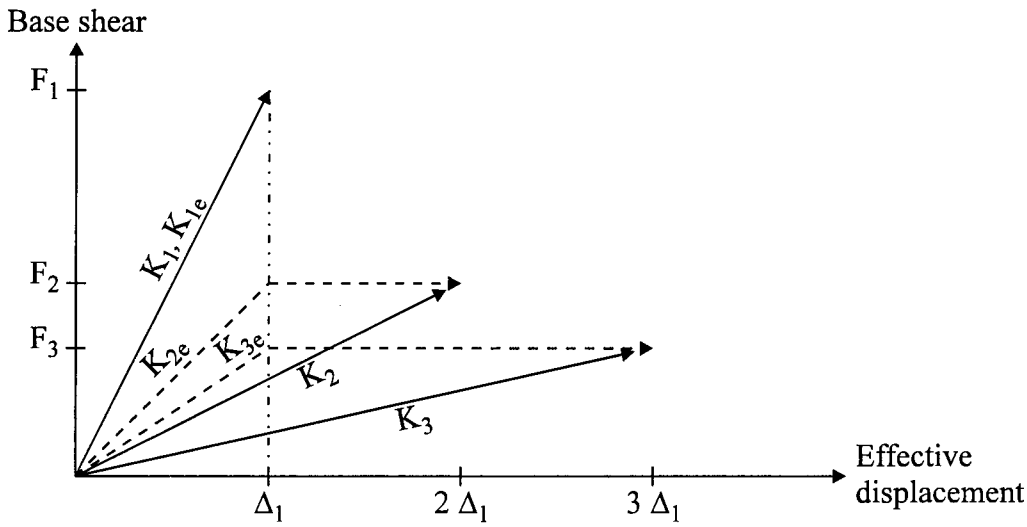

(b) Force-deformation response of SDOF systems

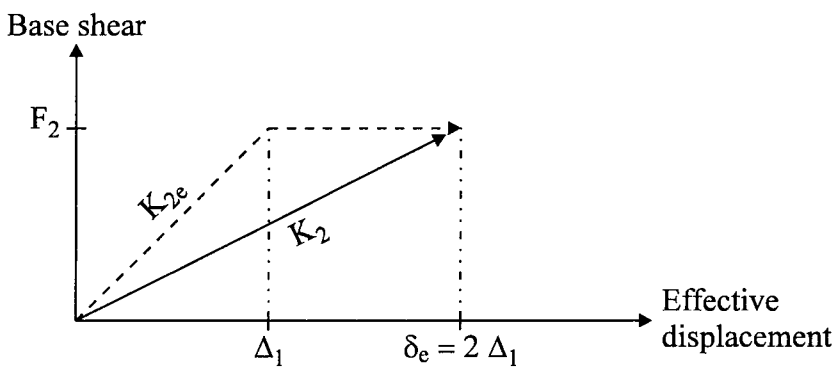

(c) Derivation of initial elastic stiffness

Fig. 10.4 Equivalent SDOF model

11. SUMMARY and CONCLUSIONS

11.1 Summary

This work consists of two distinct studies. The first study involves the seismic evaluation of single-storey and two-storey steel buildings with concentrically braced frames (CBFs) designed in accordance with the provisions of the NBCC (ACNBC 1995a) and CSA Standard S16.1-94 (CSA 1994). The systematic method of seismic rehabilitation of buildings recommended by the ATC (1995) is adapted for seismic evaluation. Criteria are developed for specification of design ground motion. A database consisting of 100 earthquake accelerograms is established for dynamic analyses. Response spectra of the accelerograms are developed and compatibility with the NBCC design spectrum is assessed to determine response levels for evaluating the results of dynamic analyses. Models for earthquake response analyses of the buildings are developed based on a review of literature on the behaviour of CBFs, steel diaphragms, non-structural elements, and from observations on the dynamic behaviour of an existing single-storey building in an ambient vibration test. The buildings are designed and analysed for five seismic zones in Western Canada with seismicities ranging from low to high. All the analytical procedures recommended by the ATC (1995) and FEMA (1994) are used to estimate the seismic response of the buildings. Based on these studies, general conclusions and recommendations for seismic design of CBFs are presented in the following section.

The second study reviews a seismic design method based on specifying limiting displacements rather than forces. This method is evaluated by applying it to the design of an 8-storey and a 2-storey building with CBFs and is verified by extensive nonlinear dynamic time history analyses. It is compared, both qualitatively and quantitatively, with the spectral acceleration-based design method currently used by seismic codes and is shown to be a viable alternative for the seismic design of steel buildings.

11.2 Conclusions from studies on low-rise steel buildings with CBFs

Specific conclusions related to several aspects of the seismic design and response of low-rise steel buildings with CBFs are first presented. Based on these conclusions, a

design strategy is proposed which considers seismic zoning, the importance of the structure, acceptable damage levels, and methods of analysis and design.

11.2.1 Period estimate for design

(a) The fundamental period, computed analytically, of all buildings in this study was significantly greater than the NBCC estimate given by [2.10]. The latter is the metric equivalent of the expression proposed by Anderson *et al.* (1952)

$$[11.1] \qquad T = \frac{0.05\,H}{\sqrt{b}}$$

where H is the height and b is the width of the building in feet. Anderson *et al.* (1952) state that this expression was calibrated against period measurements on a large number of buildings and was intentionally made to give periods that were smaller than the measured ones so as to result in conservative designs. A similar approach is still recommended by FEMA (1994). Equation [11.1] does not account for the seismic zone. Hence, with the same geometry of the CBF, the NBCC estimate results in the same design period for all seismic zones and appears to be inappropriate.

(b) In accordance with the NBCC provision, a base shear of 0.80 of the value prescribed in [2.8] with the period estimate from [2.10], was used for all buildings in this study.

(c) The NBCC estimate does not reflect the dynamic behaviour of single-storey steel buildings with a flexible roof diaphragm. Such behaviour governs the seismic response. A similar observation was made by Tremblay and Stiemer (1996).

(d) The closed form analytical expressions developed here (Appendix E) account for all significant characteristics of buildings with flexible roof diaphragms, but should be verified by field measurements.

(e) Cladding and built-up roofing characteristically exhibit marked nonlinear behaviour and at higher amplitudes of vibration, even though the damage level may still be acceptable, have much reduced contribution to the stiffness. However in ambient vibration tests, where the amplitude of vibration is relatively small, these elements contribute significantly to the lateral stiffness of the building as is reflected in relatively short measured periods. Therefore, ambient vibration tests may underestimate

considerably the period of vibration of buildings that should be used for design. Forced vibration tests with larger amplitude of vibration are considered more suitable for this purpose.

(f) For buildings with two or more storeys, the flexibility of the roof diaphragm has little influence on the fundamental period because the percentage of effective seismic mass on the roof decreases with increasing number of storeys.

(g) The stiffness contribution from non-structural elements can reduce the period of buildings significantly, particularly in low seismic zones.

11.2.2 Distribution of lateral force

(a) The NBCC recommends that the greater of the force from [2.11] and [2.12] be used for the design of floors and roofs acting as diaphragms. Equation [2.11] governed for all diaphragms in this study.

(b) A nonlinear variation of maximum shear force along the span of the diaphragm was obtained from response spectrum analysis and from dynamic time history analyses, whereas a linear distribution is usually assumed in design. Hence, the lateral force distribution recommended by the ATC (1995), even though shown to be slightly unconservative, may be used for design. This distribution is parabolic with an ordinate of 1.5 V/L at mid-span of the diaphragm, where V is the lateral force and L is the span of the diaphragm.

(c) For the two-storey building, the roof diaphragm flexibility did not influence the first mode significantly and the distribution of lateral force over the building height by [2.11] was appropriate. This force distribution will also be appropriate for regular buildings more than two-storeys high.

11.2.3 Design of brace members

(a) For the single-storey building with a flexible roof diaphragm, the maximum brace ductility demand in tension of 2.0 was obtained for the strong diaphragm-weak frame (SD-WF) design in zone 5 wherein the roof diaphragm response was elastic. Tremblay and Stiemer (1996) have reported significantly greater values for such buildings.

For the two-storey building, the maximum brace ductility demand was limited to 1.6 in seismic zones 1 to 4. In zone 5, the maximum demand was 1.6 in the first storey and 4.1 in the second storey. Hence, with the exception of the latter, the brace ductility demands are reasonable and satisfy the criterion of not exceeding the force modification factor, R, used in design. For the case with partitions absent in zone 5, current design procedures do not address this issue.

(b) Because the braces for both the single-storey and the two-storey buildings designed as strength braced frames (SBFs) did not in general meet the stringent slenderness ratio and width-thickness ratio requirements for ductile braced frames (DBFs), then attempting to design these frames as DBFs would only result in considerably greater overstrengths arising from the theoretically lesser demand based on the increased R value for the DBFs and the increased strength to meet the limitations.

(c) Class 1 HSS sections were used throughout this study because of their relative efficiency in axial compression. Symmetric open sections such as channels, double angles back-to-back, and W shapes are also used extensively in practice. The HERA (Feeney and Clifton 1995) even allows the use of round steel bars as brace members for CBFs not exceeding two storeys in height.

(d) In seismic zones 1 and 2, the compressive resistance of the braces is rather low. Hence, the assumption of tension-only concentrically braced frames is appropriate. However, in zones 3 and higher, the use of such a frame results in braces that have significant compressive resistance, which should be considered explicitly in design.

(e) Overstrength in the braces, as discussed more fully subsequently, should be avoided because it affects the design of the brace connections, beams, and columns of the CBF. Larger braces would require the remaining components to be proportionately large in size to ensure that the braces are the 'weak link' in the lateral load path and yield prior to the other elements.

(f) The maximum effective slenderness ratio, KL/r, is limited to 300 for tension members by CSA Standard S16.1-94 (CSA 1994). This constraint affected the brace selection in seismic zone 1 only.

11.2.4 Design of connections

Connection failure is the most common cause of poor seismic performance of CBFs. Brace members are designed to have greater capacity in tension and compression than required by the analysis with factored loads. This affects the connection design. The strength, stiffness, and ductility of CBFs cannot be relied upon if the connections fail prematurely because they have been designed for the factored loads and not the brace capacities which may be developed under seismic action. This behaviour is in contrast to that under other loadings which do not depend on the members provided.

(a) Brace yielding was observed in the single-storey and the two-storey buildings. Therefore the connections should develop the tensile resistance of the brace, preferably in all seismic zones, unless inelastic action in other elements in the LLRS that limits the brace force is deemed to provide satisfactory behaviour. Similarly, the force in the brace may be limited by lack of anchorage at the base of the CBF. This proposition will not be expensive if the braces are selected appropriately (overstrength is minimised). Brace cross-sectional areas provided in this study were within 11% of the design requirement, except in zone 1 wherein the brace slenderness constraint governed. The compressive resistance of the braces, if overlooked, may lead to buckling of the gusset plates. For the CBFs studied, the brace compressive capacity was low in seismic zones 1 and 2 and was significantly greater in zones 3 and higher. Hence, the connections should also develop the compressive resistance of the braces in all seismic zones.

(b) Brace connections should allow for rotation at the ends of the brace member that occurs when the brace buckles in compression.

11.2.5 Design of beams and columns

CSA Standard S16.1-94 (CSA 1994) requires columns and beams in DBFs (designed with a R factor of 3.0) to resist redistributed loads due to brace buckling or yielding. Such requirements are not specified for nominally ductile braced frames (NDBFs) and SBFs that are designed with R equal to 2.0 and 1.5, respectively. The traditional design approach for NDBFs and SBFs does not consider the actual strength of the bracing. This study has shown that inelastic response could occur in the beams and columns of such frames in zones 3 and higher. In a severe earthquake, the force applied

on the CBF connections, beams, and columns is limited by the actual strength of the bracing. Hence, capacity design checks for beams and columns, similar to those currently used for DBFs, are recommended for NDBFs and SBFs in seismic zones 3 and higher.

11.2.6 Design of diaphragms

For the single-storey and the two-storey building, there was extensive inelastic response in the roof diaphragm in seismic zones 4 and 5. The response in zone 1 was always elastic while some inelastic action was observed in zones 2 and 3. Whether inelastic action in the roof diaphragm is considered to be unsatisfactory or not is circumscribed because of a lack of experimental observations on the damage that such diaphragm assemblies can sustain during severe ground motion and on the possible remedial measures that could be undertaken. Two alternatives were explored to avoid damage to the roof diaphragm. The first alternative, use of the capacity design approach, was shown to be economically feasible for CBFs designed with a force modification factor, R, of 1.5 and 2.0. This requires provision of a strong diaphragm-weak frame design where the diaphragm has greater shear capacity than the CBF. The other alternative is to provide a ductile shear link between the diaphragm and the CBF with a yield capacity that is smaller than that of the diaphragm and the CBF so that inelastic action will concentrate at this 'weak link.' Both alternatives need to be verified by experimental investigations.

11.2.7 Design of non-structural components

(a) Non-structural components contribute significant stiffness and strength to low-rise buildings, particularly in seismic zones 1 and 2 where the lateral loads are low.

(b) In seismic zones 1 and 2, the stiffness and strength contributions of the cladding and the interior partitions, assuming that they will not be altered, could be added to that provided by the lateral load resisting system (LLRS) to affect economy in design. While these contributions could also be considered in zones 3 and higher, the designer must be willing to accept loss of such components during severe ground shaking.

(c) Non-structural elements in the plane of the vertical bracing are likely to be protected from damage because of the relatively high in-plane stiffness of the CBFs. The strength

and stiffness of such elements should be included in the analyses. They tend to share the lateral load with the CBFs and consequently the brace ductility demands are reduced in the event of inelastic response.

(d) Non-structural elements that are not in the plane of the vertical bracing should preferably be isolated from the roof or floor above so as to prevent them from being damaged by the interstorey drift. A review of literature on gypsum wallboard partitions suggests that an interstorey drift of 0.25% was adequate to initiate yield while a drift of 0.75% often caused complete failure.

11.2.8 Anticipated deformations of the structure

(a) The maximum interstorey drift in most of the buildings studied was well within the 1% limit recommended for CBFs by the ATC (1995) and the 2% limit of the NBCC. Only a few buildings with severe inelastic response exceeded these drift limits in seismic zone 5.

(b) The 2% drift limit of the NBCC is excessive for CBFs. The interstorey drift required to yield the braces in any storey is a function of the geometry of the CBF and its material properties (E, F_Y) only. A more meaningful estimate may be obtained by multiplying this yield deformation with the R factor assumed in design. Furthermore, most non-structural partitions will fail completely at drifts exceeding 1%.

(c) The NBCC recommends that the deformation of the structure obtained from a linear elastic analysis be amplified by the force modification factor, R, to obtain the anticipated inelastic deformation of the structure in the design earthquake. This approach was found to give reasonable estimates for the SBFs investigated in this study and is recommended in the absence of a better alternative.

11.2.9 Use of various analytical procedures in seismic design

(a) In the NBCC, a linear elastic structural analysis is considered adequate for seismic design by the equivalent static lateral force procedure. Member selection depends on the forces in the individual members only and the relative strength of members in the lateral load path is often neglected. This method is considered adequate in seismic zones 1 and 2 only. In zones 3 and higher, a hierarchy in the provision of strength to

elements along the lateral load path and checks to ensure that the weakest element has a ductile failure mode are essential to give an effective design by this procedure.

(b) A nonlinear static (pushover) analysis helps to determine the possible force and deformation demands on the elements of the LLRS when it is subjected to large deformations that might occur in the design earthquake. The distribution of lateral force to apply on the structure may be obtained from a response spectrum analysis. For large statically indeterminate structures, this analysis is the only alternative short of a nonlinear dynamic time history analysis. Its use should be encouraged in practical seismic design.

11.2.10 Overstrength in the LLRS

The buildings designed had greater lateral load capacity than the NBCC prescribed base shear. For the single-storey building, the ratio of the CBF strength to the prescribed base shear ranged from 1.3 to 2.8. Similarly, for the two-storey building, this ratio ranged from 1.6 to 2.4 for the first storey and from 1.5 to 3.7 for the second storey. Reasons for this overstrength are: (i) discrete size of the brace members, (ii) use of a resistance factor for calculation of member resistance in design, (iii) contribution from the compression brace in tension-only CBFs, (iv) secondary effects such as the P-Δ effect, restrictions on the effective slenderness ratio and the width-thickness ratio for brace members, and (v) contribution from the non-structural elements.

As well, in some situations brace members may be required to carry other than seismic loads, such as gravity and wind loads, or be governed by architectural considerations.

The consequences of brace overstrength are:

(a) An increase in the lateral stiffness, and hence a reduction in the period, and consequently an increase in the seismic demand on the structure.

(b) Overstrength in itself does not guarantee elastic response or inelastic response with a ductile failure mode.

(c) The relative strength of components in the lateral load path is of utmost importance. The effect of making a certain element in the load path stronger than required is likely to make some other element in the load path the 'weak link.' In a severe event, the ductility

demand will concentrate at this 'weak link.' Hence, a hierarchy in the provision of strength to components in the load path is important.

Short of reducing the size of members insofar as possible to minimise the overstrength, the designer either has to connect the overstrong braces for the forces that they can transmit or use a lower connection design load that is justified by an appropriate analysis.

Use of an elastic model for analysis gives an indication of the increased seismic demand due to overstrength. This shows where a 'weak link' may exist. With such a 'weak link', the force in the overstrong brace is limited and strengthening of components to match the brace overstrength is therefore not required.

Time history dynamic analysis is a more sophisticated method to assess the adequacy of structures with significant overstrength in the LLRS. The models chosen for such an analysis must be based on a clear visualisation of the lateral load path and must account for the strength and stiffness of various elements in the load path. This helps the designer identify the 'weak link.' Consequences of its failure can then be assessed.

11.2.11 Ambient vibration test of a single-storey steel building

(a) Flexibility of the roof diaphragm was evident in the experimental mode shapes.

(b) The flexibility of the diaphragm reduces the lateral stiffness of the structure from which it is postulated that the fundamental period is increased significantly with respect to a building with a rigid diaphragm.

(c) Even though the measured periods are significantly greater than the estimates obtained from the NBCC, they are still less than those obtained from various analytical models in which high estimates of the stiffness of non-structural elements are used.

(d) Analyses using a single degree of freedom model substantiates the significant contributions to the lateral stiffness by the non-structural cladding and partitions.

(e) Analyses indicate that the built-up roofing must stiffen the roof diaphragm considerably (for vibrations of low amplitude), in order that the analytical periods correspond to the measured periods.

(f) It is postulated that the non-structural elements and the built-up roofing exhibit a nonlinear elastic behaviour with a high tangent stiffness. Because the ambient vibrations are of low amplitude, the measurement reflects this stiffness.

(g) Although the building has several diagonal walls, it is otherwise regular in plan. A two-dimensional structural model was in good agreement with a more elaborate three-dimensional model.

11.2.12 Application of the results to other CBFs

All the CBFs in this study were designed with a force modification factor, R, of 1.5. As well, the acceleration-related seismic zone, Z_a, was assumed equal to the velocity-related seismic zone, Z_v. For convenience, a snow load of 1.6 kPa was used in all zones. Brace overstrength occurred due to limitations on the effective slenderness ratio and the discrete choice of members, and not due to tension-compression bracing. Only two aspect ratios of the diaphragm were considered.

The SBFs considered in this study would classify as NDBFs (R equal to 2.0) if the connections were designed appropriately, i.e., as required in CSA Standard S16.1-94 (CSA 1994), that the connections of NDBFs that use tension-only bracing be designed to resist 1.10 times the brace yield load in seismic zone 2 and higher. The general trend of results for the SBFs (R equal to 1.5) would also be valid for NDBFs. Some minor differences in the members selected may arise due to the lower design forces for NDBFs as compared to SBFs. However, SBFs would not classify as DBFs, even if the connections were designed for the brace resistances, because of the stringent limitations on the slenderness ratio and the width-thickness ratio for braces in DBFs. These limitations tend to result in overstrong braces and the consequent problems - at least for low-rise buildings of moderate size. Consideration should therefore be given to designing CBFs as SBFs but that the capacity design approach be followed.

For buildings designed in zones where Z_a is not equal to Z_v, or for different snow loads, the change in base shear would be proportionate to the new requirements and therefore the findings of this study would, in general, be applicable.

The question of brace overstrength, for whatever reasons, has been addresses in Chapter 6. With brace overstrength, some other element in the LLRS becomes the weak link and its influence on the system has to be assessed. For buildings with smaller plan dimensions than considered in this work, brace overstrength may be greater than in this study because of the constraint on the slenderness ratio of the braces.

The effect of roof diaphragm flexibility will increase as the aspect ratio of the diaphragm increases.

11.3 Displacement-based seismic design

11.3.1 General

In seismic design, it is not uncommon to consider significant inelastic deformation of the structure at the ultimate limit states (ULS), whereas for other loads, inelastic action, if it occurs, is quite limited. In a severe earthquake, a structure which responds inelastically is softened and limits the seismic force which it attracts. The ductile behaviour guards against collapse, even if the design earthquake is exceeded. Designing for limited strength also reduces initial costs. For the serviceability limit states (SLS), associated with earthquakes occurring relatively frequently in the life of the structure, elastic response is desired to limit damage. To avoid collapse (and limit damage) at the ULS, the maximum displacements must be limited. Similarly, at the SLS, displacements must be limited to avoid damage to the structure and its components. Therefore, a rational approach for seismic design is to use displacements as the basis of design for both the ULS and the SLS. Damage control is better achieved by limiting displacements rather than accelerations (forces). By starting with displacements rather than forces, the design process is inverted. Using target displacements, the process becomes clear and transparent.

11.3.2 Design procedure

The displacement-based design procedure is straightforward to apply, as discussed in Chapter 8. At the start of the design process, the lumped mass at each floor, the structural configuration, and material properties are estimated or established. An appropriate displaced shape is assumed for the structure. For CBFs, brace elongations are

defined as they are directly related to the displaced shape. An appropriate level of damping is selected which depends on the assumed displacements (elastic or inelastic). Structures that are modelled as multi-degree of freedom (MDOF) systems are transformed to equivalent single degree of freedom systems with an equivalent (effective) displacement and mass. Rather than using a design acceleration spectrum as is done in spectral acceleration-based design, a design displacement spectrum is used to determine an effective period corresponding to the effective (target) displacement and effective damping. The secant stiffness to this effective displacement is calculated from the effective mass and period. The base shear, calculated from the secant stiffness and the effective displacement, is distributed as lateral forces over the structure. The LLRS is then designed for this force distribution. The structure is then analysed and the displacements are compared with those assumed at start of the design process. If the displaced shapes do not agree well, iterations are performed until the desired level of matching is attained.

11.3.3 Salient features

The salient features of displacement-based seismic design that distinguish it from spectral acceleration-based design are:

(a) Target displacements are selected at the start of the design process for the ULS and the SLS to control damage as desired.

(b) Empirical equations for estimating the fundamental period of the structure to begin the design process are not required. Instead, stiffness and strength are provided to satisfy the deformation criteria.

(c) The selection of an initial displaced shape forces the engineer to consider the configuration of the LLRS and the allowable drift for the non-structural elements. The latter, as obtained from laboratory tests, could be used directly in design.

(d) The empirical and somewhat arbitrary force modification factor, R, is not required. Instead, the structure is provided with strength and stiffness to attain the target deformations which may require inelastic action in the structural members.

11.3.4 Observations

Application of the displacement-based design method to the design of an 8-storey and a 2-storey CBF in Chapters 9 and 10, respectively, leads to the following observations:

(a) The method is logical, easy to implement, and free of obfuscation.

(b) The initial displaced shape affects the base shear, the lateral force profile, and the member design requirements.

(c) Displaced shapes with large effective displacements result in lower base shears. The level of inelastic response which is related to the inelastic response of the members is selected in the first instance.

(d) In CBFs, the interstorey drift is explicitly related to the brace ductility demand. Hence, it is easy to visualise the deformed state of the brace for a given (assumed) interstorey drift.

(e) An initial displaced shape which agrees reasonably with the first mode shape is a good choice to begin the design.

(f) In tall CBFs, the responses in the higher modes increase brace ductility demands in the upper storeys. An assumed displaced shape with relatively large interstorey drifts here controls this demand. Alternatively, a portion of the base shear (15% in this study) can be applied at the roof level.

(g) The P-Δ effect and the column shortening effect can be accounted for even at the preliminary design stage.

11.3.5 Development of tentative displacement response spectra for design

Figure 11.1 shows the NBCC displacement response spectrum (DRS) for zone 1, the maximum DRS and the mean + 1 standard deviation ($\mu + 1\ \sigma$) DRS of the accelerograms used in zone 1, and a proposed DRS for seismic design in zone 1. All curves are based on an effective damping ratio of 5%. The NBCC DRS is obtained by converting the elastic design acceleration spectrum, given by the product, v S, where v is the zonal velocity ratio and S is the S factor given in Fig. 2.2. Figures 11.2 to 11.5 show similar spectra for zones 2 to 5, respectively.

Figures 11.1 to 11.5 show that the $\mu + 1\ \sigma$ DRS of the accelerograms for zones 1 to 5 agree fairly well with the corresponding NBCC DRS for the range of periods from 0 to 1 s. The $\mu + 1\ \sigma$ DRS of the accelerograms is typically lower than the NBCC DRS for periods greater than 1 s. This is attributed to the fact that the acceleration response spectra of the NBCC, from which the NBCC DRS are derived, have been adjusted upward in the medium and long period range in an attempt to account for the effect of higher modes of vibration of multi-degree of freedom structures. The maximum DRS of the accelerograms is greater than the NBCC DRS for the entire range of periods from 0 to 2 s in zones 1 and 2. However, in zones 3 and higher, the NBCC DRS is greater than the maximum DRS, typically for periods greater than 1.5 s.

Regression analyses were carried out on the $\mu + 1\ \sigma$ DRS of the accelerograms for all five zones to develop tentative DRS for design purpose. Figures 11.1 to 11.5 suggest that the $\mu + 1\ \sigma$ DRS of the accelerograms may be approximated by two lines; the first through the origin and extending for the range of periods from 0 to 1 s, and the second from 1 s to 2 s. The displacement ordinate at a period of 1 s is referred to as the 'anchor point' and is denoted by S_{d1}. Its value is taken equal to the (rounded off) ordinate of the $\mu + 1\ \sigma$ DRS of the accelerograms at a period of 1 s. This value, as seen from the figures, is approximately equal to the ordinate of the NBCC DRS at 1 s. Hence, the 'anchor points' for the proposed DRS in zones 1, 2, 3, 4, and 5 are 20 mm, 35 mm, 55 mm, 70 mm, and 110 mm, respectively.

For the range of periods from 0 to 1 s, the proposed DRS is a linear function through the origin

[11.2] $$S_d = T\ S_{d1}$$

where S_d is the spectral displacement, T is the period, and S_{d1} is the anchor point. For the range of periods from 1 s to 2 s, the regression analysis gives different slopes for a linear fit for all five seismic zones. However, using the average slope for simplicity, the following equation is proposed for all five zones

[11.3] $$S_d = (0.6\,T + 0.4)\ S_{d1}$$

The spectral displacement from [11.2] and [11.3] is plotted as the 'proposed' DRS in Figs. 11.1 to 11.5. In the range of periods from 0 to 1 s, the proposed DRS are

conservative with respect to the NBCC DRS and the $\mu + 1\,\sigma$ DRS of the accelerograms because they give a lower period for the same target displacement and thus result in the provision of greater stiffness and strength. In the range of periods from 1 s to 2 s, the proposed DRS are lower than the NBCC DRS for all five zones. Having used an average slope for the range of periods from 1 s to 2 s, the proposed DRS are below the $\mu + 1\,\sigma$ DRS for some zones and above for others. In zones 1, 2, and 4, the proposed DRS are slightly below the $\mu + 1\,\sigma$ DRS, and above in zones 3 and 5.

What is the effect of using a DRS that falls below the $\mu + 1\,\sigma$ DRS ? The designer enters the DRS with a target displacement and determines the period from the proposed DRS. This period is obviously greater than that corresponding to the $\mu + 1\,\sigma$ DRS resulting in a more flexible structure with a lower base shear. Should an earthquake corresponding to the $\mu + 1\,\sigma$ DRS occur, the displacement of the structure would be greater in the ratio of the displacements given by the $\mu + 1\,\sigma$ DRS to the proposed DRS at the effective period.

Priestley *et al.* (1996) state that design acceleration response spectra are often defined with three regions as follows; (a) for periods smaller than 0.1 to 0.2 s, the acceleration increases linearly with the period, T, (b) for periods from 0.1-0.2 s to 0.4-0.8 s, the acceleration is constant, and (c) for longer periods the acceleration decreases proportionally to 1/T. This implies that displacements vary proportionally to T^3, T^2 and T in the corresponding range of periods. Figure 11.6 shows the elastic DRS specified in Eurocode 8 (Comité European de Normalization 1994) for various levels of viscous damping and for a peak ground acceleration of 0.35 g. The portion of the DRS from 0.6 s to 3 s varies linearly with period while below 0.6 s, the variation is to a higher power. The displacement is assumed constant for periods greater than 3 s. The approximate maximum ground displacement specified by Eurocode 8 is smaller than the constant displacement specified for periods greater than 3 s and with damping less than 10% of critical. Because the NBCC design acceleration spectrum (the S factor curve of Fig. 2.2) specifies a constant acceleration for periods up to 0.25 s, the proposed DRS could be modified to make the displacement proportional to T^2 in this range of periods and thus give a better agreement with the NBCC DRS and the $\mu + 1\,\sigma$ DRS of the

accelerograms. However, the proposed DRS is simple. Similarly, for longer periods the DRS could be modified to give constant displacements as provided in Eurocode 8. It is noted that the $\mu + 1\,\sigma$ DRS for both zones 3 and 5 tend to exhibit this behaviour, but longer periods should be investigated before invoking such a measure.

11.4 Strategy for seismic design

11.4.1 Introduction

A strategy for seismic design is proposed. This strategy is compatible both with the spectral acceleration-based design currently in vogue, and the displacement-based design discussed in the previous section. In the former case, the earthquake loading would logically be based on the requirements of the NBCC (ACNBC 1995a). The proposed strategy incorporates features of seismic design existing in current design codes and guidelines, collects them into a coherent whole, and extends them to provide a unified approach consistent with the limit states design philosophy. Such a strategy is needed to bring together in a rational manner the many facets of seismic design that must be considered. The strategy helps focus the designer's attention on the fundamental coexistent requirements of stiffness, strength, and energy dissipation essential to good seismic design. Currently, some facets of seismic design may be treated in a piecemeal manner or may only be implied. The basic objectives of earthquake-resistant design (ACNBC 1995b) are for the structures to resist major earthquakes without collapse and to resist moderate earthquakes without significant damage. These objectives are embodied in the limit states design approach which considers both the ULS and the SLS. The strategy takes into account the seismicity of the site (seismic zone), the importance of the structure, tolerable damage levels at the ULS and the SLS, initial and rehabilitation costs, and methods of design and analysis consistent with these factors. A major and unique feature is that these factors are related to the seismic zones. This concept arises in part from the fact that, at least in zones of low seismicity, the additional cost of minimising damage, even under the major earthquake, may be minimal. At the commencement of the design process, for all seismic zones, the designer should assess the increase in initial costs, to reduce inelastic behaviour, relative to possible rehabilitation costs at a later date. This may require considerable judgement. In addition, the level of rigour applied in the

design and analysis process as presented depends on the seismicity and the importance of the structure.

Detailing that is required to attain the anticipated response at the ULS is not presented in the proposed strategy for seismic design. These requirements are generally given in material design standards such as CSA Standard S16.1-94 (CSA 1994) for specific framing systems. However, use of the capacity-based design procedure, as discussed subsequently, is recommended in some zones. The use of this procedure implies that the minimum requirements for a steel framing system to have a force modification factor, R, of 2.0 are met.

11.4.2 The strategy

Tables 11.1 and 11.2 present the proposed design strategy for ordinary and important buildings, respectively, for each seismic zone in terms of the anticipated response at the serviceability limit states (SLS) and the ultimate limit states (ULS). Appropriate design and analysis methods for the ULS for each zone are also suggested.

Considering Table 11.1 for ordinary buildings, the strategy calls for elastic response for the SLS in all zones. The criteria defining this response and the response at the ULS are defined in section 11.4.3. Thus, under moderate earthquakes, the deformations are limited and non-structural and structural damage is avoided. For the ULS, based on the detailed studies of one-storey and two-storey CBFs, the additional cost to achieve elastic behaviour as compared to implied inelastic behaviour using current procedures with values of the force modification factor, R, greater than 1.0, appear to be minimal in seismic zones 1 and 2. Even though the structures were designed with a R value of 1.5 (implying inelastic response), the response as determined from a total of 41 time history dynamic analyses was elastic except for 7 instances. In zone 1 in particular, the restriction on the brace slenderness ratio led to braces of greater resistance than required for the earthquake forces. Five of the 7 inelastic responses were obtained in zone 2 for the two-storey building. Even then the maximum brace ductility demand was about 1.6. Had the cladding been considered effective, the incidents of yield would be further reduced. Therefore, increasing the brace size to make the response elastic would not be of significant cost. With the spectral acceleration-based procedure, one approach

to increase the brace size would simply be to design the entire structure using a R value of 1.0. A more direct method would be to use the displacement-based design approach wherein a target displacement for the ULS not exceeding the yield displacement is selected.

For zones 4 and higher, consistent with current philosophy, inelastic response is anticipated because the ACNBC (1995b) suggests that it would be uneconomical and unwarranted to resist major earthquakes without damage as related to the relatively small likelihood of such events in Canada. Zone 3 is a transition zone where the engineer exercises judgement to determine whether or not elastic response can be afforded.

An array of procedures for design and analysis at the ULS is presented. For ordinary buildings in zones 1 and 2, the usual design procedures only are followed. Thus, the base shear and the lateral force distribution as obtained from the NBCC are used. An elastic second-order analysis is performed and the members checked to confirm that the ULS design equations are satisfied. It is further necessary to ensure that the deformation criteria for both the SLS and ULS are satisfied at their respective force levels. The governing limit state for deformations, whether the SLS or the ULS, depends on the relative magnitude of the displacement criteria to that of the earthquakes as defined in section 11.4.3. The usual design procedure does not require an assessment of or a determination of the relative strength of elements along the lateral load path. It is only necessary that the elements have a resistance greater than that associated with the base shear. The burden for designers carrying out seismic designs for zones 1 and 2 should therefore be considerably reduced while at the same time ensuring elastic behaviour of the structures for the major earthquake with little additional cost.

In zones 4 and higher, a capacity-based design procedure is recommended, while, as for the anticipated response, zone 3 represents a transition zone where the design procedure recommended depends on whether or not the structure is designed to respond elastically. The HERA (Feeney and Clifton 1995) requires capacity-based design for steel structures in general. In this procedure, elements of the primary lateral force resisting system are chosen and suitably designed and detailed for energy dissipation in a major earthquake. All other structural elements in the load path are then provided with adequate strength so that the chosen means of energy dissipation can be maintained.

[This implies that the steel framing system meets the requirements of CSA Standard S16.1-94 (CSA 1994) for a R value of 2.0.] For CBFs, the braces are the energy dissipating elements. Currently, some aspects of capacity-based design are required in CSA Standard S16.1-94 (CSA 1994) for DBFs and for NDBFs in zones 2 and higher. Alternatively, elements other than the braces may be selected to dissipate energy. For example, in Chapter 5, a ductile weak link between the roof diaphragm and the CBF isolated the roof diaphragm from the effects of ground motion and also limited the forces in the CBF. Clause 27.7.2 of CSA Standard S16.1-94 (CSA 1994) permits the use of such devices provided their behaviour is established experimentally. The proposed strategy extends the requirements for capacity-based design to all steel structures in zones 4 and higher. It is difficult to envision how a structure could in fact meet the requirement of not collapsing in a major earthquake without such a design procedure.

In applying the capacity-based design approach to multi-storey buildings, Redwood and Channagiri (1991) suggest modifications to account for the fact that the braces at different levels in a frame are unlikely to yield simultaneously. Hence the required resistance of the columns is attenuated to the square root of sum of squares of the components of the brace yield loads. Because of this approach and other issues such as the case of a dual system, it is recommended that a nonlinear static (pushover) analysis be performed in zones 4 and higher. In this analysis, as discussed in section 4.4.3, the lateral force profile is applied incrementally and yielding is monitored. The structure is deemed satisfactory if the target displacement is reached with or without inelastic behaviour. The greater the ductility attained at a given base shear, the greater is the resistance of the structure to earthquakes exceeding the design value.

For important structures such as schools, hospitals, and post-disaster structures, Table 11.2 shows that elastic response is required for the SLS in all zones. This criterion parallels that for ordinary buildings.

Again for the ULS, but now extended to zone 3, it is proposed that the response be elastic. For zones 4 and higher, consideration should be given to designing structures to remain elastic. Recognising that it may be expensive to provide elastic response, limited inelastic action may be allowed as given in section 11.4.3 provided that the structure can perform its intended function.

The usual design procedure is recommended for zones 1 and 2. In addition to the usual limit states design checks as required for ordinary buildings, it is recommended that a response spectrum analysis be performed. As discussed in section 4.2.2, this analysis, readily available in commercial structural analysis programs, determines the maximum structural response to the several modes directly from an earthquake design spectrum. For zones 3 and higher, a capacity design is recommended as is currently required for DBFs and NDBFs in zones 2 and higher. Weak links, as discussed for ordinary buildings in the higher seismic zones, may be allowed provided that the building remains functional in the major earthquake. Thus for the zones given here, the capacity design approach is followed in a parallel manner as for ordinary buildings in the higher zones.

The analysis procedures for zones 3 and higher are more stringent than for ordinary buildings. In zones 4 and higher, the analyses procedures are the most stringent requiring both a nonlinear static analysis and a nonlinear dynamic time history analysis. The nonlinear static analysis, used to verify the capacity design, is based on an assumed lateral force profile and does not provide ductility demands explicitly. The nonlinear dynamic time history analysis is considered essential for important structures in the higher zones in order to evaluate explicitly the displacement and ductility demands. In zone 3, the proposed analysis requirements are somewhat less demanding than in zones 4 and higher and require a response spectrum analysis and a nonlinear static analysis.

11.4.3 Design earthquakes and deformation criteria

Table 11.3 gives the design earthquakes and the associated deformation criteria expressed in terms of the interstorey drift ratio, the interstorey drift divided by the storey height, for both the SLS and the ULS and for ordinary and important buildings. The values for the ULS are from the NBCC.

The NBCC (ACNBC 1995a) does not stipulate either a design earthquake or deformation criteria for the SLS although Commentary J (ACNBC 1995b) states that structures designed in conformance with [the NBCC] should be able to resist moderate earthquakes without significant damage. The designer can easily check the SLS which are formally defined by the 'moderate' earthquake and appropriate drift limits. A 1 in 100 year event with a 40% probability of exceedance in 50 years is considered

reasonable for the SLS. For 12 cities in Canada, from Table J-2 of the user's guide (ACNBC 1995b), this level represents, on the mean, 0.42 of the 1 in 475 year earthquake used for the ULS with a coefficient of variation of 0.28. In Japan, the earthquake used for the SLS is 0.4 to 0.8 of the ULS earthquake depending on the value of the structural characteristics factor, D_s, which ranges between 0.25 and 0.50 for the most ductile braced frames to the least ductile (Aoyama 1981). The structural characteristics factor (comparable to 1/R) takes into account inelastic deformations and energy dissipation. An additional factor related to the irregularity of the structure would reduce the ratios quoted. The Tri-Services manual (Uang 1993) uses an earthquake with a 50% probability of exceedance in 50 years corresponding to a 1 in 73 year earthquake. This is slightly more liberal than that proposed here.

For important buildings, the Tri-Services manual gives a limiting interstorey drift ratio of 0.005. This value also appears in the Uniform Building Code 1991 (Uang 1993) for all structures with a fundamental period less than 0.7 s.

For gypsum board partitions on metal studs, Freeman (1977) states that an interstorey drift ratio of 0.0025 is considered the threshold of initial damage and 0.0050 is the lower bound of significant damage. The latter value is proposed as the limiting interstorey drift ratio for important buildings. That is to say significant damage to the non-structural partitions would not be expected to occur in the 1 in 100 year earthquake. For CBFs, neglecting the effects of column deformations, the interstorey drift, attributable to the brace deformation, is a function of the geometry of the braced bay and material properties only. When the brace is at a 45° angle and has a yield strength of 350 MPa, the interstorey drift ratio at brace yield is 0.0035. This value varies from 0.003 for braces at 40° to the horizontal to 0.004 for braces at 50°. Therefore, in order that the structural response at the SLS be elastic as stipulated in Tables 11.1 and 11.2, the interstorey drift would be governed by the structural requirement and not the non-structural damage requirement. By limiting the structural response to the elastic region, non-structural elements are protected against significant damage. Using higher yield steels would increase the elastic response of the structure proportionately. For structures with steel plate shear walls (Driver *et al.* 1997), the elastic limit is associated

with yielding of the tension diagonal of the infill plate and thus similar limits on elastic response apply.

For ordinary buildings, the limiting interstorey drift ratio for the SLS is given as the range from 0.005 to 0.010. The latter is equivalent to that given in the Tri-Services manual but would result in extensive damage to the partitions. The lower limit, as for important buildings, is the lower bound of significant damage to the partitions. The choice of a limit is therefore related to the economics of increased initial costs for a stiffer structure to possible rehabilitation costs in the future. Again, as for important buildings with CBFs, these limits would not be reached when the response is elastic at the SLS.

11.4.4 Rehabilitation of buildings

The seismic design strategy proposed here may also be used in the rehabilitation of existing buildings. This basically involves use of the capacity-based design approach. Having identified the elements in the LLRS, weak links are strengthened until the desired [ductile] failure mode is attained. If this is not possible, a supplementary LLRS should be provided.

11.5 Recommendations for further work

11.5.1 Experimental investigations

Experimental investigations are recommended on:

(a) behaviour of typical roof diaphragm assemblies under monotonic and cyclic loading to failure:

(i) evaluation of the shear stiffness, strength, damping, and deformation damage thresholds,

(ii) damage mechanisms, the extent of damage to be allowed under moderate and severe earthquake loading, and possible remedial measures,

(iii) the possible difference between the response of mechanically fastened deck assemblies, such as reported by Davies and Bryan (1982), and that of welded deck assemblies typically used in North America,

(iv) the effect of various types of insulation on the shear stiffness of deck panels under different levels of excitation representative of wind and earthquake loading,

(v) behaviour of shear links between the roof diaphragm and the CBF,

(b) behaviour of typical cladding, insulation systems, and partitions under monotonic and cyclic loading to failure to determine shear stiffness and strength characteristics, damping, and damage deformation thresholds,

(c) behaviour of typical brace assemblies with connections under monotonic and cyclic loading to failure to expand the existing database:

(i) the effect of different slenderness ratios, width-thickness ratios, local buckling, possible premature failure due to low-cycle fatigue, and cumulative damage under inelastic loading cycles,

(ii) establishment of force modification factors,

(iii) development of phenomenological hysteresis models,

(d) ambient and forced vibration tests on low-rise buildings during various stages of construction to determine:

(i) periods of vibration and damping ratios,

(ii) improved estimates of periods for the NBCC,

(iii) stiffness contribution of the bare frame, cladding, partitions, and roof deck,

(e) behaviour of full-scale CBFs including the beams and columns under gravity loading and cyclic lateral loading,

(f) forced vibration tests on steel sub-assemblages to determine periods of vibration and damping characteristics during inelastic response, for use in inelastic analyses.

11.5.2 Analytical investigations

Analytical investigations are recommended on:

(a) development of [two-dimensional] brace hysteresis models for three-dimensional inelastic dynamic time history analysis of irregular buildings where torsion is significant,

(b) development of a standard suite of earthquake accelerograms for time history dynamic analysis, for use across Canada, taking into account the acceleration-related and the velocity-related seismic zones,

(c) development of the proposed design displacement spectra in various seismic zones across Canada, and

(d) application of the displacement-based design method to other steel LLRS such as moment resisting frames, eccentrically braced frames, and steel plate shear walls, with a view to eventual inclusion in building codes.

Table 11.1 Design strategy for ordinary buildings

Zone	Anticipated response at limit state		Design procedure	Analysis procedure
	Serviceability	Ultimate		
1	Elastic	Elastic	Usual	Usual
2	Elastic	Elastic	Usual	Usual
3	Elastic	Inelastic ?	Capacity ?	NSA ?
4	Elastic	Inelastic	Capacity	NSA
5	Elastic	Inelastic	Capacity	NSA
6	Elastic	Inelastic	Capacity	NSA

Notes: NSA refers to nonlinear static analysis

Table 11.2 Design strategy for important buildings

Zone	Anticipated response at limit state		Design procedure	Analysis procedure
	Serviceability	Ultimate		
1	Elastic	Elastic	Usual	Usual + RSA
2	Elastic	Elastic	Usual	Usual + RSA
3	Elastic	Elastic	Capacity	RSA + NSA
4	Elastic	Elastic ?	Capacity	NSA + THA
5	Elastic	Elastic ?	Capacity	NSA + THA
6	Elastic	Elastic ?	Capacity	NSA + THA

Notes: RSA refers to response spectrum analysis
NSA refers to nonlinear static analysis
THA refers to nonlinear dynamic time history analysis

Table 11.3 Design earthquakes and deformation criteria

Limit state	Design earthquake	Limiting interstorey drift ratio	
		Ordinary buildings	Important buildings
Serviceability	1 in 100 year event (40% in 50 years)	0.005 - 0.010	0.005
Ultimate	1 in 475 year event (10% in 50 years)	0.020*	0.010*

Note: * current values in the NBCC 1995

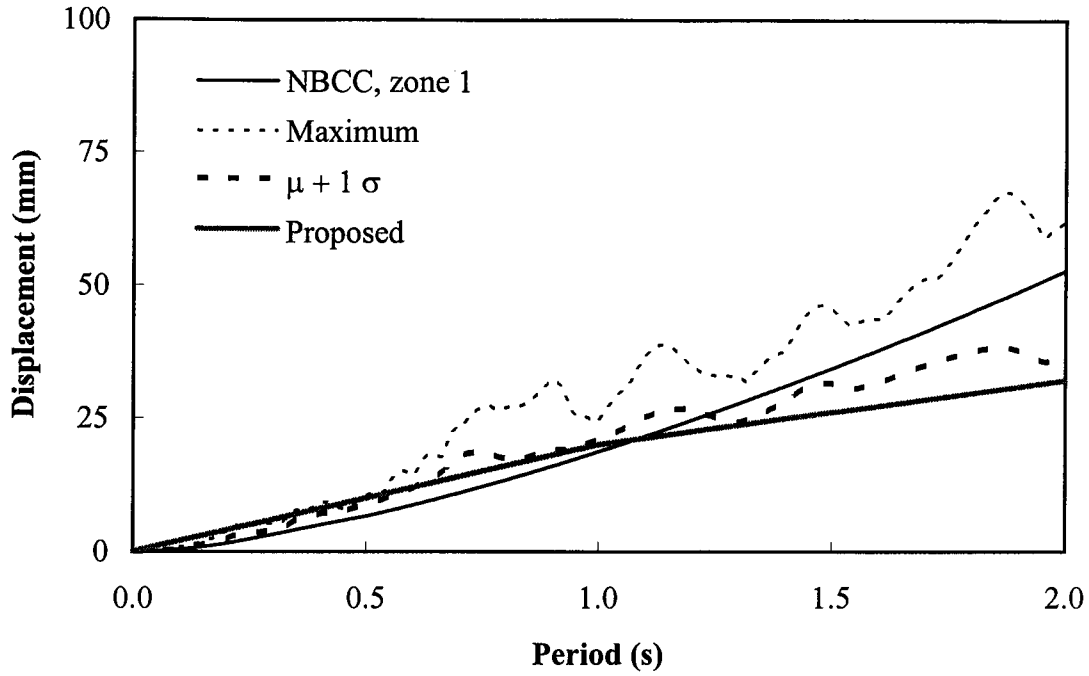

Figure 11.1 Displacement response spectra for zone 1

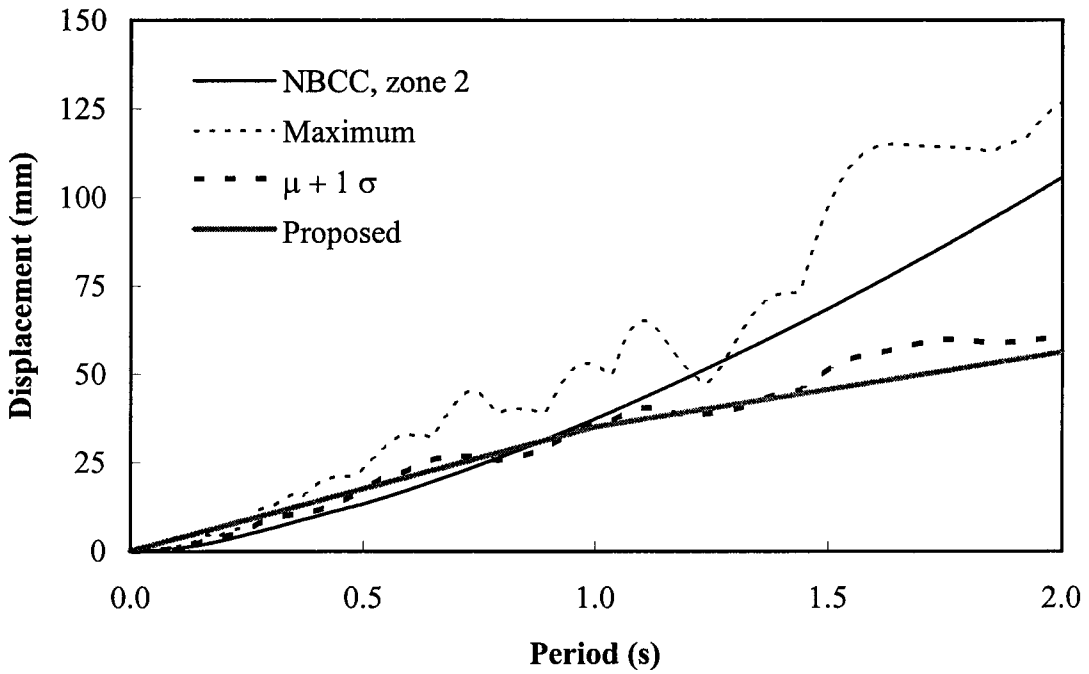

Figure 11.2 Displacement response spectra for zone 2

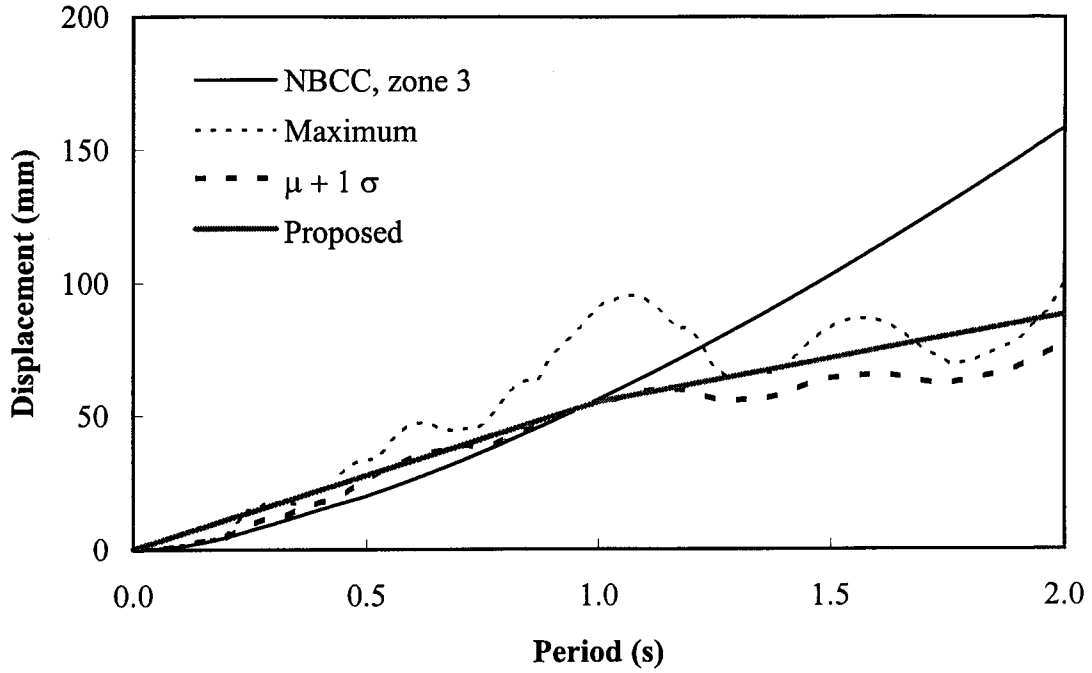

Figure 11.3 Displacement response spectra for zone 3

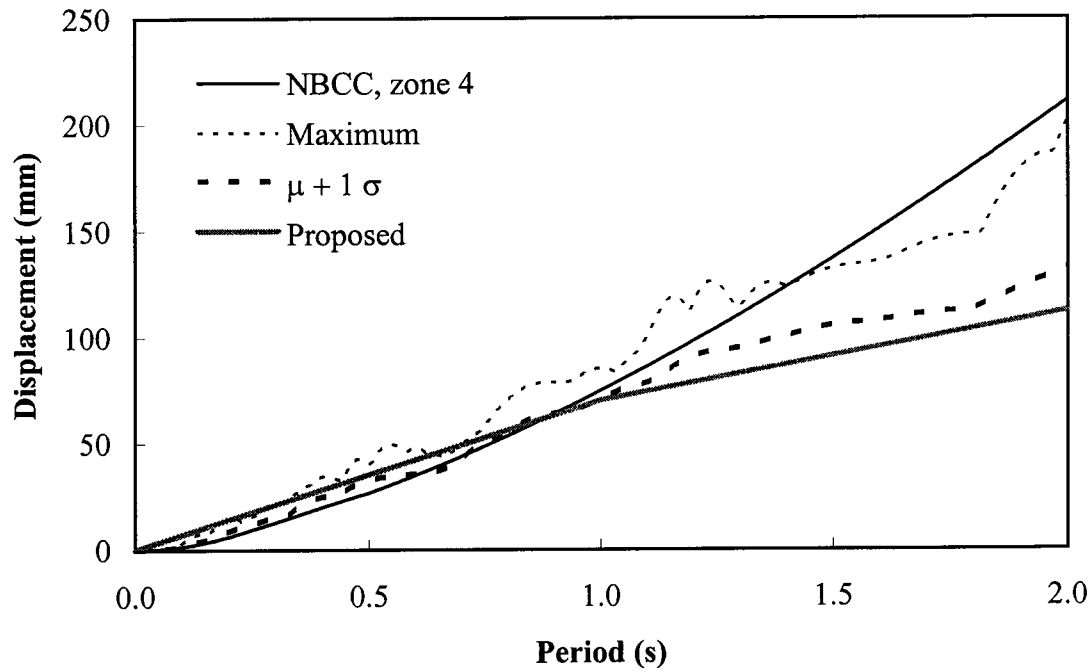

Figure 11.4 Displacement response spectra for zone 4

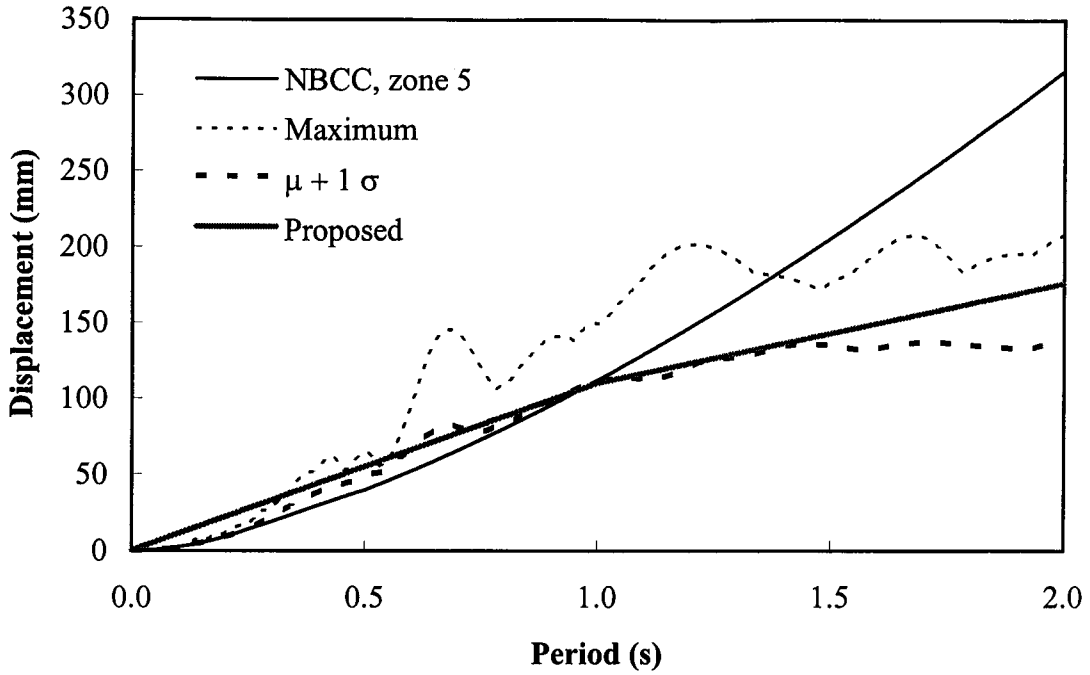

Figure 11.5 Displacement response spectra for zone 5

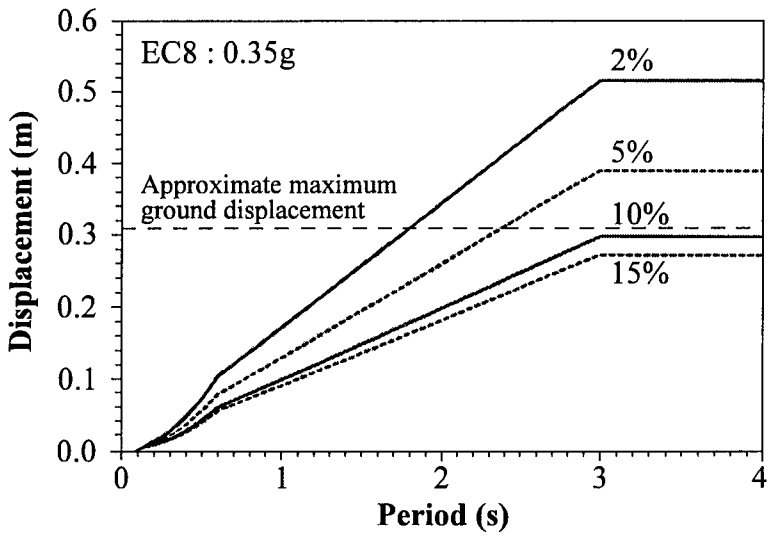

Figure 11.6 Eurocode-8 elastic displacement response spectra

REFERENCES

ACNBC. 1990. National building code of Canada. Associate Committee on the National Building Code, National Research Council of Canada, Ottawa, Ontario.

ACNBC. 1995a. National building code of Canada. Associate Committee on the National Building Code, National Research Council of Canada, Ottawa, Ontario.

ACNBC. 1995b. User's guide - NBC 1995 structural commentaries (part 4). Associate Committee on the National Building Code, National Research Council of Canada, Ottawa, Ontario.

Acronym Software. 1994. SODA, structural optimization, design, and analysis. Version 3.2.5a, Acronym Software Inc., Waterloo, Ontario.

Adham, S.A., Avanessian, V., Hart, G.C., Anderson, R.W., Elmlinger, J., and Gregory, J. 1990. Shear wall resistance of lightgage steel stud wall systems. Earthquake Spectra, **6**(1): 1-14.

AISC. 1978. Specification for the design, fabrication and erection of structural steel for buildings. American Institute of Steel Construction Inc., Chicago, Illinois.

AISC. 1992. Seismic provisions for structural steel buildings - load and resistance factor design. American Institute of Steel Construction Inc., Chicago, Illinois.

AISI. 1991. The performance of steel buildings in past earthquakes. American Iron and Steel Institute, Washington, D.C.

Anderson, A.W., Blume, J.A., Degenkolb, H.J., Hammill, H.B., Knapik, E.M., Marchand, H.L., Powers, H.C., Rinne, J.E., Sedgwick, G.A., and Sjoberg, H.O. 1952. Lateral forces of earthquake and wind. Transactions of the ASCE, paper no. 2514, **117**: 716-780.

Andreaus, U., and Gaudenzi, P. 1989. Modelling of cyclic behaviour of steel braces. Res Mechanica, **26**: 267-288.

Aoyama, H. 1981. Outline of earthquake provisions in the recently revised Japanese building code. Bulletin of the New Zealand National Society for Earthquake Engineering, **14**(2): 63-80.

Astaneh-Asl, A., Goel, S.C., and Hanson, R.D. 1985a. Cyclic in-plane buckling of double angle bracing. Journal of Structural Engineering, ASCE, **110**(9): 2036-2055.

Astaneh-Asl, A., Goel, S.C., and Hanson, R.D. 1985b. Cyclic out-of-plane buckling of double-angle bracing. Journal of Structural Engineering, ASCE, **111**(5): 1135-1153.

Astaneh-Asl, A., Goel, S.C., and Hanson, R.D. 1986. Earthquake-resistant design of double-angle bracings. Engineering Journal, American Institute of Steel Construction, **4**: 133-147.

ATC. 1995. Guidelines for the seismic rehabilitation of buildings (75% complete draft). Report ATC-33.03. Applied Technology Council, Redwood City, California.

Bathe, K.J. 1982. Finite element procedures in engineering analysis. Prentice Hall, Englewood Cliffs, New Jersey.

Bonacci, J.F. 1994. Design forces for drift and damage control: A second look at the substitute structure approach. Earthquake Spectra, **10**(2): 319-331.

Calvi, G.M., and Kingsley, G.R. 1995. Displacement-based seismic design of multi-degree-of-freedom bridge structures. Earthquake Engineering and Structural Dynamics, **24**: 1247-1266.

Campbell, K.W. 1985. Strong motion attenuation relations: a ten-year perspective. Earthquake Spectra, **1**(4): 759-804.

Chien, E. 1985. Single storey building design aid. Canadian Institute of Steel Construction, Willowdale, Ontario.

Chien, E. 1987. Multi-storey steel building design aid. Canadian Institute of Steel Construction, Willowdale, Ontario.

Chien, E. 1991. Low rise office building design aid. Canadian Institute of Steel Construction, Willowdale, Ontario.

Chopra, A.K. 1995. Dynamics of structures - theory and applications to earthquake engineering, Prentice Hall, Upper Saddle River, New Jersey.

Clough, R.W., and Penzien, J. 1993. Dynamics of structures. McGraw-Hill Inc., New York, N.Y.

Cohen, J.M., and Powell, G.H. 1993. A design study of an energy-dissipating cladding system. Earthquake Engineering and Structural Dynamics, **22**: 617-632.

Comité European de Normalization. 1994. Eurocode 8 design provisions for earthquake resistance of structures, Part I: General rules, ENV 1993-2. Brussels.

Cornell, C.A. 1968. Engineering seismic risk analysis. Bulletin of the Seismological Society of America, **58**: 1583-1606.

Crouse, C.B. 1991. Ground-motion attenuation equations for earthquakes on the cascadia subduction zone. Earthquake Spectra, **4**: 201-236.

CSA. 1989. Limit states design of steel structures. CAN/CSA-S16.1-M89, Canadian Standards Association, Rexdale, Ontario.

CSA. 1994. Limit states design of steel structures. CAN/CSA-S16.1-94, Canadian Standards Association, Rexdale, Ontario

CSMIP. California Strong Motion Instrumentation Program, Division of Mines and Geology, Department of Conservation, Sacramento, California. www site at ftp://ftp.consrv.ca.gov/pub/dmg/csmip.

CSSBI. 1991. Design of steel deck diaphragms. Canadian Sheet Steel Building Institute, publication no. CSSBI B13-91, Willowdale, Ontario.

Davies, J.M. 1976. Calculation of steel diaphragm behavior. Journal of the Structural Division, ASCE, **102**(ST7): 1411-1430.

Davies, J.M. 1977. Simplified diaphragm analysis. Journal of the Structural Division, ASCE, **103**(ST11): 2093-2109.

Davies, J.M., and Bryan, E.R. 1982. Manual of stressed skin diaphragm design. Granada, New York, N.Y.

Driver, R.G., Kulak, G.L., Kennedy, D.J.L., and Elwi, A.E. 1997. Seismic behaviour of steel plate shear walls. Structural Engineering Report no. 215, Department of Civil and Environmental Engineering, University of Alberta, Edmonton, Alberta.

Dumanoglu, A.A., and Severn, R.T. 1985. Dynamic behaviour of clasp-type buildings. Earthquake Engineering and Structural Dynamics, **13**: 481-505.

El-Tayem, A.A., and Goel, S.C. 1986. Effective length factor for the design of X-braced systems. Engineering Journal, American Institute of Steel Construction, **1**: 41-45.

Fan, B.H., Vandenberg, G., and Katrichak, A.M. 1994. Seismic withstand of buildings in a west coast electric utility. Proceedings of the 5th U.S. national conference on earthquake engineering, Chicago, Earthquake Engineering Research Institute, Oakland, California, Vol. I: 189-198.

Feeney, M.J., and Clifton, G.C. 1995. Seismic design procedures for steel structures. HERA report R4-76, New Zealand Heavy Engineering Research Association, Manukau City, New Zealand.

FEMA. 1994. National Earthquake Hazards Reduction Program recommended provisions for the development of seismic regulations for new buildings. Building Seismic Safety Council, Washington, D.C.

Filiatrault, A., and Tremblay, R. 1996. Behaviour of tension-only concentrically braced steel frames under simulated earthquake loads. Proceedings of the International Conference on Advances in Steel Structures, Hong Kong, paper no. 57: 1047-1052.

Freeman, S.A. 1977. Racking tests of high-rise building partitions. Journal of the Structural Division, ASCE, **103**(ST8): 1673-1685.

Friberg, P.A., and Susch, C.A.T. 1990. A user's guide to STRONGMO: Version 1.0 of NCEER's strong-motion data access tool for PCs and terminals, Lamont-Doherty Geological Observatory, Columbia University, Palisades, New York.

Gulkan, P., and Sozen, M.A. 1974. Inelastic response of reinforced concrete structures to earthquake motions. Journal of the American Concrete Institute, paper no. 71-41, December, pp. 604-610.

Gupta, A.K. 1990. Response spectrum method in seismic analysis and design of structures. Blackwell Scientific Publications, Boston, Massachusetts.

Gupta, A.K., and Moss, P.J. 1993. Guidelines for design of low-rise buildings subjected to lateral forces. CRC Press, Boca Raton, Florida.

Hanson, R.D. 1966. Comparison of static and dynamic hysteresis curves. Journal of the Engineering Mechanics Division, ASCE, proceedings paper 4949, **92**(EM5): 87-113.

Higginbotham, A.B., and Hanson, R.D. 1976. Axial hysteretic behavior of steel members. Journal of the Structural Division, ASCE, **102**(ST7): 1365-1381.

ICBO. 1997. Uniform building code, volume 2. Structural engineering design provisions, International Conference of Building Officials, Whittier, California.

Idriss, I.M. 1993. Procedures for selecting earthquake ground motions at rock sites. Report NITS GCR 93-625, U.S. Department of Commerce.

Ikeda, K., and Mahin, S.A. 1986. Cyclic response of steel braces. Journal of Structural Engineering, ASCE, **112**(2): 342-361.

Jain, A.K., and Goel, S.C. 1978. Hysteresis models for steel members subjected to cyclic buckling or cyclic end moments and buckling; User's guide for DRAIN-2D: EL9 and EL10. Report no. UMEE 78R6, Department of Civil Engineering, University of Michigan, Ann Arbor.

Jain, A.K., Goel, S.C., and Hanson, R.D. 1978. Inelastic response of restrained steel tubes. Journal of Structural Engineering, ASCE, **104**(ST6): 897-910.

Jain, A.K., Goel, S.C., and Hanson, R.D. 1980. Hysteretic cycles of axially loaded steel members. Journal of the Structural Division, ASCE, **106**(ST8): 1777-1795.

Johnson, B.G. (Editor). 1966. Guide to design criteria for metal compression members. John Wiley and Sons Inc., New York.

Kahn, L.F., and Hanson, R.D. 1976. Inelastic cycles of axially loaded steel members. Journal of the Structural Division, ASCE, **102**(ST5): 947-959.

Kannan, A.E., and Powell, G.H. 1973. DRAIN-2D: A general purpose computer program for dynamic analysis of inelastic plane structures, Report no. EERC 73-6, University of California, Berkeley, California.

Kowalsky, M.J., Priestley, M.J.N., and Macrae, G.A. 1995. Displacement-based design of RC bridge columns in seismic regions. Earthquake Engineering and Structural Dynamics, **24**: 1623-1643.

Lawson, R.S., Vance, V., and Krawinkler, H. 1994. Nonlinear static push-over analysis - why, when, and how? Proceedings of the 5th U.S. national conference on earthquake engineering, Chicago, Earthquake Engineering Research Institute, Oakland, California, Vol. I: 283-292.

Léger, P., and Romano, A. 1992. Seismic analysis of short-period structures subjected to the 1988 Saguenay earthquake. Canadian Journal of Civil Engineering, **19**(3): 510-520.

Little, T.E., and Meidal, K.M. 1994. Ground motion studies for a west coast electric utility. Proceedings of the 5th U.S. national conference on earthquake engineering, Chicago, Earthquake Engineering Research Institute, Oakland, California, Vol. III: 261-270.

Luttrell, L.D. 1981. Steel deck institute diaphragm design manual. Department of Civil Engineering, West Virginia University, Morgantown, West Virginia.

Mahin, S.A., and Lin, J. 1983. Construction of inelastic response spectra for single degree of freedom systems, Report no. UCB/EERC-83/17, University of California, Berkeley, California.

Maison, B.F., and Popov, E.P. 1980. Cyclic response prediction for braced steel frames. Journal of the Structural Division, ASCE, **106**(ST7): 1401-1416.

Mazzolani, F.M. 1994. Thin-walled metal construction: research, design and codification. Proceedings of the 50th anniversary conference, Structural Stability Research Council, Bethlehem, Pennsylvania.

Mazzolani, F.M., De Matteis, G., and Landolfo, R. 1996. Analytical models for cladding panels under monotonic and cyclic shear loads. Proceedings, Stability Problems in Designing, Construction and Rehabilitation of Metal Structures, 5th International Colloquium on Structural Stability, Rio de Janeiro, Brazil, pp. 163-174.

McGuire, R.K. 1976. Fortran computer program for seismic risk analysis. U.S.G.S. Open File Report 76-67.

Mondkar, D.P., and Powell, G.H. 1975. ANSR-1: General purpose program for analysis of nonlinear structural response, Report no. EERC 75-37, University of California, Berkeley, California.

Montgomery, C.J. 1981. Influence of P-Delta effects on seismic design. Canadian Journal of Civil Engineering, **8**(1): 31-43.

Montgomery, C.J., and Hall, W.J. 1979. Seismic design of low-rise steel buildings. Journal of the Structural Division, ASCE, **105**(ST10): 1917-1933.

Naeim, F. 1989. The seismic design handbook. Chapman & Hall, New York, N.Y.

Nakashima, M., and Wakabayashi, M. 1992. Analysis and design of steel braces and braced frames in building structures. In Stability and Ductility of Steel Structures under Cyclic Loading, Fukumoto, Y., and Lee, G., editors, CRC press, Florida.

Naman, S.K., and Goodno, B.J. 1986. Seismic evaluation of a low rise steel building. Engineering Structures, **8**(1): 9-16.

Nau, J.M., and Hall, W.J. 1984. Scaling methods for earthquake response spectra. Journal of Structural Engineering, ASCE, **110**(7): 1533-1548.

NAVFAC. 1982. Seismic design for buildings. TM 5-809-10, NAVFAC P-355, AFM 88-3, Department of the Army, the Navy, and the Air Force, Washington, D.C.

Newmark, N.M. 1959. A method of computation for structural dynamics. Journal of Engineering Mechanics Division, Proceedings of the ASCE, **85**(EM3): 67-94.

Newmark, N.M., and Hall, W.J. 1982. Earthquake spectra and design. Earthquake Engineering Research Institute, Oakland, California.

Nonaka, T. 1977. Approximation of yield condition for the hysteretic behaviour of a bar under repeated axial loading. International Journal of Solids and Structures, **13**: 637-653.

Osteraas, J., and Krawinkler, H. 1989. The Mexico earthquake of September 19, 1985 - Behavior of steel buildings. Earthquake Spectra, **5**(1): 51-88.

Palsson, H., Goodno, B.J., Craig, J.I., and Will, K.M. 1984. Cladding influence on dynamic response of tall buildings. Earthquake Engineering and Structural Dynamics, **12**: 215-228.

Patton, R.N. 1985. Analysis and design methods. Bulletin of the New Zealand National Society for Earthquake Engineering, **18**(4): 329-334.

Popov, E.P., and Black, R.G. 1981. Steel struts under severe cyclic loadings. Journal of the Structural Division, ASCE, **107**(ST9): 1857-1881.

Powell, G.H. 1993. DRAIN-2DX Element description and user guide, version 1.10, Report no. UCB/SEMM-93/18, Department of Civil Engineering, University of California, Berkeley, California.

Prakash, V., Powell, G.H., and Campbell, S. 1993. DRAIN-2DX Base program description and user guide, version 1.10, Report no. UCB/SEMM-93/17, Department of Civil Engineering, University of California, Berkeley, California.

Prathuangsit, D., Goel, S.C., and Hanson, R.D. 1978. Axial hysteresis behavior with end restraints. Journal of the Structural Division, ASCE, **104**(ST6): 883-896.

Priestley, M.J.N. 1993. Myths and fallacies in earthquake engineering - conflicts between design and reality. Bulletin of the New Zealand National Society for Earthquake Engineering, **26**(3): 329-341.

Priestley, M.J.N., Seible, F., and Calvi, G.M. 1996. Seismic design and retrofit of bridges. John Wiley and Sons, Inc., New York.

Rabinovitch, J.S., and Cheng, J.J.R. 1993. Cyclic behavior of steel gusset plate connections. Structural Engineering Report no. 191, Department of Civil Engineering, University of Alberta, Edmonton, Alberta.

Redwood, R.G., and Channagiri, V.S. 1991. Earthquake resistant design of concentrically braced steel frames. Canadian Journal of Civil Engineering, **18**(5): 839-850.

Redwood, R.G., and Jain, A.K. 1992. Code provisions for seismic design of concentrically braced steel frames. Canadian Journal of Civil Engineering, **19**(6): 1025-1031.

Redwood, R.G., Lu, F., Bouchard, G., and Paultre, P. 1991. Seismic response of concentrically braced steel frames. Canadian Journal of Civil Engineering, **18**(6): 1062-1077.

Rezai, M.K. 1995. First phase of the experimental modal analysis of the steel plate shear wall frame built at the University of Alberta. Research report, Department of Civil Engineering, The University of British Columbia, Vancouver.

Rihal, S.S. 1986. Earthquake resistance and behaviour of wood-framed building partitions. Proceedings of the 3rd U.S. national conference on earthquake engineering, Charleston, S.C., Earthquake Engineering Research Institute, Oakland, California, Vol. II: 1297-1310.

SEAOC. 1990. Recommended lateral force requirements and commentary. Seismology Committee, Structural Engineers Association of California, San Francisco, California.

Shibata, A., and Sozen, M.A. 1976. Substitute-structure method for seismic design in R/C. Journal of the Structural Division, ASCE, **102**(ST1): 1-18.

Sockalingam, B., Montgomery, D., Schiff, S., and Sparks, P. 1994. Diaphragm action of cladding in low-rise metal buildings. Proceedings, Structures Congress XII, Atlanta, Georgia, Vol. 2, pp. 1048-1053.

Sockalingam, B. 1988. A dynamic procedure for analysing low-rise metal buildings. M.S. Thesis, Clemson University, South Carolina.

Strnad, M., and Pirner, M. 1978. Static and dynamic full-scale tests on a portal frame structure. Structural Engineer, **56B**(3): 45-52.

Tomasetti, R.L., Gutman, A., Joseph, L.M., and Beer, D. 1984. One Mellon Bank Center: the skin is more than beauty deep. Modern Steel Construction, **3**: 5-10.

Tremblay, R. 1993. Seismic design and behavior of friction concentrically braced frames. Ph.D. thesis, Department of Civil Engineering, The University of British Columbia, Vancouver, B.C.

Tremblay, R. and Stiemer, S.F. 1996. Seismic behaviour of single-storey steel structures with a flexible roof diaphragm. Canadian Journal of Civil Engineering, **23**(1): 49-62.

Tremblay, R., Timler, P., Bruneau, M., and Filiatrault, A. 1995. Performance of steel structures during the 1994 Northridge earthquake. Canadian Journal of Civil Engineering, **22**(2): 338-360.

Tremblay, R., Bruneau, M., Nakashima, M., Prion, H.G.L., Filiatrault, A., and DeVall, R. 1996. Seismic design of steel buildings: lessons from the 1995 Hyogo-ken Nanbu earthquake. Canadian Journal of Civil Engineering, **23**(3): 727-756.

Tso, W.K., Zhu, T.J., and Heidebrecht, A.C. 1992. Engineering implication of ground motion a/v ratio. Soil Dynamics and Earthquake Engineering, **11**: 133-144.

Uang, C.-M. 1993. An evaluation of two-level seismic design procedure. Earthquake Spectra, **9**(1): 121-135.

Ventura, C.E. 1995. Ambient vibration test of the Safeway store. Research report by the UBC Ambient Vibration Team, Department of Civil Engineering, The University of British Columbia, Vancouver.

VicWest Steel. 1991. Steel deck-shear diaphragm design manual. Edmonton, Alberta.

Wakabayashi, M., Nakamura, T., Iwai, S., and Hayashi, Y. 1984. Effects of strain rate on the behavior of structural members subjected to earthquake force. Proceedings of the 8 th World Conference on Earthquake Engineering, San Francisco, California, Vol. IV: 491-498.

Walpole, W.R. 1985. Concentrically braced frames. Bulletin of the New Zealand National Society for Earthquake Engineering, **18**(4): 351-354.

Walpole, W.R. 1995. Behaviour of cold-formed steel RHS members under cyclic loading. Proceedings of the NZNSEE Conference, Rotorua, New Zealand, New Zealand National Society for Earthquake Engineering, Waikanae, New Zealand.

Weaver, W., Timoshenko, S.P., and Young, D.H. 1990. Vibration problems in engineering. John Wiley and Sons, New York, N.Y.

Wilson, E.L., and Habibullah, A. 1987. Static and dynamic analysis of multi-story buildings, including P-Delta effects. Earthquake Spectra, **3**(2): 289-298.

Zhu, T.J., Tso, W.K., and Heidebrecht, A.C. 1988. Effect of peak ground a/v ratio on structural damage. Journal of Structural Engineering, ASCE, **114**(5): 1019-1037.

APPENDIX A

A.1 Introduction

BC Hydro, the third largest electric utility in Canada, has recently carried out ground motion studies for seismic evaluation and upgrade of all components of its system including dams, electric systems, and buildings (Little and Meidal 1994, Fan *et al.* 1994). The approach adopted by BC Hydro for arriving at the design ground motion at a given site is outlined. Recommendations of BC Hydro for selection of time histories are then listed.

A.2 Approach of BC Hydro for specifying design ground motion

The design ground motion is obtained from probabilistic seismic hazard analyses based on the Cornell-McGuire method (Cornell 1968, McGuire 1976). The steps in such an analysis may be summarised as follows:

(a) Areas where significant earthquakes can occur are identified and brought together on a seismogenic zone model. The zonation is based on the following: (i) historical seismicity patterns, that is, locations where earthquakes have occurred in the past, (ii) the cause of past earthquakes, and (iii) what might cause future earthquakes. Each zone has an equal probability of a given magnitude earthquake occurring per unit of area.

(b) For each source zone, the rate at which earthquakes of different magnitude can occur and the maximum credible magnitude is estimated. A review of past data indicates that a magnitude 4.5 earthquake near a populated area causes damage occasionally. Hence, a magnitude of 4.5 is selected as the lower cut-off.

(c) Attenuation relationships are used to give the intensity of shaking as a function of the earthquake magnitude and distance from the epicentre. As no attenuation relationship is available for Western Canada due to lack of strong motion data, expressions developed by Idriss (1993) and Crouse (1991) are used.

(d) The above data is processed by the computer program EQRISK (McGuire 1976) to obtain the peak horizontal acceleration, PHA, versus the annual probability of exceedance at any site. A contour map for the PHA can be obtained by joining locations with a given

probability level. The PHA contours may be used for scaling the appropriate time histories for dynamic analysis.

(e) Uniform hazard response spectra are also computed for various annual probabilities of exceedance. They may be used as a 'Target' response spectrum for adjustment of time histories to produce spectrum compatible accelerograms.

(f) The seismic hazard analysis also indicates the magnitude-distance contribution to each site. Thus, the major contribution to the hazard at a site may be from a moderate magnitude event close to the site. This also assists in the selection of appropriate time histories for dynamic analysis.

A.3 Recommendations for selection of time histories

(a) Time histories should be from a seismotectonic setting similar to the area of interest. The selection process should consider factors such as source mechanism (e.g., strike-slip fault, thrust fault, or subduction interface), magnitude and epicentral distance.

(b) Attention is also given to the foundation condition. Typically, time histories recorded on rock or firm soil sites are considered. Local site effects are accounted for by applying the time history to the bottom of a vertical soil column and propagating the motion upwards to the base of the structure.

(c) Time histories selected should have a PGA similar to the design PHA of the site in question. Time histories are often considered for which the PGA are scaled within a range of 0.5 to 2.0.

(d) If a design target response spectrum is specified, then the response spectra for the time histories selected should be similar, particularly in the period range of interest.

(e) Several choices are available for scaling of time histories; no scaling, scale the PGA to equal the PHA of the site, or scale to match the design spectral shape. Sensitivity tests are recommended.

(f) A minimum of three representative time histories should be used. This selection should be reviewed and increased if the results are highly variable.

APPENDIX B

B.1 Introduction

DRAIN-2D (Kannan and Powell 1973) uses the constant-average acceleration method for solving the equations of dynamic equilibrium. This method is a particular case of a general method proposed by Newmark (1959). In the following, the equation of motion is first cast into an incremental form that makes it amenable for the solution of nonlinear systems. Newmark Beta methods are then described. The constant-average acceleration method is obtained by substituting the appropriate constants. Use of this method to develop an earthquake response spectrum is also discussed.

B.2 Incremental equation of motion

The equation of motion of a multi-degree of freedom system is

[B.1] $$M\,\ddot{U} + C(\dot{U})\,\dot{U} + F_s(U,\dot{U}) = P(t)$$

where M is the mass matrix, C is the damping matrix, F_s is the restoring force vector, P(t) is the external forcing vector, and $\ddot{U}$, $\dot{U}$, and U, are the acceleration, velocity and displacement vectors, respectively. Assume that the mass remains constant. Consider [B.1] at time instant t_i and at instant t_{i+1}.

[B.2] $$M\,\ddot{U}_i + C_i(\dot{U})\,\dot{U}_i + (F_s)_i = P_i$$

[B.3] $$M\,\ddot{U}_{i+1} + C_{i+1}(\dot{U})\,\dot{U}_{i+1} + (F_s)_{i+1} = P_{i+1}$$

The incremental equation of motion is obtained by taking the difference between [B.2] and [B.3] to obtain

[B.4] $$M\,\Delta\ddot{U}_i + C_T\,\Delta\dot{U}_i + K_T\,\Delta U_i = \Delta P_i$$

where C_T and K_T are the tangent values of the damping and stiffness matrices at time t_i. The other incremental quantities are defined as follows:

[B.5] $$\Delta\ddot{U}_i = \ddot{U}_{i+1} - \ddot{U}_i$$

[B.6] $$\Delta\dot{U}_i = \dot{U}_{i+1} - \dot{U}_i$$

[B.7] $$\Delta U_i = U_{i+1} - U_i$$

[B.8] $$K_T\,\Delta U_i = \left((F_s)_{i+1} - (F_s)_i\right) \text{ and } C_T\,\Delta\dot{U}_i = \left(C_{i+1}(\dot{U})\,\dot{U}_{i+1} - C_i(\dot{U})\,\dot{U}_i\right)$$

[B.9] $\Delta P_i = P_{i+1} - P_i$

Equation [B.4] introduces approximations for a nonlinear system due to the use of tangent damping and stiffness matrices. Direct time integration schemes solve this equation by using the known acceleration, velocity, and displacement at time t_i and by making assumptions on the variation of these quantities between time instants t_i and t_{i+1}. In essence, the equation of dynamic equilibrium, [B.1], is only being satisfied at discrete time intervals Δt apart, where $\Delta t = t_{i+1} - t_i$.

B.3 Newmark Beta methods

Newmark (1959) proposed a family of time-stepping methods based on the following expressions for final velocity and displacement

[B.10] $$\dot{U}_{i+1} = \dot{U}_i + \left((1-\gamma)\,\Delta t\right)\ddot{U}_i + \left(\gamma\,\Delta t\right)\ddot{U}_{i+1}$$

[B.11] $$U_{i+1} = U_i + \Delta t\,\dot{U}_i + \left(\left(\frac{1}{2}-\beta\right)(\Delta t)^2\right)\ddot{U}_i + \left(\beta\,(\Delta t)^2\right)\ddot{U}_{i+1}$$

The parameter γ provides a linearly varying weighting between the influence of the initial and final accelerations on the change of velocity. It also controls the amount of artificial damping induced by the step-by-step procedure (Clough and Penzien 1993). There is no artificial damping for γ equals 1/2. Similarly, the parameter β provides for weighting the contribution of the initial and final accelerations to the change of displacement. Equations [B.10] and [B.11] are implicit formulations that are inconvenient because iteration is required at each step to determine the acceleration at the end of the step. They are converted to an explicit form by using the incremental equation of motion, [B.4]. Equations [B.10] and [B.11] may be expressed in terms of incremental quantities to give

[B.12] $$\Delta\dot{U}_i = \Delta t\,\ddot{U}_i + \left(\gamma\,\Delta t\right)\Delta\ddot{U}_i$$

[B.13] $$\Delta U_i = \Delta t\,\dot{U}_i + \left(\frac{1}{2}(\Delta t)^2\right)\ddot{U}_i + \left(\beta\,(\Delta t)^2\right)\Delta\ddot{U}_i$$

In the above equations, $\Delta\ddot{U}_i$, $\Delta\dot{U}_i$, and ΔU_i are unknowns. Equation [B.13] gives

[B.14] $$\Delta\ddot{U}_i = \left(\frac{1}{\beta\ (\Delta t)^2}\right) \Delta U_i - \left(\frac{1}{\beta\ \Delta t}\right) \dot{U}_i - \left(\frac{1}{2\,\beta}\right) \ddot{U}_i$$

Substituting [B.14] into [B.12] and rearranging the terms gives

[B.15] $$\Delta\dot{U}_i = \left(\frac{\gamma}{\beta\ \Delta t}\right) \Delta U_i - \left(\frac{\gamma}{\beta}\right) \dot{U}_i + \left(1 - \frac{\gamma}{2\,\beta}\right) \Delta t\, \ddot{U}_i$$

Equations [B.14] and [B.15] on substitution into the incremental equation of motion, [B.4], result in an expression with only one unknown, ΔU_i, given by

[B.16] $$\hat{K}_i\, \Delta U_i = \Delta\hat{P}_i$$

where

[B.17] $$\hat{K}_i = K_T + \left(\frac{\gamma}{\beta\ \Delta t}\right) C_T + \left(\frac{1}{\beta\ (\Delta t)^2}\right) M$$

[B.18] $$\Delta\hat{P}_i = \Delta P_i + \left(\frac{\gamma}{\beta} C_T + \frac{M}{\beta\ \Delta t}\right) \dot{U}_i + \left[\frac{M}{2\,\beta} + \left(\frac{\gamma}{2\,\beta} - 1\right) \Delta t\, C_T\right] \ddot{U}_i$$

Equation [B.16] is solved for ΔU_i and the increments in acceleration and velocity are obtained from [B.14] and [B.15], respectively. Thus, the state of the system at time t_{i+1} is completely determined. Computations for the next time step follow the same procedure.

For the specific case of earthquake excitation at the base of a structure, the incremental force in [B.18] is given by

[B.19] $$\Delta P_i = - M \{1\} \Delta\ddot{U}_g$$

where $\Delta\ddot{U}_g$ is the increment in ground acceleration between time instant t_i and t_{i+1}.

B.4 Constant-average acceleration method

The constant-average acceleration method assumes that the acceleration within any time step is the average of the acceleration at the beginning of the time step and that at the end of the time step. It is a special case of Newmark's method and is obtained by assuming parameter γ equal to 1/2 and β equal to 1/4. Equations [B.17] and [B.18] simplify to

[B.20] $$\hat{K}_i = K_T + \left(\frac{2}{\Delta t}\right) C_T + \left(\frac{4}{(\Delta t)^2}\right) M$$

[B.21] $$\Delta\hat{P}_i = \Delta P_i + \left(2\,C_T + \frac{4\,M}{\Delta t}\right)\dot{U}_i + 2\,M\,\ddot{U}_i$$

This method is unconditionally stable as the errors are not amplified from one time step to the next (Bathe 1982). Hence, the time step may be selected by considering only the need for defining properly the earthquake ground motion and the vibration characteristics of the structure. The accelerograms selected in Chapter 4 are digitised at a minimum time step of 0.005 s. A time step of 0.001 s was selected for analyses with DRAIN-2D because sensitivity tests indicated that a smaller time step was unnecessary.

B.5 Development of an earthquake response spectrum

The equation of motion of a SDOF system of mass, M, damping, C, and stiffness, K, that is subjected to earthquake ground acceleration, $\ddot{U}_g$, is given by

[B.22] $$M\,\ddot{U} + C\,\dot{U} + K\,U = -\,M\,\ddot{U}_g$$

The mass, M, is related to the damping, C, and stiffness, K, by

[B.23] $$C = 2\,\xi\,\omega\,M$$

[B.24] $$K = \omega^2\,M$$

where ξ is the damping ratio and ω is the circular frequency. Substitute [B.23] and [B.24] into [B.22] and simplify to obtain

[B.25] $$\ddot{U} + 2\,\xi\,\omega\,\dot{U} + \omega^2\,U = -\,\ddot{U}_g$$

Equation [B.25] is integrated numerically with the mass, M, taken equal to 1.0 and with the following substitutions in [B.20] and [B.21]

[B.26] $$C_T = 2\,\xi\,\omega$$

[B.27] $$K_T = \omega^2$$

[B.28] $$\Delta P_i = -\left(\left(\ddot{U}_g\right)_{i+1} - \left(\ddot{U}_g\right)_i\right) = -\,\Delta\ddot{U}_g$$

Thus, [B.20] and [B.21] simplify to

[B.29] $$\hat{K}_i = \omega^2 + \frac{4\,\xi\,\omega}{\Delta t} + \frac{4}{(\Delta t)^2}$$

[B.30] $$\Delta\hat{P}_i = -\,\Delta\ddot{U}_g + \left(4\,\xi\,\omega + \frac{4}{\Delta t}\right)\dot{U}_i + 2\,\ddot{U}_i$$

The increment in displacement is given by [B.16]. The response spectra shown in Fig. 4.1 to 4.10 are developed by this procedure. A time step of 0.001 s is used.

APPENDIX C

C.1 EL9 buckling element

The EL9 buckling element was developed and incorporated into the DRAIN-2D computer program by Jain *et al.* (1978, 1980). It is a truss element with four degrees of freedom that are the two translations at each end. Large displacement effects are not considered in that the direction cosines of the element and its displacement transformation matrix are assumed to remain constant. The element behaviour is based on a multi-linear phenomenological model that mimics the hysteresis behaviour of a brace. The general behaviour of this hysteresis model is described below.

C.2 Description of the hysteresis model

The hysteresis model is constructed with the following parameters for the brace; length, cross-sectional area, radius of gyration, effective length factor, K, elastic modulus, E, tension yield force, P_{yp}, the first cycle buckling load, P_{yn}, and a strength reduction factor to arrive at the second and subsequent cycle buckling load, P_{ync}.

Referring to Fig. C.1(a), assume that an initially straight member is loaded first in tension. It follows segment AE elastically. The member yields at E and follows path EE′. On reversal of displacement at E′, the member unloads elastically. Continued compression results in the first buckling of the member at point B, at load P_{yn}. The buckling load used in the second and subsequent cycles, P_{ync}, is smaller than P_{yn}. After buckling at point B, the member follows segment BC. The control point C corresponds to a compressive displacement equal to five times the yield elongation of the member, Δ_Y. If the direction of axial displacement is again reversed at L, the member follows segment LL′ parallel to the initial elastic slope A′B until it attains the post-buckling load level, P_{ync}. If the direction of axial displacement is reversed at L′, the member follows segment L′ L″ that is parallel to segment BC. Point L″ lies at load level P_{ync}.

Continued compression beyond point C or L″ results in segment CD or L″ D. The point D represents the maximum compressive displacement of the brace. If the direction of axial displacement is reversed at D, it results in the compressive load

decreasing to zero and is followed by an increasing tensile load along path DFE″. To locate the point F, a line A″ F′ is drawn from the new origin A″ (A′A″ = E′ E″) at a slope of 1/3 times the initial elastic slope A′ E′ or A′ B, that intersects the line DE″ at F′. Intercept A″ F is taken as 60/(KL/r) times the distance A″ F′. Distance E′ E″ is the residual elongation obtained from the percentage residual strain

$$[C.1] \qquad \varepsilon = 0.0175\left(\frac{0.55\,\Delta}{KL/r} + 0.0002\,\Delta^2\right)$$

where Δ is the maximum displacement in compression (point D) and KL/r is the effective slenderness ratio of the brace. This empirical equation is based on experimental data obtained from small square steel tube specimens (Jain *et al.* 1980).

Figure C.1(b) describes the hysteresis rules adopted in the post-buckling region. The line FG drawn parallel to the initial elastic slope is used to distinguish the loading history in region DFG from that in region A″ E″ FG. If the direction of axial displacement is reversed along DF″, the member retraces the same path. If the displacement reverses at point H, the member follows segment HI that is parallel to segment A′ B. Continued compression results in segment I I′. If the direction of axial displacement is reversed at I′, the member follows segment I′ H. If the direction of axial displacement is reversed at J, the member follows segment JK. Continued compression results in segment KK′ or in segment KK″. If reversal occurs at K′, the member follows segment K′J. If the member surpasses point G and returns from K″, it follows K″ F and then FE″. New control points are determined if the member surpasses points D or E″ during a cycle. In all subsequent cycles, the maximum compression load is P_{ync}.

The KL/r ratio controls the amount of pinching in the hysteresis loop. For a KL/r ratio less than 60, the hysteresis loop is convex outwards along path DF″FE″ in Fig. C.1(b). If the KL/r ratio is greater than 60, the hysteresis loop is concave outwards along this path. The length and radius of gyration of the brace member depend on the geometry and the brace cross section used. The effective length factor, K, depends on the rotational restraint provided by the end connections.

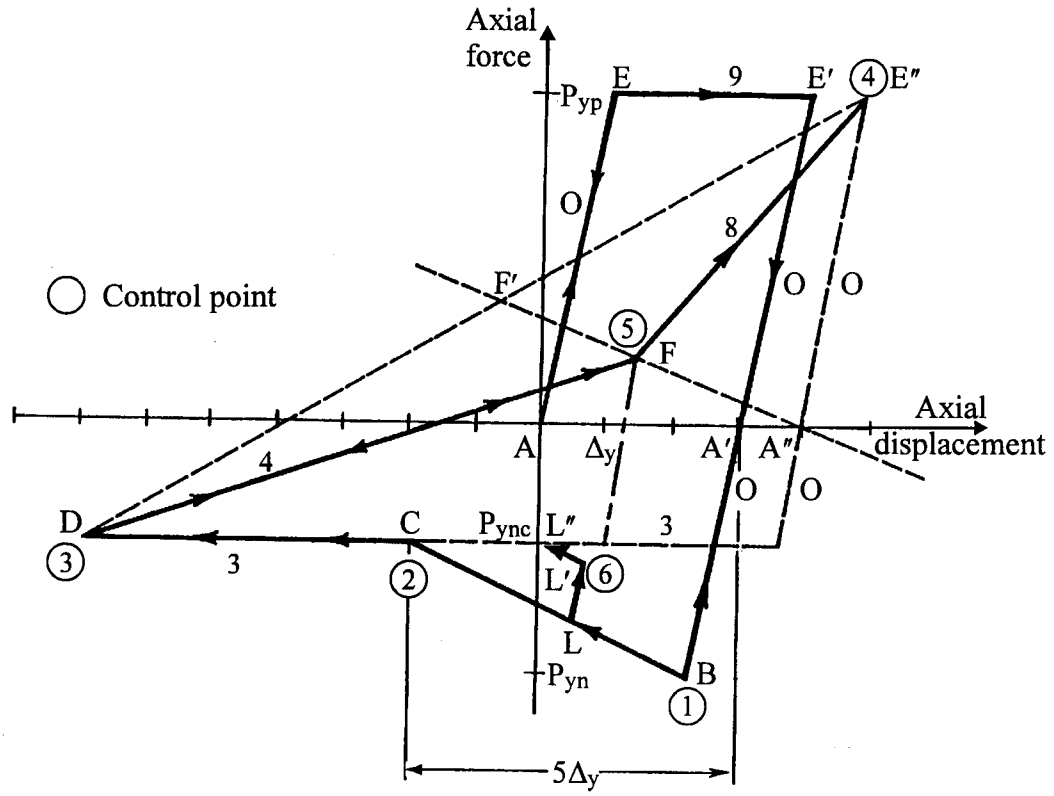

(a) Overall behaviour

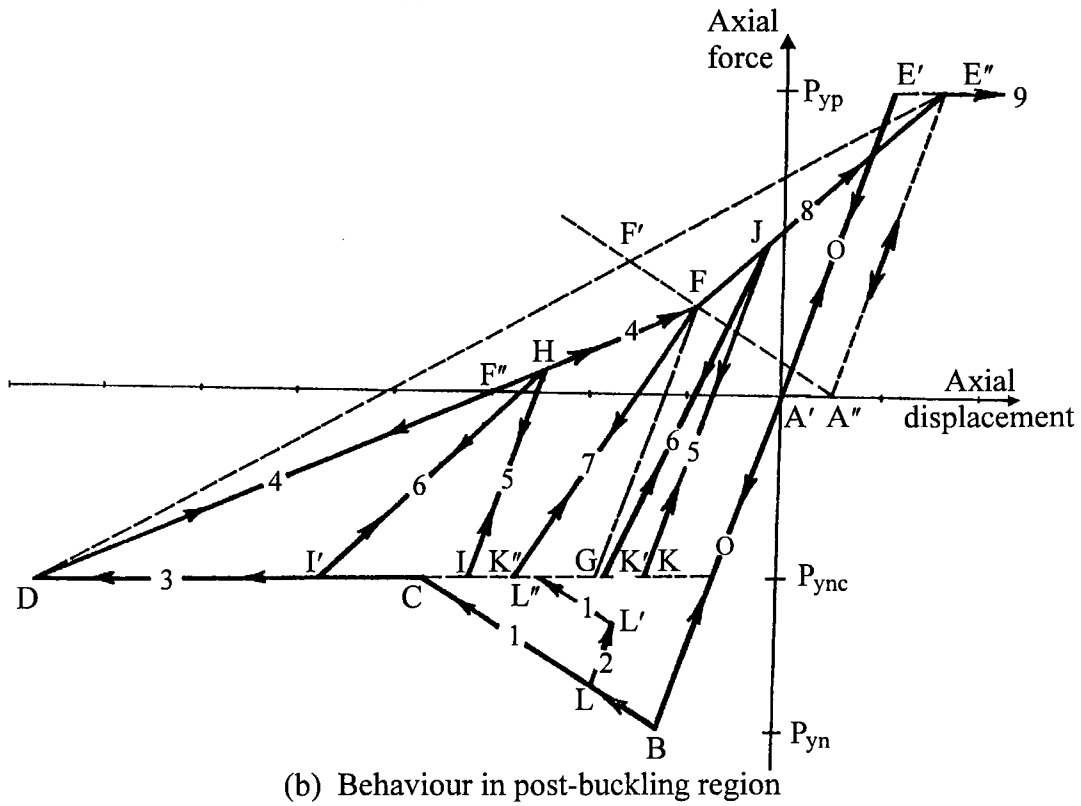

(b) Behaviour in post-buckling region

Figure C.1 Axial-hysteresis behaviour of the EL9 element

APPENDIX D

D.1 Introduction

The Safeway store at Bonnie Doon Mall, Edmonton, Alberta, is a single-storey building that relies on a steel roof diaphragm and on concentrically braced frames (CBFs) for lateral stiffness and stability. Non-structural elements comprise exterior cladding and a few interior partitions. Experimental studies of its dynamic behaviour were carried out by the Ambient Vibration Team of the University of British Columbia on 16th June, 1995 (Ventura 1995). Analytical studies of the dynamic behaviour of the building are reported here. The studies were made possible with the aid of architectural drawings, shop details, and building specifications that were provided by C. J. Montgomery of The Cohos Evamy Partners, Edmonton.

D.2 Objectives

The objectives of this study are to

(a) measure the periods and mode shapes of the building with ambient vibration tests,
(b) study the mode shapes for evidence of flexible deck diaphragm behaviour,
(c) compare the experimental period with the empirical estimate of the NBCC,
(d) develop analytical models to represent the dynamic behaviour of the building,
(e) investigate the sensitivity of the models to the modelling parameters,
(f) formulate tentative recommendations for the seismic analysis of such buildings, and
(g) make recommendations for further experimental work.

As an outcome of the analyses, the contribution of the non-structural elements to the lateral stiffness is also assessed.

D.3 Description of the building

The Safeway store is located at the south end of Bonnie Doon Mall on 82nd Avenue and 85th Street, Edmonton, Alberta. It consists of a single-storey steel building with an irregular plan as shown in Fig. D.1. It is approximately 62.0 m in the North-South (N-S) direction and 74.5 m in the East-West (E-W) direction, with a main floor area of 4413 m^2. The floor to ceiling height is about 7.8 m. It has a steel roof deck

and relies on diaphragm action to transfer lateral loads to the CBFs that are present along the exterior wall. The main entrance to the store faces the south and has an elaborate facade. Two small mezzanine floors that comprise 5% of the main floor area are suspended from the roof and are stabilized by diagonal braces tied back to the roof structure.

The roof deck spans in the N-S direction and supports a built-up roof. The deck is supported by roof joists that span in the E-W direction. The joists have a nominal depth of 1050 mm. The area of cross section of the joist chords ranges from 490 mm^2 to 1280 mm^2. Tie joists frame into the interior columns. The joists are supported by roof girders that span the N-S direction. The girders are wide flange sections with depths ranging from 450 mm to 1200 mm. They constitute a cantilever-suspended-span system and are continuous over the interior columns. The latter are typically HSS 203 x 203 with a maximum wall thickness of 13 mm. CBFs 1 and 5 are aligned in the N-S direction and CBFs 3 and 4 are aligned in the E-W direction. CBF 2 is present along the north-west exterior wall and contributes stiffness to both directions. Each CBF is typically one bay wide and two levels high.

Figure D.2 shows the layout of the non-structural elements. The exterior cladding consists of a 102 mm (4 inch) Exterior Insulation Finish System (EIFS), air/vapor barrier, 12.7 mm (1/2 inch) exterior grade gypsum sheathing, two layers of 64 mm (2 1/2 inch) and 203 mm (8 inch) metal studs, and 12.7 mm (1/2 inch) gypsum board forming the interior surface. The EIFS is present on the west and the north face of the store. The south face has a number of glazed panels and partitions along the entrance facade. The east wall is made up of a 12.7 mm (1/2 inch) gypsum board partition and separates the store from the adjacent mall. Interior partitions exist in the north and north-west areas as shown.

D.4 Experimental periods and mode shapes

The experimental periods and mode shapes are obtained from an ambient vibration test. Details of the test set-up and the methodology are given by Rezai (1995) and Ventura (1995). To measure the vibrations in the N-S and E-W directions, accelerometers are placed on the roof above the frames along grid lines 6 and H,

respectively. The peaks of the power spectral density function of the ambient vibration records determine the potential natural frequencies of the building. The periods of the first three modes of vibration in the N-S and E-W direction are summarized in Table D.1. The corresponding mode shapes are shown in Figs. D.3 and D.4. These mode shapes clearly show the flexibility of the roof diaphragm. Hence, analytical models developed to study the dynamic behaviour of such buildings should account for diaphragm flexibility.

D.5 NBCC estimate of the period

The NBCC (ACNBC 1995a) estimate of the period of a CBF is given by

[D.1] $$T = \frac{0.09\ h_n}{\sqrt{D_s}}$$

where h_n and D_s are the height and width of the braced frame in metres, respectively. The CBFs have an average height of 7.3 m. In [D.1], the term D_s appears to be a measure of the stiffness. The total stiffness of the CBFs in any direction is considered to be proportional to the sum of the widths of the CBFs in that direction. The stiffness of a CBF at 45°, can be shown to contribute one-half this value in the N-S and E-W directions. Table D.2 compares the NBCC estimate of the fundamental period determined on this basis with the measured period. The NBCC underestimates the period significantly.

D.6 Structural properties

Before carrying out a dynamic analysis, the mass and stiffness of the building must be estimated. These estimates follow

D.6.1 Specified loads

The gravity loads specified on the structural drawings are: (a) dead load of 1.68 kPa, (b) snow load of 1.44 kPa, and (c) a maximum ponding load intensity of 2.39 kPa. Some mechanical units with a total weight of 149 kN are present on the roof.

D.6.2 Estimate of mass

About 95% of the plan area of the building is single-storey high with the remainder accounted for by the two mezzanine floors. Hence, the mass is assumed to be distributed uniformly over the plan. The ambient vibration test was carried out on a dry day. Hence, only the roof dead load was contributing to the structural mass. The best estimate of this load, based on the architectural drawings and the specifications, is given in Table D.3. The miscellaneous item on line 9 includes allowance for ceiling work, ductwork, roof fixtures, and some allowance for the mezzanine floors. The dead load estimate of 0.90 kPa is significantly less than the specified dead load of 1.68 kPa indicated on the drawings. The structural mass is 0.4 kN s^2/mm.

D.6.3 Estimate of lateral stiffness

This building obtains its lateral stiffness from: (a) CBFs along the exterior wall, (b) interior frames in both directions, and (c) non-structural elements such as the EIFS and interior partitions. An estimate of the roof deck stiffness is also required for the analytical models that consider diaphragm flexibility. The stiffness contribution of the CBFs, interior frames, and the deck diaphragm is well defined. In contrast, the stiffness of non-structural elements is difficult to quantify. In the following, the stiffnesses of the former three are quantified. The stiffness contribution of the non-structural elements is estimated from a single degree of freedom (SDOF) idealization of the building.

D.6.3.1 Lateral stiffness of the CBFs

The details of the CBFs and their lateral stiffness are given in Fig. D.5. The stiffness contribution in the N-S and E-W direction is 94 kN/mm and 96 kN/mm, respectively.

D.6.3.2 Lateral stiffness of interior frames

Interior frames in the N-S direction are present along grid lines B, C, F, H, and K. They consist of the cantilever-suspended-span system together with the supporting columns that are typically HSS 203 x 203 x 13. The girders are continuous over the columns. Hinges are assumed to be present in the girders where the suspended span is

connected to the cantilevers. The in-plane stiffness of these frames is calculated assuming the column bases to be fixed, and is given in Table D.4.

Interior frames in the E-W direction are present along grid lines 4, 5, 6, 7, and 8. These frames are made up of the tie joists that have their top and bottom chords attached to the column and are capable of transferring moment to it. The roof joists that span E-W are supported by girders at the top flange only. They are not capable of transferring any significant moment and are considered to not contribute to frame action. The in-plane stiffness of the E-W interior frames is given in Table D.5.

The interior frames contribute relatively little to the lateral stiffness in each direction because the columns are very slender with a clear height of at least 7 m. Thus, even if the columns are assumed to be restrained against rotation at the top due to infinitely stiff girders, the resulting lateral stiffness contribution is still small.

D.6.3.3 Stiffness of the roof deck

The roof deck was fabricated by VicWest Steel Incorporated. The deck profile is 38 mm deep with a sheet width of 914 mm. Gage 22 sheets with a core thickness of 0.76 mm are used over most of the roof. Gage 20 sheets are used at locations of snow drift accumulation but these are small in extent. The roof joists are at an average spacing of 1.8 m. The deck sheets are typically continuous over 4 spans. Each deck sheet is fastened to the supporting joist with 7 fasteners (22 mm diameter puddle welds) at the end supports and 4 fasteners at the intermediate supports. The sheets are button punched at 600 mm on center along the sidelap. They are connected to the rafters (girders) with welds at a spacing of 760 mm. A continuous angle with a cross sectional area of 778 mm^2 is welded to the deck along its perimeter and functions as the flange member.

The sheet to joist fastener layout is not standard and thus the shear stiffness of the deck cannot be obtained directly from the deck design manual provided by VicWest Steel (1991). Hence, the stiffness for the actual layout is first estimated by the 'European' method (Davies and Bryan 1982). The stiffness from the VicWest Steel design manual is then interpolated as indicated in Table D.6. The roof specifications indicate that the 16 mm (5/8 inch) gypsum board is screwed to the deck sheets with at least 20 fasteners per board. The two can be expected to act integrally for vibrations of

low amplitude. The shear stiffness, G′, of the gypsum board is estimated as 1.1 kN/mm based on a tangent modulus of rigidity of 69 MPa (Freeman 1977). This contribution increases the shear stiffness of the deck from 6.35 kN/mm to 7.45 kN/mm. In addition, the built-up roofing over the gypsum board is composed of the following: a layer of tar felt, 102 mm (4 inch) phenolic board rigid insulation, 25.4 mm (1 inch) fiberboard, 3 layers of asphalt, and gravel ballast at the top. No stiffness estimate could be made for this built-up roofing due to lack of experimental data. Numerical models are used to investigate the effect of stiffness contribution of the built-up roofing.

D.6.3.4 Lateral stiffness of non-structural elements

A single degree of freedom (SDOF) model is used to estimate the stiffness of the non-structural elements. This model assumes a rigid roof diaphragm supported by three springs in parallel that represent the stiffness of the CBFs, K_{cbf}, the interior frames, K_{if}, and the non-structural elements (exterior cladding and a few interior partitions), K_c. The period of this model is given by

$$T_r = 2\pi\sqrt{\frac{M}{(K_{cbf} + K_{if} + K_c)}} \qquad [D.2]$$

The mass, M, and the stiffnesses, K_{cbf} and K_{if}, were estimated in the previous sections. The value of K_c is varied from 0 to 100 kN/mm and the period T_r is calculated from [D.2]. Figure D.6 shows the graph of T_r versus K_c for the N-S and E-W direction. The experimentally observed period of the first mode is also shown. If K_c is neglected, the period obtained in the N-S and E-W direction is 0.39 s and 0.40 s, respectively, and is greater than the corresponding measured period. This suggests that the non-structural elements must contribute significant lateral stiffness. Equation [D.2] gives

$$K_c = \left(\frac{4\pi^2 M}{T_r^2} - K_{cbf} - K_{if}\right) \qquad [D.3]$$

The stiffness of non-structural elements can be obtained by assuming the period of the SDOF system, T_r, equal to the measured period of the first mode. This stiffness is lower than the actual stiffness because of the following: (a) the period of the building with a

rigid diaphragm will certainly be smaller than the measured period of the first mode that includes the effect of diaphragm flexibility, and (b) the stiffness of interior frames, K_{if}, is calculated assuming the column bases are fixed. Figure D.6 gives a value of 33 kN/mm and 88 kN/mm for K_c in the N-S and E-W direction, respectively. Table D.7 gives the relative stiffness contribution of the CBFs, interior frames, and the non-structural elements to the SDOF model. The contribution of the latter in both directions is significant.

The stiffness K_c has to be apportioned to the components of the exterior cladding and the interior partitions in the N-S and E-W direction. Figure D.2 gives the location, type, and the approximate length of the non-structural partitions that are assumed to only possess in-plane stiffness. An effective shear modulus, G, is determined from the stiffness K_c by

$$[D.4] \qquad K_c = \frac{G \ t \ L}{H}$$

where t, L, and H are the effective thickness, length, and height of the partitions, respectively.

No estimates are available for the shear stiffness of the EIFS that depends on its material properties and connection details. Hence, the 102 mm (4 inch) EIFS is assumed to be equivalent to a 25.4 mm (1 inch) thick gypsum board partition. This is about 1 1/2 times the stiffness of the metal cladding considered for the single-storey building in Chapter 5. One half the length of each inclined wall (at 45° in plan) is effective in the N-S and E-W direction. The effective length of the EIFS in the N-S direction is 63 m and that of the gypsum board, including that in the exterior cladding, is 142 m. Using the stiffness of 33 kN/mm for K_c (non-structural stiffness in the N-S direction) in [D.4], gives an effective modulus of 50 MPa for the 25.4 mm (1 inch) gypsum board. Freeman (1977) has reported shear moduli ranging from 40 MPa to 120 MPa for such partitions.

Similarly, in the E-W direction, the non-structural stiffness, Kc, is 88 kN/mm. The effective length of the EIFS and gypsum board partitions are 67 m and 129 m, respectively. When these are assumed to have the same shear modulus as established for the N-S direction, the remaining contribution to stiffness must be due to the glazed panels

and partitions of 49 m length along the entrance facade. If these panels are also assumed to be 25.4 mm (1 inch) thick, an equivalent shear modulus of 345 MPa is obtained for them from [D.4], which is almost 7 times that obtained for gypsum board partitions. Although the stiffness estimates for the non-structural elements are high relative to the CBFs, this stiffness has to be present in order to give the period of the first mode with the SDOF model (that assumes a rigid diaphragm). In fact, flexibility of the diaphragm should be compensated by a further increase in stiffness of the non-structural elements.

D.7 Classical beam on elastic foundation model

The first, second, and third experimental mode shapes shown in Figs. D.3 and D.4 correspond to the first symmetric, first anti-symmetric, and the second symmetric mode shapes of a simply supported beam. This observation suggests that the building may be modelled by an equivalent beam on elastic foundation analogy as shown in Fig. D.7. Appendix E describes an approximate solution that uses this analogy to determine the fundamental period of a single-storey steel building with a flexible roof diaphragm. The equations used are [E.19] and [E.21] to [E.26], with some pertinent parameters given in Table D.8. The diaphragm mass, M_d, is taken as 90% and 85% of the total mass, M, in the N-S and E-W direction, respectively, with the remainder assigned to the respective endframes. A continuous angle welded to the diaphragm perimeter functions as the flange member. The lever arm, D, for calculating the moment of inertia is taken as the distance between grid lines 4 and 9 (49 385 mm) in the N-S direction, and grid lines C and M (56 040 mm) in the E-W direction. The moment of inertia is given by

[D.5] $$I = 2\, A_f \,(D/2)^2$$

where A_f is the area of the flange member. The shear area, A_s, is given by

[D.6] $$A_s = G'\, d \;/\; G$$

where G′, d, and G are the shear stiffness, width, and shear modulus of the diaphragm, respectively. The diaphragm stiffness, K_d, is obtained from [E.21]. The endframe stiffness in each direction, K_f, is the sum of the stiffnesses of the CBFs, K_{cbf}, and the non-structural elements, K_c. The "subgrade" stiffness, $K_i L$, is assumed equal to the

stiffness of the interior frames, K_{if}. The lateral stiffness provided to the diaphragm by the inclined walls to the west is neglected.

The classical model gives a period of 0.69 s in the N-S direction and 0.57 s in the E-W direction. Both periods are significantly greater than the corresponding measured periods of 0.34 s and 0.29 s. This model is suitable for studying the sensitivity of the fundamental period to the modelling parameters. Figure D.8 shows the effect of change in moment of inertia, I, and shear area, A_s, on the period in the N-S direction. The minimum period of 0.40 s on the plot is still greater than the measured period of 0.34 s and suggests that the stiffness of the non-structural elements and the subgrade modulus (from interior frames) need to be significantly greater than assumed in order to equal the measured period.

D.8 Numerical beam on elastic foundation analogy

The classical model is applicable to regular buildings and provides an estimate of the fundamental period only. Hence, a numerical analogy of the classical model is developed to account for the irregular building layout and obtain periods and mode shapes of the higher modes. The building is modelled with an equivalent non-prismatic beam with flexural rigidity, EI, and shear rigidity, GA_s, as shown in Fig. D.7. The lateral stiffnesses of the CBFs, interior frames, and non-structural elements are modelled by discrete spring supports to the beam at appropriate nodes along its length. The roof mass is lumped at the nodes in proportion to their tributary area and rotational inertia is neglected.

In the numerical experiments with this model, only two values of the diaphragm shear stiffness are considered. A stiffness of 7.45 kN/mm based on actual specifications of the deck, as discussed in section D.6.3.3. Tremblay[1] suggests that at very low load levels, the shear stiffness is much higher than the published values. A stiffness of 59.6 kN/mm is obtained by assuming the corrugated deck equivalent to a flat plate of 0.76 mm thickness. Both these estimates neglect any contribution from the built-up

[1] Tremblay, R. 1996. Personal communication.

roofing except for the 16 mm (5/8 inch) gypsum board that is fastened to the metal deck. [A preliminary analysis with a rigid diaphragm gives a fundamental period of 0.34 s and 0.29 s in the N-S and E-W direction, respectively, as expected because the non-structural stiffness has been calibrated so.]

Periods from this model are compared with the experimental ones in Table D.9. With a diaphragm stiffness of 7.45 kN/mm, the numerical model gives periods for the first three modes that are significantly greater than the measured values. The period of the first mode of 0.61 s and 0.48 s in the N-S and E-W direction, respectively, is less than the corresponding period of 0.69 s and 0.57 s obtained with the classical model in section D.7. An increase in the diaphragm stiffness from 7.45 kN/mm to 59.6 kN/mm reduces the period of the third mode significantly while the first and second modes are affected to a lesser extent. The period of these modes is reduced further only if additional stiffness is attributed to the non-structural elements and interior frames that provide subgrade stiffness to the model.

D.9 Three-dimensional model

The previous models introduce approximations due to the non-uniform layout of the building. Hence, a three-dimensional model is developed as it is capable of representing the behaviour of the building more appropriately. The modelling details are as follows.

(a) A space frame is generated with the orthogonal interior frames. The mezzanine floors and the entrance facade are not modelled for simplicity.

(b) All columns are modelled with a fixed base. A rigid end zone equal to the depth of the shallower member that frames into the column is specified at the top. Torsional inertia and shear areas are neglected.

(c) Each CBF is modelled as a truss. Moment continuity for the interior frames in the N-S direction that form the cantilever-suspended-span system is modelled appropriately. In the E-W direction, only frames with tie joists are modelled.

(d) The roof deck is modelled with plane stress elements with an effective thickness equal to the ratio of the deck shear stiffness, G′, to the shear modulus, G. An effective thickness of 0.095 mm is obtained for a deck shear stiffness of 7.45 kN/mm and is about 1/8th of the actual sheet thickness of 0.76 mm. This simply accounts for the fact that a

'flat' plane stress element has considerably greater shear stiffness than a corrugated deck sheet of the same thickness. The plane stress elements that model the roof deck are attached to nodes that are at the top of the columns only. Thus, these elements are not 'stitched' to the beams (N-S) or the tie joists (E-W). This implies that the axial stiffness of the beams and the joists and their lateral (out-of-plane) bending stiffness is not considered to contribute to the bending stiffness of the deck assembly. This approximation will result in somewhat longer periods. In reality, the roof deck is attached to the top flange of the beams and the top chord of the tie joists. Because it is not attached to these members at their mid-plane, full out-of-plane stiffness of the beams and tie joists may not be mobilized.

(e) The non-structural cladding and partitions are also modelled with plane stress elements. The effective shear modulus is assumed as derived in section D.6.3.4

(f) Translational mass is specified in both horizontal directions in the plane of the roof.

Results with this model are presented in Table D.10. [A preliminary analysis with a rigid roof diaphragm gives a fundamental period of 0.36 s and 0.29 s in the N-S and E-W direction, respectively.] The symbols G_g, G_{EIFS}, and $G_{g\&p}$ in Table D.10 refer to the shear modulus of the gypsum board, EIFS, and the glazed panels and partitions along the entrance, respectively. A description of each case in Table D.10 follows:

(a) Case 1 assumes shear stiffness of the roof deck and shear moduli for the non-structural elements as derived in sections D.6.3.3 and D.6.3.4, respectively. The mode shapes that correspond to the experimental ones in the N-S and E-W direction are shown in Figs. D.9 and D.10, respectively. They are qualitatively similar to the experimental ones; however, the periods are significantly greater. A comparison of periods with case (a) in Table D.9 shows good agreement with the numerical beam on elastic foundation model.

(b) In case 2, the shear modulus of the gypsum board partitions is increased to the maximum value suggested by Freeman (1977). A small change in periods is observed.

(c) In case 3, the non-structural elements are made rigid. The period of the first mode in the N-S direction becomes less than that measured, while that in the E-W direction is still greater than that measured. The periods of the second and third modes are still greater than that those measured.

(d) In case 4, the shear stiffness of the roof deck is increased to 59.6 kN/mm. The non-structural elements are as in case 1. There is a significant reduction in the period of the third mode in both directions with the period becoming smaller than the measured one. The period of the first mode is still considerably greater than that measured. A similar observation is made with the numerical beam model; case (b) in Table D.9.

(e) In case 5, the deck shear stiffness is as in case 4, and the non-structural elements are as in case 2. The periods obtained for the three modes in both directions are now close to those measured.

A comparison of the period of the third mode obtained for cases 1, 2, and 3 with that obtained for cases 4 and 5 suggests that the shear stiffness of the roof deck has to be significantly greater than the estimate of 7.45 kN/mm given in section D.6.3.3. The stiffness, as apparently measured by the ambient vibration tests, is likely to be marginally less than 59.6 kN/mm because the period of the third mode in cases 4 and 5 is less than the measured value. The non-structural elements are certainly stiffer than the estimate established in section D.6.3.4.

D.10 Conclusions

The following conclusions can be drawn

(a) The empirical estimate of the period obtained from the NBCC (ACNBC 1995a) of 0.15 s in the N-S direction and 0.16 s in the E-W direction are significantly less than the measured periods of 0.34 s and 0.29 s, respectively.

(b) The measured periods are in turn significantly less than those obtained from the various analytical models even when high estimates are used for the stiffness of the non-structural elements. In the N-S direction, the estimated period of the first mode ranges from 0.57 s to 0.37 s, and in the E-W direction from 0.47 s to 0.30 s. Some possible reasons for this discrepancy follow.

(c) Analyses with the SDOF model suggest that non-structural cladding and partitions must contribute even more stiffness to the building than considered appropriate.

(d) Analyses with the numerical beam model and the 3-D model suggest that the built-up roofing stiffens the roof diaphragm significantly. The period of the third mode is influenced significantly by the shear stiffness of the diaphragm only; the stiffness of the

cladding, partitions, and the CBFs have little influence on it because these elements are present on the periphery of the diaphragm. Analysis with a diaphragm shear stiffness of 59.6 kN/mm gives a period for the third mode that is close to the measured value.

(e) The deck shear stiffness of 59.6 kN/mm is significantly greater than that suggested by diaphragm design manuals. This stiffness could result due to the following; (i) the built-up roofing acting integrally with the steel deck for vibrations of low amplitude, (ii) the 16 mm (5/8 inch) gypsum board that is fastened to the metal deck with screws may result in 'closing' the cells of the corrugated deck profile and thereby increasing its shear stiffness significantly, and (iii) the girders and joists of the roof structure may contribute some lateral stiffness to the roof deck.

(f) It is also possible that the non-structural elements and the built-up roof exhibit a nonlinear elastic behaviour with a high tangent stiffness. Because the ambient vibrations are of low amplitude, only this stiffness is apparent in the measurements.

D.11 Recommendations

D.11.1 Seismic analysis of low-rise buildings

(a) The non-structural elements contribute significant stiffness to low-rise buildings. This effect should be considered in dynamic analyses because any stiffening action will result in greater response to earthquake loading (due to a reduction in period), at least until these elements are damaged significantly.

(b) With the same modelling parameters, the two-dimensional beam on elastic foundation model gives periods that are in reasonable agreement with those from the more elaborate three-dimensional model. Hence, the former is considered to be adequate for dynamic analysis of reasonably symmetric buildings.

D.11.2 Further studies

Further studies on such buildings should address the following issues:

(a) Stiffness of typical roof deck panel assemblies under monotonic and cyclic loading.

(b) Effect of various types of insulation on the stiffness of deck panels under different levels of excitation representative of wind and earthquake loading on such buildings.

(c) Stiffness of common non-structural elements, such as, masonry, wood veneer, and gypsum wallboard on metal studs.

(d) Stiffness of exterior insulation and finish systems.

(e) Response from ambient and forced vibration tests during various stages of construction. This would allow the effect of addition of various components on the dynamic behaviour to be determined.

Table D.1 Period from ambient vibration test

Mode	Direction	
	North-South	East-West
	Period (s)	
1	0.34	0.29
2	0.18	0.13
3	0.12	0.10

Table D.2 Comparison of NBCC estimate with measured period

	Period (s)		
Direction	NBCC	Measured	Ratio
N-S	0.15	0.34	0.44
E-W	0.16	0.29	0.55

Table D.3 Estimate of roof dead load

Line	Description	Intensity (kPa)
1	Girders (N-S)	0.10
2	Roof joists (E-W)	0.10
3	38 mm (1 1/2 inch) steel deck	0.10
4	16 mm (5/8 inch) gypsum board	0.13
5	102 mm (4 inch) phenolic board insulation	0.07
6	25 mm (1 inch) fibreboard	0.05
7	Gravel with 3 ply asphalt	0.22
8	Mechanical equipment on roof	0.03
9	Miscellaneous	0.10
	Total =	0.90

Table D.4 Lateral stiffness of interior N-S frames

Frame at grid	Stiffness (kN/mm)
B	0.93
C	2.71
F	1.71
H	1.53
K	1.85
Total =	8.73

Table D.5 Lateral stiffness of interior E-W frames

Frame at grid	Stiffness (kN/mm)
4	1.12
5	0.84
6	0.62
7	0.45
8	0.67
Total =	3.70

Table D.6 Estimate of shear stiffness of the roof deck

Design Manual	number of sheet/joist fasteners per sheet width	Shear stiffness G′ (kN/mm)
Davies & Bryan	4	2.21
1982	actual layout	4.84
	7	5.79
VicWest Steel	4	2.93
1991	actual layout (interpolation)	6.35
	7	7.53

Table D.7 Relative stiffness contribution from SDOF model

Direction	K_{cbf}	K_{if}	K_c
N-S	0.69	0.06	0.24
E-W	0.51	0.02	0.47

Table D.8 Parameters used in the classical model

Parameter	Direction	
	N-S	E-W
Mass of diaphragm, M_d (kN s^2/mm)	0.36	0.34
Mass of end frame, M_f (kN s^2/mm)	0.04	0.06
Span of diaphragm, L (mm)	74 495	61 735
Area of flange member, A_f (mm^2)	778	778
Lever arm (mm)	49 385	56 040
Moment of inertia, I (x 10^{12} mm^4)	0.95	1.22
Shear area, A_s (mm^2)	5891	7108
Diaphragm stiffness, K_d (kN/mm)	26	48
Endframe stiffness, K_f (kN/mm)	94 + 33	96 + 88
Subgrade stiffness, K_i L (kN/mm)	8.7	3.7

Table D.9 Comparison of periods - numerical beam model vs. experiment

Mode	Direction					
	N-S			E-W		
	Model	Expt.	Ratio	Model	Expt.	Ratio
	(a) Diaphragm shear stiffness G′ = 7.45 kN/mm					
1	0.61	0.34	1.80	0.48	0.29	1.67
2	0.32	0.18	1.79	0.26	0.13	1.99
3	0.21	0.12	1.72	0.17	0.10	1.73
	(b) Diaphragm shear stiffness G′ = 59.6 kN/mm					
1	0.52	0.34	1.54	0.39	0.29	1.34
2	0.24	0.18	1.34	0.20	0.13	1.51
3	0.14	0.12	1.15	0.11	0.10	1.08

Table D.10 Periods from the three-dimensional model

Case	Model parameters	Direction	Mode 1	Mode 2	Mode 3
			Period (s)		
	Ambient vibration test	N-S	0.34	0.18	0.12
		E-W	0.29	0.13	0.10
1	G′ = 7.45 kN/mm; G_g = 50 MPa; G_{EIFS} = 12.5 MPa; $G_{g\&p}$ = 346 MPa				
		N-S	0.57	0.30	0.20
		E-W	0.47	0.25	0.17
2	G′ = 7.45 kN/mm; G_g = 120 MPa; G_{EIFS} = 30 MPa; $G_{g\&p}$ = 346 MPa				
		N-S	0.53	0.29	0.19
		E-W	0.44	0.24	0.16
3	G′ = 7.45 kN/mm; Non-structural partitions made rigid				
		N-S	0.24	0.19	0.14
		E-W	0.33	0.20	0.18
4	G′ = 59.6 kN/mm; G_g = 50 MPa; G_{EIFS} = 12.5 MPa; $G_{g\&p}$ = 346 MPa				
		N-S	0.41	0.20	0.09
		E-W	0.32	0.12	0.07
5	G′ = 59.6 kN/mm; G_g = 120 MPa; G_{EIFS} = 30 MPa; $G_{g\&p}$ = 346 MPa				
		N-S	0.37	0.18	0.09
		E-W	0.30	0.11	0.07

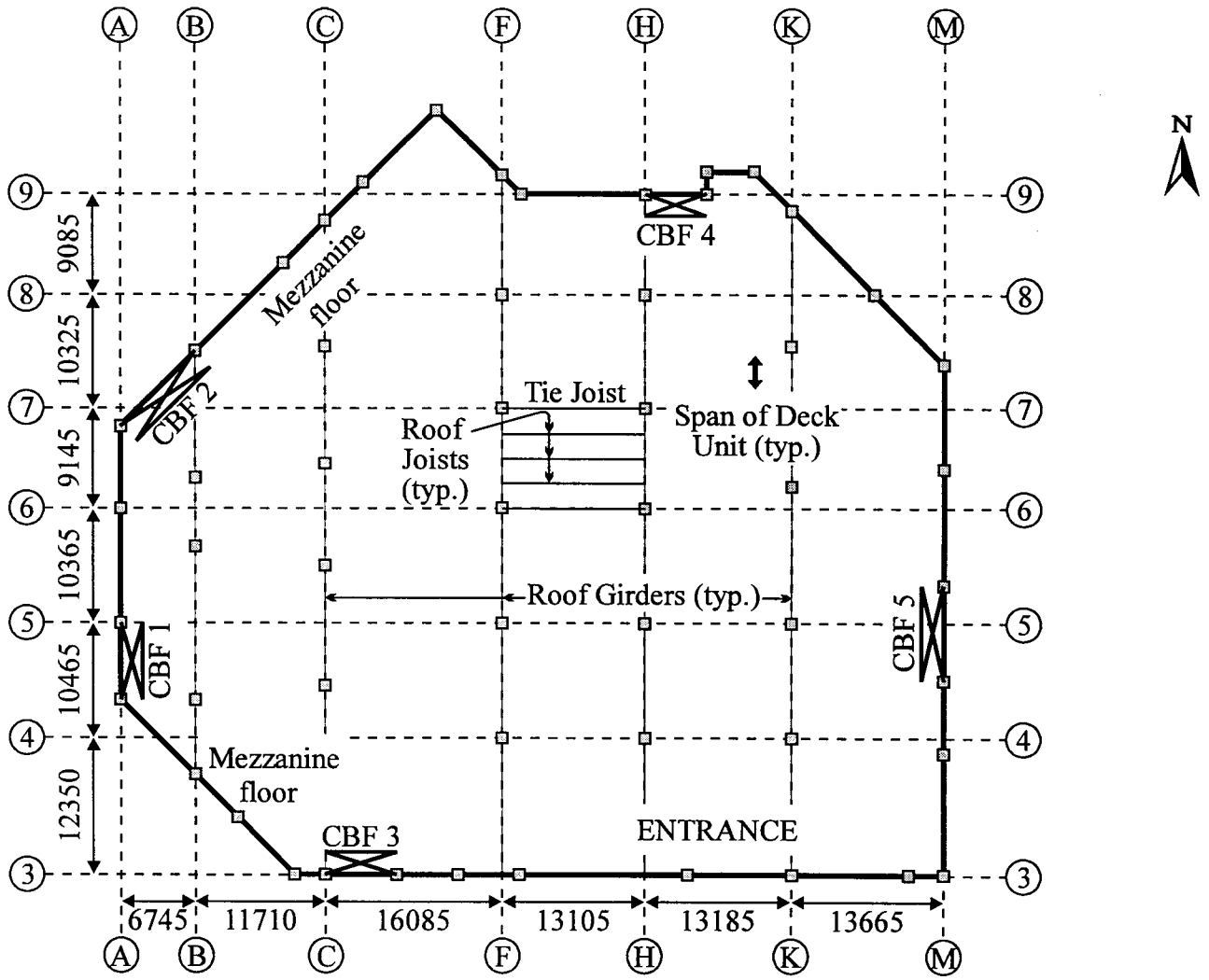

Figure D.1 General layout of Safeway store at Bonnie Doon Mall, Edmonton

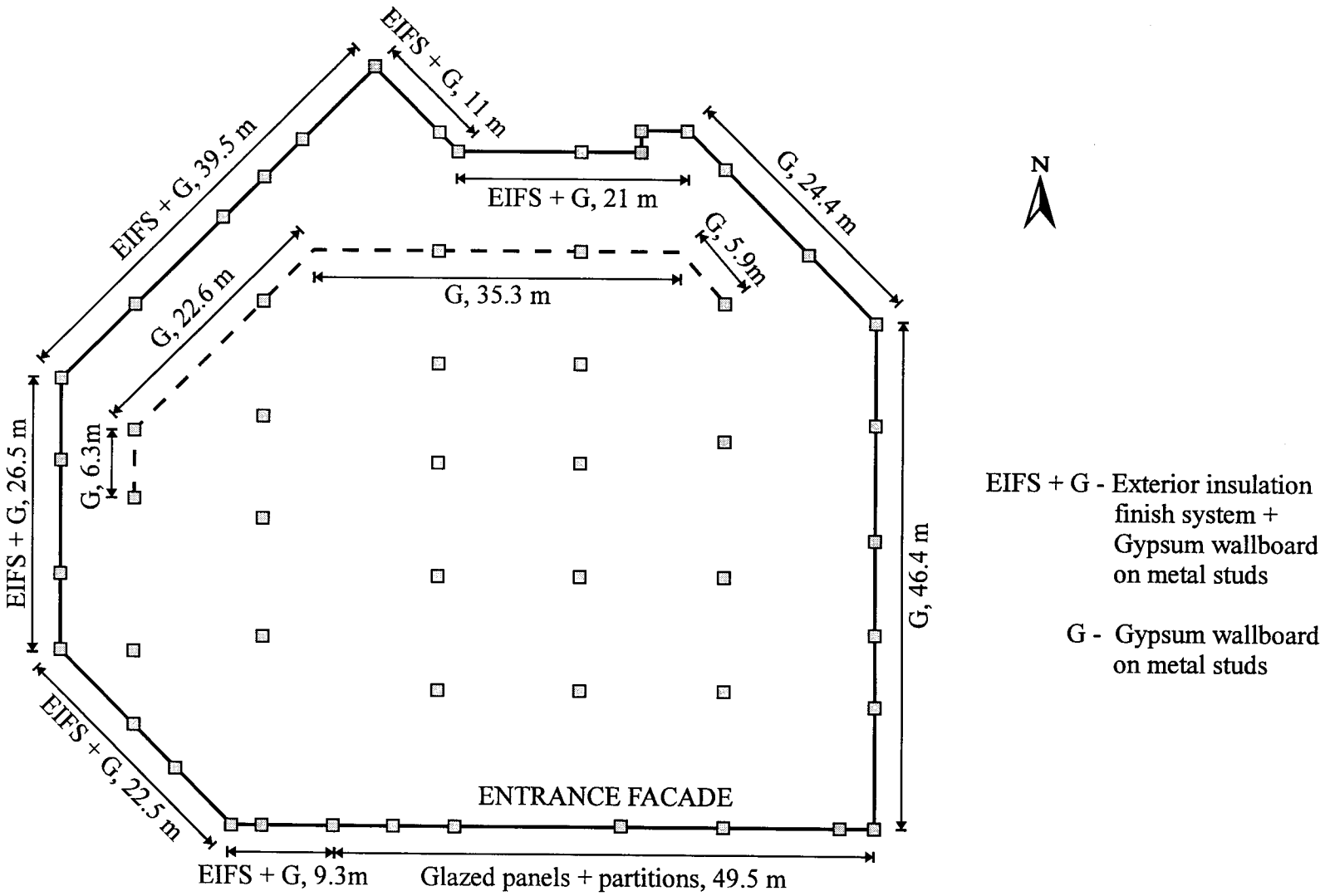

Figure D.2 Layout of non-structural elements

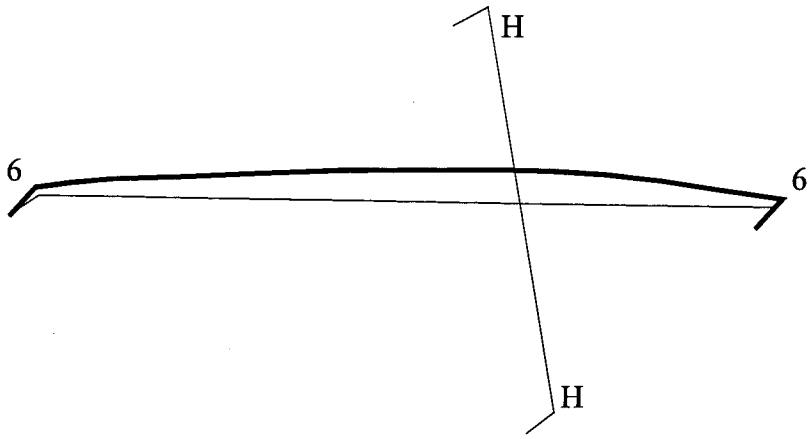

(a) Mode 1 (T = 0.34 s)

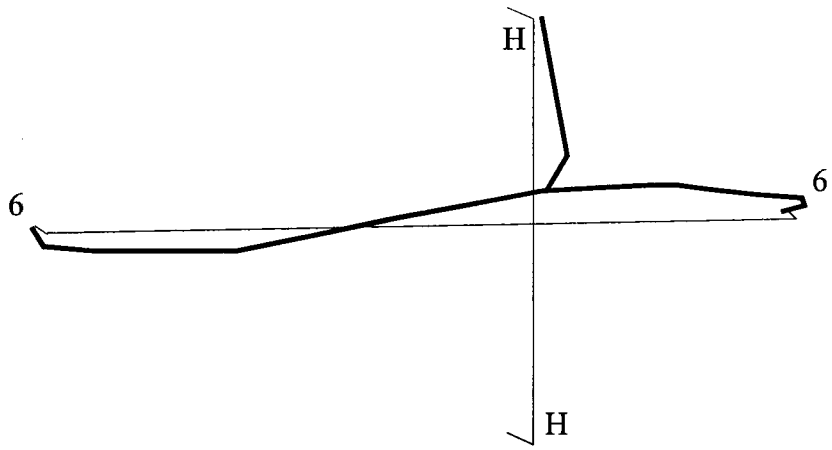

(b) Mode 2 (T = 0.18 s)

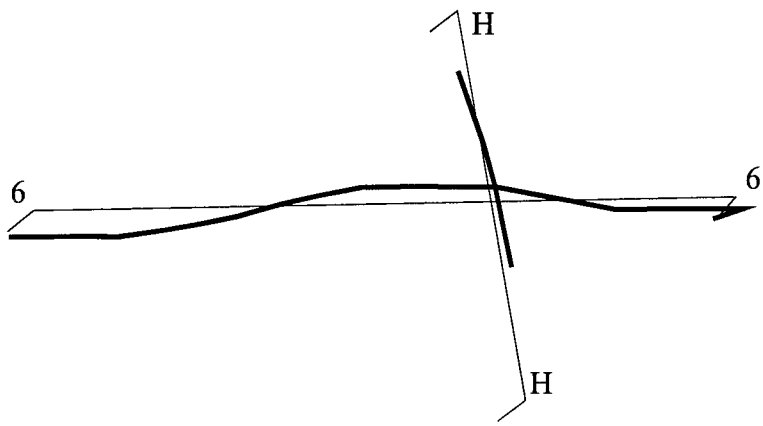

(c) Mode 3 (T = 0.12 s)

Figure D.3 Experimental mode shapes in N-S direction

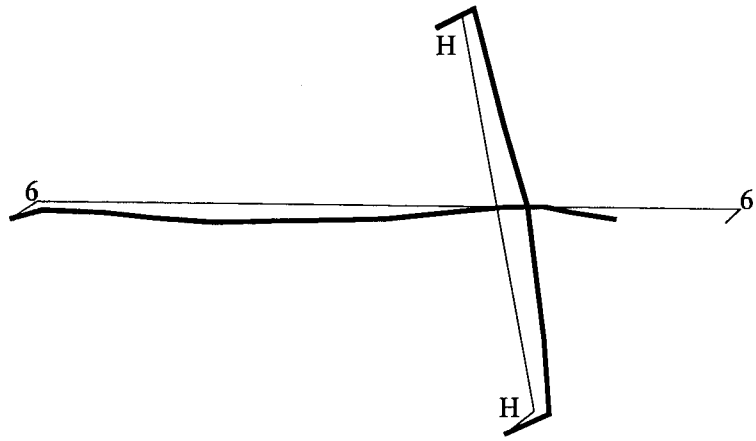

(a) Mode 1 (T = 0.29 s)

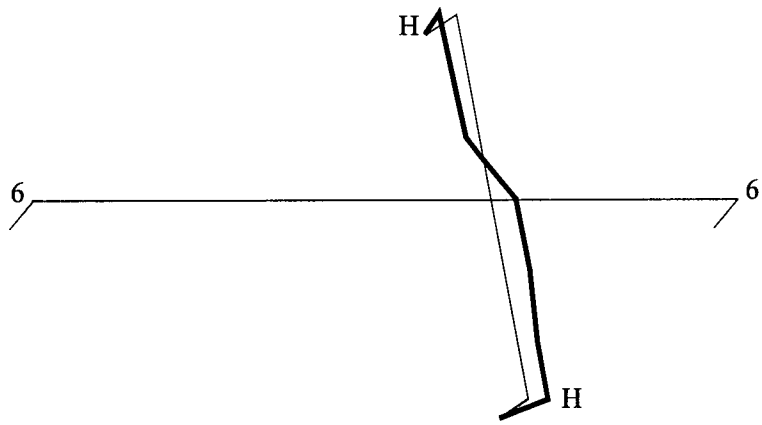

(b) Mode 2 (T = 0.13 s)

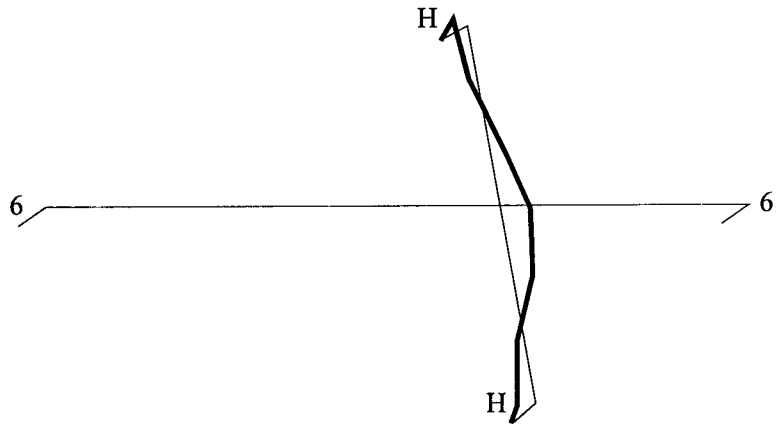

(c) Mode 3 (T = 0.10 s)

Figure D.4 Experimental mode shapes in E-W direction

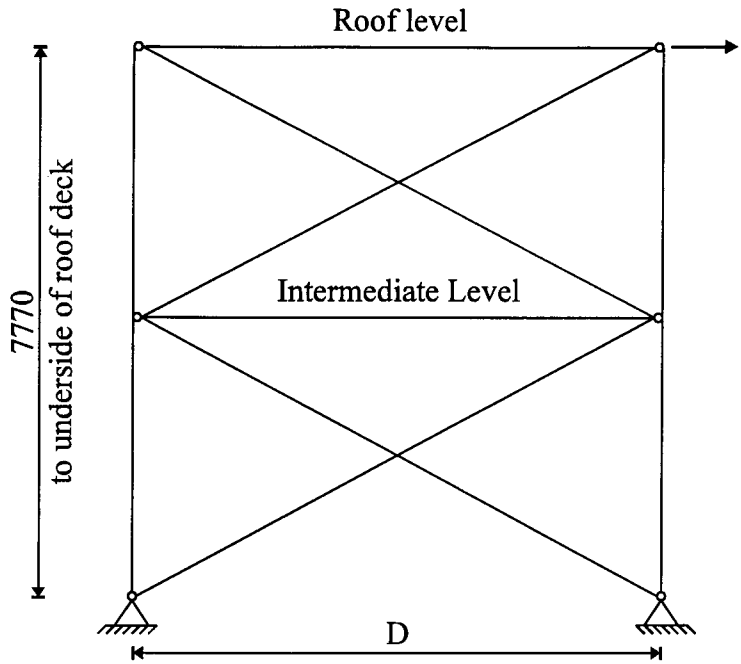

CBF	D (mm)	Roof beam	Stiffness (kN/mm)
1	7025	W460x67	39
2	9540	W460x82	36
3	6530	W460x67	40
4	5505	W410x54	38
5	8690	W460x89	37

Columns - HSS 203 x 203 x 13

Intermediate beam - HSS 203 x 203 x 13

Braces - C 200 x 17, Area = 2170 mm^2

Stiffness for lateral drift at roof level

Figure D.5 Lateral stiffness of CBFs

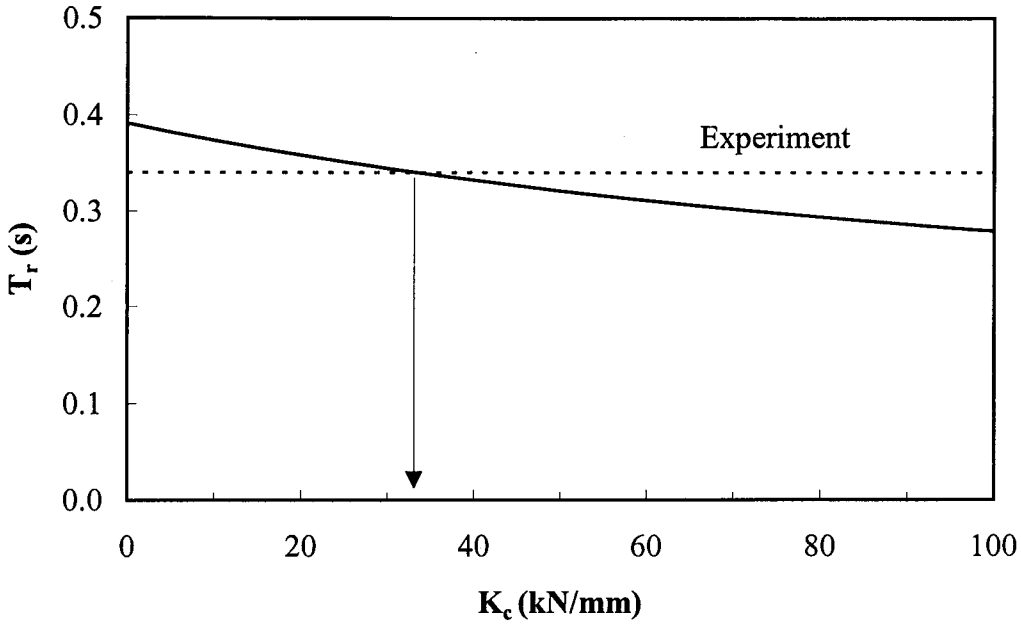

(a) North-South direction

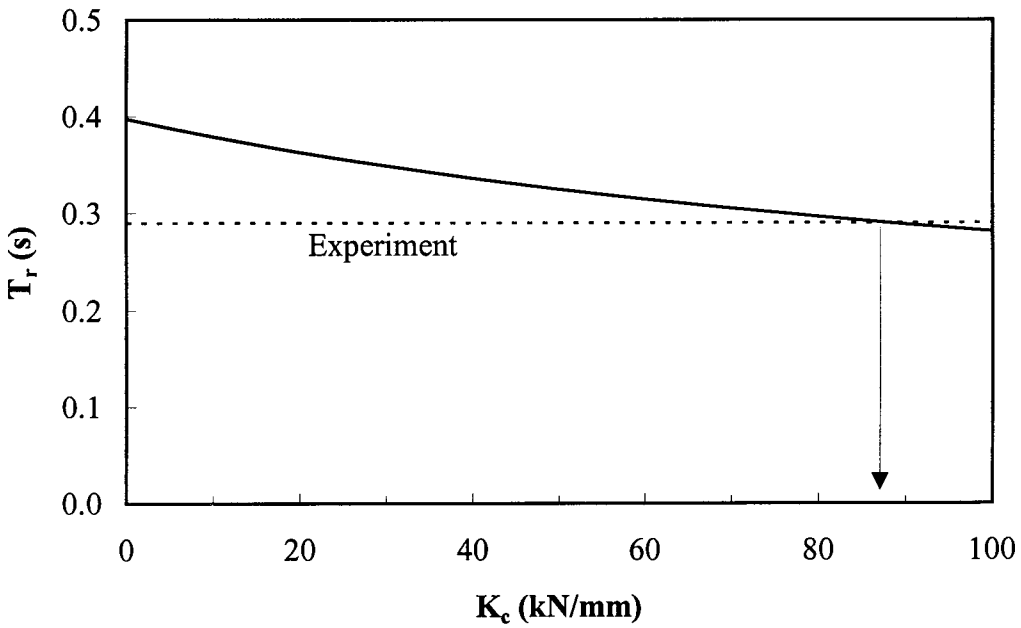

(b) East-West direction

Figure D.6 Estimate of nonstructural stiffness from SDOF model

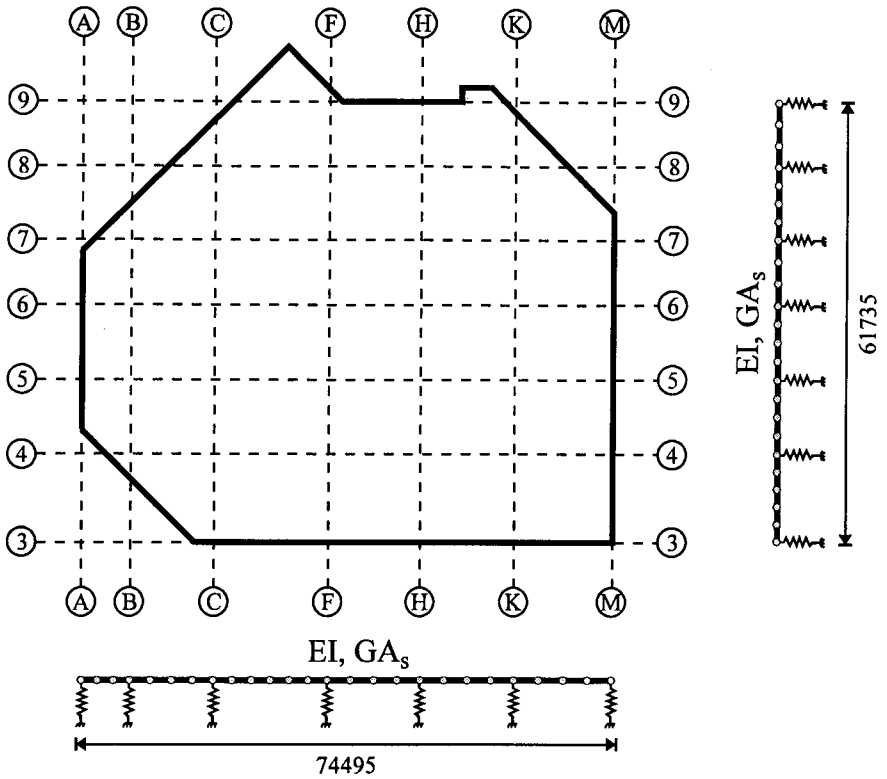

Figure D.7 Beam on elastic foundation analogy

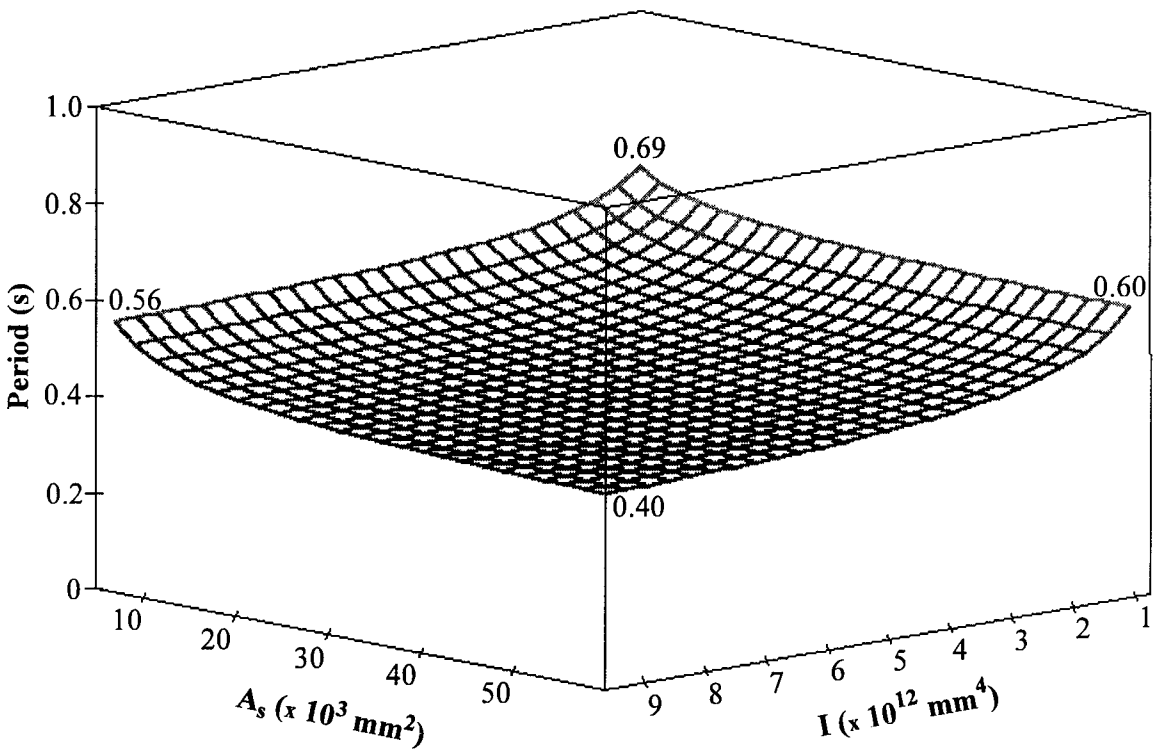

Figure D.8 Fundamental period in N-S direction from classical model

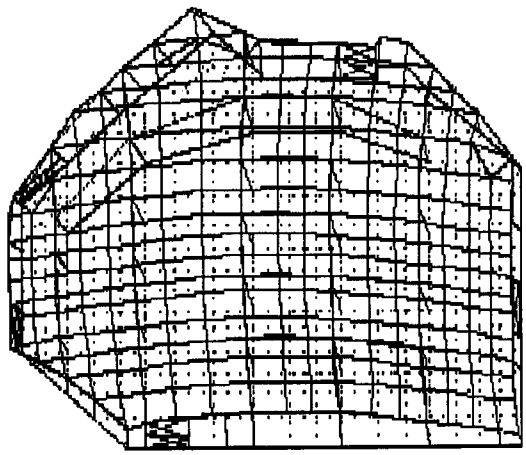

(a) T = 0.57 s

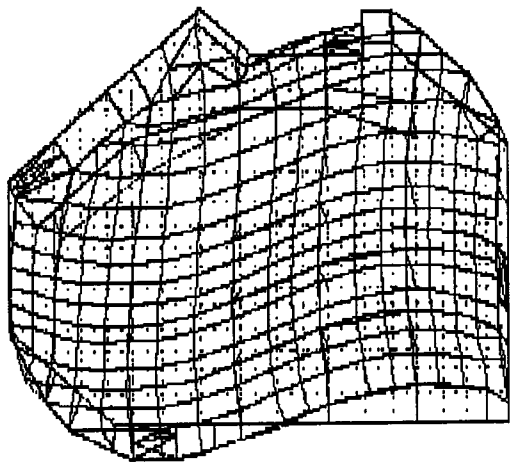

(b) T = 0.30 s

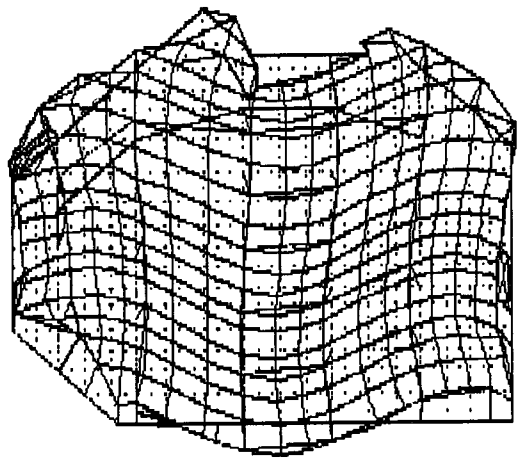

(c) T = 0.20 s

Figure D.9 Mode shapes in N-S direction from 3-D model

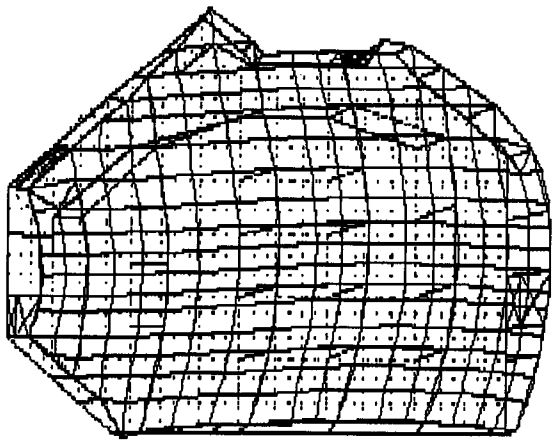

(a) T = 0.47 s

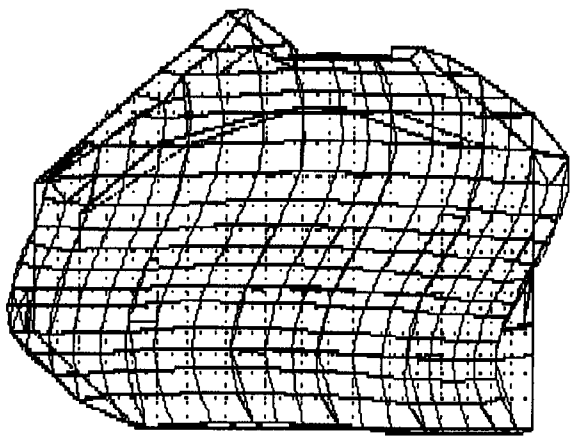

(b) T = 0.25 s

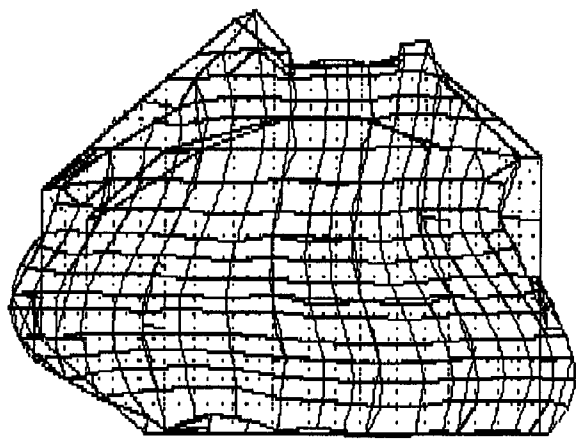

(c) T = 0.17 s

Figure D.10 Mode shapes in E-W direction from 3-D model

APPENDIX E

E.1 Introduction

Consider a single-storey steel building with a flexible roof diaphragm that is supported by frames at its ends as shown in Fig. E.1(a). The mass of the diaphragm is assumed to be distributed uniformly along it while that of the frames is lumped at each frame. Interior partitions may also be present that contribute stiffness to the diaphragm along its span. The building may be represented by an equivalent beam shown in Fig. E.1(b). The fundamental period of vibration of the latter is found by an approximate closed-form solution that is derived below.

E.2 Natural frequency of a simply supported diaphragm

Consider a prismatic roof diaphragm that is simply supported at its ends. The stiffness of the diaphragm is characterised by flexural rigidity, EI, provided by the flange members, and shear rigidity, GA_s, provided by the web. The translational mass of the diaphragm, M_d, is assumed to be distributed uniformly along it. Rotational inertia of the diaphragm is neglected. In the following, the fundamental period of vibration of this diaphragm is derived from first principles.

The deflection of the diaphragm, y(x,t), is a sum of the deflection due to bending, $y_b(x,t)$, and that due to shear, $y_s(x,t)$. Thus,

[E.1] $$y(x,t) = y_b(x,t) + y_s(x,t)$$

Figure E.2 shows the free body diagram of a differential element of length dx of the diaphragm that is assumed to be vibrating in a steady-state. Using D'Alembert's principle, the equilibrium of forces in the Y direction results in

[E.2] $$\frac{\partial V(x,t)}{\partial x} + p(x,t) = \rho A \frac{\partial^2 y(x,t)}{\partial t^2}$$

where ρ is the mass density per unit volume. Summing the moment of the elemental forces about point C and neglecting second-order terms gives

[E.3] $$\frac{\partial M(x,t)}{\partial x} = V(x,t)$$

The bending moment, M(x,t), and the shear force, V(x,t), are given by

[E.4] $$M(x,t) = -EI\frac{\partial^2 y_b(x,t)}{\partial x^2}$$

[E.5] $$V(x,t) = GA_s\frac{\partial y_s(x,t)}{\partial x}$$

Substitute [E.5] into [E.2] to obtain

[E.6] $$\frac{\partial}{\partial x}\left(GA_s\frac{\partial y_s(x,t)}{\partial x}\right) + p(x,t) = \rho A\frac{\partial^2 y(x,t)}{\partial t^2}$$

Substitute [E.4] and [E.5] into [E.3] and obtain

[E.7] $$GA_s\frac{\partial y_s(x,t)}{\partial x} + \frac{\partial}{\partial x}\left(EI\frac{\partial^2 y_b(x,t)}{\partial x^2}\right) = 0$$

Equations [E.6] and [E.7] are coupled in $y_s(x,t)$ and $y_b(x,t)$. The solution depends on the boundary and initial conditions. Assume that the external forcing, $p(x,t)$, is zero. Rearrange [E.6] to obtain

[E.8] $$\frac{\partial^2 y_s(x,t)}{\partial x^2} = \frac{1}{GA_s}\left(\rho A\frac{\partial^2 y(x,t)}{\partial t^2}\right)$$

Differentiate [E.1] with respect to x twice to obtain

[E.9] $$\frac{\partial^2 y(x,t)}{\partial x^2} = \frac{\partial^2 y_b(x,t)}{\partial x^2} + \frac{\partial^2 y_s(x,t)}{\partial x^2}$$

Equations [E.4] and [E.8] can be used to replace the right hand side of [E.9] to give

[E.10] $$\frac{\partial^2 y(x,t)}{\partial x^2} = -\frac{M(x,t)}{EI} + \frac{1}{GA_s}\left(\rho A\frac{\partial^2 y(x,t)}{\partial t^2}\right)$$

Differentiate [E.10] with respect to x and substitute [E.3] to obtain

[E.11] $$\frac{\partial^3 y(x,t)}{\partial x^3} = -\frac{V(x,t)}{EI} + \frac{1}{GA_s}\left(\rho A\frac{\partial^3 y(x,t)}{\partial x\partial t^2}\right)$$

Differentiate [E.11] with respect to x, substitute for the shear term from [E.2], and rearrange to obtain the differential equation of the diaphragm as

[E.12] $$EI\frac{\partial^4 y(x,t)}{\partial x^4} + \rho A\frac{\partial^2 y(x,t)}{\partial t^2} - \frac{\rho AEI}{GA_s}\frac{\partial^4 y(x,t)}{\partial x^2\partial t^2} = 0$$

Assume that the diaphragm is in simple harmonic motion. The deflection, y(x,t), may be expressed as the product

[E.13] $$y(x,t) = \Phi(x)\,\xi(t)$$

where $\Phi(x)$ is a spatial (shape) function and $\xi(t)$ is a temporal function. Differentiate [E.13] as required and substitute into [E.12] to obtain

[E.14] $$EI\,\Phi^{IV}(x)\,\xi(t) + \rho A\,\Phi(x)\,\ddot{\xi}(t) - \frac{\rho AEI}{GA_s}\,\Phi^{II}(x)\,\ddot{\xi}(t) = 0$$

Because the response is harmonic, $\xi(t)$ is taken as

[E.15] $$\xi(t) = \sin(\omega t)$$

Differentiate [E.15] with respect to t twice and substitute into [E.14] to obtain

[E.16] $$\left(EI\,\Phi^{IV}(x) - \rho A\omega^2\,\Phi(x) + \frac{\rho A\omega^2 EI}{GA_s}\,\Phi^{II}(x)\right)\sin(\omega t) = 0$$

For a non-trivial solution, the quantity in brackets in [E.16] must be equal to zero. Because the diaphragm is simply supported, the spatial function is taken as

[E.17] $$\Phi(x) = A_n \sin\left(\frac{n\pi x}{L}\right)$$

The assumed solution, [E.17], does not satisfy the boundary conditions rigorously, nor is it the general solution of [E.12]. Differentiate [E.17] as required and substitute into [E.16] to obtain

[E.18] $$\left(EI\left(\frac{n\pi}{L}\right)^4 - \rho A\omega^2 - \frac{\rho A\omega^2 EI}{GA_s}\left(\frac{n\pi}{L}\right)^2\right) A_n \sin\left(\frac{n\pi x}{L}\right) = 0$$

For a non-trivial solution, the expression in the large bracket in [E.18] must be equal to zero. This expression, on suitable rearrangement, gives the natural frequency of the diaphragm as

[E.19] $$\omega^2 = \frac{EI}{\rho A}\,\frac{(n\pi/L)^4}{\left(1 + \frac{EI}{GA_s}\left(\frac{n\pi}{L}\right)^2\right)}$$

To check the validity of the above derivation, consider the case of a simply supported diaphragm with flexural rigidity, EI. To ignore shear deformations, the shear

rigidity is assumed to be infinitely large. Hence, take limits as GA_s tends to infinity in [E.19] and simplify to obtain the natural frequency of an Euler-Bernoulli beam (Weaver *et al.* 1990) as

[E.20] $$\omega^2 = \left(\frac{n\pi}{L}\right)^4 \frac{EI}{\rho A}$$

E.3 Application to single-storey buildings

The equivalent beam shown in Fig. E.1(b) is itself represented by a two degree of freedom model shown in Fig. E.3, where M_f is the mass of the frames, M_d is the mass of the roof diaphragm, K_f is the lateral stiffness of the frames, K_i is the subgrade modulus (equal to the smeared lateral stiffness provided by the interior partitions), and K_d is a calibrated stiffness of the diaphragm given by

[E.21] $$K_d = \omega_1^2 M_d$$

where ω_1 is the fundamental frequency of the simply supported diaphragm obtained from [E.19] with n taken equal to 1. The total mass of the building, M, is the sum of M_f and M_d. The fundamental frequency of the building, ω_b, is obtained by solving the characteristic equation of the equivalent two degree of freedom system that may be simplified into the quadratic equation

[E.22] $$\alpha \lambda^2 + \beta \lambda + \gamma = 0$$

where $\lambda = \omega_b^2$ and the constants α, β, and γ are given by

[E.23] $$\alpha = M_f M_d$$

[E.24] $$\beta = -\left(M K_d + M_d K_f + M_f K_i L\right)$$

[E.25] $$\gamma = K_f K_d + K_i L \left(K_f + K_d\right)$$

The fundamental period of the building, T_b, is given by

[E.26] $$T_b = 2\pi / \omega_b$$

E.4 Verification of the expression

The analytical estimate of the period derived above is applied to the single-storey building considered in Chapter 5. The results are reported in Table 5.7. Note that interior

partitions are neglected in the building. Hence, some additional numerical results are presented to verify the equation.

Consider the single-storey building shown in Fig. 5.1. Assume the details of the diaphragm, concentrically braced frame (CBF), and cladding for zone 5 from Table 5.6. The total mass, M, corresponds to a weight of 6710 kN. The mass of the diaphragm, M_d, is taken to be 0.82 M, while the remainder is attributed to the end frames. The interior partitions are assumed of gypsum wallboard on wood studs with an effective thickness of 25.4 mm. They extend the entire length of 60 000 mm in the E-W direction, are spaced 5250 mm apart in the N-S direction, and are anchored to the floor below and the underside of the diaphragm above. The shear modulus, G, of such partitions is typically between 40 MPa and 120 MPa (Freeman 1977). The racking stiffness of the partitions is

$$\frac{V}{\Delta} = \frac{G\,t\,L}{h} \qquad [E.27]$$

where V is the lateral load, Δ is the interstorey drift, t is the effective thickness, L is the length, and h is the height of the partition. Table E.1 compares the fundamental period from the classical model with that from the MDOFN model of Chapter 5. The lateral stiffness of the two end frames is 85 kN/mm in all six cases. The shear modulus for case 2 and 3 in Table E.1 is calibrated so that the total lateral stiffness provided by the interior partitions is 10% and 50% of that provided by each end frame, respectively. In case 6, the total lateral stiffness provided by the partitions is just over three times that of the two end frames. The results show excellent agreement with the numerical estimates.

E.5 Initial estimate of period for design

The analytical expressions developed before may be used to obtain the fundamental period of single-storey buildings when all the properties are known. However, at the start of the design, the stiffnesses of the CBFs and the roof diaphragm are not yet available. Hence, an initial estimate of the period is required. The building is then designed and once the stiffness characteristics are known, a refined estimate of the period can then be made.

An initial estimate of the period is made assuming a rigid roof diaphragm. The period of a building of mass, M, and lateral stiffness, K, is

[E.28] $$T = 2\pi\sqrt{\frac{M}{K}}$$

The base shear capacity of the building, V, is given by

[E.29] $$V = M S_a = K \Delta$$

where S_a is the spectral acceleration and Δ is the lateral drift required to yield the lateral load resisting system. Rearrange [E.29] to obtain

[E.30] $$\frac{M}{K} = \frac{\Delta}{S_a}$$

For a CBF, the lateral (storey) drift required to yield the brace, Δ, is

[E.31] $$\Delta = \frac{\Delta_Y}{\cos\theta} = \frac{F_Y L_b}{E \cos\theta} = \frac{F_Y L_b^2}{E D_s}$$

where Δ_Y is the yield elongation of the brace, θ is the angle of inclination of the brace with the horizontal, F_Y is the yield stress, L_b is the brace length, E is the elastic modulus, and D_s is the width of the CBF. Substituting for Δ from [E.31] into [E.30], and substituting the resulting expression for M/K into [E.28] gives

[E.32] $$T = 2\pi\sqrt{\frac{F_Y L_b^2}{E D_s S_a}}$$

From Fig. 2.2, assuming Z_a equal to Z_v, the spectral acceleration, S_a, is related to the period, T, by

[E.33] $$S_a = \left(3.0 - 3.6\,(T - 0.25)\right) g\, v \qquad \text{for } 0.25\text{ s} < T < 0.50\text{ s}$$

[E.34] $$S_a = \frac{1.5\, g\, v}{\sqrt{T}} \qquad \text{for } T > 0.50\text{ s}$$

where g is the acceleration due to gravity and v is the zonal velocity ratio. The expression for S_a given by [E.33] or [E.34] may be substituted into [E.32] to give an initial estimate of the period, T.

Table E.1 Comparison of period for classical model vs. MDOFN model

Case	Shear modulus G MPa	Subgrade modulus kN/mm^2 K_i	Period (s) Classical model (a)	MDOFN model (b)	Ratio (b/a)
1	0	0	0.71	0.72	1.01
2	4	1.25E-04	0.65	0.66	1.02
3	19	6.23E-04	0.51	0.52	1.03
4	40	1.29E-03	0.41	0.42	1.03
5	80	2.59E-03	0.32	0.33	1.03
6	120	3.88E-03	0.27	0.28	1.03

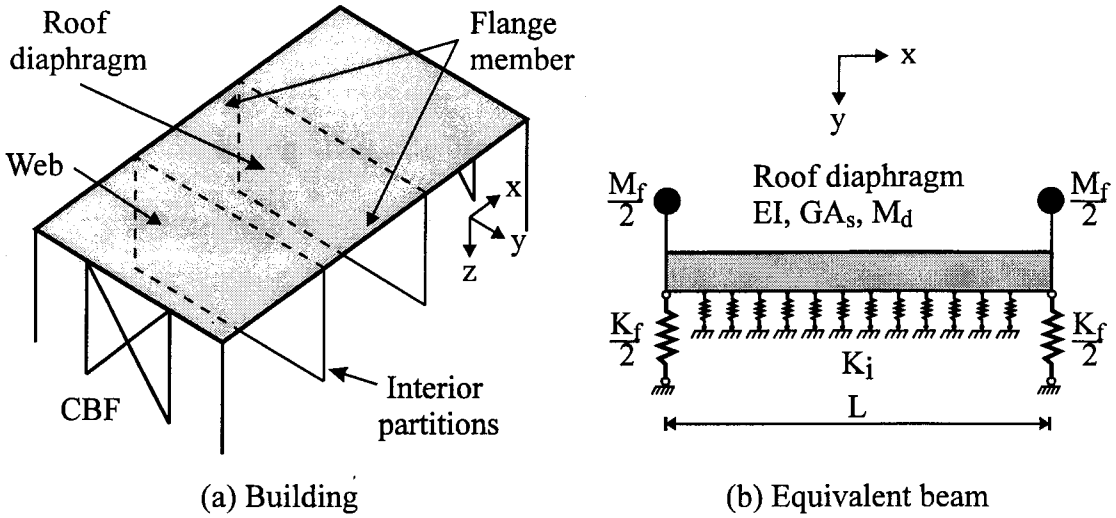

Figure E.1 Single-storey building and equivalent beam analogy

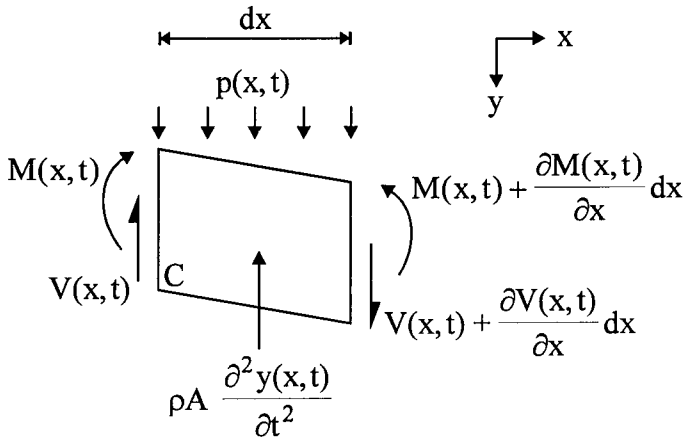

Figure E.2 Free body diagram of differential element of diaphragm

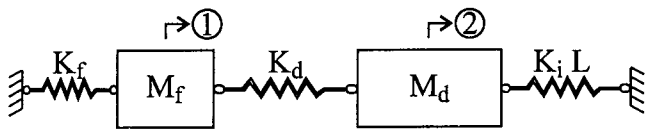

Figure E.3 Equivalent two degree of freedom model